PUNCHING SHEAR IN FLAT SLABS SUPPORTED ON RE-ENTRANT CORNER COLUMNS

JOÃO PAULO DE ALMEIDA SIQUEIRA

TESE DE DOUTORADO EM ESTRUTURAS E CONSTRUÇÃO CIVIL

DEPARTAMENTO DE ENGENHARIA CIVIL E AMBIENTAL

FACULDADE DE TECNOLOGIA

UNIVERSIDADE DE BRASÍLIA

UNIVERSIDADE DE BRASÍLIA
FACULDADE DE TECNOLOGIA
DEPARTAMENTO DE ENGENHARIA CIVIL E AMBIENTAL

PUNCHING SHEAR IN FLAT SLABS SUPPORTED ON RE-ENTRANT CORNER COLUMNS

JOÃO PAULO DE ALMEIDA SIQUEIRA

ORIENTADOR: GUILHERME SALES SOARES DE AZEVEDO MELO
COORIENTADOR: MIGUEL FERNÁNDEZ RUIZ (UPM)

TESE DE DOUTORADO EM ESTRUTURAS E CONSTRUÇÃO CIVIL

PUBLICAÇÃO: xxx/25
BRASÍLIA-DF
2025

UNIVERSIDADE DE BRASÍLIA
FACULDADE DE TECNOLOGIA
DEPARTAMENTO DE ENGENHARIA CIVIL

PUNCHING SHEAR IN FLAT SLABS SUPPORTED ON RE-ENTRANT CORNER COLUMNS

JOÃO PAULO DE ALMEIDA SIQUEIRA

Tese submetida ao Departamento de Engenharia Civil e Ambiental da Faculdade de Tecnologia da Universidade de Brasília como parte dos requisitos necessários para a obtenção do grau de Doutor em Estruturas e Construção Civil.

Tese de Doutorado aprovada pela Banca Examinadora, constituída por:

Prof. Guilherme Sales Soares de Azevedo Melo, *Ph*.D.
Universidade de Brasília
(Presidente e Orientador)

Prof. Marcos Honorato de Oliveira, *D.Sc*
Universidade de Brasília
(Examinador Interno)

Prof. Válter José da Guia Lúcio, *D.Sc*
Universidade Nova de Lisboa
(Examinador Externo)

Prof. Elyson Andrew Pozo Liberati, *D.Sc*
Universidade Estadual de Maringá
(Examinador Externo)

A ata da defesa, com as respectivas assinaturas dos membros, encontra-se no SEI/UnB e na Secretaria do Programa da Unidade.

Brasília-DF, 08 de dezembro de 2025.

FICHA CATALOGRÁFICA

SIQUEIRA, JOÃO PAULO DE ALMEIDA
Punching shear in flat slabs supported on re-entrant corner columns
[Brasília, Distrito Federal] 2025. xxi, 158., 210 x 297 mm (ENC/FT/UnB, Doutor, Estruturas e Construção Civil, 2025). Tese de Doutorado - Universidade de Brasília. Faculdade de Tecnologia. Departamento de Engenharia Civil e Ambiental.
1. Punção 2. Lajes lisas
3. Armadura de cisalhamento 4. Pilar de Canto Reentrante
I. ENC/FT/UnB II. Título (Doutor)

REFERÊNCIA BIBLIOGRÁFICA

SIQUEIRA, J. P. A. (2025). *Punching shear in flat slabs supported on re-entrant corner column*. Tese de Doutorado em Estruturas e Construção Civil, Publicação E.DM-XX/25, Departamento de Engenharia Civil e Ambiental, Universidade de Brasília, Brasília, DF, 158p.

CESSÃO DE DIREITOS

AUTOR: João Paulo de Almeida Siqueira

TÍTULO: Punching shear in flat slabs supported on re-entrant corner columns

GRAU: Doutor ANO: 2025

João Paulo de Almeida Siqueira.
Av. Juscelino Kubitschek de Oliveira, N° 1290 - Planalto
38660-000 Buritis - MG - Brasil.
e-mail: joaopaulodealmeida28@gmail.com

Dedicatória

Dedico este trabalho à minha mãe, Juliana (in memoriam),
minha eterna fonte de amor, força e inspiração.
Sua dedicação e luta resultam nessa nossa conquista.

AGRADECIMENTOS

Considero-me extremamente privilegiado por ter passado os últimos oito anos na Universidade de Brasília, inicialmente como aluno de mestrado e, posteriormente, de doutorado no Programa de Pós-Graduação em Estruturas e Construção Civil. Esse período foi marcado por significativo crescimento pessoal, acadêmico e profissional, além do desenvolvimento do rigor científico, da paixão e da dedicação indispensáveis à atuação como professor e pesquisador.

Muitas pessoas contribuíram para tornar este trabalho possível, às quais desejo expressar minha mais sincera gratidão.

Em primeiro lugar, agradeço imensamente ao meu orientador Prof. Guilherme Sales de Melo, por me acolher em seu grupo de pesquisa. Muito obrigado pela confiança depositada em mim e por todo incentivo ao longo desses anos, bem como pela orientação, pelo apoio constante, pela atenção e pela amizade. Sinto-me muito honrado em ser seu aluno.

E também agradeço ao Prof. Paul Regan (*in memoriam*), que concebeu os ensaios que deram origem a esta pesquisa.

Agradeço à Prof. Elaine Albuquerque, que antecedeu este trabalho e cuja pesquisa tive a oportunidade e a honra de dar continuidade.

Gostaria de agradecer, também, ao Prof. Miguel Fernández Ruiz, pela paciência e atenção com que me recebeu durante o período de doutorado sanduíche em Madrid, bem como pela disponibilidade constante em compartilhar seu conhecimento.

Agradeço ao Prof. Marcos Honorato, chefe do Laboratório de Estruturas da Universidade de Brasília, pelo envolvimento neste trabalho, bem como pelos valiosos comentários e sugestões. Estendo meus agradecimentos aos colegas de laboratório: Aparecida, Júlia, Caio, Nataniel. Ao técnico de laboratório, Sr. Magno, e aos colaboradores, em especial ao Zé Paulo e ao Hagamenon.

Agradeço aos membros examinadores externos desta tese, Prof. Elyson Liberati e Prof. Valter Lúcio, pelo tempo e esforço dedicados à leitura, pela revisão criteriosa, pelas contribuições e sugestões construtivas para o aprimoramento do trabalho, bem como pela discussão extremamente enriquecedora durante a defesa.

Esta pesquisa não teria sido possível sem o apoio financeiro da FAPDF, do CNPq e da CAPES, que viabilizaram a aquisição dos materiais e equipamentos necessários, além da concessão de bolsas para o doutorado no país e para o período de doutorado sanduíche.

Agradeço à empresa Trejor pelo fornecimento das armaduras de cisalhamento (*double headed studs*), à Ciplan pelo fornecimento do concreto e ao SENAI-DF pelo apoio nos ensaios de caracterização dos materiais.

À minha família e aos amigos, por acreditarem em mim desde o início e por estarem presentes em cada etapa desta caminhada. Agradeço aos meus pais (Juliana e José), que me deram a vida e que, dentro de suas possibilidades, contribuíram de forma decisiva para minha formação como ser humano.

Por fim, gostaria de agradecer a Deus por tudo, por ter me sustentado com saúde e determinação nos momentos mais desafiadores desta trajetória acadêmica.

"Nem tudo está perdido como parece... sabe, coisas extraordinárias só acontecem a pessoas extraordinárias, vai ver é um sinal que você tem um destino extraordinário, algum destino maior do que você pode ter imaginado."

C.S.Lewis - Crônicas de Nárnia

ABSTRACT

Punching Shear in Flat Slabs Supported on Re-entrant Corner Column.
Author: João Paulo de Almeida Siqueira.
Supervisor: Guilherme Sales S. de A. Melo and Miguel Fernández Ruiz.
Programa de Pós-graduação em Estruturas e Construção Civil
Brasilia, December of 2025.

Slab-column connections in re-entrant corners are less common than connections to internal, edge and corner. They can occur with some frequency. Normative codes provide detailed guidelines for designing inner, edge, and corner columns. These provide explicit means of calculating punching capacities by considering the moment transfer between slabs and columns, and a simplified approach applicable to structures with approximately equal adjacent spans. However, the connections to re-entrant corners are not mentioned.

The punching response of flat slabs with re-entrant corner regions is a complex phenomenon. Herein, the resistance and deformation capacity are coupled. Additionally, the distribution of shear forces near the supported area plays a major role in the mechanical response, with potential concentrations depending on the load eccentricity. Furthermore, the available literature on this situation is limited.

An experimental programme was conducted on the punching behaviour of re-entrant corner columns to provide comprehensive data on this topic and enhance the knowledge. The tests were aimed at investigating the influence of the flexural reinforcement ratio, edge reinforcement near the re-entrant corner, load eccentricity, and shear reinforcement on the punching resistance of slab-column connections. The results reveal that the flexural reinforcement ratio, load eccentricity, and presence of shear reinforcement significantly influence the state of deformations (rotations and strain of the reinforcements) and the ultimate load of the specimens.

The thesis also presents an approach that extends the critical shear crack theory (CSCT) to punching shear cases of re-entrant columns. A comparison between the analytical and experimental results revealed that the approach developed combined with the failure criterion used in the CSCT accurately predicts strength and deformation capacity.

Keywords: flat slab, punching shear, re-entrant corner, shear reinforcement, CSCT.

RESUMO

Punção em Lajes Lisas Apoiadas em Pilares de Canto Reentrante.
Autor: João Paulo de Almeida Siqueira.
Orientadores: Guilherme Sales S. de A. Melo and Miguel Fernández Ruiz.
Programa de Pós-graduação em Estruturas e Construção Civil
Brasília, dezembro de 2025.

As ligações entre lajes e pilares em cantos reentrantes são menos comuns do que as ligações internas, bordas e cantos. Elas podem ocorrer com alguma frequência. Os códigos normativos fornecem orientações detalhadas sobre o projeto de pilares internos, de borda e de canto. Eles fornecem meios explícitos de calcular as capacidades de punção levando em conta a transferência de momento entre a laje e o pilar, e uma abordagem simplificada aplicável a estruturas com vãos adjacentes aproximadamente iguais. No entanto, não há menção às ligações de cantos reentrantes.

A resposta da punção em lajes lisas em regiões de cantos reentrantes é um fenômeno complexo, em que a resistência e a capacidade de deformação estão acopladas. Além disso, a distribuição das forças de cisalhamento perto da área apoiada desempenha um papel importante na resposta mecânica, com possíveis concentrações dependendo da excentricidade da carga. Além disso, a literatura disponível sobre essa situação é limitada.

Um programa experimental sobre o comportamento à punção em pilares de canto reentrantes é apresentado para fornecer dados sólidos sobre esse tópico e avançar no conhecimento. Os ensaios tinham como objetivo investigar a influência da taxa de armadura de flexão, a borda da laje próxima ao canto reentrante, a excentricidade da carga e a armadura de cisalhamento na resistência à punção das ligações entre laje e pilar. Os resultados mostram que a proporção da armadura de flexão, a excentricidade da carga e a presença da armadura de cisalhamento influenciam significativamente o estado das deformações (rotações das lajes e deformações das armaduras), bem como a carga de ruptura dos espécimes.

Também é apresentada uma abordagem que amplia a Teoria da Fissura Crítica de Cisalhamento (CSCT) para casos de punção em pilares de canto reentrantes. A comparação entre os resultados analíticos e experimentais mostra que a abordagem desenvolvida, combinada com o critério de falha usado na CSCT, fornece previsões precisas da capacidade de resistência e deformação.

Palavras-Chave: laje lisa, punção, pilar de canto reentrante, armadura de cisalhamento, CSCT.

RESUMEN

Punzonamiento en Losas Planas Apoyadas en Columnas de Esquina Reentrante.
Autor: João Paulo de Almeida Siqueira.
Directores: Guilherme Sales S. de A. Melo and Miguel Fernández Ruiz.
Programa de Pós-graduação em Estruturas e Construção Civil
Brasilia, diciembre de 2025.

Las conexiones losa-columna en esquinas reentrantes no son tan comunes como las conexiones a interior, borde y esquina. Sin embargo, pueden presentarse con una frecuencia apreciable. Los códigos normativos proporcionan directrices detalladas para el diseño de pilares interiores, de borde y de esquina. Ofrecen medios explícitos para calcular las capacidades de punzonamiento teniendo en cuenta la transferencia de momentos entre losas y pilares, así como un enfoque simplificado aplicable a estructuras con vanos adyacentes aproximadamente iguales. Sin embargo, no hay mención a las conexiones con esquinas reentrantes.

La respuesta al punzonamiento de losas planas con esquinas reentrantes es un fenómeno complejo, en el que la resistencia y la capacidad de deformación están acopladas. Además, la distribución de los esfuerzos cortantes cerca de la zona apoyada desempeña un papel importante en la respuesta mecánica, con concentraciones potenciales que dependen de la excentricidad de la carga. Además, la bibliografía disponible sobre esta situación es limitada.

Un programa experimental sobre el comportamiento de punzonamiento de columnas de esquinas reentrantes se presenta para proporcionar datos sólidos sobre este tema y dar un paso adelante en el conocimiento. Los ensayos tenían por objeto investigar la influencia de la relación de armadura de flexión, la armadura de borde cerca de la esquina reentrante, la excentricidad de la carga, así como la armadura de cortante en la resistencia al punzonamiento de las conexiones losa-columna. Los resultados muestran que la relación de armadura de flexión, la excentricidad de la carga y la presencia de armadura de cortante influyen significativamente en el estado de deformaciones (rotaciones y deformación de las armaduras) así como en la carga última de las probetas.

También se presenta un enfoque que extiende la Teoría de la Fisura Crítica (CSCT) a los casos de cortante por punzonamiento de columnas reentrantes. La comparación entre los resultados analíticos y experimentales muestra que el enfoque desarrollado combinado con el criterio de rotura utilizado en la CSCT proporciona predicciones precisas de la capacidad resistente y de deformación.

Palabras-clave: losa plana, punzonamiento, esquina reentrante, refuerzo de cortante, CSCT.

SUMÁRIO

LIST OF TABLES

LIST OF FIGURES

LIST OF SYMBOLS

Below is the nomenclature of symbols that have been used throughout this thesis.

Roman lower-case letters:

a_{px} a_{py}	Distances from the axis of the support area to the zero radial bending moment according to EN 1992-1-1:23
b_u	Diameter of a circle with the same surface as the region inside the control perimeter according to *fib* MC 2010:13
b_s	Width of the support strip for calculating m_E
b_b	Geometric mean of the minimum and maximum overall widths of the control perimeter, according to EN 1992-1-1:23
$b_{b,min}$	Minimum overall widths of the control perimeter, according to EN 1992-1-1:23
$b_{b,max}$	Maximum overall widths of the control perimeter, according to EN 1992-1-1:23
c	Column side length
d_g	Maximum aggregate size
d_{g0}	Reference aggregate size
d	Average punching effective depth of the slab
d_v	Shear-resisting effective depth of reinforcement
e_R	Eccentricity with respect to the centroid of column at failure
f_c	Concrete compressive strength measured on a cylinder
f_{ys}	Yield strength of flexural reinforcement
f_{yw}	Yield strength of shear reinforcement
f_u	Ultimate strength of flexural reinforcement
k_{pb}	Shear gradient enhancement coefficient for punching (EN 19\z92-1-1:23)
k_e	Coefficient of eccentricity
k_ψ	Coefficient for rotations
k_{dg}	Coefficient for aggregate size
m_E	Bending moment per unit width
m_R	Flexural strength per unit width
n_r	Number of radii of shear reinforcement
n_s	Number of shear reinforcements per radius
r_s	Distance between the axis of the supported area ant the line of contraflexure
s_0	Radial spacing of the first perimeter from the face of the loaded area
s_r	Radial spacing between the perimeters of shear reinforcement
γ_v	Ratio of moment between slab and column that is considered transferred by eccentricity of shear according to ACI 318:19
$v_{perp,max}$	Maximum value of the shear force projected in the direction perpendicular to the control perimeter

Roman upper-case letters:

A_{sw}	Area of shear reinforcement provided in each perimeter
E_c	Modulus of elasticity of concrete
E_s	Modulus of elasticity of flexural reinforcement
J_c	Property analogous to polar moment of inertia, according to ACI 318:19
M_E	Design value of the applied internal bending moment
V_E	Value of the applied shear force
V_{flex}	Flexural resistance of a slab-column connection in punching
V_R and $V_{R,test}$	Ultimate punching capacity of a slab-column connection in the test
$V_{R,c}$	Calculated punching resistance of a slab without shear reinforcement
$V_{R,max}$	Calculated maximum punching resistance of a slab with shear reinforcement
$V_{R,cs}$	Calculated punching resistance of a shear-reinforced slab
$V_{R,out}$	Calculated punching resistance outside the shear reinforced region

Greek letters:

β_e	Coefficient accounting for concentrations of the shear forces (EN 1992-1-1:23)
ε_y	Yield strain of flexural reinforcement
ε_c	Concrete bottom strain measured on the test
ρ	Flexural reinforcement ratio
ψ	Slab rotation
ψ_x	Rotation in the x direction
ψ_y	Rotation in the y direction
ψ_{xy}	Rotation in the diagonal direction

Acronyms and abbreviations:

CSCT	Critical Shear Crack Theory
EC2	EN1992:1-1: 2004
MC	Model CodeLVDT
LVDT	Linear Variable Differential Transducer
prEC2	Draft for next generation of Eurocode 2

Symbols:

Ø	Diameter of the flexural reinforcement
$Ø_{sw}$	Diameter of the shear reinforcement

1. INTRODUCTION

Reinforced concrete flat slabs have been widely used in building structures owing to their structural efficiency, convenience of construction, and architectural flexibility. This type of system eliminates the use of exposed beams. Thus, it provides higher freedom in the layout of interior spaces. Additionally, it simplifies the construction process and facilitates the passage of pipes and electrical and hydraulic installations. Fig. 1.1 compares different structural solutions in reinforced concrete. It encompasses the conventional system (composed of slabs and beams) and flat slabs.

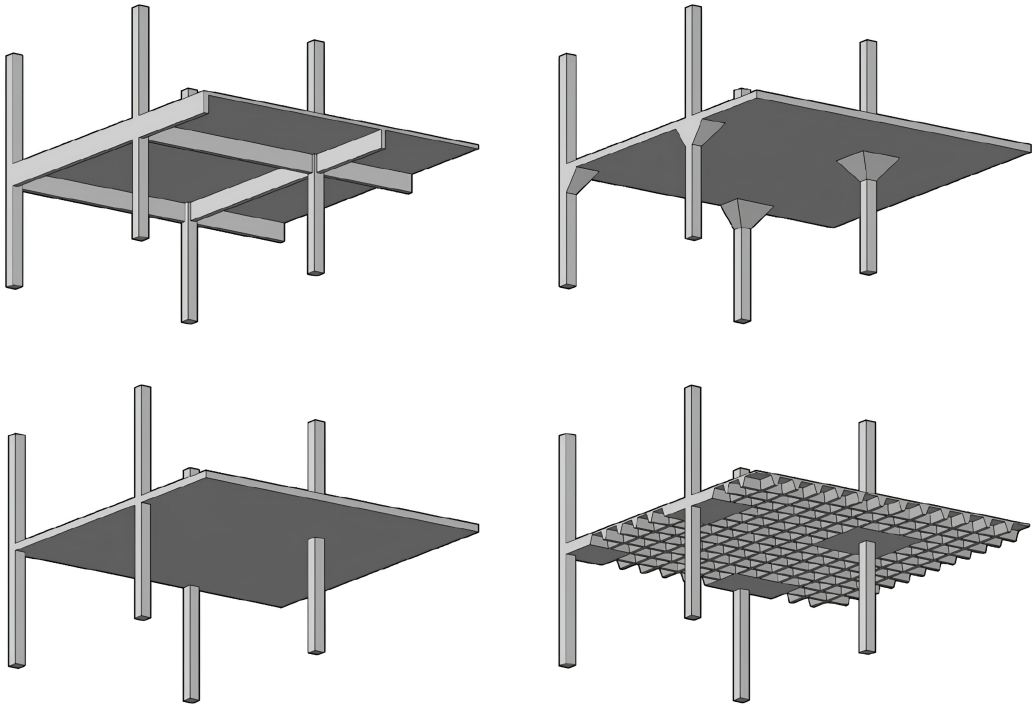

Fig. 1.1 - Structural systems for concrete structures. (from [1])

However, these advantages are accompanied by a more complex structural behaviour, particularly in the slab-column connection region, where high shear forces and bending moments are concentrated, which may lead to the punching shear phenomenon. In this situation, the slab tends to be *"punched through"* by the supporting column, resulting in a brittle and abrupt failure, usually without prior warning, which makes it especially undesirable from a structural safety standpoint.

Furthermore, the flat-slab structural system presents some disadvantages when compared to the conventional beam-and-slab system, requiring greater attention to excessive deflections in floor spans and to the reduction of the overall stiffness of the building in resisting lateral loads.

1.1. Punching Shear

Punching shear is a localized failure mode at the slab-column connection (Fig. 1.2-a) under concentrated loading. An analogous phenomenon occurs in direct foundations, such as isolated footings (Fig. 1.2-b), which are similarly subjected to concentrated reactions. In both cases, failure develops abruptly in a brittle manner and may trigger progressive collapse, particularly in the absence or insufficiency of shear reinforcement. In an inner slab-column connection, failure occurs along a truncated conical or pyramidal surface caused by diagonal tension cracking around the column or concentrated load. This mechanism results in the loss of the load-carrying capacity of the connection and is regarded as critical for structural safety owing to its abrupt characteristic.

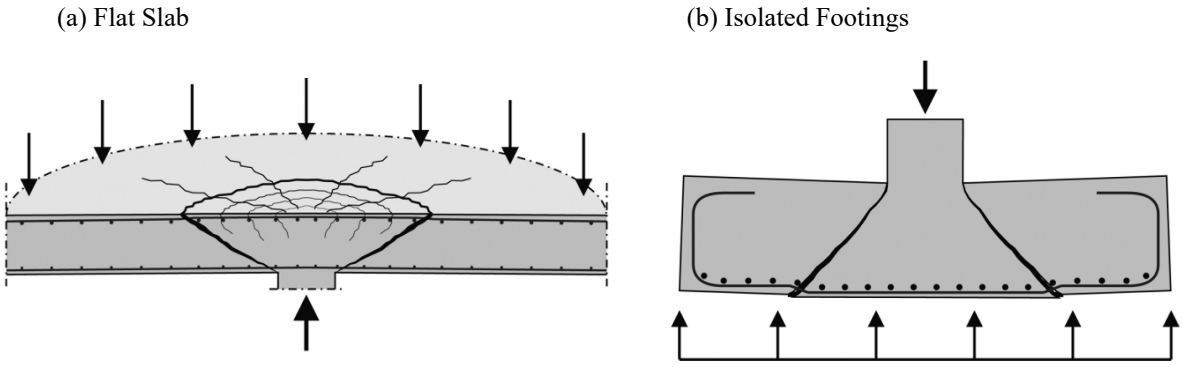

Fig. 1.2 - Punching cone in a flat slab and a foundation. (from Ungermann *et al.*[2])

Thus, the critical aspect in the design of flat slabs lies in the dimensioning of the slab-column connection. A localized failure can cause an abrupt redistribution of internal forces to other regions of the structure, which are generally not designed to withstand such increases in demand. This process may evolve into a partial or total collapse of the building. Such a mechanism (in which the extent of damage is disproportionately higher than the initial cause) is referred to as progressive collapse.

To enhance the punching shear capacity of flat slabs, several parameters can be adjusted (see, Fig. 1.3). Among the most relevant are the compressive strength of the concrete (f_c), flexural reinforcement ratio (ρ), dimensions and geometry of the column, and size effect (ξ); it accounts for the useful height of the slab and presence of shear reinforcement. Thus, the designer can address these factors to mitigate the risk of punching shear failure. However, the practical implementation of such measures generally involves technical, constructional, architectural, and economic constraints. These need to be considered meticulously during the design process.

For example, using high-strength concrete throughout the entire slab is occasionally infeasible technically or economically. Similarly, an increased longitudinal reinforcement ratio may yield limited enhance the resistant capacity and may hinder effective concrete compaction owing to the high reinforcement density near the column region. Similarly, an increase in the column dimensions may interfere with the architectural layout and reduce the usable floor area.

Another potential strategy is to increase the slab thickness. Although it improves the punching resistance, it increases the self-weight of the structure. This results in higher global internal forces and potentially adversely affects the design of other structural elements such as foundations.

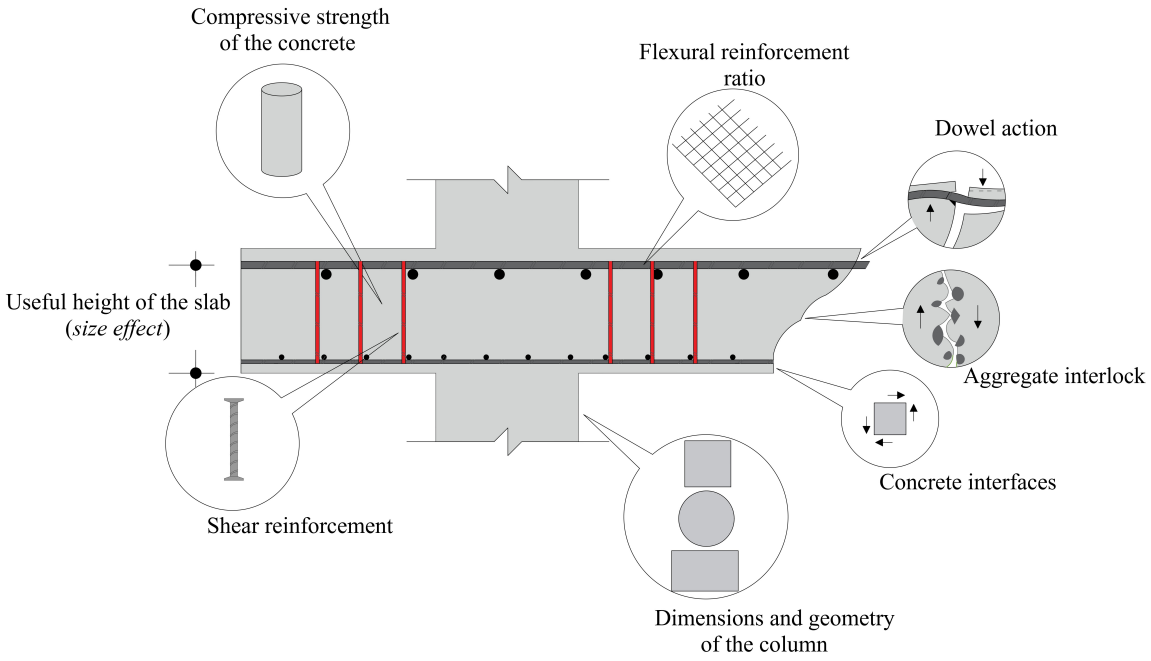

Fig. 1.3 - Some parameters involved in the rupture by punching shear.

The punching shear capacity of a slab is also influenced by factors such as the transfer of shear through the interlocking of aggregates and dowel action, as well as the residual tensile strength of the concrete. Significantly, the presence of openings at the slab-column connection [3]-[9], utilisation of fibres in the concrete [10]-[15], and use of capitals or drop panels [16]-[21] can significantly affect the punching shear capacity of a flat-slab system. Furthermore, prestressing [22]-[23] may provide a dual beneficial effect, as it reduces the applied punching shear demand by inducing compressive stresses in the slab and, simultaneously, enhances the punching shear resistance by delaying cracking and increasing the effective contribution of concrete in shear transfer mechanisms.

Although the previously mentioned parameters contribute to an increase in punching shear resistance, these provide limited improvements in the connection ductility. The most widely adopted solution for enhancing the strength and ductility of flat slabs in slab-column connection regions simultaneously is to introduce transverse reinforcement throughout the slab thickness. This reinforcement enables punching shear failure to occur in a more gradual and controlled manner, with clear pre-collapse indicators such as large deflections and visible cracking.

Slabs reinforced against shear have a significantly higher punching shear capacity. The magnitude of this capacity depends on the type, amount, and arrangement of the reinforcement used (see, Fig. 1.4). These structures generally display a more ductile response, thereby sustaining larger deformations prior to failure. Numerous studies have shown that the incorporation of shear reinforcement, such as studs or stirrups [24]-[27], can significantly enhance the punching shear capacity and provide a more ductile response. This results in a failure mode characterised by considerable deflection.

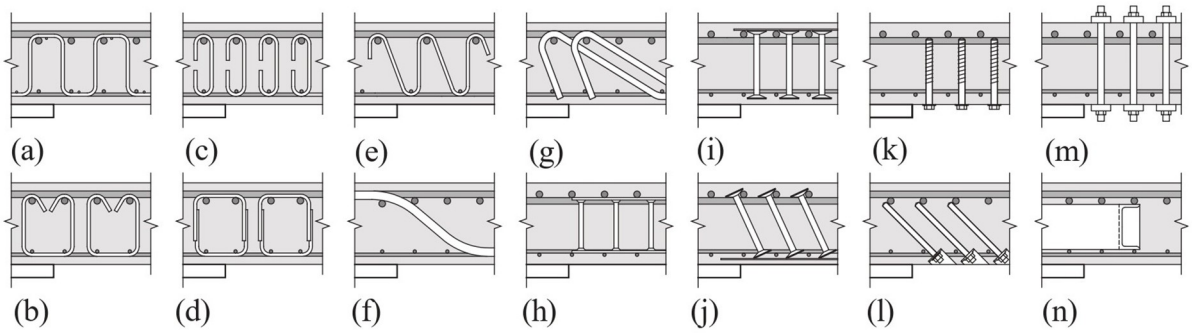

Fig. 1.4 - Punching shear reinforcement systems for RC flat slabs include (a-e) bend bar details (continuous stirrups, single or double legged elements, individual links); (f-g) bent-up bars; (h-j) headed bars (single or double headed bars, ladder type); (k-m) post-installed elements (screws or threaded bars); and (n) shearhead made of steel profiles. (from [28])

Shear reinforcement can be incorporated into the structure at different stages. In general, it is installed around the columns during the assembly of the slab reinforcement, prior to casting. This allows for a complete integration with the flexural reinforcement. Alternatively, it may be post-installed as a structural rehabilitation technique aimed at restoring or enhancing the punching shear capacity of existing structures, particularly in situations where shear deficiencies or increased loads have been identified.

1.2. Brief Historical Overview

Since the early 20th century, extensive research has been conducted to understand the shear behaviour of slab-column connections [2]. Flat slab systems have been used for over a century. The first applications are attributed to C.A.P. Turner (1905) in the United States and Robert Maillart (1908) in Europe. These early developments established the basis for the structural system known today as flat slabs. These are acknowledged for their architectural flexibility and efficient load transfer.

The first systematic study on punching shear was by Talbot (1913). The author tested 197 isolated footings. His work introduced two key concepts that are still being used in design: the identification of a critical control perimeter and the description of a truncated conical failure surface that initiates at the column face and extends through the slab thickness.

The subsequent research by Moe (1961) represents a significant advancement in design formulation. Moe defined the control perimeter (located at a distance of 0.5d from the column face) and introduced the c/d ratio (where c is the column width). He also established that the concrete shear strength is proportional to the square root of the compressive strength. This assumption was subsequently adopted by design codes. Based on Moe's observations, the ACI Committee 326 incorporated a simplified empirical expression for estimating punching shear capacity in 1963. It became the foundation for subsequent ACI provisions.

The first analytical model to describe the punching behaviour of flat slabs was proposed by Kinnunen and Nylander (1960) [29]-[32]. Through tests on axisymmetric circular slabs without shear reinforcement supported by circular columns, the authors developed a mechanically consistent model that considers the combined effects of bending and shear. The model conceptualizes the slab as a series of radial sectors separated by cracks and supported on a conical shell. Each sector rotates around a centre of rotation (CR) near the root of the shear crack. Meanwhile, the slab portion above the column remains undeformed.

This model represents a major conceptual advance. It provided the first physical interpretation of punching as a rotation-controlled phenomenon. Additionally, it served as the basis for the advanced mechanical models and design formulations that followed in the ensuing decades.

In this context, it is important to note that over the years, several theoretical models have been proposed to predict punching shear behaviour. Among the most significant are the formulations developed by Shehata and Regan 1989 [33], Gomes and Regan [30]-[31], Broms [34]-[35], Hallgren [36], Kueres and Hegger [37], and the critical shear crack theory (CSCT) proposed by Muttoni [38].

During the 1980s and 1990s, Regan [39]-[41] initiated investigations into punching in flat slabs, considering cases with and without shear reinforcement, at the Polytechnic of Central London. Regan was a member of the CEB-FIP Model Code 1990 Committee from 1985 to 1991, contributed with papers to several CEB bulletins from 1978 to 1993 and co-authored fib Bulletin 168 on Punching Shear of Reinforced Concrete. Within Professor Regan's research group, Shehata [42]-[43] proposed a model for slabs without shear reinforcement, drawing on the theoretical framework established by Kinnunen and Nylander. Later, Gomes extended Shehata's model by implementing the contribution of the shear reinforcement [30]-[31].

Broms (2016) introduced the Tangential Strain Theory (TST) [35]. It adapts several concepts from the original model proposed by Kinnunen and Nylander (1960). According to Broms, punching failure occurs when the compression zone outside the column collapses as a result of the development of radial tensile strains. Another relevant contribution is the two-parameter kinematic theory proposed by Kueres and Hegger (2018). Herein, the shear resistance is determined based on the deformed configuration of the slab, considering two degrees of freedom: flexural and translational deformations.

One of the most influential contributions to punching shear research was the formulation and validation of the CSCT by Fernández Ruiz and Muttoni [44]. The CSCT is a mechanically consistent model developed to describe and predict the punching shear behaviour of flat slabs. It is based on the premise that the opening of a critical shear crack progressively reduces the concrete's capacity to transfer shear stresses and ultimately causes failure. According to this mechanical approach, the crack opening (w) is assumed to be proportional to the product of the slab rotation (ψ) and effective depth (d). This establishes a direct relationship between the flexural response of the slab and its shear resistance. Muttoni (2008) assumed that the aggregate size influences the critical crack roughness and the capacity of shear transfer by aggregate interlock. This theoretical framework has been widely acknowledged and incorporated into advanced design standards including the fib Model Code 2010 and its 2020 revision. It also serves as the theoretical foundation for the new generation of Eurocode 2 (EC2:2023).

1.3. Punching Shear in Flat Slab: Open Questions

In the existing literature, symmetric punching shear is the most extensively investigated experimentally, numerically, and through analytical approaches. In contrast, non-symmetric (or eccentric) punching shear has been studied less thoroughly. This is notwithstanding its equal or higher practical relevance.

In cases of eccentric punching, the shear stresses along the critical control perimeter are distributed non-uniformly owing to the moment transfer between the slab and column. This transfer is balanced by a combination of shear forces, bending moments, and torsional moments. These interact in a complex manner within the slab-column connection region.

The origins of moment transfer from slabs to columns can be attributed to several factors. These include asymmetric loading, the differences in stiffness or span length between adjacent panels, the position of the columns within the structural layout, shrinkage and creep effects, and the horizontal actions induced by wind or seismic loads.

With regard to the position of the columns within the structure, slab-column connections are generally classified into interior, edge, and corner types. Although most experimental and analytical studies have focused on interior connections, a substantial portion of real structures includes edge and corner columns [45]-[63], which exhibit distinct structural behaviours. However, the number of experimental investigations addressing these configurations remains limited. This was emphasized by Hernandez Fraile *et al.* (2023). As illustrated in Fig. 1.5, approximately 73% of the reported tests were performed on inner columns, 20% involved edge columns, and 7% investigated corner column connections.

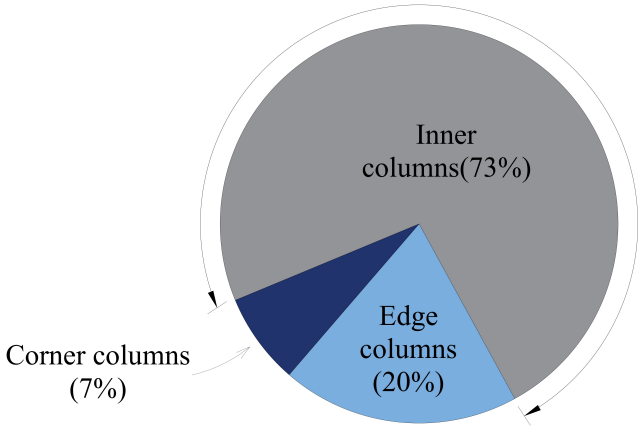

Fig. 1.5 - Available punching tests on various types of connections. (adapted from [15])

Among the various slab-column configurations, slabs supported on re-entrant corner columns represent one of the most complex and least understood cases. In such configurations, the column is located within an internal recess of the slab. This generates highly localized stress concentrations and complex load-transfer mechanisms. Notwithstanding their practical relevance, these cases have been largely overlooked in previous investigations. This has resulted in a significant deficiency in both literature and design standards [64]-[69].

Re-entrant corner columns are commonly observed in architectural layouts with H-, L-, T-, or U-shaped floor plans, as well as in inner patios. This geometry induces non-uniform stress distributions and significant unbalanced moments, which are not captured adequately by conventional design approaches developed for interior, edge, or corner columns. Consequently, the behaviour of these connections remains insufficiently understood, particularly in terms of punching shear resistance and failure mechanisms.

To address this research deficiency, the present thesis provides the results of a comprehensive experimental investigation involving fifteen slab-column connection specimens at re-entrant corners. Of these, eight specimens were constructed without shear reinforcement, whereas seven were reinforced with different ratios of shear studs. The loading schemes were designed to simulate various eccentricities, thereby reproducing realistic structural conditions.

Throughout the testing, detailed measurements of the reinforcement strains, slab rotations, and column deformations were collected to capture the mechanical response of each specimen. The resulting data provide new insights into the structural behaviour, failure patterns, and influence of shear reinforcement on the punching performance of flat slabs at re-entrant corner columns. Accordingly, the results presented in this thesis contribute to improving the understanding of the behaviour of flat slabs supported on re-entrant corner columns.

1.4. Objectives of the Thesis

Following the context described above, the main objectives of this work are to:

- Contribute with new experimental data on the punching shear resistance of flat slabs supported on re-entrant corner columns.
- Increase the knowledge on the punching behaviour of flat slabs supported on re-entrant corner columns by means of detailed experimental measurements.
- Evaluation of current code provisions for punching shear design in ACI 318-19, *fib* Model Code 2010, ABNT NBR 6118:2023, Eurocode 2 (2004) and the new generation of Eurocode 2 adpatds for re-entrant corners.
- Develop a rational approach based on the CSCT to calculate the punching shear strength and deformation capacity with outcomes from linear elastic finite element analyses.

1.5. Structure of the Thesis

This thesis is organized into seven chapters, including the present one written as an introduction. A brief description of each chapter is given below:

Chapter 2 shows the code provisions, and the formulations (punching shear and flexural capacities) used for the calculation within this research.

Chapter 3 is part of the article entitled "*Punching shear in flat slabs with re-entrant corner columns*", which has been accepted for publication in the *IBRACON Structures and Materials Journal*. The article comprises a slab without shear reinforcement supported on a re-entrant corner column and compares it to a similar inner connection with comparable characteristics.

Chapter 4 is part of an article being prepared for submission to a scientific journal.

Chapter 5 comprises the scientific article "*Punching shear tests in flat slabs supported on re-entrant corner columns*", published in the *Journal Engineering Structures*. It presents and discusses the main aspects and experimental results of seven tests performed on re-entrant slab-column connections.

Chapter 6 includes the scientific article "*Punching shear in flat slabs with re-entrant corner columns and shear reinforcement*", published in the *Journal Engineering Structures*. It presents and discusses the main aspects and experimental results of eight tests performed on re-entrant slab-column connections, five with shear reinforcement and three without.

In Chapters 3 to 6 (scientific journal articles), the numbering of figures, tables and equations has been changed to adapt to the format of this document. In addition, as this is a thesis that compiles different journal articles, each chapter includes its own introduction (with a brief state of the art), conclusions and references.

Chapter 7 summarizes the main conclusions of this thesis and discusses topics for future research.

1.6. List of Publications

The research was conducted at the Structural Laboratory of the Universidade de Brasília (Labest - UnB) resulting in the following publications:

- Siqueira J. P. A., Albuquerque E. J. P., Fernández Ruiz M., Melo G. S., *Punching shear tests in flat slabs supported on re-entrant corner columns*, Engineering Structures, Vol. 308, 20 p., 2024. DOI: 10.1016/j.engstruct.2024.117954.
- Siqueira J. P. A., Albuquerque E. J. P., Fernández Ruiz M., Melo G. S., *Punching shear in flat slabs with re-entrant corner columns and shear reinforcement*, Engineering Structures, Vol. 310, 24 p., 2024. DOI: 10.1016/j.engstruct.2024.118098.
- Siqueira J. P. A., Cartaxo A. E., Melo G. S., *Punching shear in flat slabs with re-entrant corner columns*, Revista IBRACON de Estruturas e Materiais, Vol. 18, n. 2, e18202, 2025. DOI: 10.1590/S1983-41952025000200002.

Other publications accomplished during the doctorate include:

- Siqueira J. P. A., Melo G. S., *Punching shear in flat slabs with open stirrups as shear reinforcement*, Structural Concrete, Vol. 24, n. 2, p. 2827–2843, 2023. DOI: 10.1002/suco.202200050.

1.7. References

[1] Ferreira, M. P. (2010). Punção em Lajes Lisas de Concreto Armado com Armaduras de Cisalhamento e Momentos Desbalanceados. Tese de Doutorado em Estruturas e Construção Civil, Publicação E.TD – 007 A/10 Departamento de Engenharia Civil e Ambiental, Universidade de Brasília, Brasília, DF, 275p.

[2] Ungermann, J.; Kalus, M.; Claßen, M.; Hegger, J. (2022) *100 Jahre Durchstanzen im Massivbau - Alles erforscht?* Beton- und Stahlbetonbau 117, H. 8, S. 613-624. https://doi.org/10.1002/best.202200039

[3] Moe J., Shearing strength of reinforced concrete slabs and footing under concentrated loads, Development department bulletin D47, Portland Cement Association, 1961.pp 135.

[4] Teng S, Cheong HK, Kuang KL, Geng JZ. Punching shear strength of slabs with openings and supported on rectangular columns. Acids Struct J 2004,V. 101: 678-87.

[5] Liberati EAP, Marques MG, Leonel ED, Almeida LC, Trautwein LM. Failure analysis of punching in reinforced concrete flat slabs with openings adjacent to the column. Engineering Structures, Vol. 182. Elsevier, 2019, p. 331-43. https://doi.org/10.1016/j.engstruct.2018.11.073

[6] Augustin T, Fillo L, Halvonik J. Punching resistance of slab-column connections with openings. Struct Concr 2019:1-13. https://doi.org/10.1002/suco.201900158

[7] Santos J. B.; Souza R. M.; Melo G. S.; Gomes R. B. Punching resistance of flat slabs with openings adjacent to the columns. ACI Structural Journal, V. 119, n°.1, pp 41-53, 2022. doi: 10.14359/51734216

[8] Santos J. B.; Muttoni A.; Melo G. S., Enhancement of the punching shear verification of slabs with openings. Structural Concrete, 18 p., 2022. dx.doi.org/10.1002/suco.202200714

[9] dos Santos JB, Melo GdS, Fernández Ruiz M. Punching performance of flat slabs with openings accounting for the influence of moment transfer and shear reinforcement. Eng Struct 2024;303:1-19. https://doi.org/10.1016/j.engstruct.2024.117461

[10] Swamy RN, Ali SAR. Punching shear behavior of reinforced slab-column connections made with steel fiber concrete. Acids J 1982;79:392-406 (USA).

[11] Narayanan R, Darwish IYS. Punching shear tests of steel-fiber-reinforced micro-concrete slabs. Mag Concr Res 1987;39(N◦138):42-50 (London, UK).

[12] Alexander SDB, Simmonds SH. Punching shear tests of concrete slab-column joints containing fiber reinforcement. Acids Struct J 1992;89(4):425-32 (USA).

[13] Harajli MH, Maalouf D, Khatib H. Effect of fibers on the punching shear strength of slab-column connections. Cem Concr Compos 1995;17:161-70.

[14] Gouveia AV, Lapi M, Orlando M, Faria DMV, Ramos AP. Experimental and theoretical evaluation of punching strength of steel fiber reinforced concrete slabs. Struct Concr 2018;Vol. 19-1:217-29.

[15] Fraile DH, Faccin E, Minelli F, Plizzari G, Muttoni A. Fibre orientation in SFRC slabs and consequences for punching shear and flexural resistance. Eng Struct 2024;302:117364. https://doi.org/10.1016/j.engstruct.2023.117364.

[16] Wey, E. H., 1991. Seismic response of slab-column connections with shear capitals. PhD Thesis, Rice University. Houston, Texas.

[17] Megally, S. H., and Ghali, A., 2002, Cautionary Note on Shear Capitals, Concrete International, V. 24, No. 3, Mar., pp. 75-83.

[18] Lima Neto, Aarão Ferreira. Punção em lajes cogumelo de concreto armado com capitéis. 2012. xxii, 167 f., il. Tese (Doutorado em Estruturas e Construção Civil)—Universidade de Brasília, Brasília, 2012.

[19] K. Qian, B. Li, Experimental study of drop-panel effects on response of reinforced concrete flat slabs after loss of corner column, ACI Struct. J. 110 (2) (2013) 319-329.

[20] A. Kai, "Title Experimental study of drop panel effects on response of reinforced concrete flat slabs after loss of corner column (Experimental and analytical analysis)," 2013.

[21] D.Z. Yankelevsky, Y.S. Karinski, A. Brodsky, V.R. Feldgun, Dynamic punching shear of impacting RC flat slabs with drop panels, Eng. Fail. Anal. 129 (2021) 105682, https://doi.org/10.1016/j.engfailanal.2021.105682.

[22] Clément, T. (2012). Influence de la précontrainte sur la résistance au poinçonnement de dalles en béton armé. PhD Thesis, Laboratoire de Construction en Béton, École Polytechnique Fédérale de Lausanne (EPFL), Lausanne, Switzerland.

[23] Barbán, V. V., Melo, G. S. S. A., & Carvalho, A. L. (2019). Punching shear tests of post-tensioned flat slabs supported on edge columns. *Structural Concrete*, 20(6), 1–15. https://doi.org/10.1002/suco.201900160

[24] Birkle G, Dilger WH. Influence of slab thickness on punching shear strength. ACI SJ 2008;105(2):180-8.

[25] Lips S, Fernández Ruiz M, Muttoni A. Experimental investigation on punching strength and deformation capacity of shear-reinforced slabs. ACI SJ 2012;109(6):889-900.

[26] Ferreira MP, Melo GS, Regan PE, Vollum RL. Punching of reinforced concrete flat slabs with double-headed shear reinforcement. ACI SJ 2014;111(2):363-73.

[27] Schmidt P, Kueres D, Hegger J. Punching shear behavior of reinforced concrete flat slabs with a varying amount of shear reinforcement. Struct Concrete 2019:1-12.

[28] Brantschen, F. (2016). *Influence of bond and anchorage conditions of the shear reinforcement on the punching strength of reinforced concrete slabs* [PhD Thesis]. École Polytechnique Fédérale de Lausanne (EPFL).

[29] Kinnunen, S., & Nylander, H. (1960). *Punching of Concrete Slabs without Shear Reinforcement*. Transactions of the Royal Institute of Technology, No. 158, Stockholm.

[30] Gomes, R. B. and Regan, P. E., Punching Resistance of RC Flat Slabs with Shear Reinforcement, ASCE Journal of Structural Engineering, Vol. 125, No. 6, pp. 684-692, Reston, USA, 1999a.

[31] Gomes, R. B. and Regan, P. E., Punching strength of slabs reinforced for shear with offcuts of rolled steel I-section beams, Magazine of Concrete Research, Vol. 51, No. 2, pp. 121-129, London, UK, 1999b.

[32] Kinnunen, S. (1963). *Punching of Concrete Slabs with Two-Way Reinforcement*. Kungl. Tekniska Högskolans Handlingar, No. 198, Stockholm.

[33] Shehata, I. A. E. M and Regan, P. E., Punching in R.C. Slabs, Journal of Structural Engineering, Vol. 115, No. 7, pp. 1726-1740, USA, 1989.

[34] Broms, C. E. (2005) Concrete flat slabs and footings – Design method for punching and detailing for ductility [PhD Thesis]. KTH Stockholm.

[35] Broms, C. E. Tangential Strain Theory for Punching Failure of Flat Slabs, *ACI Structural Journal*, Vol. 113, No. 1, pp. 87–102, USA, 2016. DOI: https://doi.org/10.14359/51687942

[36] Hallgren, M. (1996) Punching shear capacity of reinforced high strength concrete slabs [PhD Thesis]. Royal Institute of Technology (KTH).

[37] Kueres, D.; Hegger, J. (2018) Two-parameter kinematic the teory for punching shear in reinforced concrete slabs without shear reinforcement. Engineering Structures 175, pp. 201 216. https://doi.org/10.1016/j.engstruct.2018.08.023

[38] Muttoni A. Punching shear strength of reinforced concrete slabs without transverse reinforcement. ACI Struct J 2008; 105(4):440-50. https://doi.org/10.14359/19858

[39] Regan, P. E., Punching Shear in Prestressed Concrete Slab Bridges, Engineering Structures Research group, Polytechnic of Central London, 230 pp., London, UK, 1983.

[40] Regan, P. E., Shear Combs, Reinforcement against Punching, The Structural Engineering, Vol. 63B, No. 4, pp. 76-84, 1985.

[41] Regan, P. E., Symmetric Punching of Reinforced Concrete Slabs, Magazine of Concrete Research, Vol. 38, pp. 115-128, England, 1986.

[42] Shehata, I. A. E. M, Rational Method for Designing RC Slabs to Resist Punching, Journal of Structural Engineering, Vol. 116, No. 7, pp. 2055-2060, USA, 1990.

[43] Shehata, I. A. E. M, Theory of punching in RC slabs, Ph.D Thesis, Polytechnic of Central London, UK, 1985.

[44] Fernández Ruiz M, Muttoni A. Applications of the critical shear crack theory to punching of R/C slabs with transverse reinforcement. ACI Struct J 2009; 106-4:485-94. https://doi.org/10.14359/56614

[45] Hanson, N.W.; Hanson, J.M. (1968) Shear and Moment Transfer between Concrete Slabs and Columns. J. PCA Res. Dev. Lab., 11, 2-16. Available online: https://www.concrete.org/publications/internationalconcreteabstractsportal/m/details/id/19463

[46] Stamenkovic, A. (1970) Local Strength of Flat Slabs at Column Heads. Ph.D. Thesis, Imperial College London, London, UK.

[47] Narayani, N. (1971) Shear Reinforcement in Reinforced Concrete Column Heads. Ph.D. Thesis, Faculty of Engineering, Imperial College of Science and Technology, London, UK.

[48] Zaghlool, E. R. F. (1971) Strength and behaviour of corner and edge column-slab connections in reinforced concrete flat plates [PhD-Thesis]. The University of Calgary.

[49] Beukel, A. van den (1976) Punching Shear at Inner, Edge and Corner Columns. *HERON* 21, Nr. 3, pp. 1-30.

[50] Walker,P.R.; Regan, P.E. (1987) Corner column-slab connections in concrete flat plates. ASCE J. Struct. Eng. 113, 704-720.

[51] Gilbert, S. G.; Glass, C. (1987) Punching failure of reinforced concrete flat slabs at edge columns. *The Structural Engineer* 65B, No. 1 , pp. 16-28.

[52] Mortin JD, Ghali A. (1991) Connection of flat plates to edge columns, ACI Structural Journal, Vol. 88-2, pp. 191-198, USA, Doi:10.14359/2683.

[53] Hammil,N.; Ghali, A. (1994) Punching Shear Resistance of Corner Slab-Column Connections. ACI Struct. J., 91, 697-707.

[54] Desayi, P.; Seshadri, H.K. (1997) Punching shear strength of flat slab corner column connections. In Part 1. Reinforced Concrete Connections; Department of Civil Engineering, Indian Institute of Science: Bangalore, India.

[55] El-Salakawy EF, Polak MA, Soliman MH. (2000) Reinforced concrete slab-column edge connections with shear studs. Canad J Civ Eng; 27-2:338-48. https://doi.org/10.1139/l99-062

[56] Sudarsana, I. K. (2001) Punching shear in edge and corner column slab connections of flat plate structures [PhD-Thesis]. University of Ottawa.

[57] Hegger, J.; Tuchlinski, D. (2006) Zum Durchstanzen von Flachdecken - Einfluß der Momenten-Querkraft-Interaktion und der Vorspannung. Beton-und Stahlbetonbau 101, H. 10, 742-753. https://doi.org/10.1002/best.200600508

[58] Ritchie M, Ghali A, Dilger W, Gayed RB. (2006) Unbalanced moment resistance by shear in slab-column connections: experimental assessment, ACI Structural Journal, Vol. 103-1, pp. 74-82, USA. Doi:10.14359/15088.

[59] Hegger, J. et al. (2007) Versuche zum Durchstanzen im Bereich von Randstützen mit und ohne Durchstanzbewehrung. *Bauingenieur* 82, H. 6, S. 270-278.

[60] Zaghloul, A. Punching Shear Strength of Interior and Edge Column-Slab Connections in CFRP Reinforced Flat Plate Structures Transferring Shear and Moment. Ph.D. Thesis, Department of Civil and Environmental Engineering, University of Ottawa, Ottawa, ON, Canada, February 2007.

[61] Albuquerque, N.G.B.; Melo, G.S.; Vollum, R.L. (2016) Punching Shear Strength of Flat Slab-Edge Column Connections with Outward Eccentricity of Loading. ACI Struct. J., 113, 1117-1129.

[62] Giduquio, Marnie B., Min-Yuan Cheng, and Langa S. Dlamini. (2019) Reexamination of strength and deformation of corner slab-column connection with varied slab reinforcement ratio. *ACI Structural Journal* 116.2: 53-63.

[63] Fraile DH, Setiawan A, Santos JB, Muttoni A. (2023) Punching tests on edge slab-column connections with refined measurements. Eng Struct; 288:1-24. https://doi.org/10.1016/j.engstruct.2023.116166

[64] ABNT NBR 6118:2023 - Projeto de Estruturas de Concreto. Associação Brasileira de Normas Técnicas, Rio de Janeiro, Brazil, 2023, 260 pp.

[65] Design of Concrete Structures - General Rules and Rules for Buildings, EN 1992-1-1. Brussels, Belgium: CEN European Committee for Standardization; 2004, 225 p.

[66] EN 1992-1-1:2023. Eurocode 2: Design of concrete structures - Part 1-1: General rules and rules for buildings, bridges and civil engineering structures. Brussels, Belgium: CEN European Committee for Standardization; 2023, 408 p.

[67] Comité Euro-International du Béton/Fédération Internationale de la Précontrainte: Model Code for Concrete Structures; 1990.

[68] ACI Committee 318. Building Code Requirements for Structural Concrete (ACI 318- 19) and Commentary, 624. Farmington Hills, USA: American Concrete Institute; 2019.

[69] *fib* Model Code for Concrete Structures 2010, *fib*. First Edition UK 2013. https://doi.org/10.1002/9783433604090

2. PUNCHING SHEAR PROVISIONS IN DESIGN CODES

In the following, a brief description of the design formula of the codes is presented. This chapter does not provide a complete summary of all aspects of design, but it does give an overview of the most relevant design provisions, with a focus on slab-column re-entrant corner connections. Thus, the design formula terms associated with internal, edge, and corner columns are not covered here. It is recommended to read the original code for complete information. Additional background information, provisions for detailing and derivations of the design concepts are also available in Santos [1].

The definition of the control perimeter is provided by a line situated in the plane of the slab, at a predetermined distance from the loaded area, which varies according to the standard under consideration (see, Fig 2.1). In the case of NBR 6118 and Eurocode 2 (EC2:2004), the perimeter is located between the edge of the loaded area and a distance of $2d$. In addition, the corners must be rounded, and the perimeter can be reduced in length near openings or edges of the slab. The next generation of EC2 (EC2:2023), *fib* Model Code (MC2010) and the ACI position the control perimeter $0.5d$ from the edge of the loaded area. It is important to note that while the MC2010 and prEC2 employ rounded corners, the ACI utilises straight corners.

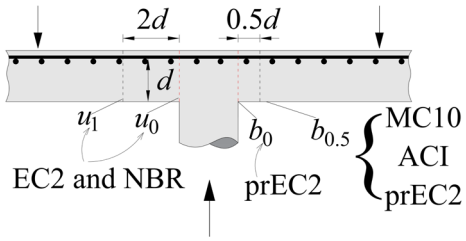

Fig. 2.1 - Control perimeters for punching verification in codes.

The design approaches to consider the load eccentricity in the slab-column connections vary. For instance, EN1992-1-1:2004 and NBR 6118:2014 employ a plastic distribution and empirical approaches, taking the coefficient β into account to address shear force concentrations. The Brazilian standard does not explicitly mention the coefficient β, but its concept can be considered implicitly. The value of β depends on the ratio between the length of the control perimeter (u_1) and W_1 (function of control perimeter). In contrast, the ACI 318:2019 employs an elastic stress distribution, increasing the acting shear stress due to the unbalanced moment to account for load eccentricity. The *fib* Model Code, conversely, addresses eccentricity by utilising a factor k_e, which reduces the length of the control perimeter on the resistance side.

2.1. ACI 318:2019

The punching shear provisions in ACI 318:19 [2] are primarily based on the empirical equation proposed by Moe (1961). In 2019, the American code was updated and included a size effect factor, derived by Dönmez and Bažant (2017) [3]. However, the American standard continues to neglect the influence of the flexural reinforcement ratio in the design for punching shear.

ACI 318 calculates the design shear stress v_E on a critical section of length b_0 located at $0.5d$ from the column face (see, Fig. 2.2).

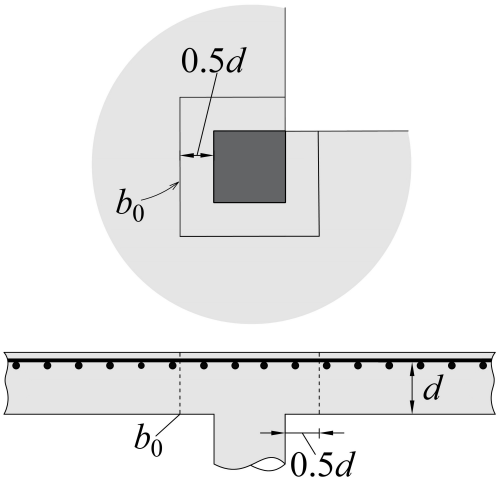

Fig. 2.2 - Control perimeter according to ACI 318, adapted for re-entrant corner columns.

The shear stress is calculated using Eq. (2.1):

$$v_E = \frac{V_E}{b_0 d} \pm \frac{\gamma_v M_{sc} c_{AB}}{J_c} \tag{2.1}$$

where V_E is the shear force, M_{sc} is the moment about the centroid of the critical section (for simplicity $M_{sc} = V_E e_u$) and $e_u = e_R - e_{cg,i}$, where e_R is the eccentricity of the load relative to the column centre and $e_{cg,i}$ is the distance between the centre of gravity of the critical section and the axis of the column ($e_{cg,0} \approx 28$ mm for the perimeter b_0, in the presented tests). The parameter c_{AB} is the distance from the centroid of the critical section to the point where the shear stress is calculated and J_c is analogous to the polar moment of inertia of the critical section. Equation (2.2) and (2.3) give the value of J_c that determine the distribution of shear stress v_E. Generally, the critical section perimeter can be considered as composed of straight segments. The value of J_c can be determined by summation of the contribution of the segments.

$$J_{c,x} = d \sum \left[\frac{l}{3} \left(y_i^2 + y_i y_j + y_j^2 \right) \right] \tag{2.2}$$

$$J_{c,y} = d \sum \left[\frac{l}{3} \left(x_i^2 + x_i x_j + x_j^2 \right) \right] \tag{2.3}$$

where y_i, y_j, x_i and x_j are coordinates of points i and j at the extremities of a typical segment whose length is l (see, Fig. 2.3). The proportion of unbalanced moment transmitted by uneven shear (γ_v) is given by:

$$\gamma_v = 1 - \frac{1}{1+(2/3)\sqrt{b_1/b_2}} \tag{2.4}$$

where b_1 is the dimension of the critical section measured in the direction of the span for which moments are determined and b_2 is the dimension of the critical section measured in the direction perpendicular to b_1.

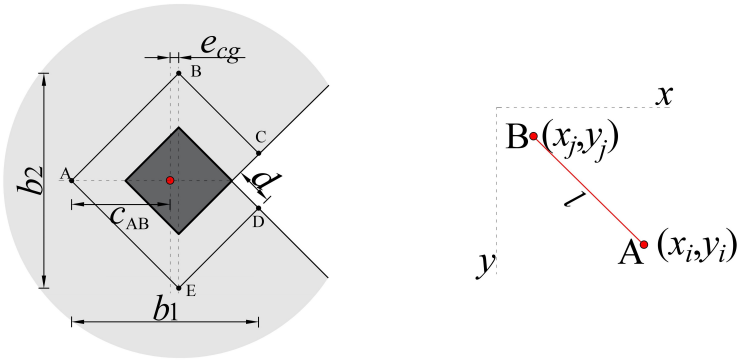

Fig. 2.3 - Properties of the critical perimeter for calculating the polar moment of inertia.

Equation (2.5) can be rewritten as:

$$v_E = \beta_0 \frac{V_E}{b_0 d} \quad \text{and} \quad \beta_0 = 1 + \frac{\gamma_v M_{sc}}{V_E} \frac{b_0}{\frac{J_c}{c_{AB} d}} \tag{2.5}$$

The punching resistance of slabs without shear reinforcement can be calculated as:

$$V_{R,c} \leq \begin{cases} \frac{1}{3} \lambda_s \lambda \sqrt{f_c} b_0 d \\ \left(0.17 + \frac{0.33}{\beta_c} \right) \lambda_s \lambda \sqrt{f_c} b_0 d \\ \left(0.17 + \frac{0.083 \alpha_s d}{b_0} \right) \lambda_s \lambda \sqrt{f_c}\, b_0 d \end{cases} \tag{2.6}$$

where β_c is the relationship between the largest and smallest column dimensions; α_s is 40 for interior columns, 30 for edge columns, and 20 for corner columns, in these calculations $\alpha_s = 40$ was used; λ is used as a modifier to reduce expected performance of lightweight concrete where the reduction is not related directly to tensile strength (the value of λ was taken as 1.0 for normal-weight concrete) and λ_s factor that considers the size effect determined by Eq. (2.7). For the slabs tested in this article are controlled by the first term of Eq. (2.6).

$$\lambda_s = \sqrt{\frac{2}{1+0{,}004d}} \leq 1 \tag{2.7}$$

According to ACI the punching resistance for failure within the shear-reinforced area can be calculated by adding the concrete and the shear reinforcement contributions, Eq. (2.8). For slabs with double-headed studs, the concrete contribution is considered 75% of the punching resistance of slabs without shear reinforcement in the first term of Eq. (2.8) and 50% for stirrups.

$$V_{R,cs} = \begin{cases} 0.25\lambda_s\lambda\sqrt{f_c}b_0 d + \dfrac{A_v f_{yt} d}{s} & \text{(for studs)} \\ 0.17\lambda_s\lambda\sqrt{f_c}b_0 d + \dfrac{A_v f_{yt} d}{s} & \text{(for stirrups)} \end{cases} \tag{2.8}$$

where: s is the spacing of the peripheral lines of shear reinforcement in the direction perpendicular to the column face; A_v is sum of all studs or stirrups leg within a line geometrically similar to the perimeter of the column section; and f_{yt} is the characteristic yield stress of shear reinforcement by:

$$f_{yt} \leq \begin{cases} 420 \text{ MPa} \\ f_{yk} \end{cases} \tag{2.9}$$

The upper limit of 420 MPa on the value of f_{yt} used in design is intended to control cracking.

The maximum punching strength of slabs is defined as Eq. (2.10).

$$V_{R,max} = \begin{cases} 0.66\sqrt{f_c}b_0\, d \text{ (for studs)} \\ 0.5\sqrt{f_c}b_0 d \text{ (for stirrups)} \end{cases} \tag{2.10}$$

And the punching resistance for punching outside of the shear reinforced area is defined as Eq. (2.11)(with values of the eccentricity coefficient taken accordingly).

$$V_{R,out} = 0.17\lambda_s\lambda\sqrt{f_c}\,b_{out}d \tag{2.11}$$

where b_{out} is a control perimeter set at a distance of $d/2$ from the last line of shear reinforcement shown in Fig. 2.4.

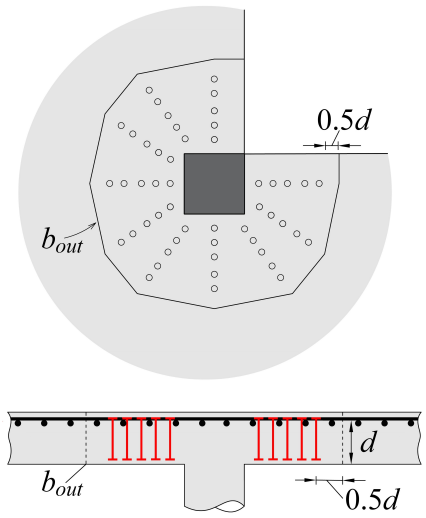

Fig. 2.4 - Control perimeter for punching shear verification outside the shear- reinforced area according to ACI 318, adapted for re-entrant corner columns.

2.2. Eurocode 2:2004

The punching shear provisions in Eurocode 2:2004 [4] are based on the empirical calculation methods introduced in the Model Code (1990) [5]. Section 6.4 of Eurocode 2:2004 is dedicated to the design of flat slabs. Where the support reaction is eccentric with regard to the control perimeter, the maximum shear stress should be taken as:

$$v_{\mathrm{E}}=\beta_i \frac{V_{\mathrm{E}}}{u_i d} \tag{2.12}$$

where u_i is the length of the control perimeter being considered (see, Fig. 2.5a) and β_i accounts for concentrations of the shear forces (increasing the value of the action). In case there are eccentricities in both orthogonal directions and for re-entrant corner column connections, β_i is determined using the following expression:

$$\beta_i = \frac{u_i}{u_i^*} + K\frac{e_u u_i}{W_i} \tag{2.13}$$

where u_i^* is the reduced length of the control perimeter being considered (see Fig. 2.5b), e_u is the eccentricity of the resultant of shear forces with respect to the centroid of the basic control perimeter calculated as $e_u = e_{\mathrm{R}} - e_{cg,i}$. The eccentricity e_{R} is the eccentricity of the load relative to the column centre and $e_{\mathrm{cg},i}$ refers to the eccentricity of the axis through the centroid relative to the column centre of the control perimeter being considered (for the tests presented, $e_{cg,1} \approx$ 86 mm for the perimeter u_1).

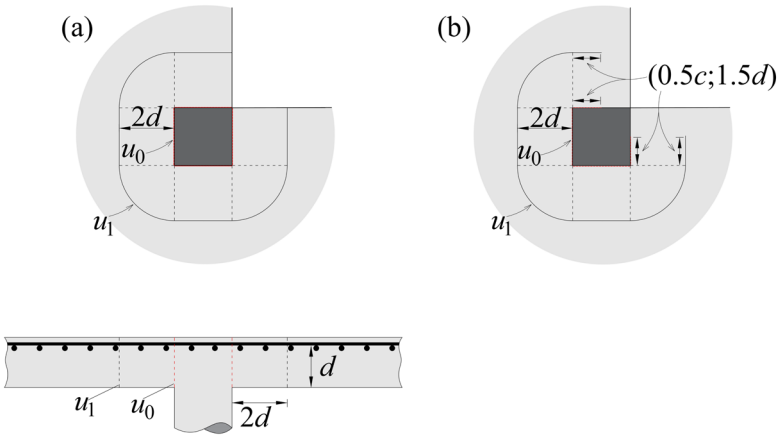

Fig. 2.5 - Control perimeter adapted for re-entrant corner columns: (a) Eurocode 2:2004; (b) Reduced basic control perimeter Eurocode 2:2004.

The parameter K is a function of the dimensions of the column, with $K = 0.6$ for square sections. W_i corresponds to a distribution of shear and is a function of the basic control perimeter u_i (as illustrated in Fig. 2.6). For the perimeters u_0 and u_1, W_i was calculated from Eq. (2.15) and (2.16) for square column, respectively:

$$W_i = \int_0^{u_i} |e| dl \tag{2.14}$$

$$W_0 = c^2\sqrt{2} \tag{2.15}$$

$$W_1 = c^2\sqrt{2} + 4cd\sqrt{2} + \frac{\pi dc\sqrt{2}}{2} - 4d^2\sqrt{2} + 16d^2\cos\theta + 8d\theta e_{cg} - \pi d e_{cg} \tag{2.16}$$

where the angle θ in radians is equal to arcsin ($e_{cg}/2d$). And to calculate W_{out}, Eq. (2.14) was applied more extensively, where dl is a length increment of the perimeter e is the distance of dl from the axis about which the moment M_E acts.

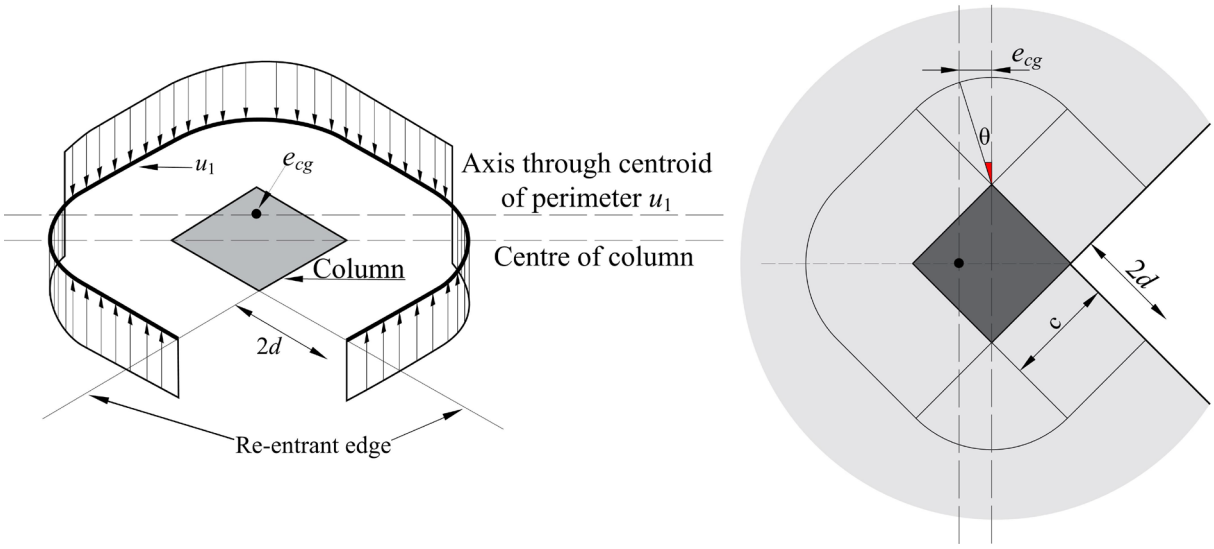

Fig. 2.6 - Shear distribution due to an un balanced moment at a slab and column at a re-entrant corner (adapted from [4]).

The punching shear resistance of the slab without shear reinforcement can be calculated as:

$$V_{R,c} = 0.18k\left(100\rho f_c\right)^{1/3} u_1 d \geq v_{min} u_1 d \tag{2.17}$$

where k is a coefficient taking into account the size effect (equal to $1 + \sqrt{200/d} \leq 2$), β_1 is the load increment factor for considering the asymmetrical distribution of shear force in the control perimeter u_1 and $\rho \leq 2$ is the flexural reinforcement ratio of the slab equal to the column width plus $3d$ each side.

It has to be noted that in this thesis the limit $k \geq 2$ is not considered for comparison to the test results (limit addressed to design of practical cases). The minimum punching shear stress is defined as:

$$v_{min} = 0.035 k^{3/2} f_c^{1/2} \tag{2.18}$$

The punching shear resistance of slabs with shear reinforcement can be calculated as:

$$V_{R,cs} = \min \begin{cases} 0.75 V_{R,c} + 1.5 \dfrac{d A_{sw} f_{yw,ef}}{s_r} \\ k_{max} V_{R,c} \end{cases} \tag{2.19}$$

where A_{sw} is the area of one perimeter of shear reinforcement around the column; s_r is the radial spacing of perimeters of shear reinforcement; $f_{yw,ef}$ is the effective design strength of the punching shear reinforcement, according to $f_{yw,ef} = (250 + 0.25d) \leq f_{yw}$; $V_{R,c}$ according to Eq. (2.17). k_{max} is a factor for limiting the maximum punching shear capacity (the recommended value is 1.5)

The punching resistance outside of the shear-reinforced area is similarly defined as for punching strength of slabs without shear reinforcement, using Eq. (2.20).

$$V_{R,out} = 0.18 k \left(100 \rho f_c\right)^{1/3} u_{out} d \tag{2.20}$$

The outermost perimeter (u_{out}) of shear reinforcement should be placed at a distance not greater than kd and the value of k recommended value is 1.5 (see, Fig. 2.7).

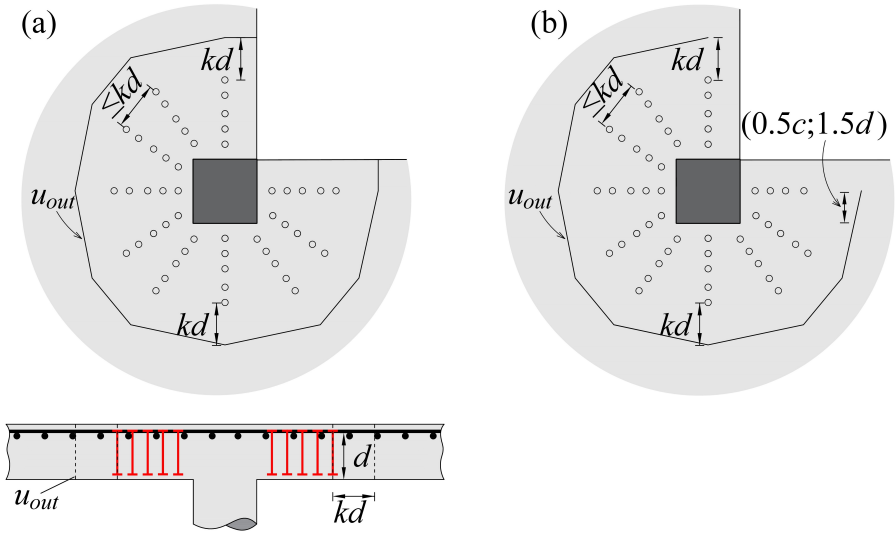

Fig. 2.7 - Control perimeter for punching shear verification outside the shear-reinforced area according to Eurocode:2004.

And the maximum punching strength is determined by Eq. (2.21).

$$V_{R,max} = 0.5 v f_c u_0 d \tag{2.21}$$

where v is a strength reduction factor for concrete cracked in shear (f_{ck} in MPa), equal to:

$$v = 0.60 \left(1 - \frac{f_c}{250} \right) \tag{2.22}$$

In these cases, the eccentricity factor β has to be calculated accordingly (outer or u_0 control perimeters).

2.3. ABNT NBR 6118:2023

The punching shear provisions of the Brazilian code [6] are also based on the CEB-FIP Model Code (1990), resulting in calculation equations similar to those in Eurocode 2 (2004). In its latest update (2023), the size effect factor is now limited in the equations of NBR 6118:2014, similar to Eurocode 2. For a given shear force V_E and moment M_E, the shear stress v_E acting on the control perimeter of the slab-column connection results:

$$v_E = \frac{V_E}{u_i^* d} + K\frac{M_E u_i}{W_i d} \tag{2.23}$$

where u_i and u_i^* are control perimeters set at $2d$ of the border of the support region with circular corners (see, Fig. 2.8), the parameters K and W_i are equal to those of EN-1992-1-1:2004 (derived from the MC 1990 [5]). In this thesis, Eq. (2.23) was represented by $v_E = \beta_i V_E/(u_i d)$, where β_i refers to the definition provided in Eq. (2.13).

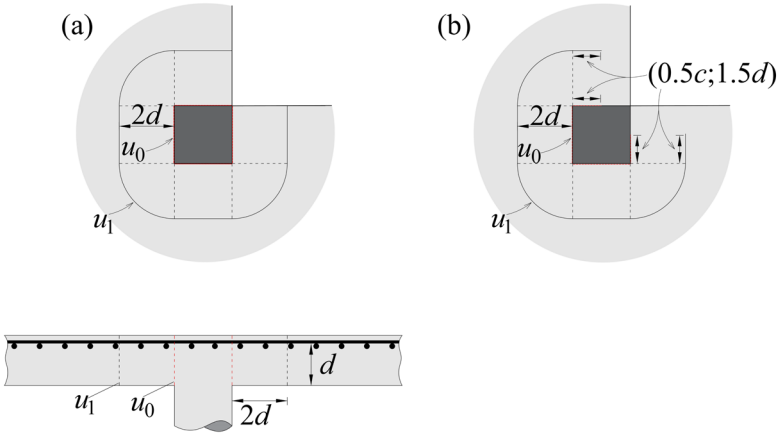

Fig. 2.8 - Control perimeter adapted for re-entrant corner columns: (a) Eurocode 2:2004; (b) Reduced basic control perimeter Eurocode 2:2004.

The design value of the punching shear resistance of the slab without shear reinforcement according to NBR 6118 is determined as:

$$V_{R,c} = 0.182 k_e \left(100\rho f_c\right)^{1/3} u_1 d \tag{2.24}$$

where k_e is a factor accounting for the size effect, which was incorporated in the latest update of the standard (equal to $1 + \sqrt{200/d} \leq 2$) and $\rho \leq 2$ is the flexural reinforcement ratio of the slab equal to the column width plus $3d$ each side. Similar to EC2, the limit on size effect was not considered.

When shear reinforcement is provided, the punching resistance of the slabs is calculated according to Eqs. (2.25), (2.26) and (2.27):

$$V_{\mathrm{R},cs} = \left[0.14k_e\left(100\rho f_c\right)^{1/3} + 1.5\frac{d}{s_r}\frac{A_{sw}f_{ywk,ef}}{u_1^* d}\right]u_1 d \tag{2.25}$$

$$V_{R,out} = 0.182k_e\left(100\rho f_c\right)^{1/3}u_{out}d \tag{2.26}$$

$$V_{R,max} = 0.27\left(1-\frac{f_c}{250}\right)f_c u_0 d \tag{2.27}$$

where A_{sw} refers to the area of one perimeter of shear reinforcement around the column, s_r is the radial spacing of perimeters of shear reinforcement, u_1^* is the reduced basic control perimeter (see, Fig. 2.8), d is the effective depth and $f_{ywk,ef}$ is the effective stress in the shear reinforcement, which results for studs $f_{ywk,ef} = \min(345\ \mathrm{MPa}; f_{yw})$. As for EN1992-1-1:2004, the value of coefficient β has to be taken accordingly to the verification performed.

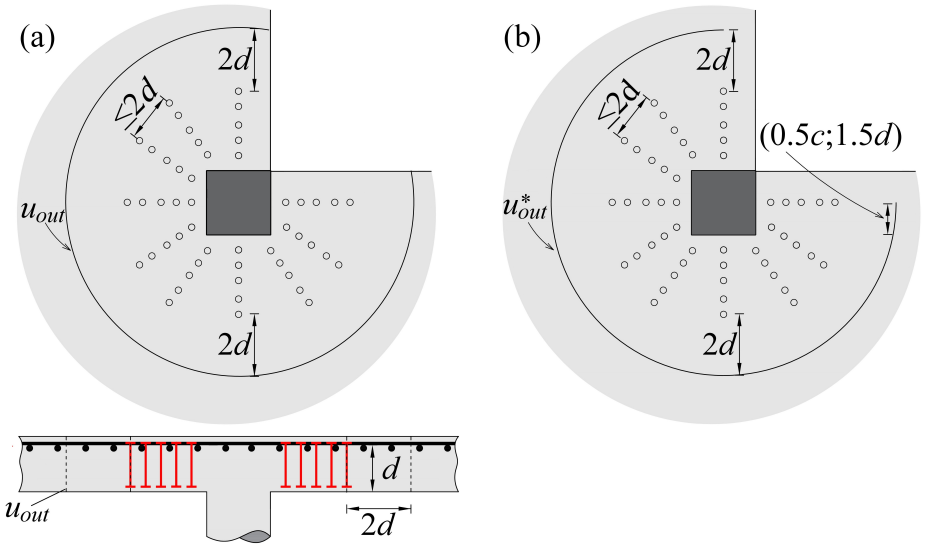

Fig. 2.9 - Control perimeter for punching shear verification outside the shear-reinforced adapted for re-entrant corner columns: (a) ABNT NBR 6118:2023 and (b) Reduced basic control perimeter.

2.4. *fib* Model Code 2010

The physically based Model Code 2010 [7] originates from the Critical Shear Crack Theory proposed by Muttoni [8]. The principal hypothesis of the critical shear crack theory is that the punching strength depends on the opening and the roughness of a critical shear crack [8]. For slabs without shear reinforcement, the punching shear strength directly depends on the opening of the critical shear crack, which can be expressed as a function of the slab rotation.

Accordingly, the punching shear strength of slabs without shear reinforcement according to MC 2010 is determined as

$$V_{R,c} = k_{\psi}\sqrt{f_c}b_0 d_v \tag{2.28}$$

where d_v is the shear-resisting effective depth of the slab (the distance from the centroid of the reinforcement layers to the supported area) and parameter k_{ψ} considers the influence of the width of the critical shear crack and depends on the slab rotation and the maximum aggregate size:

$$k_{\psi} = \frac{1}{1.5 + 0.9k_{dg}\psi d} \leq 0.6 \tag{2.29}$$

where the parameter ψ refers to the rotation of the slab around the supported area (Fig. 2.10) and k_{dg} is a factor accounting for the influence of aggregate size defined as:

$$k_{dg} = \frac{32}{16+d_g} \geq 0.75 \tag{2.30}$$

where d_g is the maximum aggregate size in mm.

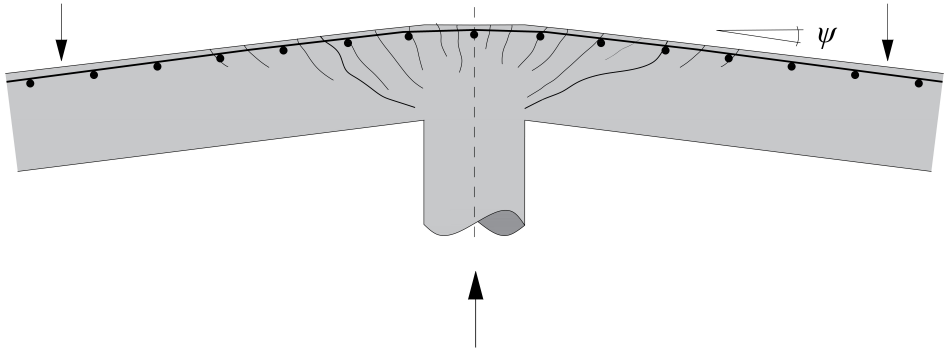

Fig. 2.10 - Rotation (ψ) of a slab.

Concentrations of the shear forces due to moment transfer between the slab and the supported area can approximately be taken into account by multiplying the length of the basic control perimeter (b_1), see Fig. 2.11, by the coefficient of eccentricity (k_e):

$$b_0 = k_e b_1 \tag{2.31}$$

where b_0 is the shear-resisting control perimeter and the coefficient of eccentricity (k_e) can be determined as a function of the moment transferred from the column to the slab as:

$$k_e = \frac{1}{1+e_u/b_u} \tag{2.32}$$

In this expression, e_u refers to the eccentricity of the resultant of shear forces with respect to the centroid of the basic control perimeter and b_u is the diameter of a circle with the same surface as the region inside the basic control perimeter.

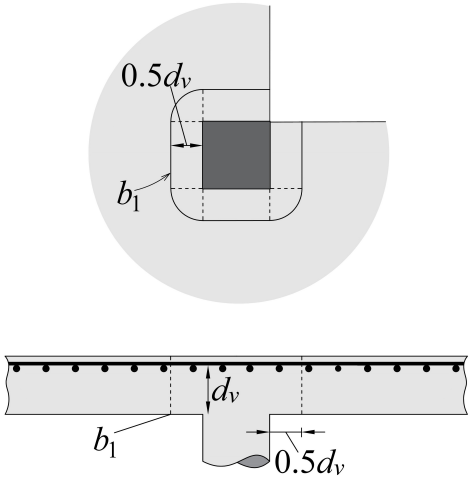

Fig. 2.11 - Basic control perimeter for re-entrant corner columns.

For Level-of-Approximation II the slab rotation can be estimated with a simplified parabolic relationship, which is a function of the ratio of moment demand to capacity:

$$\psi = 1.5\frac{r_s}{d}\frac{f_y}{E_s}\left(\frac{m_E}{m_R}\right)^{3/2} \tag{2.33}$$

where r_s is the radius of an isolated slab, (or $0.22L$ in case of a continuous slab with regular span lengths, r_s =1050 mm was considered for the tests presented in this thesis), f_y is the yield strength of the bending reinforcement, E_s is the Young's modulus of elasticity of the reinforcement, m_R is the moment capacity of the slab and m_E the average moment demand on the column strip.

The coefficient 1.5 in Eq. (2.33) can be replaced by 1.2 if: r_s is calculated using a linear elastic (uncracked) model; m_E is calculated from a linear elastic (uncracked) model as the average value of the moment for design of the flexural reinforcement over the width of the support strip (b_s).

$$m_E = V\left(\frac{1}{8} + \frac{e_R - |e_{cg,i}|}{2(b_s + b_{sr})}\right) \tag{2.34}$$

where e_R is the load eccentricity, $e_{cg,i}$ is the centroid of the column corresponds to the centroid of the control perimeter and b_s is the width of the support strip (see, Fig. 2.12).

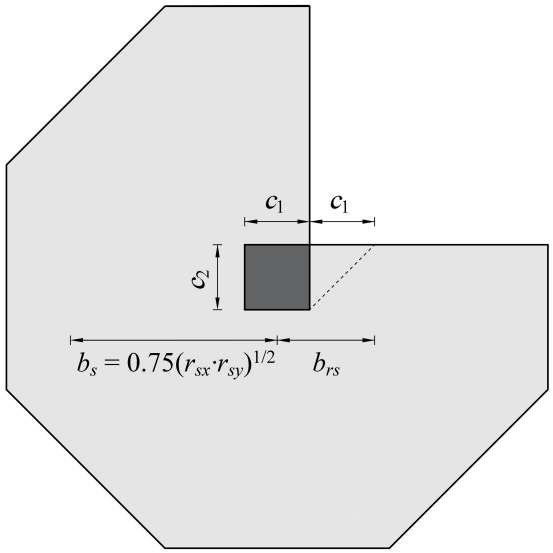

Fig. 2.12 - Support strip dimensions for re-entrant corner.

When shear reinforcement is provided, the contribution of the shear reinforcement can be calculated by multiplying the sum of the cross-sectional areas of the shear reinforcement (within an area between a distance of $0.35d_v$ and d_v from the column face) times the stresses in the shear reinforcement. Therefore, the contribution of the shear reinforcement is defined as:

$$V_{R,s} = \Sigma A_{sw} k_e \sigma_{sw} \tag{2.35}$$

The term σ_{sw} refers to the stress that is activated in the shear reinforcement and can be calculated as:

$$\sigma_{sw} = \frac{E_s \psi}{6}\left(1 + \frac{f_b}{f_{yw}}\frac{d}{\emptyset_w}\right) \leq f_{yw} \tag{2.36}$$

where f_b is the average bond stress, $\emptyset_w$ denotes the diameter of the shear reinforcement and E_s is the modulus of elasticity of the shear reinforcement.

$$f_b = \eta_1\eta_2\eta_3\eta_4(f_{ck}/25)^{0,5} \quad (2.37)$$

where η_1 is a coefficient taken as 1.75 for ribbed bars (including galvanized and stainless reinforcement), 1.4 for fusion bonded epoxy coated ribbed bars;

η_2 represents the casting position of the bar during concreting: η_2 = 1.0 when good bond conditions are obtained, as for: all bars with an inclination of 45-90° to the horizontal during concreting, and all bars with an inclination less than 45° to the horizontal which are up to 250 mm from the bottom or at least 300 mm from the top of the concrete layer during concreting;

η_2 = 0.7 for all other cases where ribbed bars are used;

η_3 represents the bar diameter: η_3 = 1.0 for Ø ≤ 25 mm; η_3 = (25/ Ø) 0.3 for Ø > 25 mm (Ø in mm);

η_4 represents the characteristic strength of steel reinforcement being anchored or lapped;

η_4 = 1.0 for f_{yk} = 500 MPa; η_4 = 1.2 for f_{yk} = 400 MPa; η_4 = 0.85 for f_{yk} = 600 MPa; η_4 = 0.75 for f_{yk} = 700 MPa; η_4 = 0.68 for f_{yk} = 800MPa

Intermediate values may be obtained by interpolation.

The concrete contribution can be calculated according to the provisions for punching of slabs without shear reinforcement Eq. (2.28). Finally, the punching strength for failure within the shear-reinforced area can be obtained by the summation of the contributions of the concrete and the shear reinforcement.

$$V_{R,cs} = V_{R,c} + V_{R,s} \quad (2.38)$$

The maximum punching shear resistance is limited by crushing of the concrete struts in the supported area:

$$V_{R,max} = k_{sys}k_{\psi}\sqrt{f_c}b_0d_v \leq \sqrt{f_c}b_0d_v \quad (2.39)$$

where the value k_{sys} can be increased as follows: k_{sys} = 2.4 for stirrups with sufficient development length at the compression face of the slab and bent (no anchorages or development length) at the tension face; k_{sys} = 2.8 for studs (diameter of heads larger or equal than three times the bar diameter).

According to MC10, the coefficient k_{sys} accounts for the performance of punching shear reinforcing systems to control shear cracking and to suitably confine compression struts at the soffit of the slab. In the absence of other data, and provided that reinforcement is detailed as per the provisions of subsection 7.13.5.3, a value k_{sys} = 2.0 can be adopted.

For failure outside the shear reinforced area, the control perimeter is set at the distance of $0.5d_{v,out}$ from the outermost shear reinforcement perimeter. The punching strength is defined as:

$$V_{R,out} = k_{\psi}\sqrt{f_c}\,b_{0,out}d_{v,out} \tag{2.40}$$

where $b_{0,out}$ is the reduced control perimeter by effect of the eccentricity of the shear force according to Eq. 2.41, and $d_{v,out}$ is the distance between the flexural reinforcement and the bottom end of the vertical branch of the shear reinforcement.

$$b_{0,out} = k_{e,out}b_{1,out} \tag{2.41}$$

$b_{1,out}$ is the outer control perimeter, see Fig. 2.13 (defined at $0.5d_{v,out}$ from the last perimeter of shear reinforcement and accounting for some limitations in the distances between the shear reinforcement units) and $k_{e,out}$ is the coefficient of eccentricity, determined as:

$$k_{e,out} = \frac{1}{1+\frac{e_{u,out}}{b_{u,out}}} \tag{2.42}$$

where $e_{u,out}$ is the eccentricity of the resultant of shear forces with respect to the centroid of the outer control perimeter ($b_{1,out}$) and $b_{u,out}$ is the diameter of a circle with the same surface as the region inside the outer control perimeter.

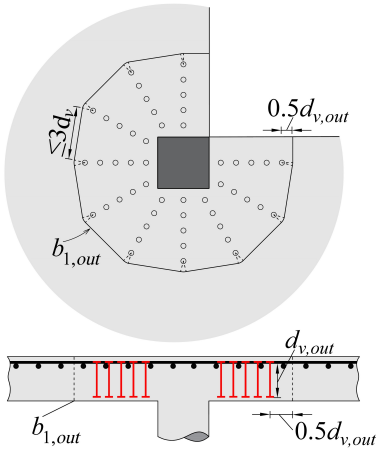

Fig. 2.13 - Control perimeter outside of the shear reinforcement region and shear-resisting effective depth.

2.5. EN 1992-1-1:2023

The punching shear provisions for the upcoming version of Eurocode 2 were developed using the framework of the Critical Shear Crack Theory (CSCT). Unlike the MC2010, the new design equations are presented in a closed form, achieved by combining simplified expressions for load-rotation relationships with the failure criteria proposed by CSCT. The shear stress (τ_E) may be calculated in accordance to EN1992-1-1:2023 [9] as:

$$\tau_E = \beta_e \frac{V_E}{b_{0.5} d_v} \tag{2.43}$$

Concerning the eccentricity of the action, it is considered by means of coefficient β_e:

$$\beta_e = 1 + 1.1 \frac{e_b}{b_b} \geq 1.05 \tag{2.44}$$

where b_b is the geometric mean of the minimum and maximum overall widths of the control perimeter (see, Fig. 2.14): $b_b = \sqrt{b_{b,min} b_{b,max}}$ and e_b is the eccentricity of the line of action of the support forces with respect to the centroid of the control perimeter ($e_b = e_R - e_{cg,i}$).

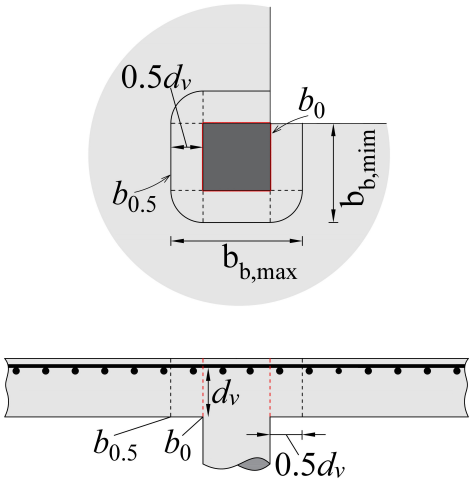

Fig. 2.14 - General definition of control perimeter according to EN1992-1-1:2023 adapted for re-entrant corner columns.

The punching shear capacity of column bases without punching shear reinforcement according to EN1992-1-1:2023 along the length of control perimeter $b_{0.5}$ is calculated as:

$$V_{R,c} = 0.6 k_{pb} \left(100 \rho_l f_c \frac{d_{dg}}{d_v} \right)^{1/3} b_{0.5} d_v \leq 0.6 f_c^{1/2} b_{0.5} d_v \tag{2.45}$$

where k_{pb} is shear gradient enhancement coefficient: $1 \leq k_{pb} = 3.6\sqrt{1-\frac{b_0}{b_{0.5}}} \leq 2.5$; d_{dg} is size parameter describing the failure zone roughness: $d_{dg} = 16 + d_g \leq 40$ mm for $f_c \leq 60$ MPa. The parameter d_v refers to the effective depth, and can be replaced for more refined estimates of the resistance by $a_{pd} = \sqrt{(a_p d_v)/8} \geq d_v$; where a_p is the distance from centroid of control perimeter to point of contraflexure: $a_p = \sqrt{a_{p,x} a_{p,y}} \geq d_v$. For columns of flat slabs where the lateral stability does not depend on frame action between the slabs and the columns, a_p may be approximated as $a_p = 0.22L$ where L is the largest span length of the adjacent bays in either the x- or y direction.

When shear reinforcement is provided, the resistance is calculated in accordance with:

$$V_{R,cs} = \eta_c V_{R,c} + \eta_s \rho_{sw} f_{yw} b_{0.5} d_v \geq \rho_{sw} f_{yw} b_{0.5} d_v \leq V_{R,max} = \eta_{sys} V_{R,c} \tag{2.46}$$

where $\eta_c = V_{R,c}/V_E$ is a factor reducing the concrete contribution, V_E and $V_{R,cs}$ depend on η_c, an iterative process between $V_E = V_{R,cs}$ can be performed to find the value of η_c for this situation where the value of the applied shear force equals the value of punching shear capacity with shear reinforcement; ρ_{sw} is the shear reinforcement ratio; η_{sys} is a factor for limiting the maximum punching shear capacity and accounting for the performance of the punching shear reinforcement system. The values of coefficient η_{sys} for shear reinforcement are:

$$\eta_{sys} = \begin{cases} 0.70 + 0.63\left(\frac{b_0}{d_v}\right)^{1/4} \geq 1.0 \text{ (studs)} \\ 0.50 + 0.63\left(\frac{b_0}{d_v}\right)^{1/4} \geq 1.0 \text{ (stirrups)} \end{cases} \tag{2.47}$$

where η_s is a factor describing the activation of shear reinforcement:

$$\eta_s = \frac{d_v}{150 \emptyset_w} + \left(15\frac{d_{dg}}{d_v}\right)^{1/2}\left(\frac{1}{\eta_c k_{pb}}\right)^{3/2} \leq 0.8 \tag{2.48}$$

Following the general approach of the CSCT, the punching resistance outside the shear reinforced region may be calculated in accordance to Eq. (2.49), considering the reduced shear-resisting effective depth $d_{v,out}$ (function of the shear reinforcement system) and the outer control perimeter $b_{0,5,out}$, located at $d_{v,out}/2$ from the outer perimeter of shear reinforcement with a length of the straight segments not exceeding $3d_{v,out}$ (see, Fig. 2.15).

The expression therefore is:

$$V_{R,out} = 0.6 k_{pb,out} \left(100 \rho_l f_c \frac{d_{dg}}{d_v} \right)^{1/3} b_{0.5,out} d_{v,out} \leq 0.6 f_c^{1/2} b_{0.5,out} d_{v,out} \tag{2.49}$$

where $d_{v,out}$ the outer shear-resisting effective depth (accounting for the possibility of delamination in compression surface) and the value of $k_{pb,out}$ is given by:

$$1 \leq k_{pb,out} = 3.6 \sqrt{\frac{d_v}{d_{v,out}}} \sqrt{1 - \frac{b_{0,out}}{b_{0.5,out}}} \leq 2.5 \tag{2.50}$$

Concerning the eccentricity of the action, it is considered by means of coefficient $\beta_{e,out}$:

$$\beta_{e,out} = 1 + 1.1 \frac{e_b}{b_{b,out}} \geq 1.05 \tag{2.51}$$

where $b_{b,out}$ is the geometric mean of the minimum and maximum overall widths of the control perimeter (see, Fig. 2.15): $b_{b,out} = \sqrt{b_{b,min,out} b_{b,max,out}}$ and $e_b = \sqrt{e_{b,x}^2 + e_{b,y}^2}$.

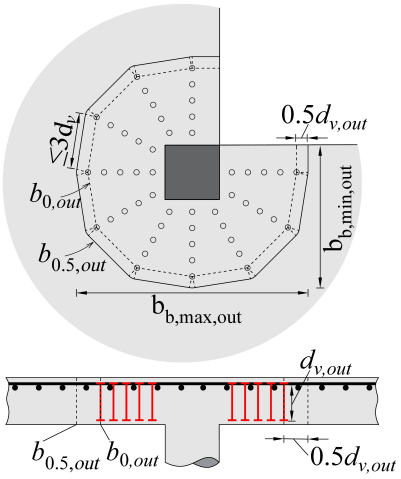

Fig. 2.15 - Control perimeters outside of the shear reinforcement region for re-entrant corner columns.

2.6. Flexural Capacities of Test Specimens

The calculation of the flexural resistance (V_{flex}) is performed on the basis of yield line mechanisms (upper-bound of limit analysis). To that aim, several mechanisms were verified and the geometry of the yield lines optimized [10] in order to obtain the minimum flexural resistance. The governing mechanism is shown in Fig. 2.16, where the flexural resistance is calculated by equalling the rate of internal work (dissipation) to the rate of external work.

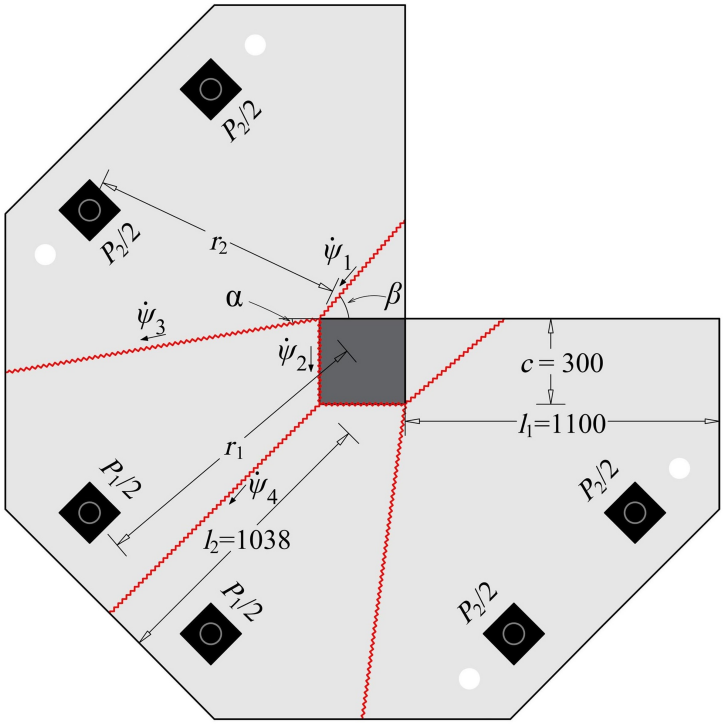

Fig. 2.16 - Yield-line pattern considered for tested slabs according to the formulation proposed by Siqueira *et al.* [11]. (dimensions in [mm])

$$\dot{W}_i = 2m_R\dot{\psi}_2\left(\frac{c}{\cos(\beta)}\frac{\cos(\alpha)}{\sin(\beta-\alpha)} + c + \frac{l_2}{\cos(\alpha)}\frac{\cos(\beta)}{\sin(\beta-\alpha)} + \frac{l_1\sqrt{2}}{2}\right) \quad (2.52)$$

$$\dot{W}_e = 2\dot{\psi}_2\left(P_1d_1 + (P_2d_2 + P_2d_3)\frac{\cos\alpha}{\sin(\beta-\alpha)}\right) \quad (2.53)$$

$$\dot{W}_i = \dot{W}_e \quad (2.54)$$

The parameters (β, α, d_1, d_2 and d_3) are optimised to minimise the failure load, where d_1, d_2, d_3, $\dot{\psi}_1$, $\dot{\psi}_3$ and $\dot{\psi}_4$ are calculated using the following expressions:

$$d_1 = r_1 \sin(\gamma_3 - \pi/2) \tag{2.55}$$

$$d_2 = r_2 \sin(\gamma_1 - \beta) \tag{2.56}$$

$$d_3 = r_2 \sin(\gamma_2 - \beta) \tag{2.57}$$

$$\dot{\psi}_1 = \frac{\dot{\psi}_2 \cos\alpha}{\sin(\beta - \alpha)} \tag{2.58}$$

$$\dot{\psi}_3 = \frac{\dot{\psi}_2 \cos(\beta)}{\sin(\beta - \alpha)} \tag{2.59}$$

$$\dot{\psi}_4 = \sqrt{2}\,\dot{\psi}_2 \tag{2.60}$$

The flexural strength V_{flex} of the slab specimens can be calculated leading to the expression:

$$V_{flex} = 6m_R \frac{\frac{c}{\cos(\beta)}\frac{\cos(\alpha)}{\sin(\beta-\alpha)} + c + \frac{l_2}{\cos(\alpha)}\frac{\cos(\beta)}{\sin(\beta-\alpha)} + \frac{l_1\sqrt{2}}{2}}{\lambda d_1 + (d_2 + d_3)\frac{\cos\alpha}{\sin(\beta-\alpha)}} \tag{2.61}$$

where m_R is the nominal moment capacity, c the column size, l_1 and l_2 were the distance from column to edge. The angles β, α, γ_1, γ_2 and γ_3 measure 49.19°, 9.71°, 115.30°, 154.70° and 220.22° respectively. The parameter λ is influenced by the applied load ratio (P_2/P_1) and takes on different values, therefore depending on the load ratios (the eccentricity of the shear force). For the P_2/P_1 load ratio is 1, λ is equal to 1. When the load ratio is 0.5, λ is equal to 2. Finally, for a load ratio of 1.5, λ is equal to 1/1.5.

Assuming a perfectly plastic behaviour of the reinforcement after yielding, a rectangular stress block for concrete in the compression zone and neglecting compression reinforcement, the moment capacity m_R of the section is then:

$$m_R = \rho f_y b d^2 \left(1 - \frac{\rho f_y}{2\eta_{fc} f_c}\right) \tag{2.62}$$

where f_y represents the yield strength of reinforcing steel, ρ is the reinforcement ratio, b the beam width, d is the effective depth to main tension reinforcement. and the uniaxial plastic concrete compressive strength ($f_{cp} = f_c \cdot \eta_{fc}$) which is obtained by multiplying the concrete compressive strength measured in cylinders (f_c) by the factor accounting for the brittleness of high-strength concrete (η_{fc}) according to Muttoni (1990) [12]. The value of η_{fc} is calculated as:

$$\eta_{fc} = \left(30/f_c\right)^{1/3} \leq 1 \tag{2.63}$$

2.7. References

[1] E. V. Santos, “Punção em lajes lisas : métodos de cálculo, prescrições normativas e exemplos de aplicação”, M. S. thesis, Fac. Tecnol., Univ. Brasília, Brasília, 2018. [Online]. Available: http://repositorio.unb.br/handle/10482/33011

[2] ACI Committee 318. Building Code Requirements for Structural Concrete (ACI 318- 9) and Commentary, 624. Farmington Hills, USA: American Concrete Institute; 2019.

[3] Dönmez A., and Bazant ZP. Size Effect on Punching Strength of Reinforced Concrete Slabs Without and With Shear Reinforcement. ACI Structural Journal, V. 114, No. 4, 2017, July-Aug., pp. 876-886. doi: 10.14359/51689719

[4] Design of Concrete Structures—General Rules and Rules for Buildings, EN 1992-1-1. Brussels, Belgium: CEN European Committee for Standardization; 2004, 225 p.

[5] Comité Euro-International du Béton/Fédération Internationale de la Précontrainte: Model Code for Concrete Structures; 1990.

[6] ABNT NBR 6118:2023 - Projeto de Estruturas de Concreto. Associação Brasileira de Normas Técnicas, Rio de Janeiro, Brazil, 2023, 260 pp.

[7] *fib* Model Code for Concrete Structures 2010, *fib*. First Edition UK 2013. https://doi.org/10.1002/9783433604090

[8] Muttoni A. Punching shear strength of reinforced concrete slabs without transverse reinforcement. ACI Struct J 2008; 105(4):440-50. https://doi.org/10.14359/19858

[9] FEN 1992-1-1:23. Eurocode 2-Design of concrete structures- Part 1-1: General rules, rules for buildings, bridges and civil engineering structures, Stable version of the draft of the 2nd generation of EN 1992-1-1:23, CEN, Brussels, Belgium, 2023, pp 405.

[10] LimitState products. LimitState: slab. Version 2.3. University of Sheffield. www.limitstate.com/slab

[11] Siqueira JPdA, Albuquerque EJP, Fernández Ruiz M, Melo GSSA. Punching shear tests in flat slabs supported on re-entrant corner columns. Eng Struct 2024;308: 1-20. https://doi.org/10.1016/j.engstruct.2024.117954

[12] Muttoni A., Die Anwendbarkeit der Plastizitätstheorie in der Bemessung von Stahlbeton, Birkhäuser Verlag, Institut für Baustatik und Konstruktion ETH Zürich, Basel, Suisse, 1990.

3. CHAPTER III: PUNCHING SHEAR IN FLAT SLABS WITH RE-ENTRANT CORNER COLUMNS

This chapter is the version of the article titled **Punching shear in flat slabs with re-entrant corner columns** published in Volume 18 of the journal Revista IBRACON de Estruturas e Materiais in 2025 (DOI: https://doi.org/10.1016/j.engstruct.2024.118098). The authors of this publication are João Paulo de Almeida Siqueira (DSc Candidate), Aparecida Evangelista Cartaxo (Professora at IFCE), and Guilherme Sales de Melo (Full Professor at UnB and thesis director). The complete reference is the following:

- Siqueira J. P. A., Cartaxo A. E., Melo G. S., *Punching shear in flat slabs with re-entrant corner columns*, Revista IBRACON de Estruturas e Materiais, Vol. 18, n. 2, e18202, 2025. DOI: 10.1590/S1983-41952025000200002.

The main contributions of João Paulo de Almeida Siqueira to the creation of this article were the following:

- Preparation of specimen S8;
- Preparation of the setup for testing specimens S8;
- Analyse the presented results;
- Production of the figures included in the article;
- Preparation of the manuscript of the article.

3.1. Abstract

Studies on slab-column connections supported on re-entrant corners are limited. Although design standards generally provide detailed guidelines for internal, edge, and corner connections, re-entrant corner connections are overlooked in these standards. To investigate the structural behaviour of re-entrant corner connections, a model without shear reinforcement was tested and compared with an inner slab-column connection with similar characteristics. The results were analysed in terms of crack pattern, ultimate loads, rotations, strains at the concrete surface and strains in the flexural reinforcement, The ultimate loads were compared with values estimated from ABNT NBR 6118 (2023), ACI 318 (2019), and EN 1992-1-1:2004 (Eurocode 2). In addition, remarks on the calculation models for slabs supported on re-entrant corner columns were provided.

Keywords: flat slab; punching shear; re-entrant corner column.

3.2. Introduction

Flat slab systems have become an increasingly popular choice for construction projects owing to their economic and functional advantages. Unlike other types of slabs, flat slabs do not have beams. This results in several advantages, such as simplifying formwork execution by reducing cutouts, facilitating reinforcement assembly, and concrete pouring.

However, despite these advantages, the absence of beams can reduce structural strength and stability, particularly in the region of the slab-column connection where large concentrations of bending moments and shear forces exist. One major concern is the possibility of punching shear failure in the region, which can catastrophically propagate through the structure [1]-[4].

Punching resistance is influenced by different factors, such as the compressive strength of concrete, flexural reinforcement ratio, dimensions and geometry of the column, openings in the slab near the columns, load eccentricity, and the use of shear reinforcement.

This complexity has led to various studies since the beginning of the 20th century. Initially, these studies focused on the resilient capacity of foundations [5] and later expanded to include flat slabs [6]-[9], both with and without shear reinforcement. Moment transfer at the slab-column connection was also considered [10].

Consequently, fewer tests are available for slab-column edge connections [11]-[19] and corner connections [15]-[16], [21]-[23]. In these connections, the effect of punching shear is intensified owing to the smaller contact section between the slab and column, involving combinations of stresses from bending, shear force, and torsional moment at the slab edges.

Re-entrant corners, although relatively less common, are not unusual and can be found in buildings of different shapes, such as H, L, T, and U (see, Fig. 3.1). Normative codes [24]-[26] provide equations and necessary details for the design of internal, edge, and corner connections, considering moment transfer between slabs and columns. However, re-entrant corner connections are not mentioned.

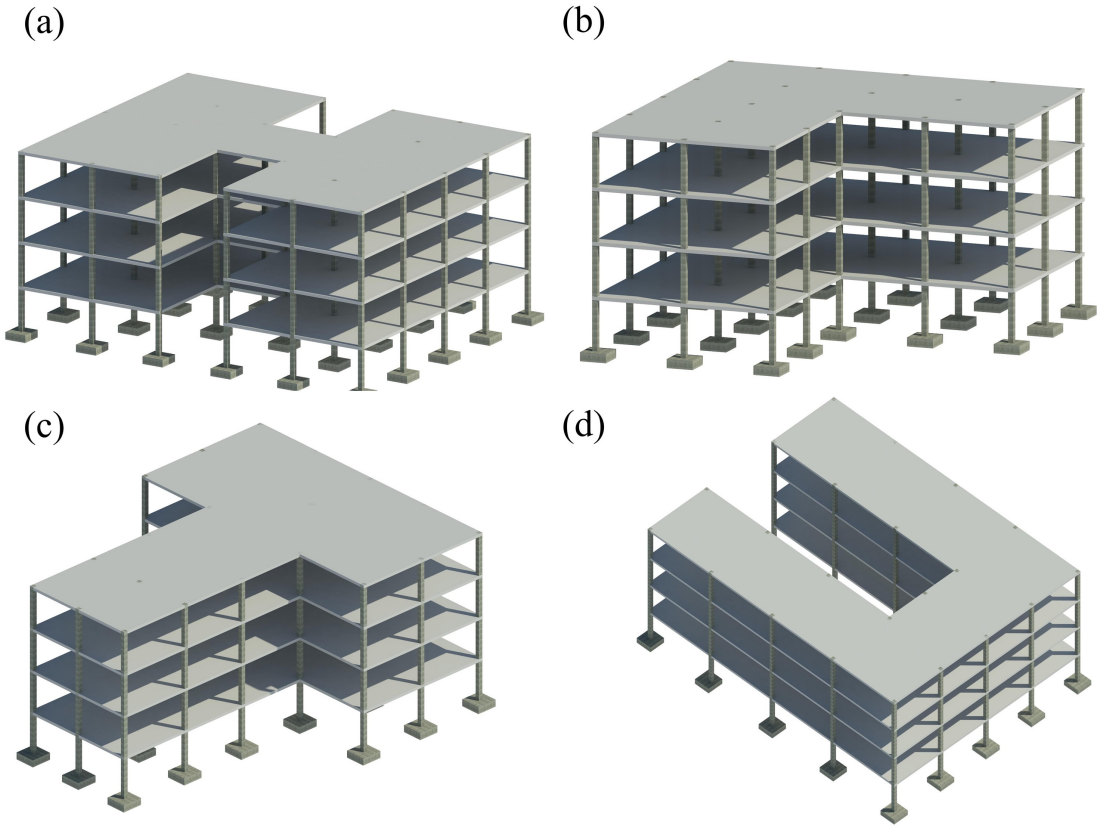

Fig. 3.1 - Building with re-entrant corner.

Furthermore, few publications have provided data on the mechanical behaviour of this connection. Only a doctoral thesis by Albuquerque [27] and one report [28], primarily consisting of testing conducted as part of the Certification Authority for Reinforcing Steels (CARES) approval process for the study system, have addressed this topic. Recently, Siqueira *et al.* [29] presented the results of a punching shear test on flat slabs supported on re-entrant corner columns based on the work of Albuquerque [27]. Seven experimental studies were conducted on specimens without shear reinforcement and subjected to different conditions by varying the load eccentricity, flexural reinforcement, and shear reinforcement arrangement at the edges.

In this context, this article presents the results of a study dedicated to this problem, including the primary results of an experimental program involving re-entrant corner slab-column connections and a comparison between a slab and an inner column. The model used in the comparison was tested by Lima [30] and had the same geometry and properties as those of similar materials, but under symmetrical loading, to demonstrate the difference in behaviour.

To evaluate current design approaches, the test results and those presented in [29] were analysed and compared with the design results according to ABNT NBR 6118:2023 [24], Eurocode 2:2004 [25] and ACI 318:2019 [26].

3.3. Experimental Programme

3.3.1. Specimen Description

The experimental program comprised two tests: one on a re-entrant corner slab and the other on an internal column. Slabs S8 and RS did not exhibit shear reinforcement. The designation "S8" was selected for consistency with the previous tests performed by the authors [29] on slabs with re-entrant corners. Slab RS was centrally supported on square columns; more information regarding this test can be found in [30]-[31].

The tests were performed at the Structural Laboratory of the Universidade de Brasília (Labest-UnB, Brazil). The models were supported on square columns with sides of 300 mm, protruding 800 and 600 mm at the top and bottom, respectively, and a thickness of 180 mm (Fig. 3.2). Table 3.1 lists the characteristics of the tested slabs. The eccentricity of shear force (e) with respect to the column axis is defined as follows:

$$e_R = \frac{M_E}{V_E} = \frac{P_1 z_1 + P_c z_c}{P_1 + 2P_2 + P_g} \tag{3.1}$$

where P_1 and P_2 are the external loads applied on the tested slab, P_g is the self-weight of the slab (19 kN) and testing equipment (6 kN), P_c is the self-weight of the slab and testing equipment unbalanced by symmetry conditions (refer to corner region A_c in Fig. 3.2a, $P_c \approx P_g/3$), z_1 is the lever arm between load P_1 and the column axis (z_1 = 1050 mm), and z_c is the lever arm between the centre of gravity of the loads unbalanced by symmetry conditions (refer to corner region A_c in Fig. 3.2a) and the column axis ($z_c \approx$ 772 mm).

Table 3.1 - Characteristics of the tested slab.

Slab	d [mm]	ρ [%]	f_c [MPa]	Ø [mm]	f_y [MPa]	ε_y [‰]	E_s [GPa]	P_2/P_1 [-]	V_R [kN]	V_{flex} [kN]
S8	144	0.96	53	16	532	2.73	195	0.5	309	386
RS	148	0.92	30	16	549	2.78	197	-	479	835

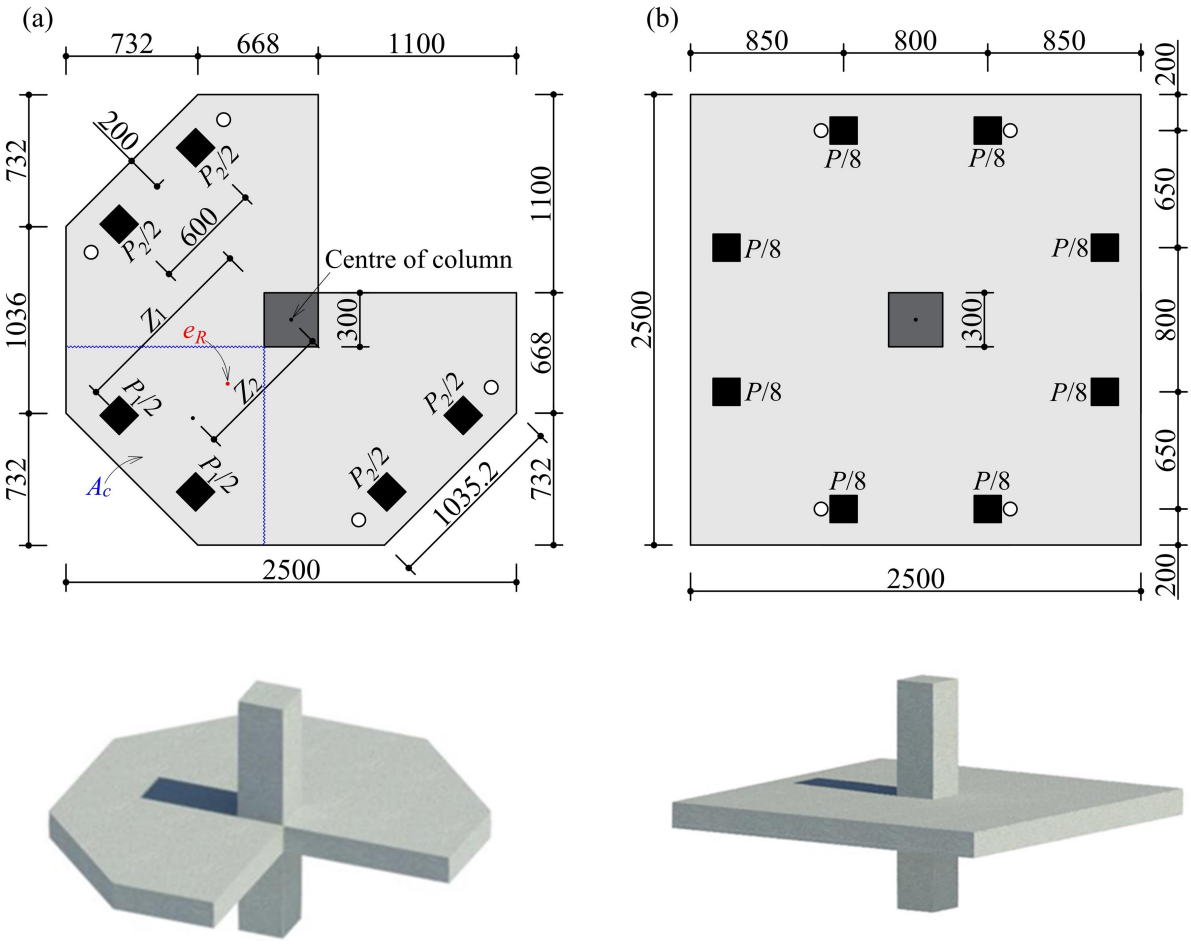

Fig. 3.2 - Dimensions in mm of the tested models: (a) Slab S8 and (b) Slab RS.

Fig. 3.3 shows the arrangement of the flexural reinforcement in the slab and column for the specimens. The specimens were reinforced with Ø 16 mm diameter bars on the top surface with a 20 mm concrete cover. The reinforcement ratio was $\rho \approx 0.9\%$. For slab S8, the bottom reinforcement in both directions comprised 25 bars Ø 10.0 mm in diameter, spaced at 100 mm intervals. The top reinforcement of slab RS comprised Ø 16 mm rebars with an average spacing of 155 mm. The hooks indicated in Fig. 3.3 were used to ensure proper anchoring of the reinforcements.

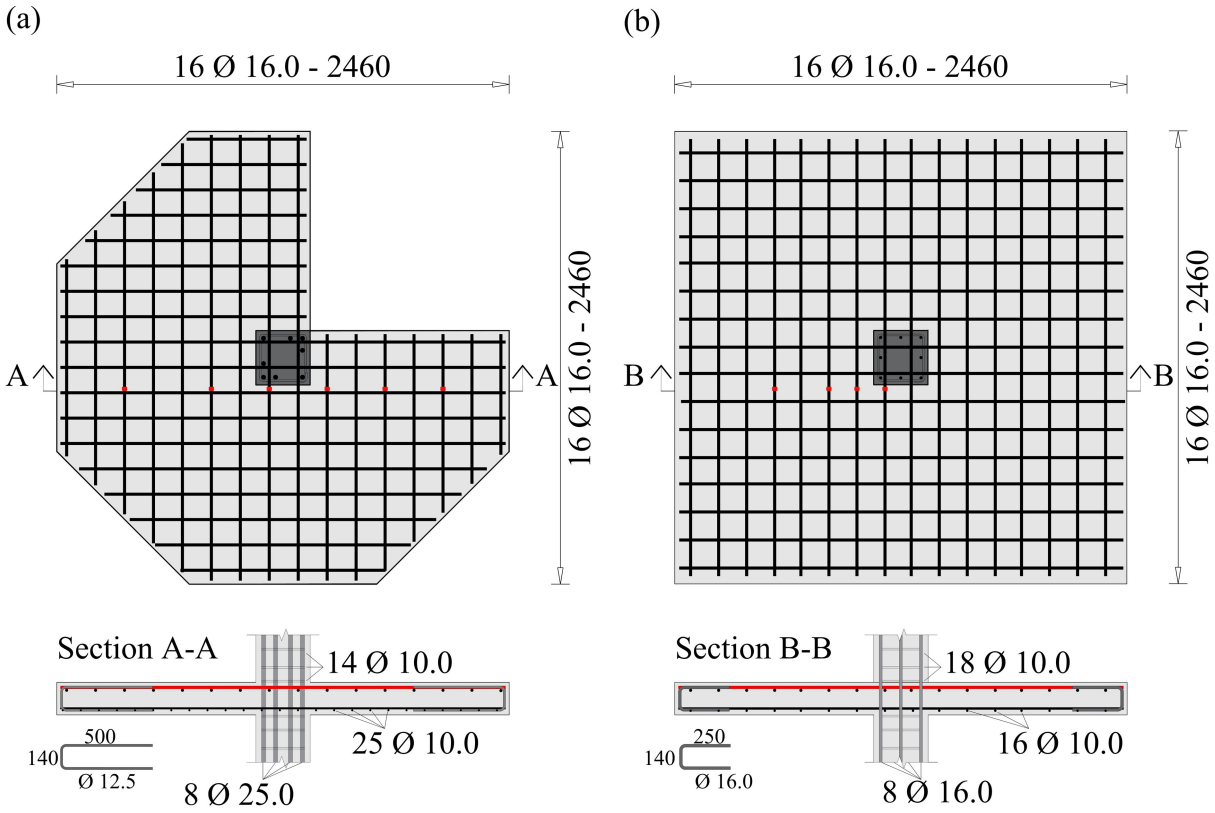

Fig. 3.3 - Flexural reinforcement of the slabs and location of strain gauges: (a) Slab S8 and (b) Slab RS.

The column was cast monolithically with the slab. In the slab with re-entrant corner, the column reinforcement comprised eight bars Ø 25.0 mm in diameter. These rebars were enclosed within Ø 10.0 mm stirrups spaced at 100 mm intervals (Fig. 3.3a). Large-diameter steel bars were required to resist high forces (torsional and tensile) owing to the resulting moment. In slab RS, the column reinforcement comprised eight longitudinal bars with a diameter of 16 mm, enclosed by stirrups with a diameter of 10 mm spaced at 80 mm intervals, as shown in Fig. 3.3b.

3.3.2. Material Properties

The characteristic compressive strengths of the concrete were 45 MPa (S8) and 30 MPa (RS), with a maximum aggregate size of 9.5 mm. The mix proportions of the concrete used for slab RS were 358 kg of quartz sand, 537 kg of artificial sand, 982 kg of gravel ranging from 4.5 to 9.5 mm diameter, 280 kg of Portland cement (CPV-ARI) and 186 kg of water. In addition, the composition of slab S8 per cubic meter of concrete was 309 kg of quartz sand, 476 kg of artificial sand, 964 kg of gravel ranging from 4.5 to 9.5 mm diameter, 420 kg of Portland cement (CPV-ARI) and 190 kg of water.

Normal-strength concrete provided by a local supplier was used for both slabs. To measure the mechanical properties of the concrete, cylindrical specimens (100 mm × 200 mm) in accordance with Brazilian codes [32]-[35] (test date for each slab). Three tests were conducted for each of the following properties: compressive strength, tensile strength and modulus of elasticity. The mechanical properties of the flexural reinforcement were determined according to normative recommendations [36]. Hot rolled steel bars (well-defined yield plateau) was used.

3.3.3. Instrumentation

The deformations of the flexural reinforcements were measured using pairs of extensometers installed on diametrically opposite sides of the longitudinal steel bars, as shown in Fig. 3.3. The radial and tangential deformations of the concrete were measured using extensometers attached to the bottom surfaces of the slabs, near the column faces (Fig. 3.4).

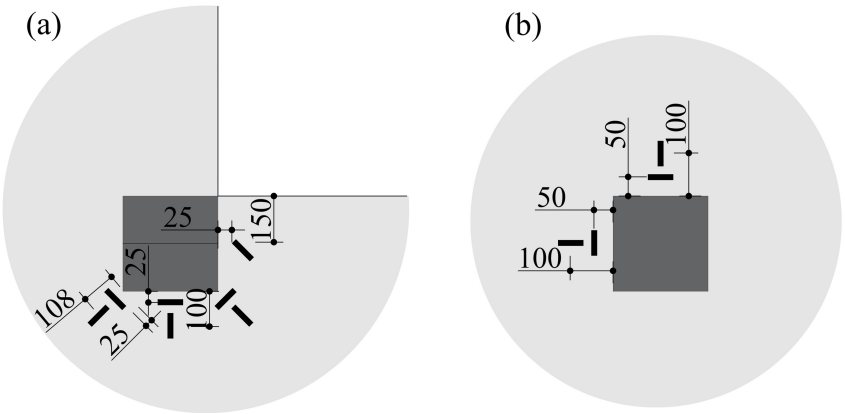

Fig. 3.4 - Instrumentation on bottom concrete surface: (a) Slab S8 and (b) Slab RS. (dimensions in [mm])

The vertical displacement of the slabs was monitored using linear variable differential transformers (LVDTs) at the locations indicated in Fig. 3.5.

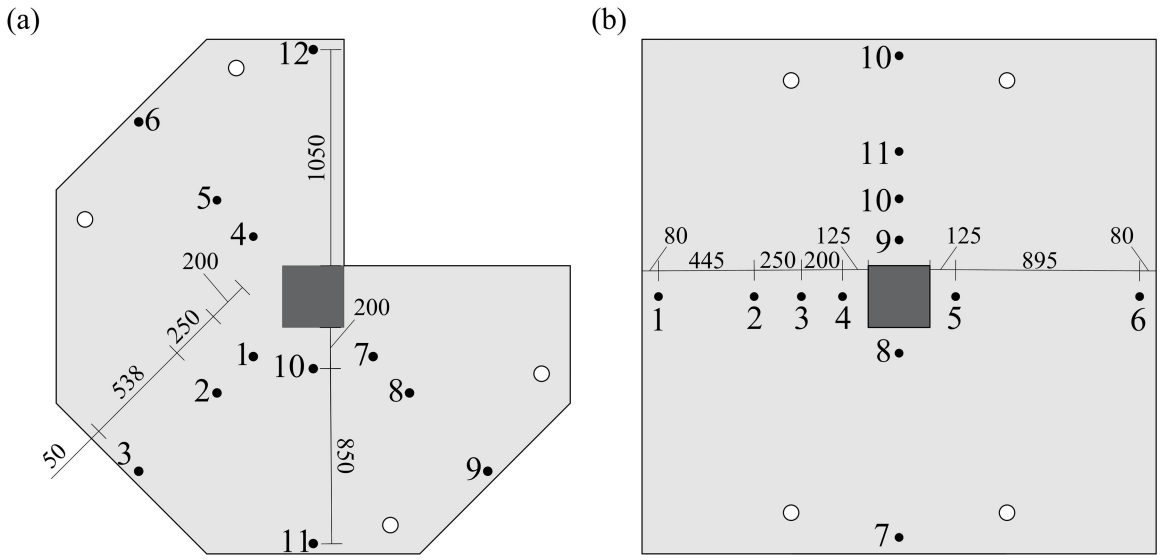

Fig. 3.5 - Position of LVDTs: (a) Slab S8 and (b) Slab RS. (dimensions in [mm])

3.3.4. Test setup

Fig. 3.6 illustrates the test system used in this study, in which the slab was fixed in the reaction frame of the Labest. The loads were applied downward by three hydraulic actuators (jacks) for slab S8 and four for slab RS and transferred by six steel plates for slab S8 and eight for slab RS. During the load increments, the cracking, displacement, and deformation evolutions of the concrete and reinforcements were monitored.

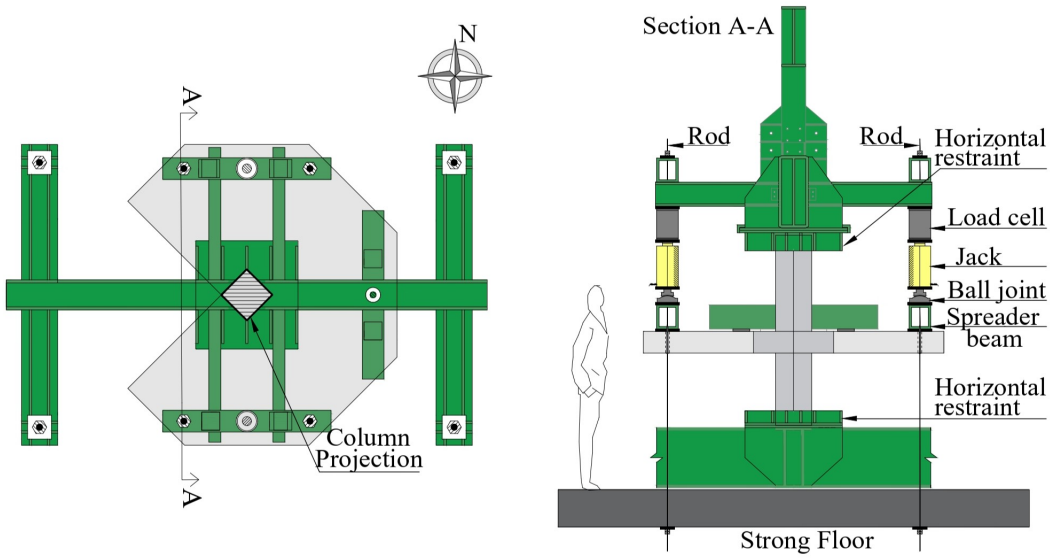

Fig. 3.6 - Test setup.

3.4. Analysis of Test Results

3.4.1. Global response and failure mode

Table 3.1 presents the failure loads and flexural strengths. The flexural strength of the slabs was determined using the equations provided by Guandalini *et al.* [37] and Siqueira *et al.* [29] for slab RS and S8, respectively. The V_u/V_{flex} ratio values ranged from 0.57 for RS to 0.80 for S8. Both specimens failed owing to punching with brittle failure. Fig 5.7 compares the unitary resistances. The failure load was normalised by a number of factors, which include the square root of the concrete strength ($\rho^{1/3}$), the cubic root of the flexural reinforcement ratio ($f_c^{0,5}$), the effective depth (d), and the basic control perimeter (b_1). The comparison of the unitary resistances revealed that the resistance was reduced by approximately 50% for the test with the re-entrant corner column compared with the interior column.

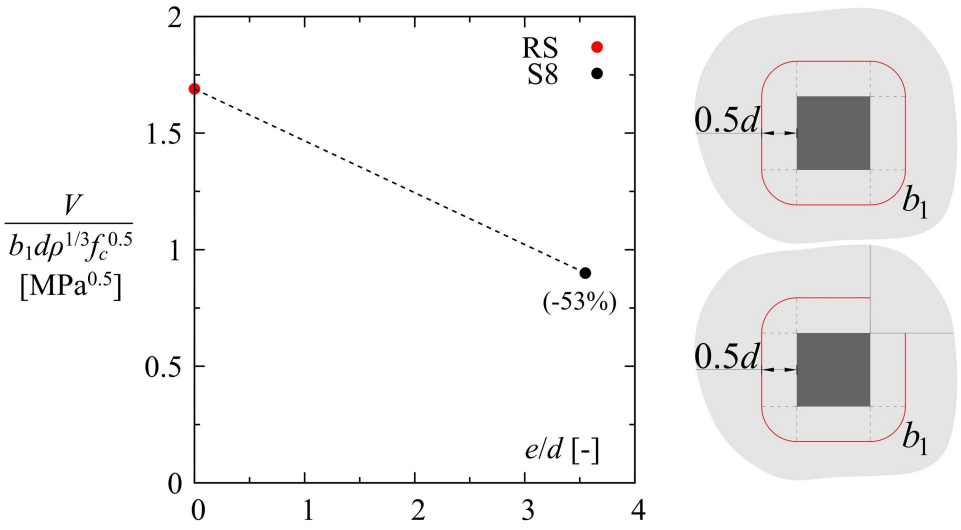

Fig. 3.7 - Normalized strength as a function of the load eccentricity of tests.

Fig. 3.8 illustrates the observed cracking pattern on the top surface, as well as the cuts of slab RS and the re-entrant corner faces of slab S8. A fully developed punching cone was identified in the slab with an inner column (without eccentricity). In slab S8, the punching cone was limited to the two inner faces of the column. Both slabs failed owing to punching shear. Radial cracks appeared at approximately 29% and 24% of the ultimate load for slabs RS and S8, respectively.

Cracking of the slab S8 began at the two inner faces of the column, with cracks along the interfaces with the column and short disconnected cracks close to them. As previously detailed by [29] and illustrated in Fig. 3.8a, the four types of cracks that developed on the top surface. Initially, cracks radiating from the inner corner of the column and running outward to the edges along more-or-less straight lines are observed. Subsequently, cracks appear substantially perpendicular to the inner column sides, also extending to the edges. Furthermore, circumferential cracks, perpendicular to the first two types, at distances from the column that increased with increasing load. Near failure, torsion cracks developed in the strips of slab adjacent to the edges forming the re-entrant corner.

For slab RS (see, Fig. 3.8b), the first cracks observed were radial, initially appearing near the faces and expanding radially toward the edges of the slab as their openings increased with increasing load. Circumferential cracks appeared only at approximately 70% of the ultimate load, forming around the column area and propagating around it until slab failure.

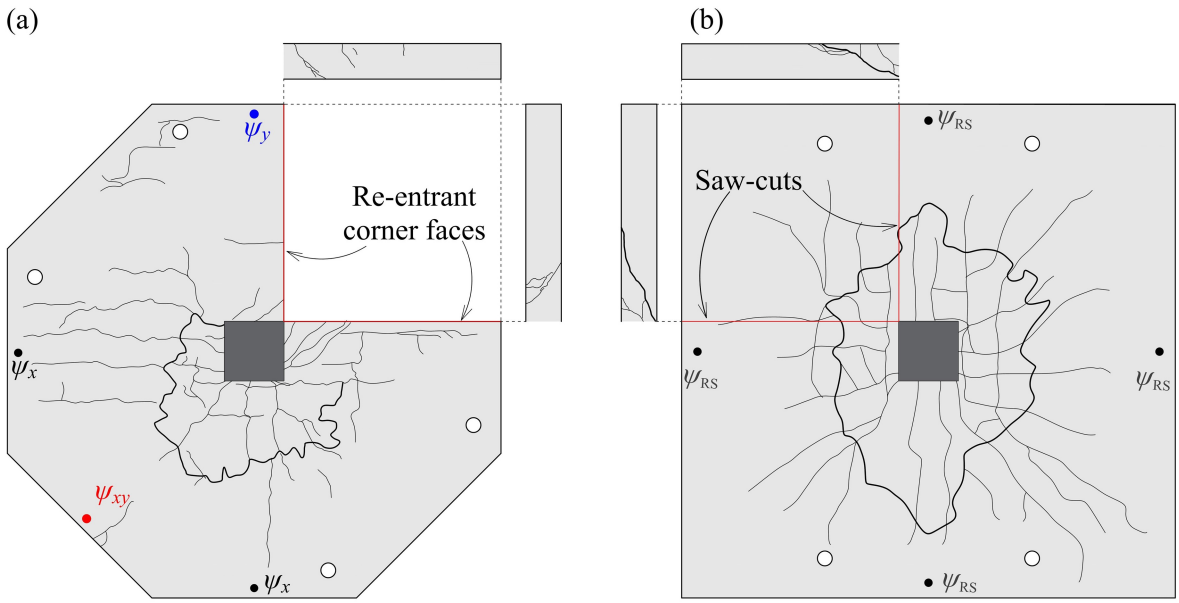

Fig. 3.8 - Crack patterns on the top surface of the slab: a) Slab S8 and b) Slab RS. (measured rotations position)

Fig. 3.9 shows the load-rotation curves for the slabs (ψ_x, ψ_y, and ψ_{xy} directions and ψ_{RS} using the average values obtained from four directions). Fig. 3.8 shows the locations of the measured rotations. Positive rotations correspond to downward slab displacements, whereas negative rotations indicate upward displacements (as measured by the LVDTs presented in Fig. 3.5).

In contrast to the inner column test, the slab with the re-entrant corner exhibited significantly larger rotations. The maximum rotations in slab S8 were larger in the *xy* direction (resulting in eccentricity).

For slab S8, a clear increase in rotations compared with the reference slab was observed, whereas the rotations were negative on the side of the re-entrant edge, consistent with the results of S1 and S3 [29]. In addition, the rotations in the x-direction of slab S8 and the average rotation of slab RS were relatively identical at failure, albeit at a substantially lower load for slab S8.

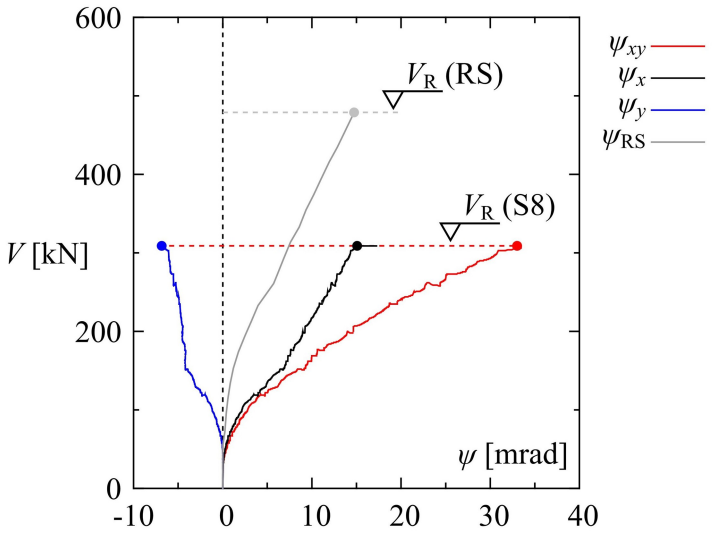

Fig. 3.9 - Load-rotation relationships of the tested specimens.

3.4.2. Strains in the top flexural reinforcement

Fig. 3.10 illustrates the deformation profile of the flexural reinforcement at a load stage near failure. The yielding of the flexural reinforcement was confined to an area close to the column, with the maximum deformations occurring within the width of the column. On the side of the column where the slab edge was discontinuous, the deformations decreased rapidly as the distance from the column increased, reaching values close to zero (Fig. 3.10a).

This behaviour was similar to that occurring in edge connections, as observed in a test (PHS1) performed by Fraile *et al.* [38]. Conversely, on the side where the slab was continuous, the decrease in strain was more gradual, similar to that of slab RS (Fig. 3.10b). However, no generalized reinforcement yielding was observed. These observations confirm the punching failure.

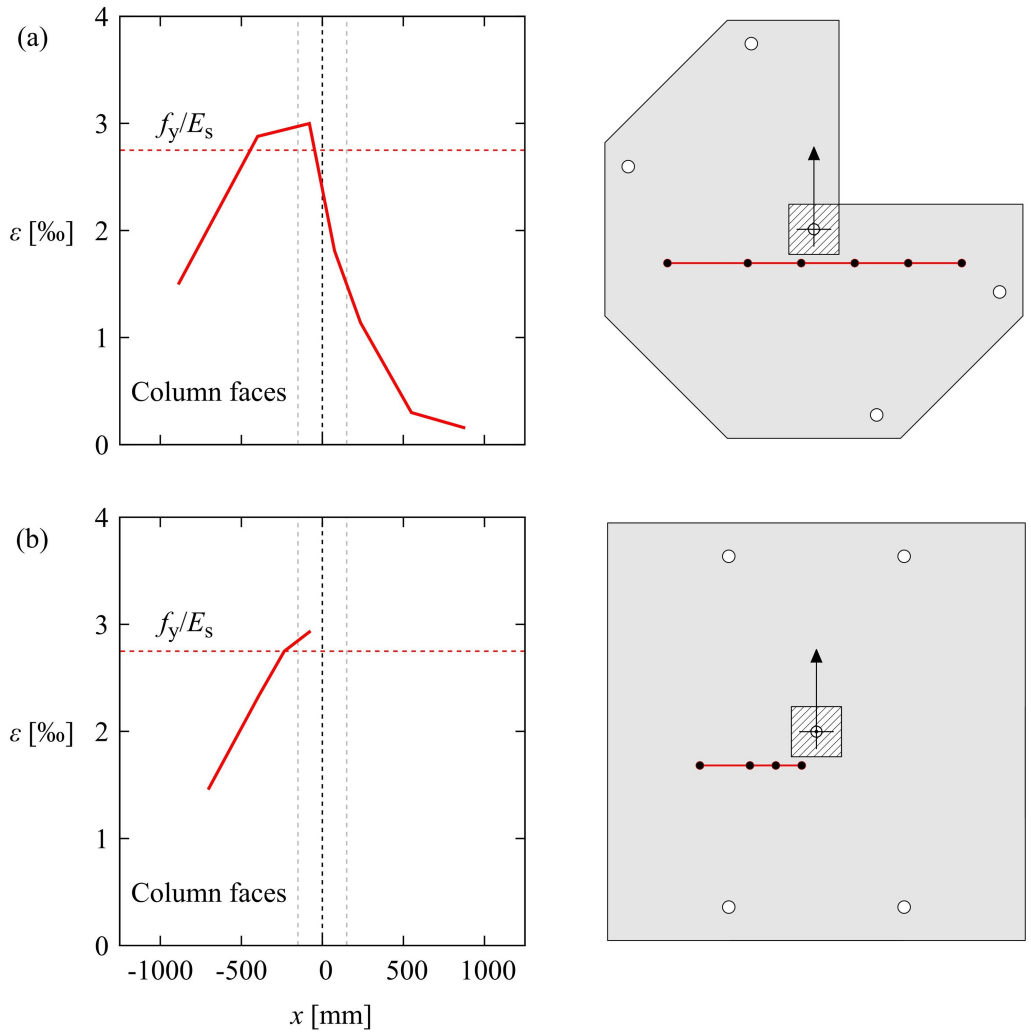

Fig. 3.10 - Profile of strains in the flexural reinforcement of tests.

3.4.3. Strains at the concrete surface

Fig. 3.11 shows the results of the radial and tangential strains on the bottom surface of the slab-column connection. The figure shows that the strains were consistently in compression, except for gauge EC7, where the tensile stresses were measured, attributable to the spalling of the concrete cover. The strains in the tangential direction were consistently higher than those in the radial direction. The tangential deformations increased monotonically with the load and reached a maximum value of approximately 1.6‰ and 1.2‰ for slabs S8 and RS, respectively. For the radial concrete strains, decompression was observed at the concrete surface near the column owing to the local bending of the compression zone. This behaviour, as explained by Muttoni [39], indicates the development of a critical shear crack close to the column face.

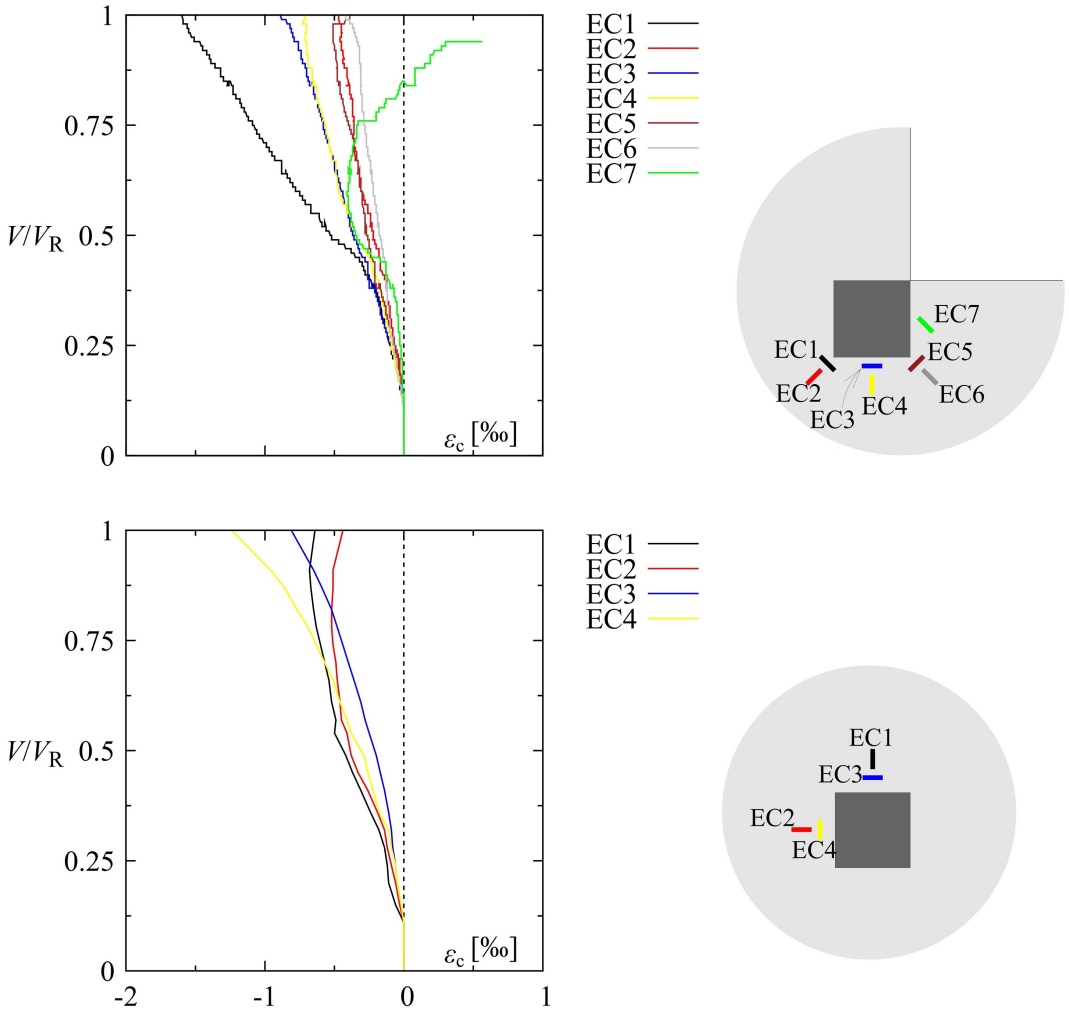

Fig. 3.11 - Surface tangential strains at the bottom surface: a) Slab 8 and b) Slab RS.

3.5. Comparison to Code Predictions

Three current design provisions were used to compare the measured and predicted punching shear capacities: ACI 318-19, EN1992-1-1:2004, and ABNT NBR 6118:2023. Chapter 2 presented details of the formulas and considerations used in the calculations. The punching shear resistances were evaluated with partial factors (γ_c and γ_s) equal to unity and the average values of the concrete strength of the cylinders obtained from the tests. The shear resistance ratio (V_R / V_{calc}) was used to compare the test results with the evaluated punching resistances.

Slabs S1 to S7 were tested by [27] and [29]. Table 3.2 lists their characteristics and comparisons with the design codes, including the results for slabs S8 and RS. The average and coefficient of variation (COV) results for slab RS were not included.

Table 3.2 - Code comparisons.

Slab	f_c	ρ	d	P_2/P_1	e_R	e_R/d	V_R	ACI 318		EN-1992		NBR 6118	
	[MPa]	[%]	[mm]	[-]	[mm]	[-]	[kN]	V_{ACI} [kN]	V_R/V_{ACI} [-]	V_{EC2} [kN]	V_R/V_{EC2} [-]	V_{NBR} [kN]	V_R/V_{NBR} [-]
S1	48	1.49	148	0.5	491	3.32	325	193	1.68	301	1.08	304	1.07
S2	48	1.49	147	1.0	344	2.34	372	238	1.57	357	1.04	361	1.03
S3	44	0.67	143	0.5	496	3.48	250	175	1.43	210	1.19	213	1.18
S4	44	0.65	145	1.0	344	2.38	282	226	1.25	257	1.10	260	1.09
S5	44	1.00	141	1.0	336	2.38	358	222	1.61	287	1.25	291	1.23
S6	44	0.94	146	1.0	341	2.35	345	230	1.50	294	1.17	298	1.16
S7	43	0.95	145	1.5	262	1.81	345	261	1.32	324	1.06	328	1.05
S8	53	0.96	144	0.5	511	3.55	309	182	1.70	251	1.23	254	1.22
RS	30	0.92	148	-	-	-	479	478	1.00	533	0.90	537	0.89
								Avge	1.45		1.14		1.13
								CoV	0.11		0.06		0.06

Fig. 3.12 compares the test results with the code predictions. ACI 318 yielded conservative predictions (the average measured to predicted strength of all experiments was 1.45). However, the predictions were less conservative for smaller load eccentricities. This can be attributed to the failure of the code equations to adequately capture the shear force concentration factors. The COV of these tests was 11%. In the absence of a specific value for the parameter α_s for re-entrant corner columns, analyses were conducted using different values (interior, edge, and

corner columns). It was observed that conservatism increased as the parameter value decreased. Therefore, a value of 40, consistent with that used for interior columns, was adopted.

By contrast, EN-1992 and NBR 6118 (derived from MC 1990 [40]) yielded good test predictions. The mean ratios of experimental to predicted strength for EN-1992 and NBR 6118 were 1.14 and 1.13, respectively, with a 6% COV.

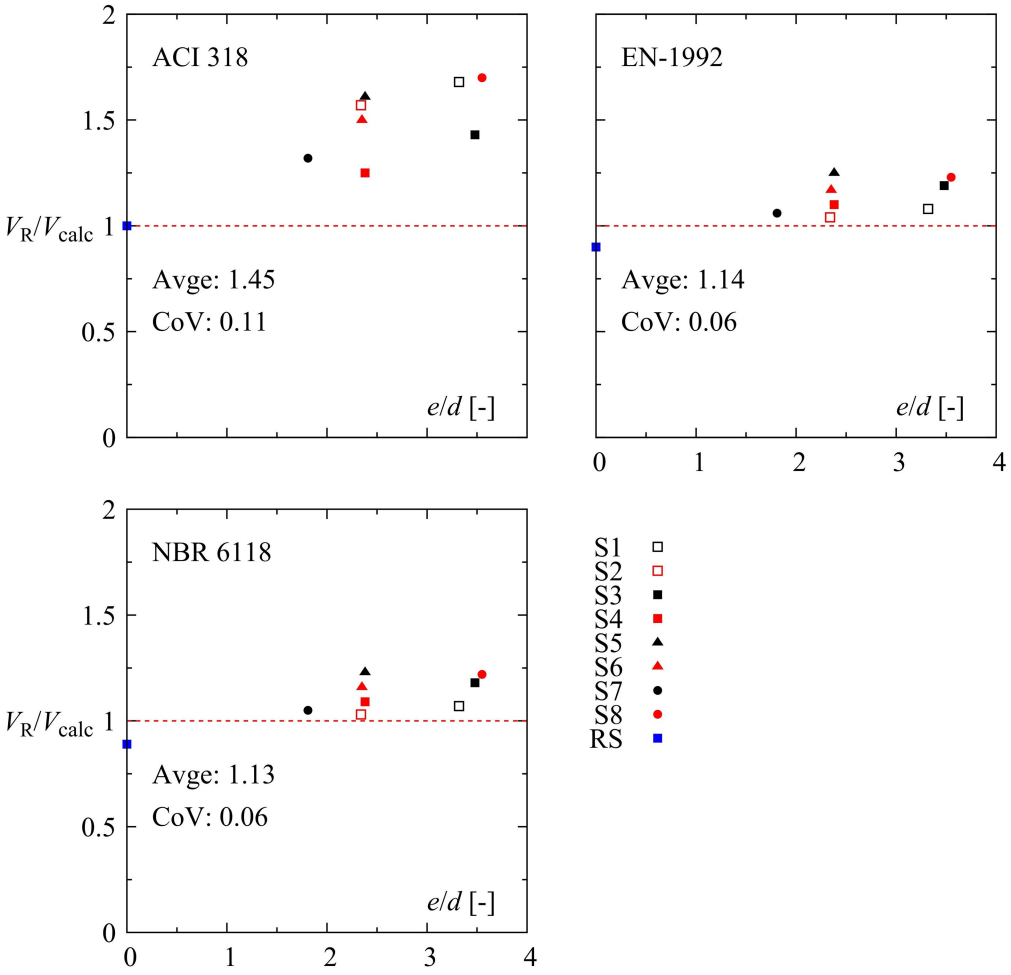

Fig. 3.12 - Comparison of test results to the codes of practice.

3.6. Conclusions

This study investigated the punching shear design of re-entrant slab-column connections and compared it with that of an inner slab-column. Based on the test results, the primary conclusions of this study are as follows:

1. The punching shear capacity was reduced by 50% for re-entrant corner connections compared with a similar slab supported on an inner column.
2. The strain distribution was similar to those at the edge and interior of the columns.
3. None of the slabs exceeded the maximum compressive strain in the concrete. The largest deformation recorded was -1.6‰.
4. The experimental ultimate loads of the slabs were satisfactorily predicted using the interpretations of EN-1992 and NBR 6118 provided in this study.
5. The design formulas of ACI 318 yielded excessively conservative strength predictions for the slabs. It is recommended a future analysis of the parameter α_s for re-entrant corners, due to the lack of specific guidelines for this situation.

This study enhances comprehension and guides the development of optimal practices for designing and evaluating re-entrant slab-column connections. However, the results presented in this study were restricted to a specific group of conditions, including the thickness of the slab, flexural reinforcement ratio, and class of concrete used. Therefore, it is noteworthy that the conclusions cannot be generalized to other situations. Additional studies and tests are necessary to obtain more conclusive results and allow future normative recommendations to adequately cover the re-entrant corner situation.

3.7. References

[1] N. J. Gardner, J. Huh, and L. Chung, “Lessons from the Sampoong department store collapse,” *Cem. Concr. Compos.*, vol. 24, no. 24, pp. 523-529, Dec., 2002, doi: 10.1016/S0958-9465(01)00068-3.

[2] J. G. M. Wood, “Pipers row car park collapse: identifying risk Concrete,” *Concrete*, vol. 37, no. 9, pp. 29-31, Oct., 2003.

[3] J. Schellhammer, N. J. Delatte, and P. A. Bosela, “Another look at the collapse of skyline Plaza at bailey’s crossroads Virginia,” *J. Perform. Constr. Facil.*, vol. 27, no. 3, pp. 354-361, Jan., 2012, doi: 10.1061/(ASCE)CF.1943-5509.0000333.

[4] X. Z. Lu *et al*. “A preliminary analysis and discussion of the condominium building collapse in surfside,” *Front. Struct. Civ. Eng*., vol. 15, pp. 1097-1110, Jun., 2021, doi: 10.1007/s11709-021-0766-0.

[5] A. N. Talbot, *Reinforced concrete wall footings and column footings*. University of Illinois, Illinois, U.S.A: Engineering Experiment Station, pp. 114. Jul., 1913.

[6] S. Kinnunen and H. Nylander, Punching of Concrete Slabs Without Shear Reinforcement (Transactions of the Royal Institute of Technology 158). Stockholm, Sweden: Elan. Boktry. Aktiebol., 1960.

[7] R. C. Elstner and E Hognestad, “Shearing Strength of Reinforced Concrete Slabs,” *J. Am. Concr. Inst. (ACI Journal Proceedings)*, vol. 53, no. 7, pp. 29-58, Jul., 1956, doi: 10.14359/11501.

[8] J. L. Andersson, (1963) Punching of Concrete Slabs with Shear Reinforcement. No. 212 .

[9] N. Narasimhan, “Shear Reinforcement in RC Column Heads,” Ph.D. thesis, Abbrev. Dept., Univ. London, City of Univ., Abbrev. State, 1971.

[10] J. Moe, *Shearing Strength of Reinforced Concrete Slabs and Footings under Concentrated Loads*, Skokie, IL, USA: Portland Cement Assoc., Res. Develop. Lab., 1961.

[11] N. W. Hanson and J. N. Hanson, "Shear and moment transfer between concrete slabs and columns", *J. PCA Res. Dev. Lab.*, vol. 10, no. 1, pp. 2-16, Jan., 1968.

[12] A. Stamenkovic, "Local strength of flat slabs at column heads", Ph.D. thesis, Imperial Coll. of Sci. and Tec., Univ. of London, London, 1969. [Online]. Available: https://spiral.imperial.ac.uk/bitstream/10044/1/16718/2/Stamenkovic-A-1970-PhD-Thesis.pdf

[13] N. Narayani, “Shear Reinforcement in Reinforced Concrete Column Heads,” Ph.D. thesis, Imperial Coll. of Sci. and Tec., Univ. of London, London, 1971. [Online]. Available: https://spiral.imperial.ac.uk/bitstream/10044/1/8032/1/Narayani_Narasimhan-1971-PhD-Thesis.pdf

[14] P. E. Regan, Tests of Connections between flat slabs and edge columns. School of Architecture and Engineering, University of Westminster, Jul., 1993.

[15] E. E. D. R. F. Zaghlool, “Strength and Behaviour of Corner and Edge Column-Slab Connections in Reinforced Concrete Flat Plates,” Ph.D. thesis, Dept. Civil Eng., Univ. Calgary, Calgary, AB, 1971.

[16] I. K. Sudarsana, “Punching Shear in Edge and Corner Column Slab Connections of Flat Plate Structures,” Ph.D. thesis, Dept. Civil Eng., Univ. Ottawa, Ottawa, ON, Cananda, 2001.

[17] M. Ritchie, A. Ghali, W. Dilger, and R. B. Gayed, “Unbalanced Moment Resistance by shear in Slab-Column Connections: Experimental Assessment.,” *ACI Struct.*, vol. 103, no. 1, pp. 74-82, Jan., 2006, doi: 10.14359/15088.

[18] A. Zaghloul, “Punching Shear Strength of Interior and Edge Column-Slab Connections in CFRP Reinforced Flat Plate Structures Transferring Shear and Moment,” Ph.D. thesis, Dep. Civil and Environmental Eng., Univ. Ottawa, Ottawa, ON, Canada, 2007.

[19] N. G. B. Albuquerque, G. S. Melo, and R. L. Vollum, “Punching Shear Strength of Flat Slab-Edge Column Connections with Outward Eccentricity of Loading,” *ACI Struct.*, vol. 113, no. 5, pp. 1117-1129, Jan., 2016, doi: 10.14359/51689156.

[20] P. Desayi and H. K. Seshadri. “Punching shear strength of flat slab corner column connections. In Part 1. Reinforced Concrete Connections,” *Proc. Inst. Civ. Engrs. Struct. Build., vol.* 122, no. 1, pp. 10-20, Feb., 1997, doi: 10.1680/istbu.1997.29163.

[21] N. Hammil and A. Ghali, “Punching Shear Resistance of Corner Slab-Column Connections,” *ACI Struct.*, vol. 91, no. 6, pp. 697-707, Nov., 1994, doi: 10.14359/1502.

[22] A. Stamenkovic and J. C. Chapman, “Local strength at column heads in flat slabs subjected to a combines vertical and horizontal loading,” *Proc. Inst. Civ*., vol. 57, no. 2, pp. 205-232, Jun., 1974, doi: 10.1680/iicep.1974.4054.

[23] P. R. Walker and P. E. Regan, “Corner column-slab connections in concrete flat plates,” *J. Struct. Eng.*, vol. 113, no. 4, pp. 704-720, Apr., 1987, doi: 10.1061/(ASCE)0733-9445(1987)113:4(704).

[24] Associação Brasileira de Normas Técnicas, *Design of Concrete Structures - Procedures*, ABNT NBR 6118, 2023.

[25] European Committee for Standardization, *Eurocode 2. Design of Concrete Structures - Part 1-1: General Rules and Rules for Buildings*, EN 1992-1-1:2004, 2004.

[26] American Concrete Institute, *Building Code Requirements for Structural Concrete and Commentary*, ACI 318, 2019.

[27] E. J. P. Albuquerque, "Punção em lajes lisas com armadura de cisalhamento e pilar de canto reentrante", Ph.D. dissertation, Fac. Tecnol., Univ. Brasília, Brasília, 2015. [Online]. Available: https://repositorio.unb.br/handle/10482/18905

[28] CARES Technical Approval Report TA7 5041, “Assessment of the Shearail, Punching Shear Reinforcement System and Quality System for Production”, Dec. 2019. [Online]. Available: http://www.ukcares.com/TAPDF/5041.pdf

[29] J. P. A. Siqueira, E. J. P. Albuquerque, M. Fernández Ruiz, and G. S. Melo. “Punching shear tests in flat slabs supported on re-entrant corner columns,” *Eng. Struct.*, vol. 308, pp. 1-20, Apr 2024, doi: 10.1016/j.engstruct.2024.117954.

[30] H. Lima, R. Palhares, G. S. Melo and M. Oliveira. “Experimental analysis of punching shear in flat slabs with variation in the anchorage of shear reinforcemen” Struct. Concr.,vol. 22, pp. 1165-1182, 2021. https://doi.org/10.1002/suco.202000158

[31] J. P. A. Siqueira and G. S. Melo, “Punching shear in flat slabs with open stirrups as shear reinforcement,” *Struct. Concr.,* vol. 24, no. 2, pp. 2827-2843, Apr., 2023, doi: 10.1002/suco.202200050.

[32] Associação Brasileira de Normas Técnicas, *Concreto - Procedimento para moldagem e cura de corpos de prova*, ABNT NBR 5738, 2015.

[33] Associação Brasileira de Normas Técnicas, *Concreto - Ensaio de Compressão de Corpos de Prova Cilíndricos*, ABNT NBR 5739, 2018.

[34] Associação Brasileira de Normas Técnicas, *Concreto e argamassa - Determinação da resistência à tração por compressão diametral de corpos de prova cilíndricos,* ABNT NBR 7222, 2011.

[35] Associação Brasileira de Normas Técnicas, *Concreto - Determinação do módulo estático de elasticidade à compressão,* ABNT NBR 8522, 2017.

[36] Associação Brasileira de Normas Técnicas, *Materiais metálicos - Ensaio de tração*, ABNT NBR 6892, 2013.

[37] S. Guandalini, O. Burdet, and A. Muttoni, “Punching tests of slabs with low reinforcement ratios,” *ACI Struct. J.*, vol. 106, no. 1, pp. 87-95, 2009 https://doi.org/10.14359/56287.

[38] D. H. Fraile, A. Setiawan, J. B. Santos, and A. Muttoni, “Punching tests on edge slab-column connections with refined measurements,” *Eng. Struct.*, vol. 288, 116166, Aug. 2023, doi: 10.1016/j.engstruct.2023.116166.

[39] A. Muttoni, "Punching shear strength of reinforced concrete slabs without transverse reinforcement," *ACI Struct. J.*, vol. 105, no. 4, pp. 440-450, Jul., 2008, doi: 10.14359/19858.

[40] Comité Euro-International du Béton, Model Code 1990 for structures. London, England: Comité Euro-International du Béton, 1993.

4. CHAPTER IV: PUNCHING SHEAR IN RE-ENTRANT CORNER COLUMN SLAB CONNECTIONS WITH SHEAR REINFORCEMENT

The main contributions of João Paulo de Almeida Siqueira to the creation of this draft paper were the following:

- Preparation of specimen S8, S8-1 and S8-2;
- Preparation of the setup for testing specimens S8, S8-1 and S8-2;
- Analyse the presented results;
- Production of the figures included in the article;
- Preparation of the manuscript of the article.

4.1. Experimental Programme

4.1.1. Specimen Description

The experimental program evaluated three types of slabs supported at a re-entrant corner column: one without shear reinforcement (reference slab) and two with different shear reinforcement ratios. These specimens were tested in the laboratory at the University of Brasília, Brazil. All three slabs had a thickness of 180 mm and were supported by a 300 mm square column as shown in Fig. 4.1. Table 4.1 lists the test parameters.

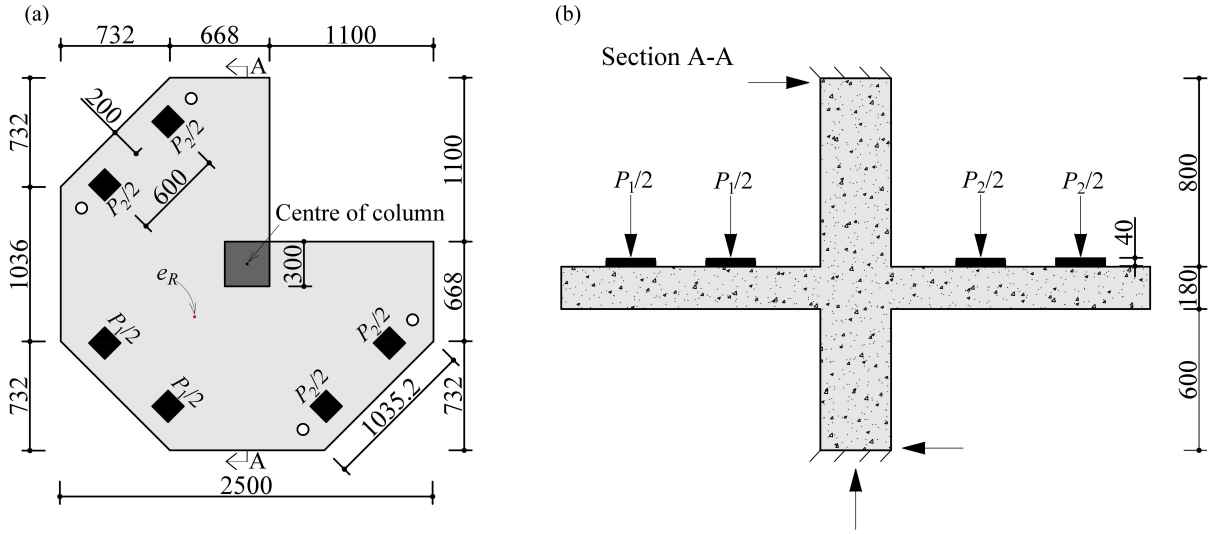

Fig. 4.1 - Specimen dimensions [mm].

Table 4.1 - Characteristics of the tested slabs.

Slab	d [mm]	$\rho^{(1)}$ [%]	$\rho_{sw}^{(2)}$ [%]	P_2/P_1 [-]	e_R [mm]	e_R/d [-]	V_R [kN]	V_{flex} [kN]
S8	144	0.96	-	0.5	511	3.32	309	386
S8-1	143	0.95	0.42	0.5	501	3.29	353	380
S8-2	141	0.97	0.66	0.5	451	2.32	375	378

The eccentricity of the load at failure (e_R) was approximately 500 mm. Fig. 4.2 shows the evolution of eccentricity during the tests.

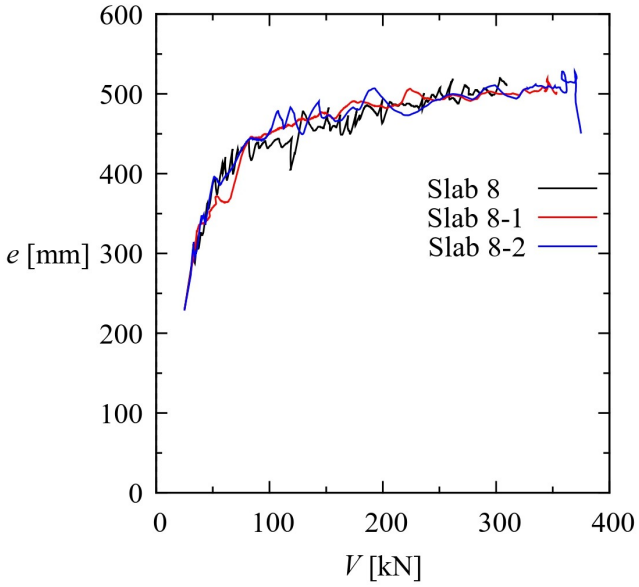

Fig. 4.2 - Specimen load eccentricity.

The flexural reinforcement consisted of 16 bars, 16 mm diameter steel bars spaced every 160 mm in the top of the slab in both directions, resulting in a flexural reinforcement ratio of approximately $\rho \approx 0.96\%$. The bottom longitudinal steel reinforcing bars were 10 mm in diameter and spaced every 100 mm in both directions with a concrete cover of 20 mm. Hooks were used to ensure reinforcement anchoring. Specimen reinforcement details are shown in Fig. 4.3a.

Each specimen column was cast monolithically with the slab. The column reinforcement consisted of 8, 25 mm diameter steel bars to facilitate moment transfer and prevent column failure. These bars were enclosed by 10 mm diameter stirrups spaced 100 mm apart.

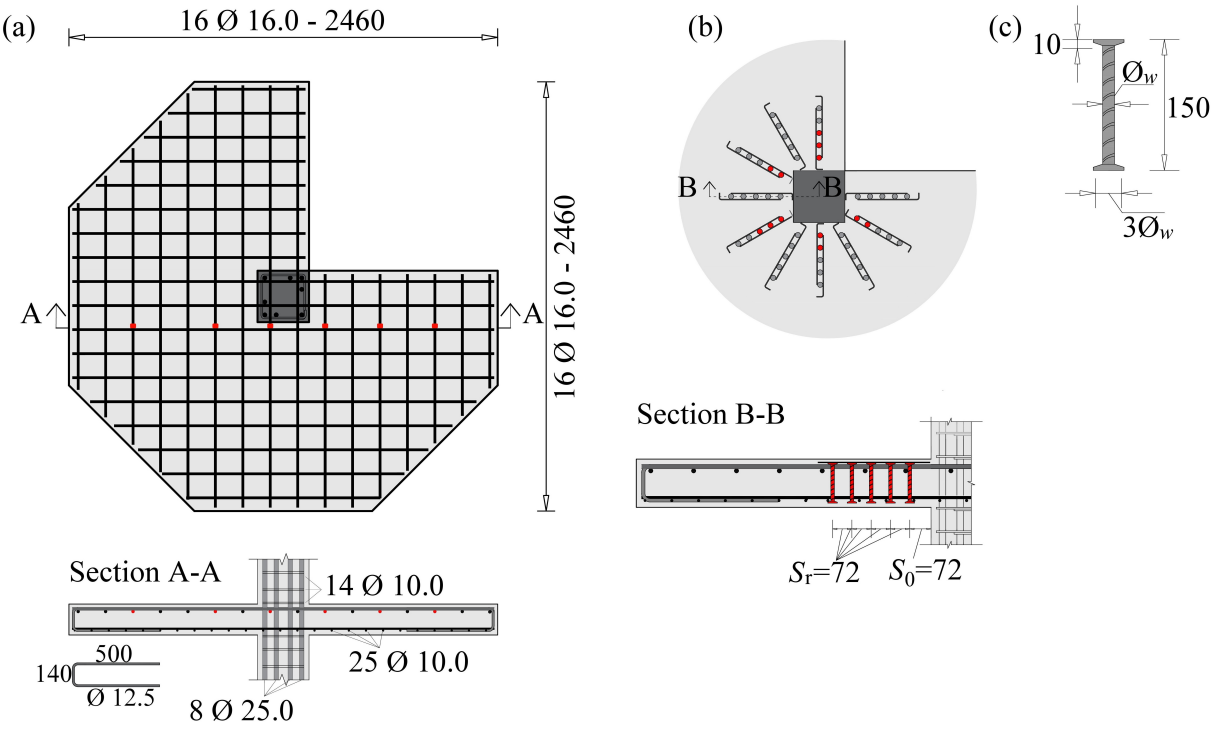

Fig. 4.3 - Detailing of the flexural and shear reinforcement configuration (the red dots represent the locations of strain gauges) [mm].

Double-headed studs manufactured were used as punching shear reinforcement. The stud heads had a diameter three times greater than the stud shank and were applied to both ends using a hot upset forging process. Specimens S8-1 and S8-2 contained studs with shank diameters of 8 and 10 mm, respectively. The distance from the outside of the first stud to the column face and the face-to-face spacing between studs was set to $s_0 = 0.5d$. Details of the adopted shear stud reinforcement scheme are shown in Fig. 4.3b and 6.3c.

Table 4.2 - Details of shear reinforcement of slabs

Slab	n_s [mm]	n_r [mm]	A_{sw} [cm²]	s_0 [mm]	s_r [mm]
S8-1	5	10	50.2	72	72
S8-2	5	10	78.5	72	72

4.1.2. Material Properties

Normal-strength concrete with a characteristic compressive strength of 45 MPa was obtained from a local supplier and used to cast the slabs and columns. One cubic metre of the concrete mixture comprised 309 kg of quartz sand, 476 kg of artificial sand, 964 kg of gravel with diameters ranging from 4.5 to 9.5 mm, 420 kg of Portland cement (CPV-ARI), and 190 kg of water.

The mechanical properties of the concrete were evaluated by testing 100 mm diameter, 200 mm long cylindrical specimens in accordance with the standards set forth in the Brazilian codes [32-35]. The compressive strength, tensile strength, and elastic modulus were determined by testing three cylinders each.

The mechanical properties of the flexural reinforcement were determined according to relevant normative recommendations [36]. Hot-rolled steel bars with well-defined yield plateaus were used as the reinforcing bars in this study. The material properties of the concrete and steel are listed in Table 4.3.

Table 4.3 - Properties of concrete and steel

Test	Concrete			Flexural reinforcement			Shear reinforcement			
	f_c [MPa]	f_{ct} [MPa]	E_c [GPa]	Ø [mm]	f_y [MPa]	E_s [GPa]	$Ø_{sw}$ [mm]	f_{yw} [MPa]	f_{uw} [MPa]	E_{sw} [GPa]
S8	53	4.5	35	16(1)	532	195	-	-	-	-
S8-1							8	652	716	226
S8-2							10	592	685	203

(1) f_u = 700 MPa

4.1.3. Instrumentation

The vertical displacements of each specimen were measured at the twelve locations shown in Fig. 6.4 using linear variable differential transducers (LVDTs; HBM model WA50) with a 50 mm stroke and 0.01 mm accuracy. The rotations of the slab in the main axes were determined from these measurements.

Type KFGS-5-120-C1-11 strain gauges (gage resistance of 119.8 Ω ± 0.2%) manufactured by Kyowa Electronic Instruments were used to measure the deformations at dix locations along the flexural reinforcement and twelve locations on the shear studs, as shown in Fig. 4.3. Two strain gauges were attached to opposite sides of the bar/stud at each location to determine the average deformation at its centre of gravity, ensuring accurate results. When one of the paired gauges obviously malfunctioned, the measured strain was taken as the value reported by the sole functional gauge.

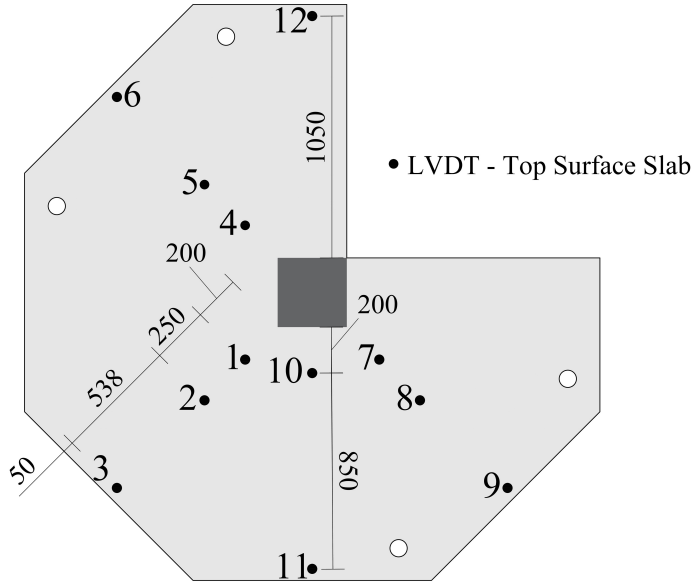

Fig. 4.4 - Locations of LVDTs [mm].

Additionally, the concrete strains were recorded at seven locations on the compression (bottom) face of each slab near the column, as shown in Fig. 4.5, using type KC-60-120-A1-11 strain gauges (gage resistance of 119.8 Ω ± 0.2%) manufactured by Kyowa Electronic Instruments.

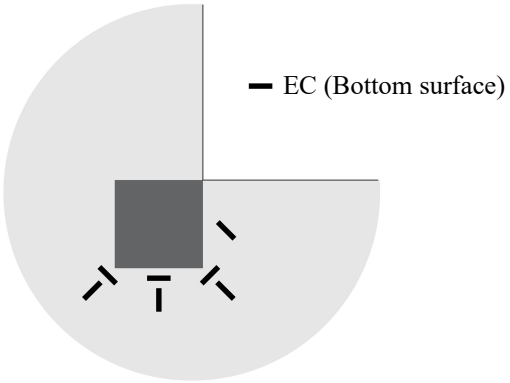

Fig. 4.5 -Strain gauges on the bottom surface of the slab.

4.1.4. Test setup

Fig. 4.6 illustrates the specimen testing system based on the LABEST reaction frame. The loads were applied in the downward direction using three hydraulic actuators (jacks), each with a capacity of 1 MN. Load cells with capacities of 500 kN were used to measure the applied force at each jack. These forces were transferred to the slab using six steel plates. Each specimen was subjected to continuous loading until failure as the concrete cracking, displacement, strain, and deformation evolution of each specimen were monitored.

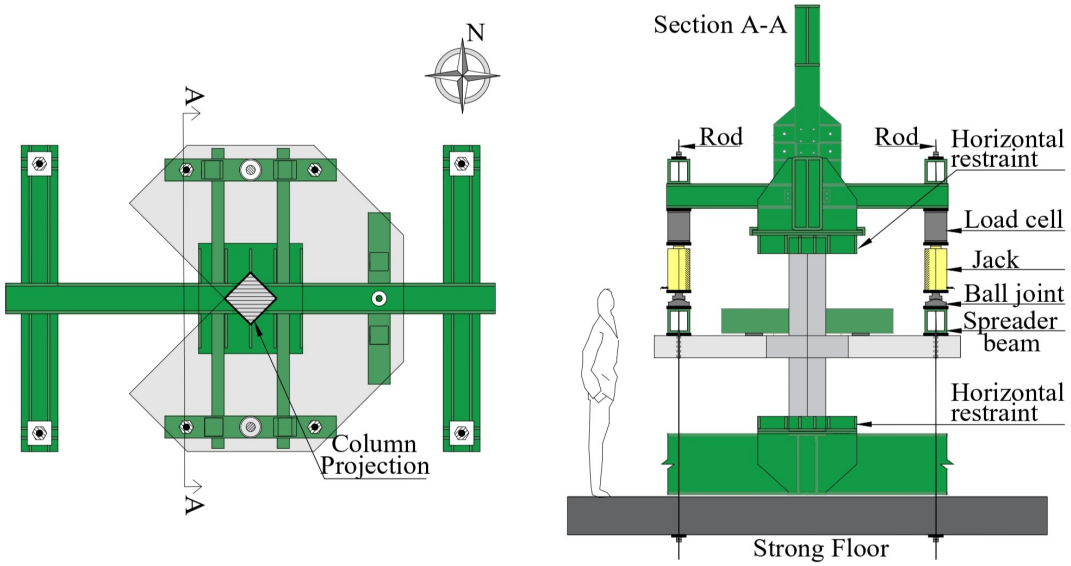

Fig. 4.6 - Test setup.

4.2. Analysis of Test Results

4.2.1. Global response and failure mode

Table 4.1 lists the failure loads and flexural strengths of the specimens. Specimen S8 failed via punching shear without exhibiting intense flexural cracking, whereas the slabs with shear reinforcement clearly exhibited flexural punching failure. To provide a consistent comparison, the failure loads were normalised considering the square root of the concrete strength, cube root of the flexural reinforcement ratio, effective depth, and length of the basic control perimeter (defined as the geometric perimeter located $0.5d$ from the end of the supported area). The normalised strengths compared in Fig. 4.7 indicate that the strengths of the specimens increased approximately 17% and 25% as the shear reinforcement ratio increased from 0 to 0.42 and 0.66, respectively. Although this increase in strength was relatively modest, the specimen without shear reinforcement failed in a sudden brittle punching failure mode whereas the specimens with shear reinforcement failed in a more ductile punching mode with significantly greater deflection.

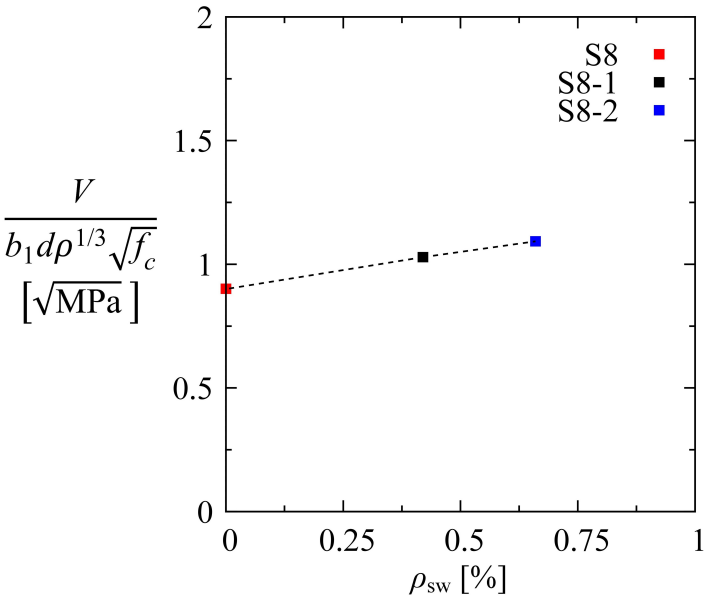

Fig. 4.7 - Normalized strength as a function of the shear reinforcement ratio of tests

The load-displacement responses of the slab specimens are illustrated in Fig. 4.8. All three specimens exhibited similar behaviours near the re-entrant column, with the displacements along the slab edges consistently increasing, particularly at point L03. As the measured slab displacement increased by approximately 45% with the increase in the shear reinforcement ratio from 0 to 0.66, the use of shear studs as reinforcement clearly increased the efficiency of the connection and significantly improved its ductility.

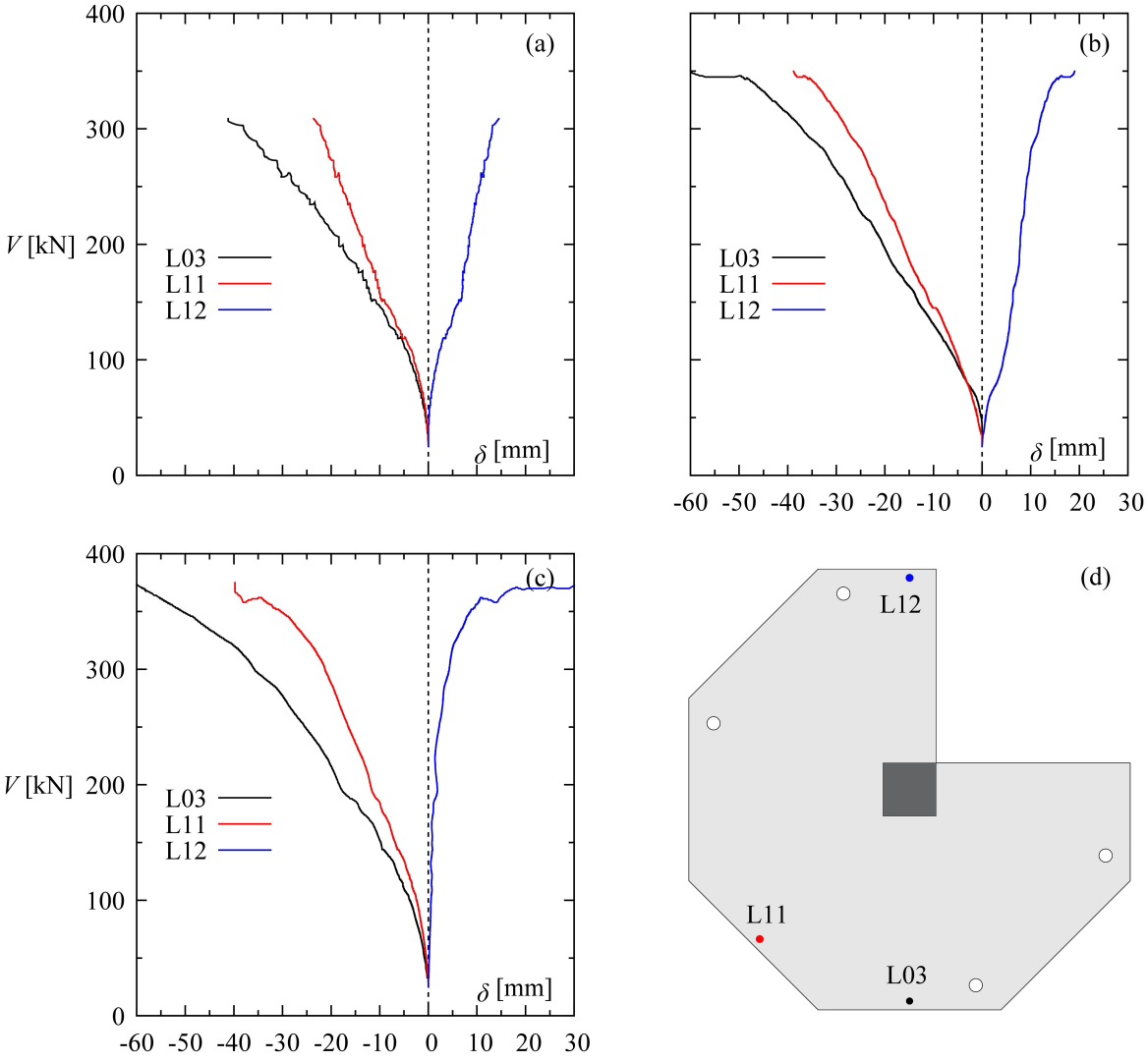

Fig. 4.8 - Load-rotation relationships of the tested specimens: a) S8, b) S8-1 and c) S8-2.

Fig. 4.9 illustrates the cracking patterns observed in the top surfaces, cuts, and re-entrant corner faces of the slabs. A punching cone was observed in the slab without shear reinforcement, whereas the slabs with shear reinforcement exhibited diagonal cracking because of the bending moment generated in the direction of eccentricity. Furthermore, characteristic torsion cracks were observed on the re-entrant and adjacent faces that formed an inverted punching cone.

Fig. 4.9 also provides detailed maps of the cracks in the cut surfaces of the slabs. All slabs exhibited an inclined critical shear crack, which is a typical characteristic of punching shear failure. This crack propagated through the shear studs of the slabs that had them

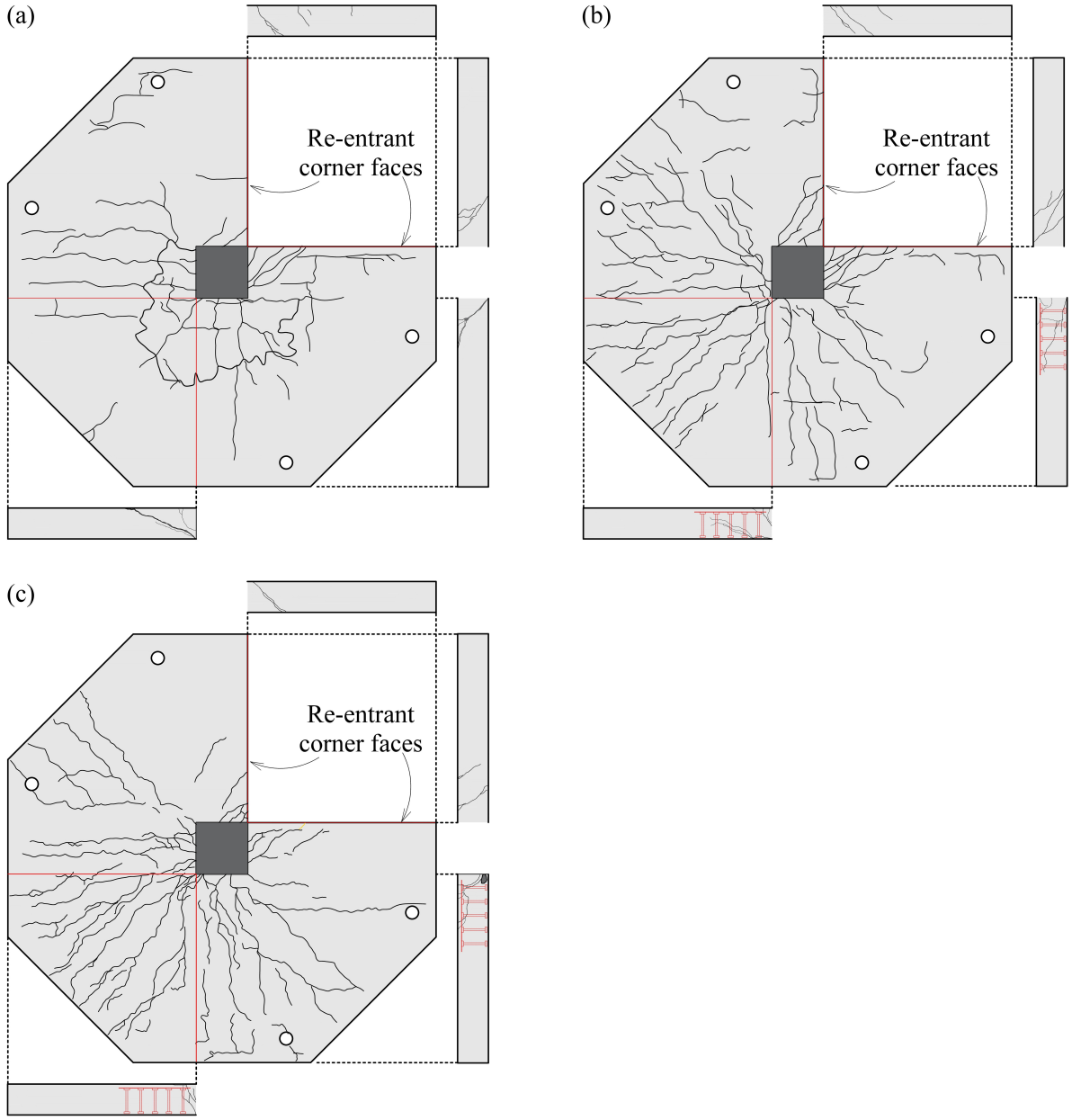

Fig. 4.9 - Crack patterns on the top surface of the slab: a) S8, b) S8-1 and c) S8-2.

4.2.2. Strains in the top flexural reinforcement and shear reinforcement

Fig. 4.10 shows the deformation profile of the flexural reinforcements instrumented near the failure. It can be seen that the yield radius of the flexural reinforcement remains confined to an area adjacent to the column, with the maximum values concentrated within its width. In the S8-2 slab, all strain gauges located in the internal area showed deformation, indicating a significant influence of the shear reinforcement, confirming the more ductile mode of failure observed in tests (S8-2 and S8-1)

The deformations along the re-entrant edges of the slab rapidly decreased with increasing distance from the column to eventually reach values close to zero. On the side of the column where the slab was continuous, the deformation decreased rapidly as the distance from the column increased.

In no case was generalised yielding observed along the instrumentation line; this is consistent with the shear punching failure mode observed in specimen S8 and the flexural punching failure modes observed in specimens S8-1 and S8-2.

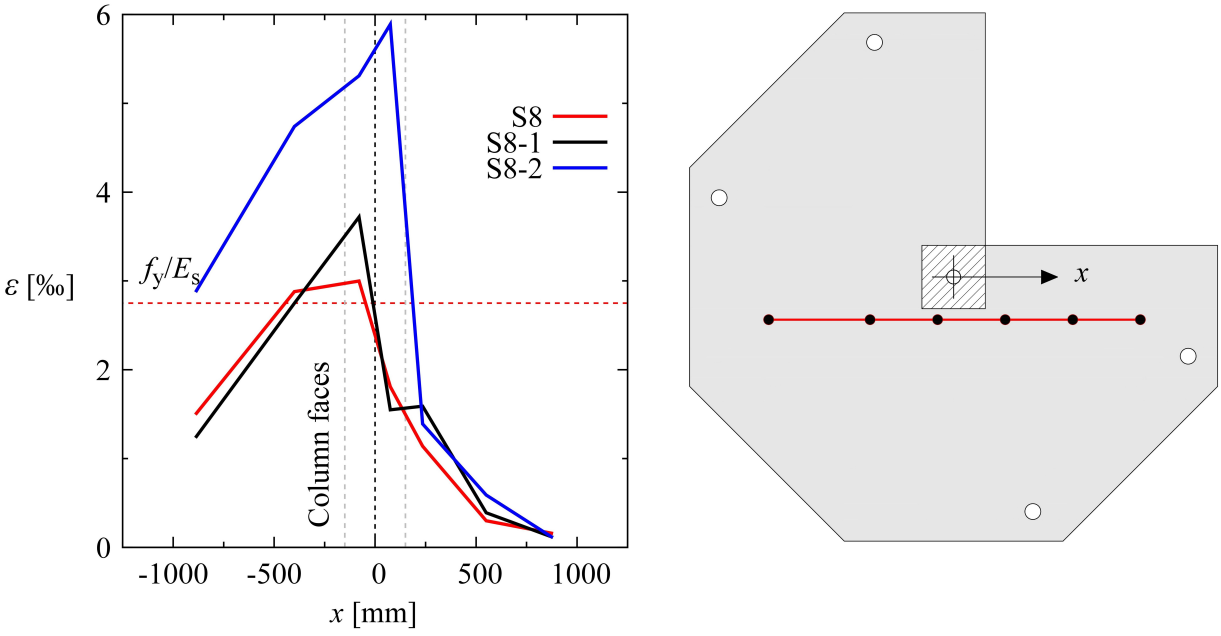

Fig. 4.10 - Profile of strains in the flexural reinforcement of tests.

Fig. 4.11 compares the performances of the shear studs in the tested slabs, in which the strain corresponding to the yield strength of the shear stud is indicated by red dashed line labelled f_y/E_s.

The studs near the axis of the symmetry/direction of eccentricity clearly reached their yield strength, whereas the strains along the other lines remained below yield closer to the re-entrant edges but were still significant, except at gauge ES1 in slab S8-1, which yielded. High stresses were consistently observed in the third shear stud in each line.

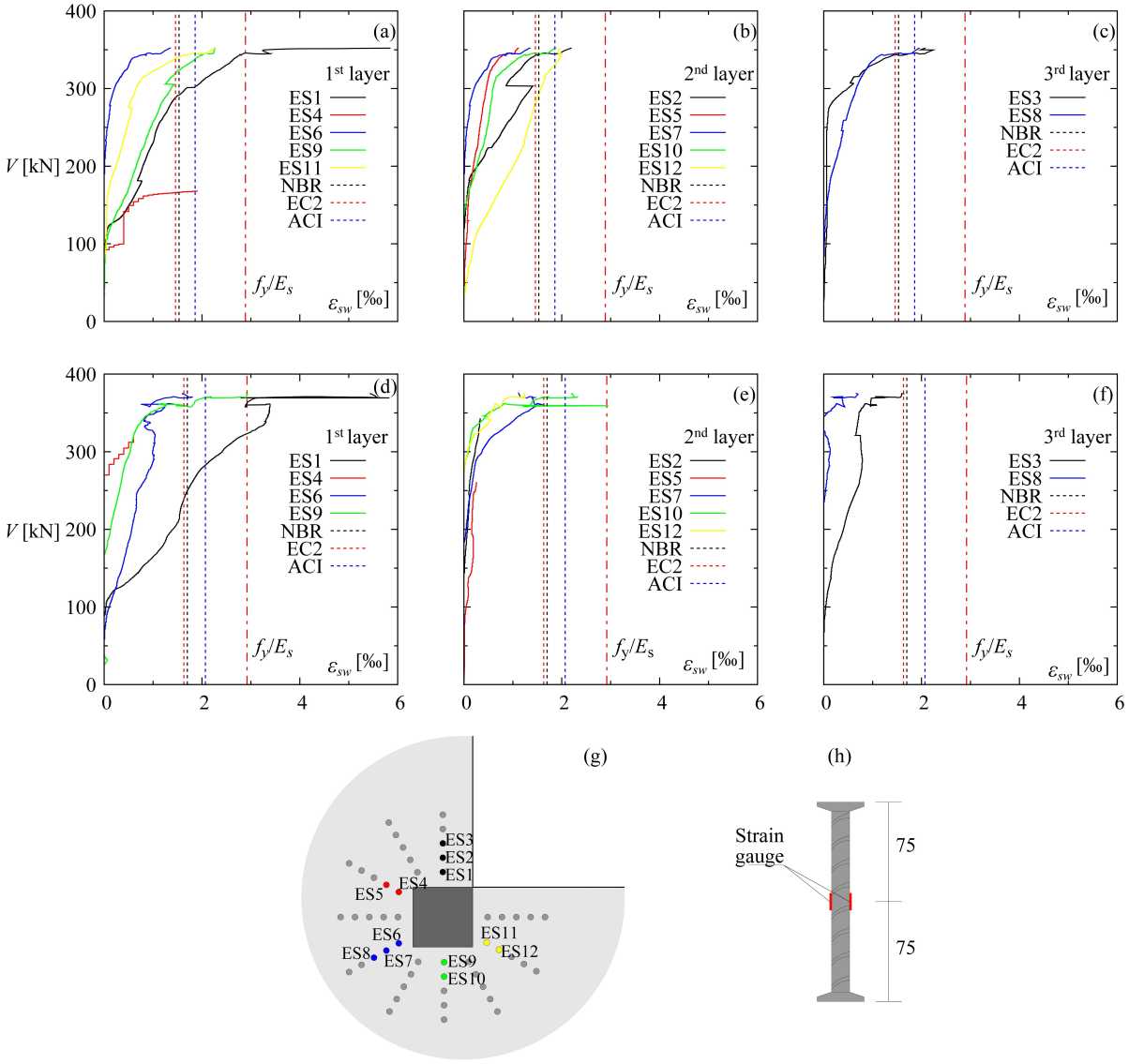

Fig. 4.11 - Measured strains in the shear reinforcement: (a-c) slab S8-1; (d-f) slab S8-2; (g) location of gauges; and (h) location of gauges in the shaft.

Fig. 4.11 also compares the effective deformation of the shear reinforcement considered in the design according to the standards: NBR (represented by the dashed black line), EC2 (by the dashed red line) and ACI (by the dashed blue line). To calculate the effective deformation, the

corresponding stress was divided by the modulus of elasticity of the steel used. The Brazilian standard limits this to 345 MPa (for studs), while the ACI defines a limit of 420 MPa. In turn, EC2 determines this effective stress as a function of the effective depth of the slab, using the following expression: $\varepsilon_{ywk,eff} = \{1.15\ (250 + 25d)/E_s \leq f_{ywk}/E_s\}$.

In the first layer monitored in both slabs, the deformation $\varepsilon_{ywk,eff}$ was reached, with the exception of two strain gauges which apparently did not functioning properly. In the second layer, it was noted that most of the strain gauges recorded deformations above the limits established by the standards. In the third layer, it was observed that in slab S8 the deformations were greater than $\varepsilon_{ywk,eff}$ while in slab S8-1 they were lower. These limitations can be attributed to the fact that by the time the shear reinforcement starts to contribute effectively, the slabs are already very cracked. This makes it difficult to achieve higher stress/strain levels, so that punching shear reinforcement often does not reach yielding before punching shear failure occurs.

4.2.3. Strains at the concrete surface

The radial and tangential strains measured on the bottom surface of the slab-column specimens are shown in Fig. 4.12. Generally, the strains in the tangential direction were higher than those in the radial direction. The tangential gauges recorded the highest strains in the slabs with shear reinforcement (S8-1 and S8-2). In these slabs, gauge EC1 reported tensile strain, indicating possible degradation in the slab stiffness associated with the formation of diagonal shear cracks; however, this increase in strain was only observed immediately before failure, and these gauges may not have functioned perfectly.

Compressive tangential concrete strains increased monotonically with load, reaching a maximum value of approximately 2.2‰ in slab S8-1 (at EC5), 1.8‰ in slab S8-2 (at EC3), and 1.6‰ in slab S8 (at EC1). The ultimate compressive strain in the concrete (ε_{cu}), defined as 3.26‰ by ABNT NBR 6118, 3.26‰ by EN1992-1-1:2004, and 3‰ by ACI 318-19, was not reached in any of the slabs.

The measured radial strains near ultimate load indicated that decompression may have occurred at the concrete surface near the column, possibly because of the local bending of the compression zone. This behaviour, as explained by Muttoni [1], could be characteristic of the development of a critical shear crack close to the column face.

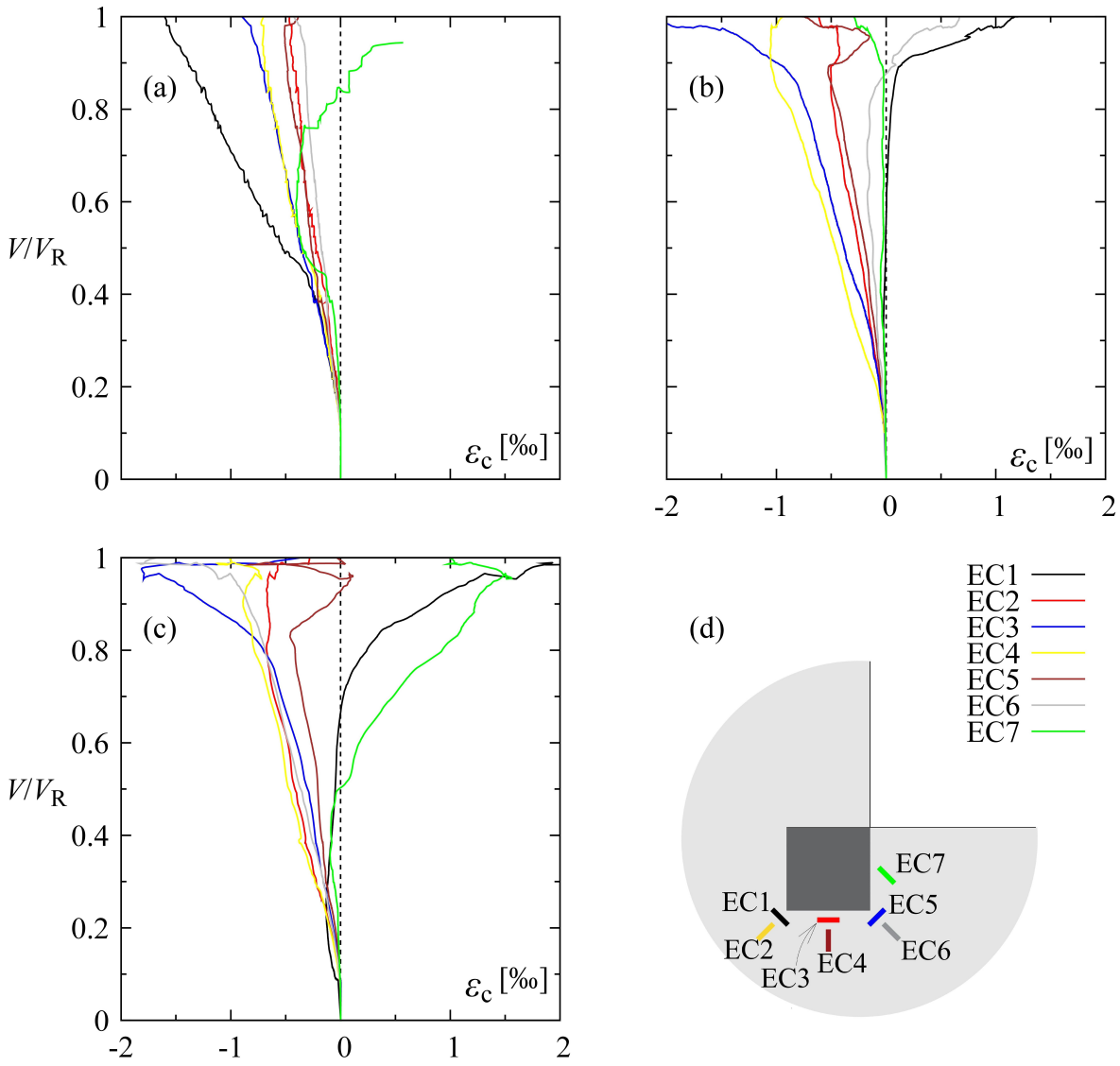

Fig. 4.12 - Tangential and radial strains on the bottom surface of slabs (a) S8, (b) S8-1 and (c) S8-2 as well as the (d) locations of gauges.

4.3. Comparison of Experimental and Code-Predicted Capacities

Five design codes were evaluated to compare the measured and predicted punching shear capacities. Chapter 2 details the equations and considerations used in these calculations. The punching shear resistances were evaluated using partial factors (γ_c and γ_s) equal to unity and the average concrete cylinder strength obtained from the tests. The shear resistance ratio (V_R/V_{calc}) was used to compare the test results to the calculated punching shear capacity.

The results indicate that ACI 318-19 was the most conservative among the considered codes, underestimating the punching shear capacity and thereby guaranteeing safe slabs. The MC2010 and EN 1992-1-1 codes provided conservative estimates for slabs without shear reinforcement; however, their predictions were more accurate for slabs with shear reinforcement.

Finally, the EN 1992-1-1 and ABNT NBR 6118 codes provided conservative estimates of the punching shear capacity of the slab without shear reinforcement but tended to overestimate these resistances for the S8-1 and S8-2 slabs with shear reinforcement, as these estimates were conditioned by the flexural capacity of the slabs.

Table 4.4 - Summary of experimental and theoretical resistances also failure modes

Slab	V_R [kN]	Failure Mode	ACI 318 $V_R/V_{R,ACI}$		EN-1992 $V_R/V_{R,EC2}$		EN-1992 $V_R/V_{R,FprEC2}$		MC 2010 - LoAII $V_R/V_{R,MC10}$		NBR 6118 $V_R/V_{R,NBR}$	
			Failure		Failure		Failure		Failure		Failure	
S8	309	V_c	1.63	V_c	1.09	V_c	1.54	V_c	1.54	V_c	1.22	V_c
S8-1	353	V_{in}	1.23	V_{in}	0.92	V_{flex}	1.03	V_{in}	1.12	V_{out}	0.92	V_{flex}
S8-2	375	V_{in}	1.07	V_{out}	0.99	V_{flex}	1.01	V_{max}	1.15	V_{out}	0.99	V_{flex}

4.4. Conclusions

This study conducted an experimental investigation of three reinforced concrete slabs at a re-entrant corner column, two with and one without shear stud reinforcement. The top and bottom reinforcement ratios and eccentricity were maintained for all specimens while the shear reinforcement ratio was varied by changing the shear stud diameter. The following conclusions were drawn based on the test results:

1. The addition of shear stud reinforcement increased the punching resistance of the reinforced concrete slab.
2. Slabs with shear reinforcement exhibited high flexural strength, particularly S8-2, demonstrating the effectiveness of shear studs in resisting punching shear.
3. The monitored studs exhibited suitable performance and contributed significantly to the punching shear resistance in both slabs; the first and second studs from the column were particularly effective.
4. None of the slabs exceeded the concrete crushing strain of 3.5‰; the largest strain was 2.0‰ in slab S8-1.
5. A crack analysis revealed radial and tangential cracks in the slabs with shear reinforcement and a punching cone in the slab without shear reinforcement. Therefore, the failure mode of S8 was classified as shear punching failure, whereas the failure modes of S8-1 and S8-2 were classified as flexural punching failure.
6. The evaluated design codes generally provided conservative predictions of slab shear capacity, with only the NBR providing unsafe capacity predictions for slabs with shear reinforcement. This can be partly attributed to the fact that the codes were calibrated for inner columns, edges, and corners; the re-entrant corner configuration has not yet been considered in any standard.

4.5. References

[1] Muttoni, "Punching shear strength of reinforced concrete slabs without transverse reinforcement," ACI Struct. J., vol. 105, no. 4, pp. 440-450, Jul., 2008, doi: 10.14359/19858.

5. CHAPTER V: PUNCHING SHEAR TESTS IN FLAT SLABS SUPPORTED ON RE-ENTRANT CORNER COLUMNS

This chapter is the postprint version of the article titled **Punching shear tests in flat slabs supported on re-entrant corner columns** published in Volume 308 of the journal Engineering Structures in 2024 (DOI: https://doi.org/10.1016/j.engstruct.2024.117954). The authors of this publication are João Paulo de Almeida Siqueira (DSc Candidate), Elaine Jaricuna Pereira de Albuquerque (Professora at UFRR), Miguel Fernández Ruiz (Professor at UPM and DSc advisor during Sandwich Program) and Guilherme Sales de Melo (Full Professor at UnB and thesis director). The complete reference is the following:

- Siqueira J. P. A., Albuquerque E. J. P., Fernández Ruiz M., Melo G. S., *Punching shear tests in flat slabs supported on re-entrant corner columns*, Engineering Structures, Vol. 308, 20 p., 2024. DOI: 10.1016/j.engstruct.2024.117954.

The main contributions of João Paulo de Almeida Siqueira to the creation of this article were the following:

- Performing all the calculations presented in article;
- Analyse the presented results;
- Production of the figures included in the article;
- Preparation of the manuscript of the article.

5.1. Abstract

Despite the great variety of cases concerning slab-column connections found in practice, most research has concentrated so far on the punching resistance of inner columns without moment transfer. Other cases, such as edge or corner columns, have attracted less research attention despite their practical relevance. Within this context, re-entrant corner columns are a commonly used detail in practice (i.e. columns at corners of openings) where almost no experimental evidence is available and design codes typically extrapolate design recommendations from other cases. In order to advance the knowledge in this field, this paper presents an experimental and theoretical investigation on the punching resistance of slab-column connections in re-entrant corners. The research is addressed at specimens with and without shear reinforcement and introduces the results of an experimental programme on specimens reproducing realistic conditions in terms of size and loading arrangement. The experimental results are first analysed according to several design guidelines, highlighting their shortcomings. On that basis, a theoretical approach for punching design is proposed based on the Critical Shear Crack Theory. Such approach is aimed at understanding the mechanics of punching failure and to lead to consistent predictions on the resistance and deformation capacity of the slab-column connections.

Keywords: Flat slab, Punching shear, Re-entrant corner, Shear reinforcement, Critical Shear Crack Theory.

5.2. Introduction

Slabs with flat soffit, such as flat slabs, have been one of the most widespread construction solutions for residential and office buildings. This has been motivated by a number of advantages, such as the simplicity for construction and relatively low cost as well as for the potential to integrate technical equipment. In particular, the possibility of arranging openings and defining the edges of the slab with a high degree of freedom has enhanced the capacity to tailor the structure to the architectural needs.

At ultimate limit state, flat slabs are governed by their punching resistance at the slab-column connections, where high bending moments and shear forces develop. This aspect, together with the control of deflections at serviceability limit state, determine the thickness of the slab, ruling the economy of the solution and the amount of materials used. As it can be noted, the thickness of a flat slab at mid-span is governed by the punching resistance at a small region (over supports) and this leads in many cases (mostly for high bay spans) to a poor use of the material, with large amounts of concrete used under its potential [1]. Even for solutions saving material in the regions located at mid span (such as flat slabs supported on column capitals [1], slabs with drop panels [3], bubble-deck systems [4]-[5] or waffle slabs [6]-[7]) their design present a solid portion of slab at the connection with columns and their strength and deformation capacity is also controlled by the local punching resistance.

Concerning the phenomenon of punching shear, it has been acknowledged as highly complex and implying the combined action of several shear-resisting actions [8], such as the dowel action of tensile reinforcement [9], aggregate interlock [9]-[10], compressive resistance [11] and residual tensile strength along the crack [12]. Theoretical efforts have allowed for significant steps forward in the understanding of the phenomenon [13]-[18].

Such efforts have been addressed to a large extent to the response of interior slab-column connections. However, a significant fraction of the slab-column connections refer in fact to edge or corner columns, where the response has some differences, both in the action (distribution of shear forces in the slab near the column, reduced membrane action) and resistance (contribution of edge reinforcement, torsion effects) [19]. Unfortunately, the experimental evidence is scanty with reference to edge [19]-[29] and corner [24]-[26],[30]-[33] connections as highlighted by Fraile *et al.* [19].

Different experimental setups have been used to assess the response of corner slab-column connections under combined gravity load and unbalanced moment, as shown for some representative cases of corner columns in Fig. 5.1. In general, the tests are performed on isolated specimens representing a portion of the slab near the connection (Fig. 5.1a,b) or on full-systems (Fig. 5.1c). The former setup has the advantage to control in a precise manner the eccentricity of the shear force during the test while the latter allows for a realistic consideration of redistribution of internal forces.

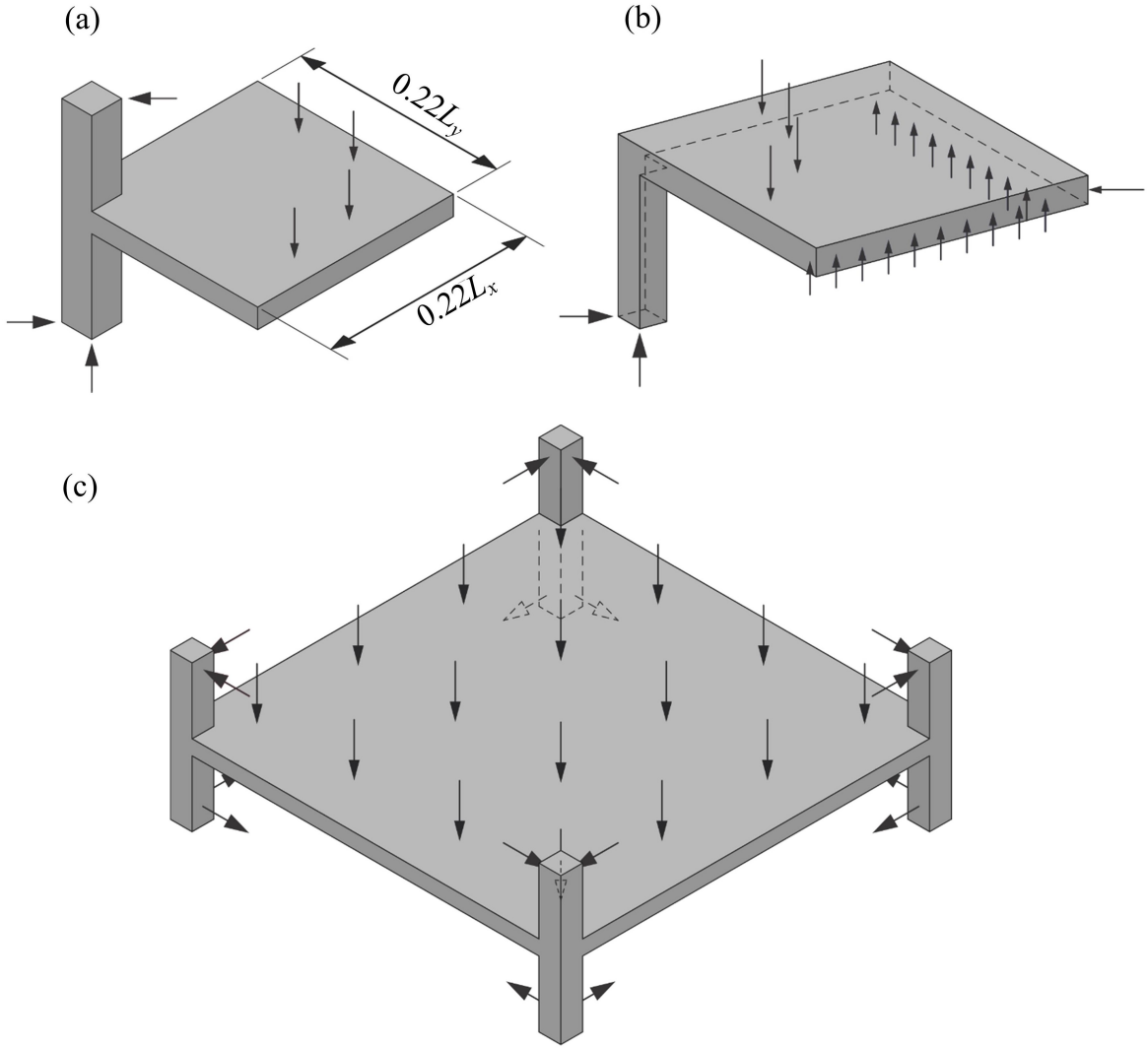

Fig. 5.1 - Instances of test setups used for slab-column corner connections: (a) isolated model [24],[29]-[30]; (b) simulating slab continuity (Vocke and Eligehausen [33]); and (c) full system (as tested by Walker and Regan [31])

Based on the knowledge acquired through experimental evidence, design approaches were provisioned in different codes of practice [36]-[41]. These approaches have been based on empirical formulae [36]-[39] but also on mechanical models [40]-[41] and provide detailed treatment for internal, edge and corners connections. The design equations allow accounting namely for the geometry of the supported area as well as for the moment transfer (eccentricity of the shear force). These approaches can therefore be adapted to other situations, but extrapolations may be compromised accounting for the complexity of the phenomena (membrane forces, presence of edge reinforcement…).

It is interesting to note that re-entrant corners have not been investigated in the scientific literature so far by means of dedicated experimental programmes. Consequently, design equations might be simply extrapolated for this case by analogy. This is however not straightforward as re-entrant corners are not mechanically similar to edge, corner or interior connections. In order to provide sound data on this topic and to make a step forward in the knowledge, this paper investigates the response of re-entrant corners by means of a dedicated experimental programme. The tests are aimed at reproducing the critical region located near the column.

As shown in Fig. 5.2, the selected sector reproduces the region where negative bending moments are expected. This configuration, as for tests on corner columns, allows for a precise control of the interior forces (namely of the eccentricity of the shear force) although it does not intend to represent redistributions of internal forces potentially occurring. To that aim, seven re-entrant slab sectors were tested under different configurations, designed with dimensions, loading conditions and reinforcement detailing reproducing realistic practical cases.

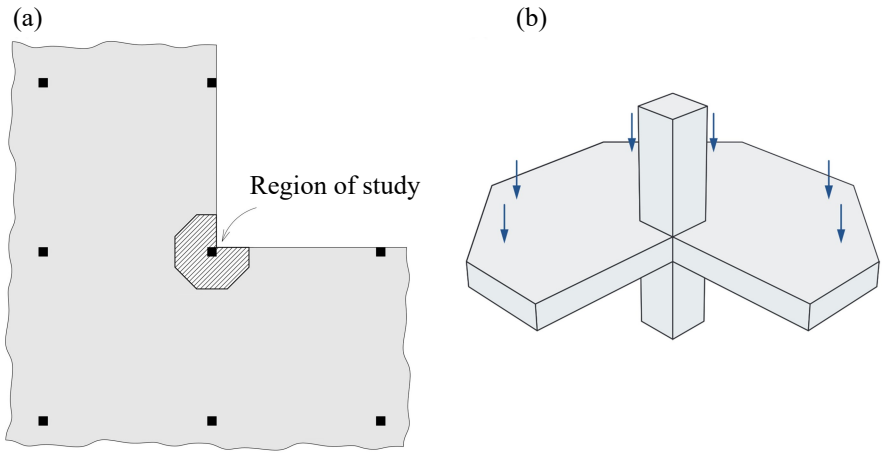

Fig. 5.2 - Re-entrant corner: (a) full slab and (b) detail of tested specimen (slab sector) reproducing the shear-critical region.

The results of the experimental programme comprised refined measurements, allowing for detailed understanding of the response of the specimens. The punching resistance is later compared to a number of codes, highlighting their shortcomings. Finally, the results are investigated on the basis of a mechanical model for punching shear. To that aim, the Critical Shear Crack Theory (CSCT) is used [16] by means of a detailed analysis of the shear field in the shear-critical region. The CSCT is shown to provide consistent results in terms of failure mode and shear strength, improving the approaches of current design codes and clarifying a number of physical considerations.

5.3. Experimental Programme

This section describes the experimental programme consisting of seven tests performed within this research. All tests were conducted in the Structural Laboratory of Universidade de Brasília (Labest-UnB, Brazil).

5.3.1. Specimen Description

The specimens were seven reinforced concrete slabs designed to represent the portion of a slab near a re-entrant corner as shown in Fig. 5.2, with the possibility of varying the eccentricity of the shear force at the supported area. The main dimensions are shown in Fig. 5.3. The specimens had nine sides, with a total in-plane width of 2500 mm and a thickness of 180 mm. They were supported on square reinforced concrete columns (300-mm side), protruding 800 mm on top and 600 mm on bottom, where they were clamped. The nominal concrete cover was 20 mm for all specimens.

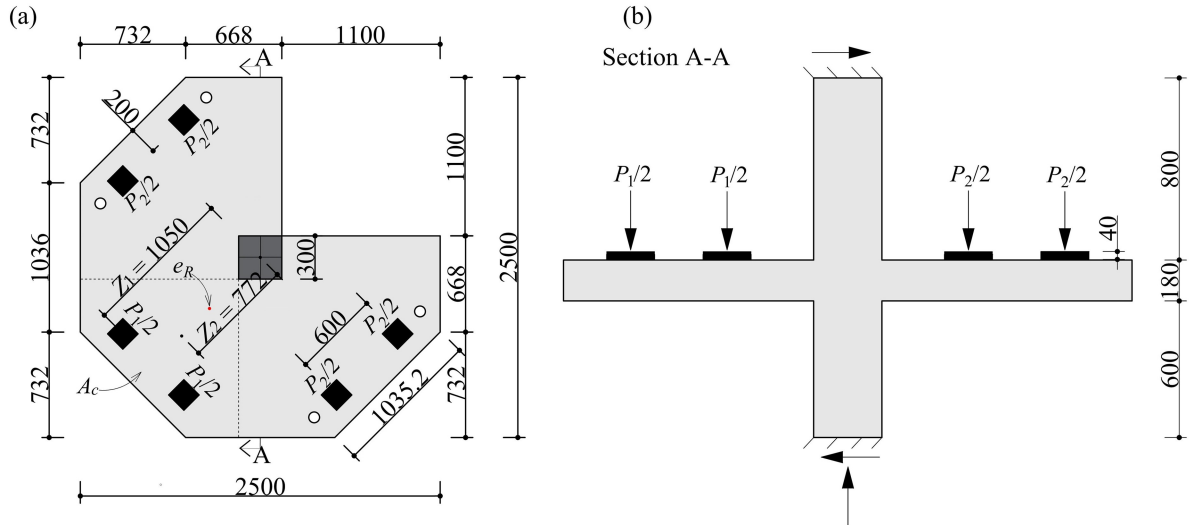

Fig. 5.3. Slabs dimensions.

The main investigated variables were the eccentricity of the shear force (e), the flexural reinforcement ratio, as well as the edge of the slab near the re-entrant corner. Details for each specimen are given in Table 5.1 (including also mean values of effective depths obtained from direct measurements in saw cuts of the specimens after testing).

Table 5.1 - Main parameters and characteristics of the tested specimens

Test	d [mm]	f_c [MPa]	ρ [%]	P_2/P_1 [-]	e_R [mm]	e_R/d [-]	V_R [kN]	$\frac{V_R}{b_1 \cdot d \cdot \sqrt{f_c}}$ (1)
S1	148.0	48	1.49	0.5	491	3.32	325	0.20
S2	147.0		1.49	1.0	344	2.34	372	0.23
S3	142.5		0.67	0.5	496	3.48	250	0.17
S4	144.5	44	0.65	1.0	344	2.38	282	0.19
S5	141.0		1.00	1.0	336	2.38	358	0.25
S6	145.5		0.94	1.0	341	2.35	345	0.23
S7	145.0	43	0.95	1.5	262	1.81	345	0.24

(1) b_1 is the perimeter located at $0.5d$ of the edge of the supported area.

Concerning the eccentricity of the shear force (e) with respect to the column axis, it is defined as follows:

$$e = \frac{M_E}{V_E} = \frac{P_1 \cdot z_1 + P_c \cdot z_c}{P_1 + 2 \cdot P_2 + P_g} \tag{5.1}$$

where: M_E refers to the transferred moment from the slab to the column and V_E to he applied shear force, P_1 and P_2 are the external loads applied on the tested slab, P_g is the self-weight of the slab (19 kN) and of the testing equipment (6 kN), P_c is the self-weight of the slab and of the testing equipment which is not balanced by symmetry conditions (refer to corner region A_c in Fig. 5.3, $P_c \approx P_g/3$), z_1 is the lever arm between the load P_1 and the column axis ($z_1 = 1050$ mm), z_c is the lever arm between the centre of gravity of the loads which are not balanced by symmetry conditions (refer to corner region A_c in Fig. 5.3) and the column axis ($z_2 = z_c \approx 772$ mm).

It shall be noted that the eccentricity varied slightly during the test as the values of z_1 (lever arm of external actions) and z_2 (lever arm of self-weight and instrumentation) were different. In Table 5.1, the values at failure (e_R) are thus reported, varying between $3.48d$ (test S3) and $1.81d$ (test S7) and covering the range of typical eccentricities for such connections.

With respect to the reinforcement, the top layers consisted of bars diameter 16 mm, except for specimens S3 and S4, where 12.5 mm bars were used. The reinforcement was uniformly distributed with some local adaptions near the column region.

In the following, the different specimens will be characterised by their average amount of flexural reinforcement (ρ), defined as follows:

$$\rho = \frac{A_s}{s \cdot (d_x + d_y)/2} \tag{5.2}$$

Fig. 5.4 and Fig. 5.5 illustrate the distribution of flexural reinforcement for reinforcement rates of 1.5% (S1 and S2), 0.96% (S5, S6 and S7), and 0.65% (S3 and S4), respectively. The bottom flexural reinforcement was 12.5 mm bars in all slabs, as shown in Fig. 5.5b.

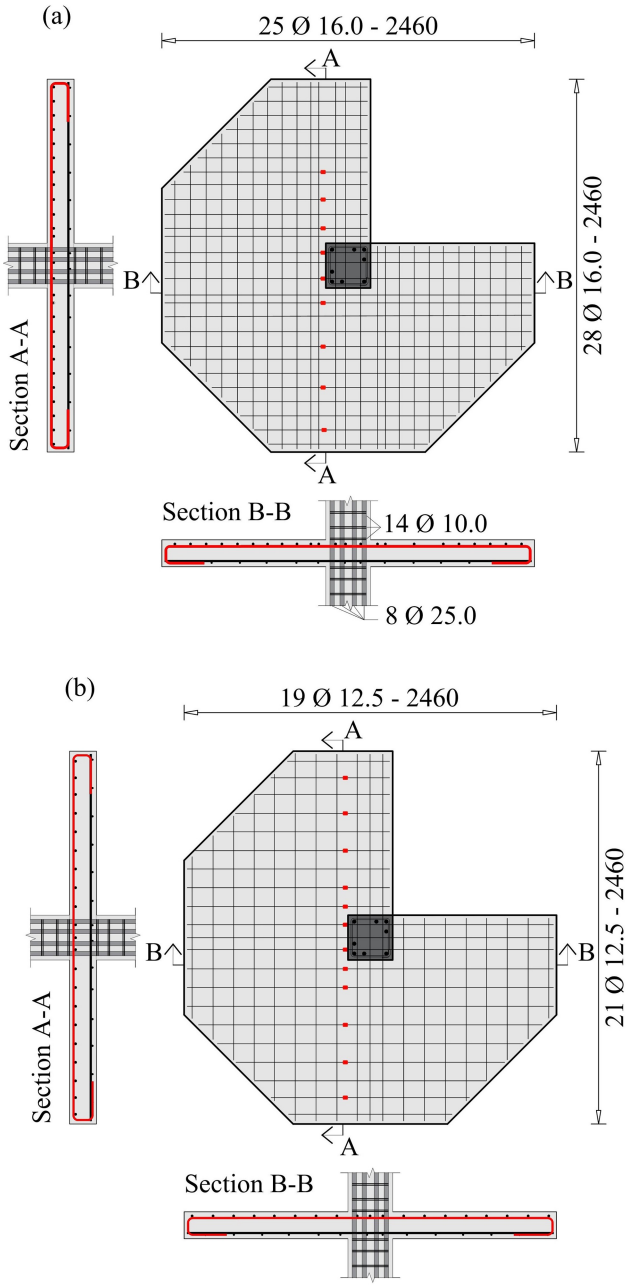

Fig. 5.4 - Flexural reinforcement of slabs and location of strain gages: (a) Slabs S1 and S2; (b) Slabs S3 and S4.

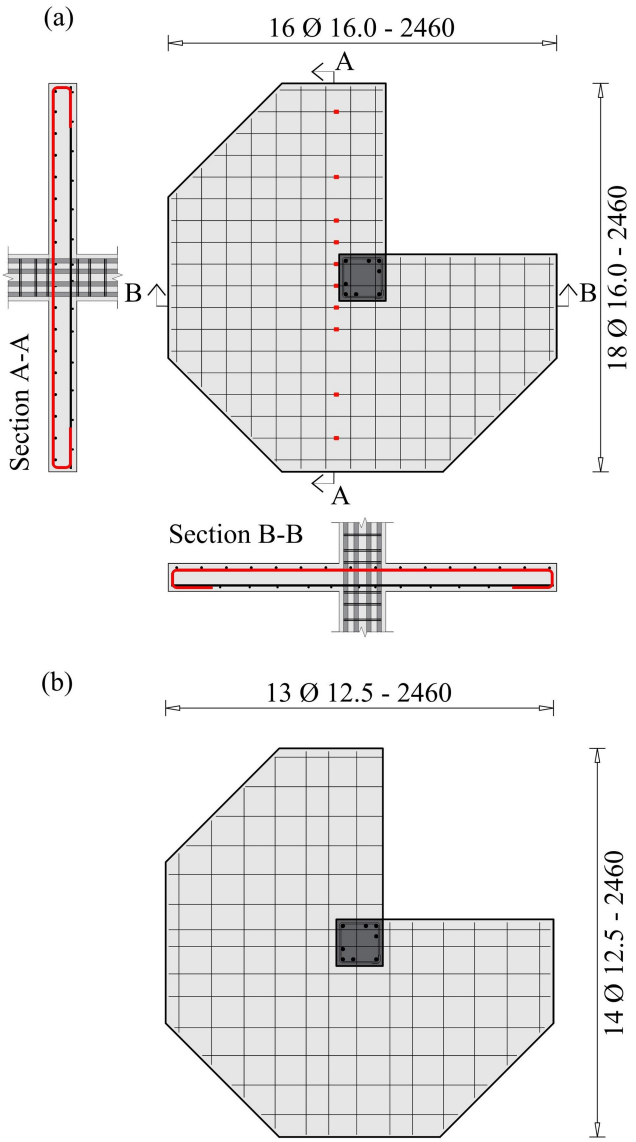

Fig. 5.5 - Flexural reinforcement of slabs and location of strain gages: (a) Slabs S5 to S7; (b) bottom flexural reinforcement.

Concerning the detailing of the reinforcement at the edges, hooks were provided for the top reinforcement, while the bottom reinforcement was straight (as well as used by [42]-[43]). This does not correspond to typical detailing of edges (where anchorage is provided by means of L-shaped reinforcement or hooks are provided for the bottom layer) but aims at ensuring a full anchorage for the top reinforcement during testing.

For specimen S6 (nominally identical to S5) edge stirrups were added in addition to the hooks, see Fig. 5.6, to investigate on its influence in the specimen's response. Such reinforcement consisted of 10 mm stirrups placed at the re-entrant corners of slab S6, together with three bars diameter 12.5 mm to ensure accurate positioning of the stirrups.

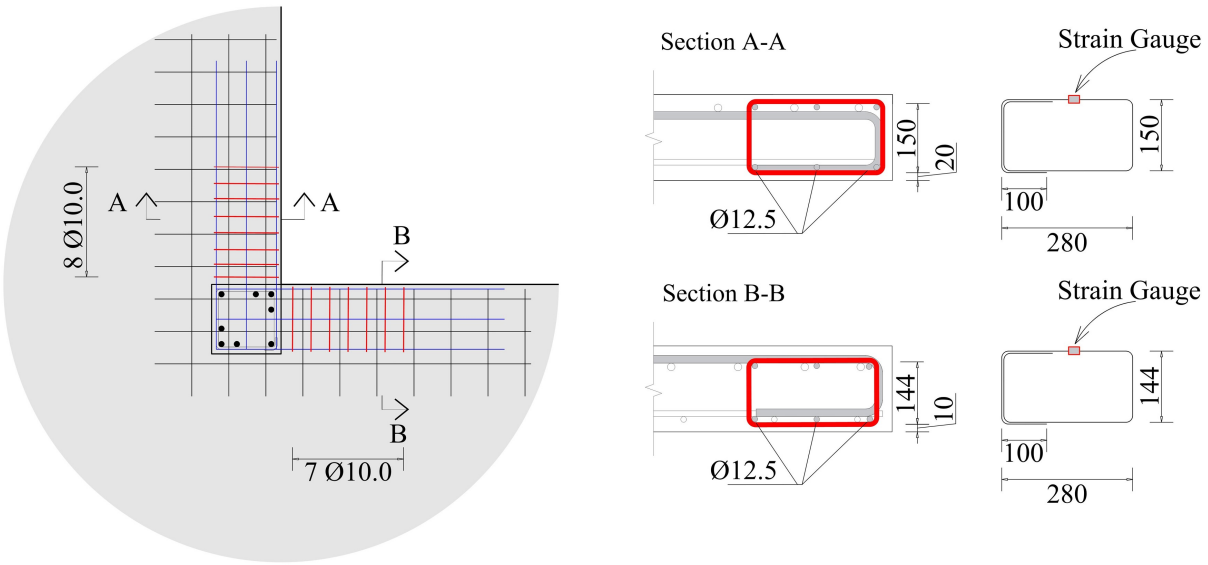

Fig. 5.6 - Detailing of edge reinforcement of specimen S6.

5.3.2. Material Properties

The characteristic compressive strength for the concrete was 40 MPa. In the concrete dosage, 50% CEM I and 50% CEM III were used. The water/cement ratio was approximately 0.47. Crushed limestone sand and gravel were used as aggregate, with 9.5 mm of maximum sieve size for the coarse aggregate. The average slump of the concrete mix was 120 mm and the slabs were moist cured for 7 days.

The compressive strength of concrete, tensile strength and the modulus of elasticity were determined for each group of slabs by testing cylinders (100 mm diameter by 200 mm high). The characterization of concrete was performed for three test series. All specimens of a given series were cast on the same day and tested on the same day or in two consecutive days (with testing age varying between 28 days (S7) and 111 days (S2)). The first series includes slabs S1 and S2, the second series comprises slabs S3 to S6, and the third series consists of the slab S7. The compressive strength varied somewhat between the series, ranging between 43 and 48 MPa.

Concerning the flexural reinforcement, hot-rolled bars were used, exhibiting a well-defined yield plateau in the material characterization tests. The values given in Table 5.2 are based on the average of the three control specimens. The measured yield strength in direct tension tests varied between 472 MPa and 568 MPa for the diameter 16 mm bars and between 569 MPa and 585 MPa for the 12.5 mm bars.

Table 5.2 - Properties of concrete and steel

Test	Concrete			Flexural reinforcement			
	f_c [MPa]	f_{ct} [MPa]	E_c [GPa]	Ø [mm]	f_y [MPa]	f_u [MPa]	E_s [GPa]
S1	48	3.4	29.4	16	558	700	192
S2	48	3.4	29.4	16	558	700	192
S3	44	3.1	30.1	12.5	577	721	201
S4	44	3.1	30.1	12.5	577	721	201
S5	44	3.1	30.1	16	570	712	201
S6	44	3.1	30.1	16	570	712	201
S7	43	3.5	32.9	16	572	710	208

5.3.3. Instrumentation

To track the response of the specimens, the vertical displacements of the slab were measured using Linear Variable Displacement Transducers (LVDTs). The LVDTs were positioned at 12 points on the soffit of the slab as shown (targets 1-11 and 16 in Fig. 5.7) and four LVDTs measured column displacement (targets 12-15). The high number of deflections measured allowed to calculate the rotations at multiple locations and directions.

Selected flexural bars were also instrumented at various locations to measure the reinforcement strains, see Fig. 5.4. Each bar was equipped with two strain gages (KFG-5-120-C1-11, with dimensions of 5.0 × 1.4 mm) positioned at the same section, one on top and the other on bottom. The strain in the reinforcement was thus calculated as the average of the two readings.

In addition, surface deformations were measured on the concrete surface with strain gages (KC-70-120-A1-11, with dimensions of 80 × 7.5 mm). For slabs S1 and S2, the strains on the concrete surface were monitored at nine points (see blue gauges in Fig. 5.7).

Following the readings of these slabs and the location where highest strains were recorded, in slabs S3 to S7, the strain gauges were installed near to the column in various directions (see black gauges in Fig. 5.7). Additionally, for these specimens, gauges were also glued on the top surface (refer to red gauges in Fig. 5.7). The readings were taken at each load increment. In this paper, only selected strain and deflection measurements will be presented and discussed.

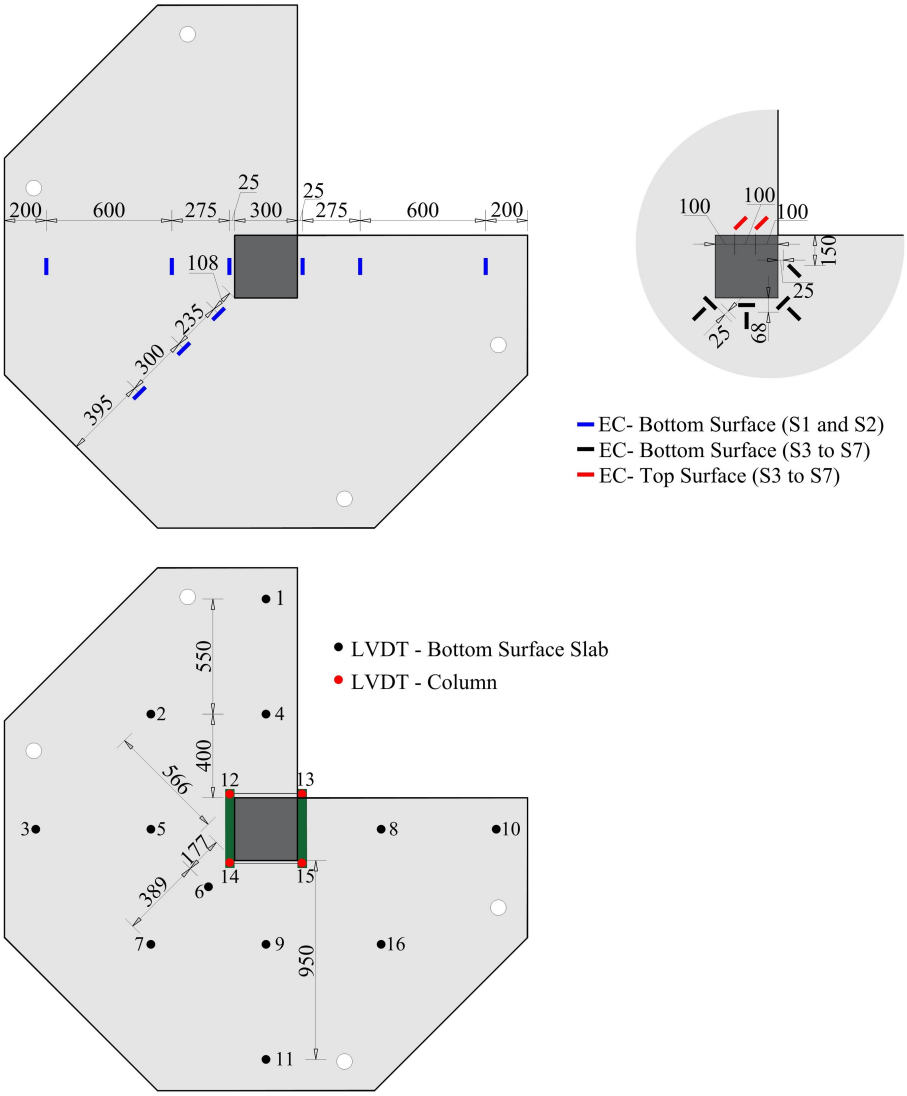

Fig. 5.7 - Location of measurements: (a) strain gages; and (b) LVDTs on slabs.

5.3.4. Test Setup

Testing of the specimens was performed in a custom test rig shown in Fig. 5.8. The specimens were loaded by means of three hydraulic jacks (1 MN capacity each) connected to two hydraulic pumps. This allowed ensuring, as shown in Fig. 5.3, the same load P_2 at two sides of the specimen and P_1 at the third. The loads, measured by means of load cells, were introduced via spherical hinges on spreader beams supported on square steel plates (side equal to 150 mm and 40 mm thick).

The ends of the columns were horizontally fixed to the rig to prevent rotations and to allow for a moment transfer between the slab and the column. The load was applied monotonically until failure, by performing a series of loading steps. Between loading steps, crack development on the surface was manually tracked and drawn, both on the top and lateral sides.

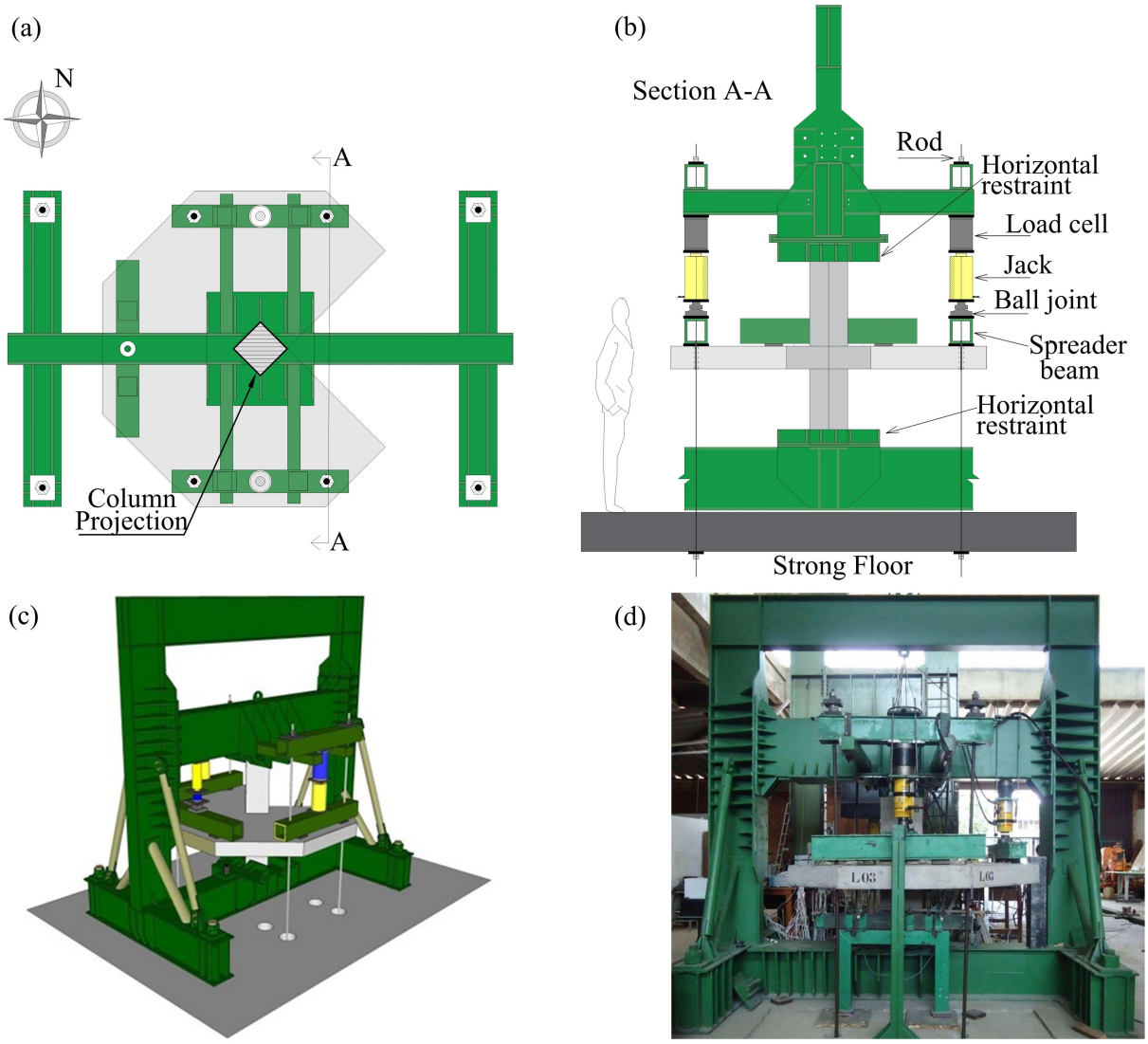

Fig. 5.8. Tests setup: (a) plan view; (b) section A-A; (c) 3D visualization section; and (d) specimen prepared.

5.4. Analysis of Test Results

5.4.1. Cracking, rotations and failure mode

For all specimens, the failure mode was punching shear, with development of a punching cone that could be clearly observed in the saw-cuts (Fig. 5.9). This failure surface extended from the bottom side of the column plate in the slab to the flexural reinforcement layer. Fig. 5.9 provides the load-rotation curves for all slabs (ψ_x, ψ_y and ψ_{xy} directions) cracking pattern on the top surface, cracks at of the re-entrant corner face and saw cut in a selected direction. The slab rotations are obtained for each considered direction using the corresponding LVDTs (for instance, LVDTs 1 and 4 in Fig. 5.7 for the ψ_y direction). This value is finally corrected by the measured column rotation (obtained using LVDTs 12-15 in Fig. 5.7). The rotations for the last load steps were obtained through extrapolation (dashed lines) from the obtained results before removing the LVDTs.

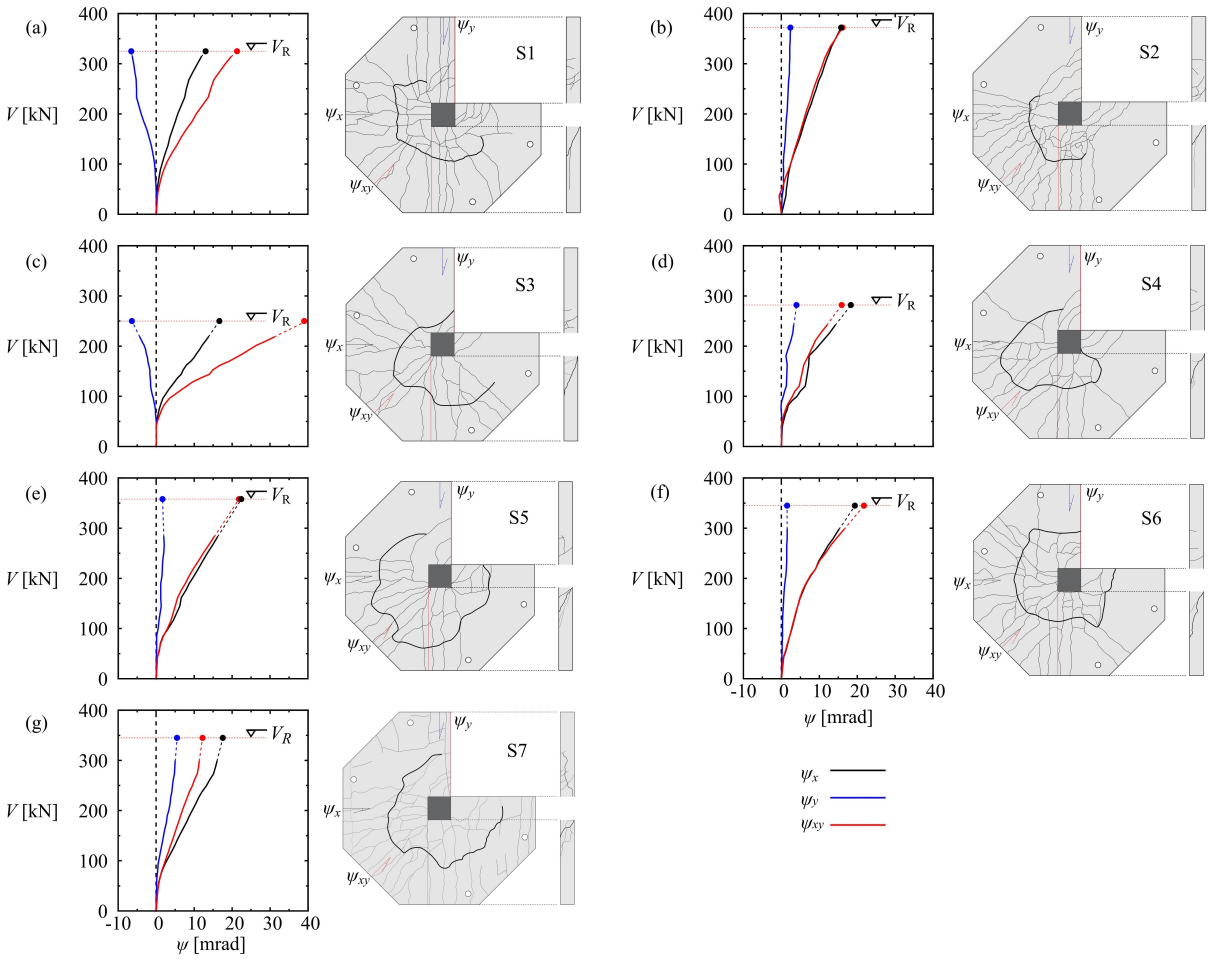

Fig. 5.9 - Load-rotations, top cracking pattern, side cracking pattern and cracks at selected saw cuts: (a) S1; (b) S2; (c) S3; (d) S4; (e) S5; (f) S6 (with edge reinforcement); and (g) S7.

Cracking on the top surface began at the two inner faces of the column (opposed to the re-entrant edges), with cracks along the interfaces with the column at approximately 19% to 32% of the ultimate load. The patterns that developed subsequently comprised four types of cracks on the top surface: (1) cracks radiating from the inner corner of the column and developing outward to the edges, (2) cracks substantially perpendicular to the inner column sides, also developing to the edges, (3) circumferential cracks, perpendicular to the previous, at distances from the column that increased with increasing load, (4) torsion cracks in the strips of the slab adjacent to the edges of the re-entrant corner.

A fully developed punching cone is identified for all tests. For the tests with a flexural reinforcement of 1.0% and lower eccentricity, the cracking reaches the re-entrant corners. With increasing reinforcement ratio, the punching cone was restricted to the two inner faces of the column. Shear cracking was also observed to reach one of the re-entrant corners for slab S3 and S4 (Fig. 5.9c-d).

The torsion cracks present at the re-entrant corner are also influenced by the eccentricity. In cases of lower eccentricities, torsion cracks were observed at the re-entrant edges at locations more distant from the connection. For larger eccentricities, the cracks were steeper and reached the re-entrant corner at points closer to the column. The presence of torsion reinforcement in the slab 6 reduced the number of cracks that could be observed near the re-entrant edges.

The load-rotation curves of all slabs are presented in Fig. 5.9a-b, showing that the load eccentricity has a significant influence on the rotations and failure load of the slab. After development of the first cracks and the consequent decrease in the stiffness of the slab, a notable increase in rotations was observed. In general, the increase in rotations is associated with a reduction in the ultimate load supported by the slab. For instance, comparing slabs S1 and S2 (nominally identical, but S1 with higher eccentricity), it can be noted that the maximum rotations (ψ_{xy}) in slab S1 were higher than those in slab S2, but associated to a lower failure load. However, the rotations in the x direction are practically identical between the two slabs. At the re-entrant edges, the higher load eccentricity results in negative rotations of 6.6 mrad for slab S1, while slab S2 exhibits positive rotations of about 2.3 mrad.

Fig. 5.9c-d shows the load-deflection curves of slabs S3 and S4, which have a lower reinforcement ratio. It is possible to observe a consistent response in terms of deflections when compared to slabs with higher reinforcement ratio (as slabs S1 and S2).

Comparing slabs S5 and S6 (where specimen S6 is nominally identical to S5 but with edge reinforcement), no major influence can be observed on the rotations or failure load (Fig. 5.9e-f). The slab S7 (test with lowest eccentricity) showed that the rotation in the *x* direction was clearly the highest (Fig. 5.9g), contrary to all other specimens (where the rotation in the *xy* direction was higher or comparable). In addition, slab S7 recorded a significant increase in the *y* (rotation along the re-entrant corner).

To compare the unitary resistance of the specimens with different eccentricity and flexural reinforcement ratio, the ultimate load was normalised by the square root of the concrete strength, effective depth, and basic control perimeter (defined as the geometrical perimeter located at 0.5*d* of the edge of the supported area). The results are presented in Fig. 5.10 By comparing the unitary resistance, it can be concluded that the increase in the reinforcement ratio resulted in higher unitary resistance, while the increase in the load eccentricity resulted in lower of resistance.

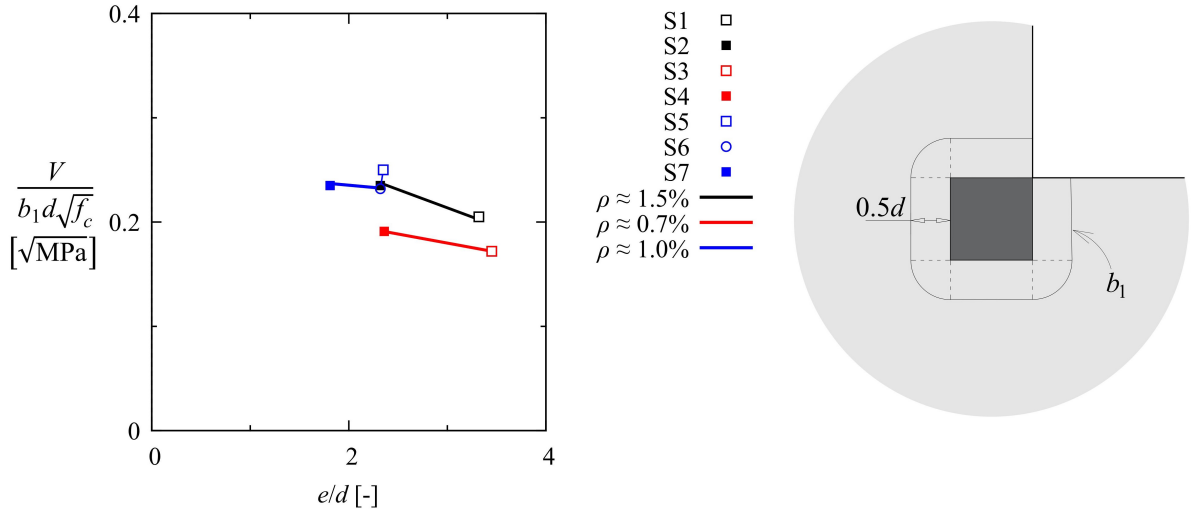

Fig. 5.10 - Normalized strength as a function of the load eccentricity of all tests.

5.4.2. Detailed measurements

5.4.2.1 Strains in top flexural reinforcement

Fig. 5.11 shows the profile of strains measured in the flexural reinforcement right before failure. The recorded strains were higher for the bars located near to the column. On the side of the re-entrant edge, the strains decrease rapidly with increasing distance to the column. On the other side (where the slab was continuous), the decrease in deformation occurs at a lower pace.

As it can be noted, the amount of flexural reinforcement had a direct impact on the deformation observed in the reinforcement (with higher levels of strain associated to lower reinforcement ratios). Yielding of the rebars was recorded in the specimens with lower reinforcement ratio ($\rho \approx 0.7\%$ and $\rho \approx 1.0\%$), while all instrumented bars remained elastic for the highest reinforcement ratio ($\rho \approx 1.5\%$).

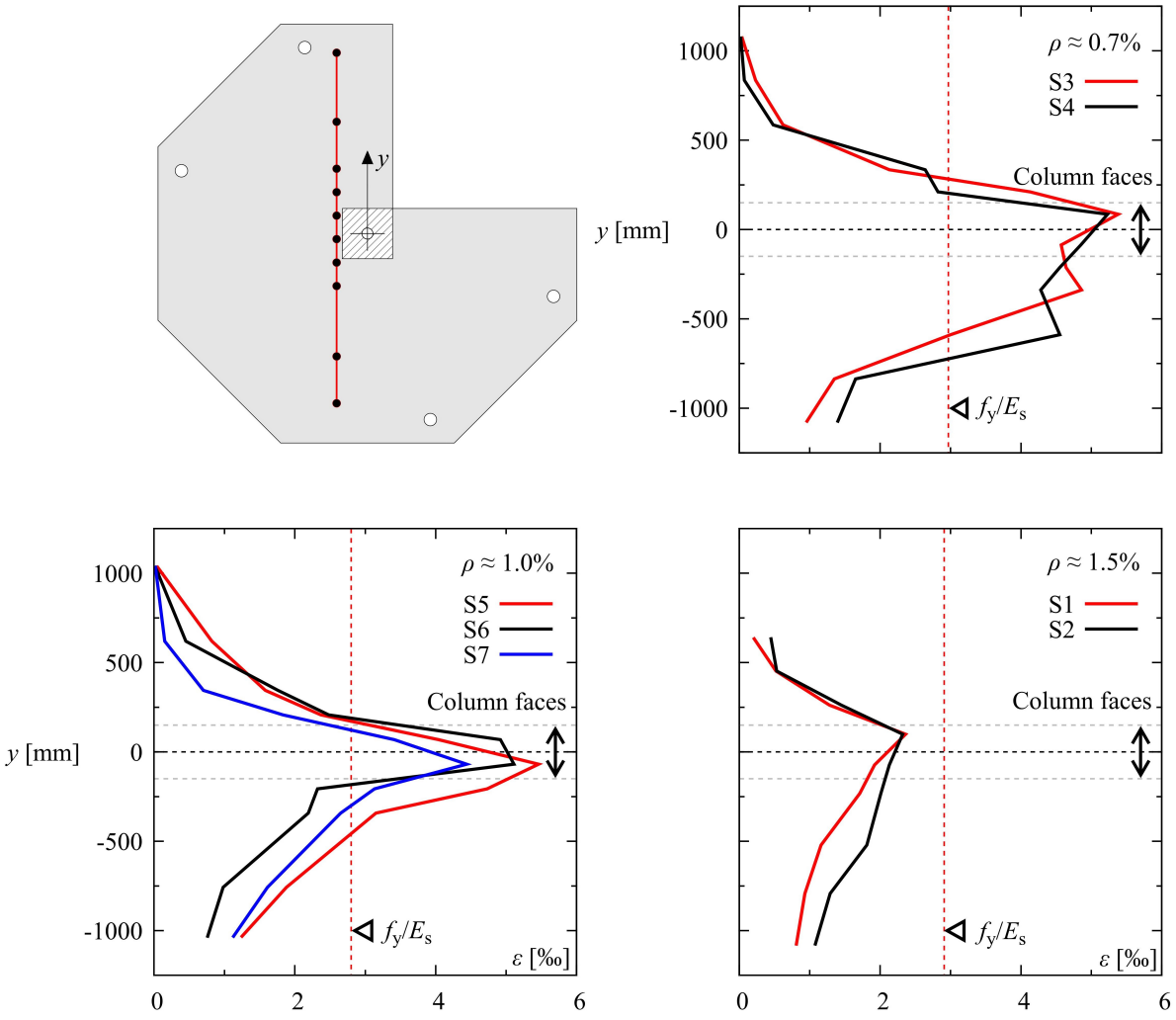

Fig. 5.11. Profile of strains in the flexural reinforcement of all tests.

The presence of torsion reinforcement in slab S6 did not show a significant change on the reinforcement stress when compared to the comparable slab S5 in the region of the free edge. This similar response is again in accordance with the fairly similar observed response in terms of failure load and associated deformation capacity. Further insight of the role of the edge reinforcement is shown in Fig. 5.12, depicting the strains in the edge reinforcement close to the column (according to the location of gages provided in Fig. 5.6).

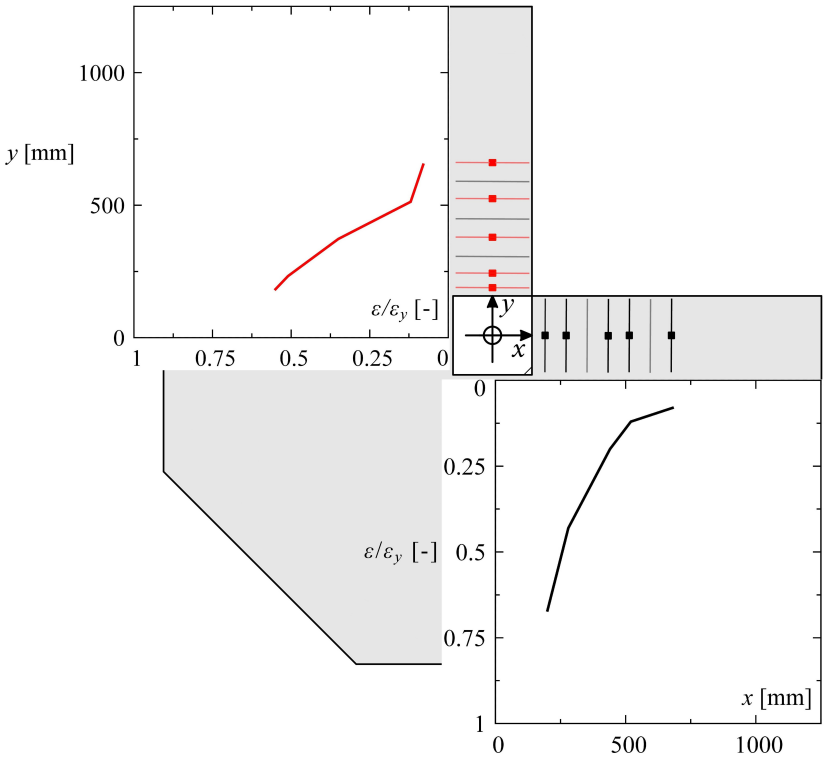

Fig. 5.12. Strains in edge reinforcement

The stirrups closest to the column showed a higher activation, in agreement to the location where torsion cracks were observed, reaching values close to 1.7‰. Such measurements show the significance of this reinforcement in the local control of torsional cracks, although the global response of the specimen was not significantly modified.

5.4.2.1 Strains at the concrete surface

Following the arrangement of gauges presented in Fig. 5.7, readings of the surface strains were recorded. The tangential and radial strains of concrete in specimens S1 and S2 are illustrated in Fig. 5.13. The radial strains were typically under compression, although near the rupture, some regions near the column developed tensile strains. This phenomenon is consistent with the development of a critical shear crack [16]. The highest values were observed near the column, in the internal region of slab, while the points located at the re-entrant corner presented significantly lower values. Concerning the tangential strains, they showed increasing compressive strains (as expected in such regions [16]). A similar trend was also observed for lower flexural reinforcement ratios (Fig. 5.14) or for moderate ratios (Fig. 5.15).

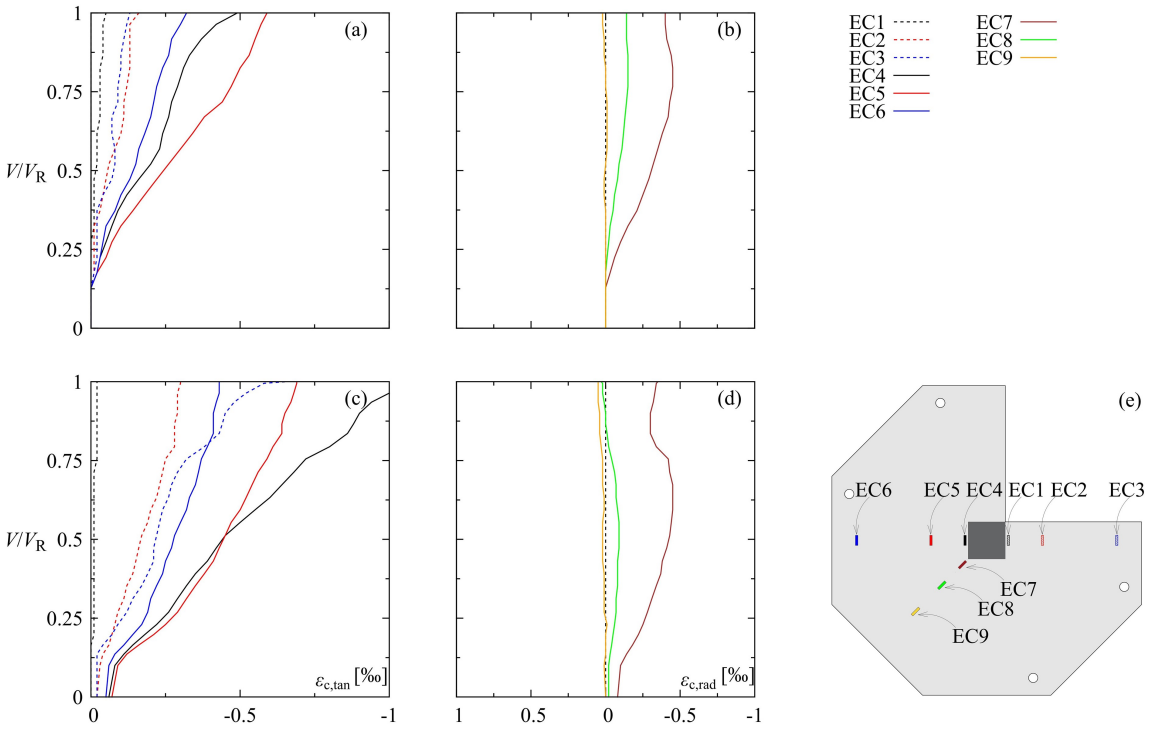

Fig. 5.13 - Surface strains at bottom surface: S1: (a-b) tangential and radial strains; and S2: (c-d) tangential and radial strains; and (e) location of gauges.

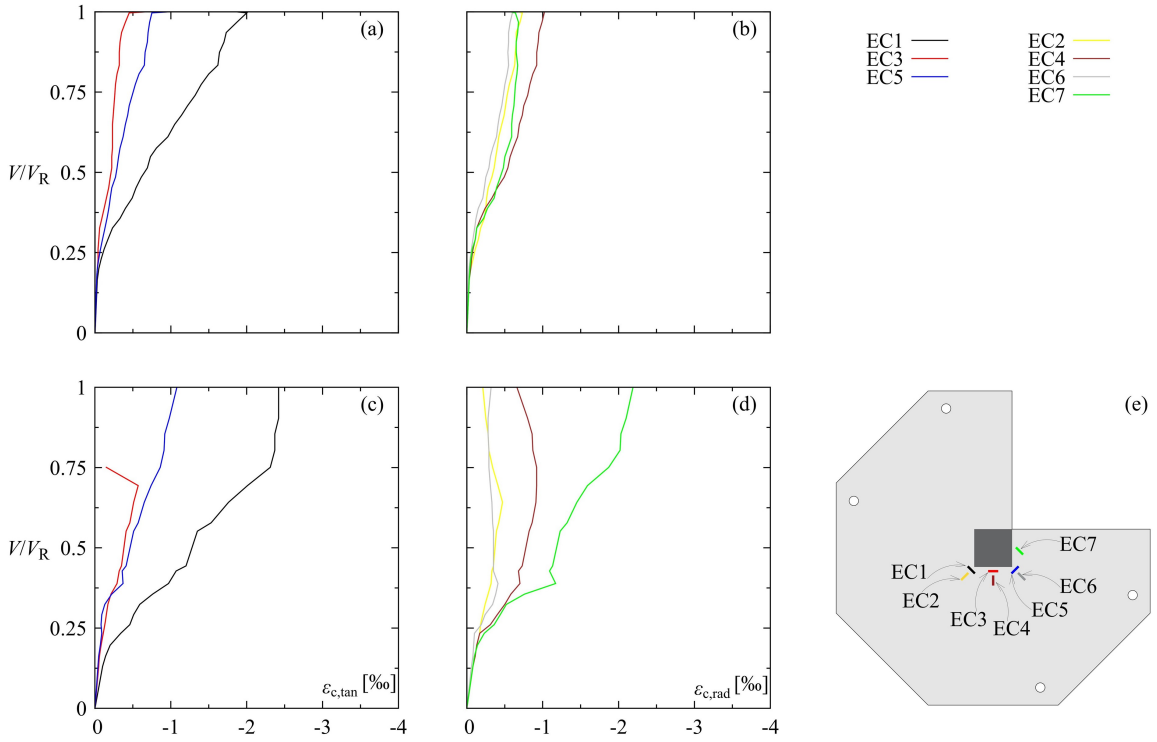

Fig. 5.14 - Surface strains at bottom surface: S3: (a-b) tangential and radial strains; and S4: (c-d) tangential and radial strains; and (e) location of gauges.

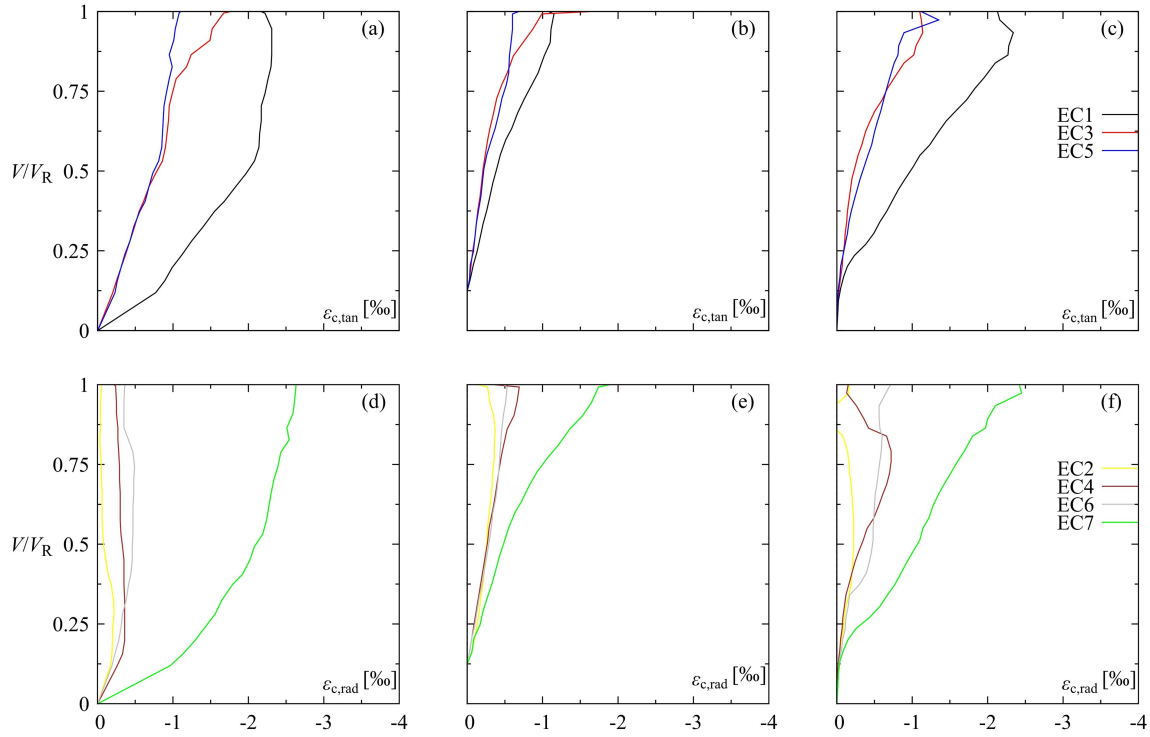

Fig. 5.15 - Surface strains at bottom surface: (a,d) S5; (b,e) S6; and (c,f) S7 (for location, refer to Fig. 5.14e).

Concerning the recorded deformations on the top surface (Fig. 5.16), surface gauges were arranged at 45° in an effort to align them with the potential compression struts originating due to torsion moments in this region. Compressive strains were recorded in several gauges indicating potentially relevant torsional moments (Fig. 5.16) but the measurements were not conclusive as the gauges intercepted in several cases flexural cracks (recording tensile strains).

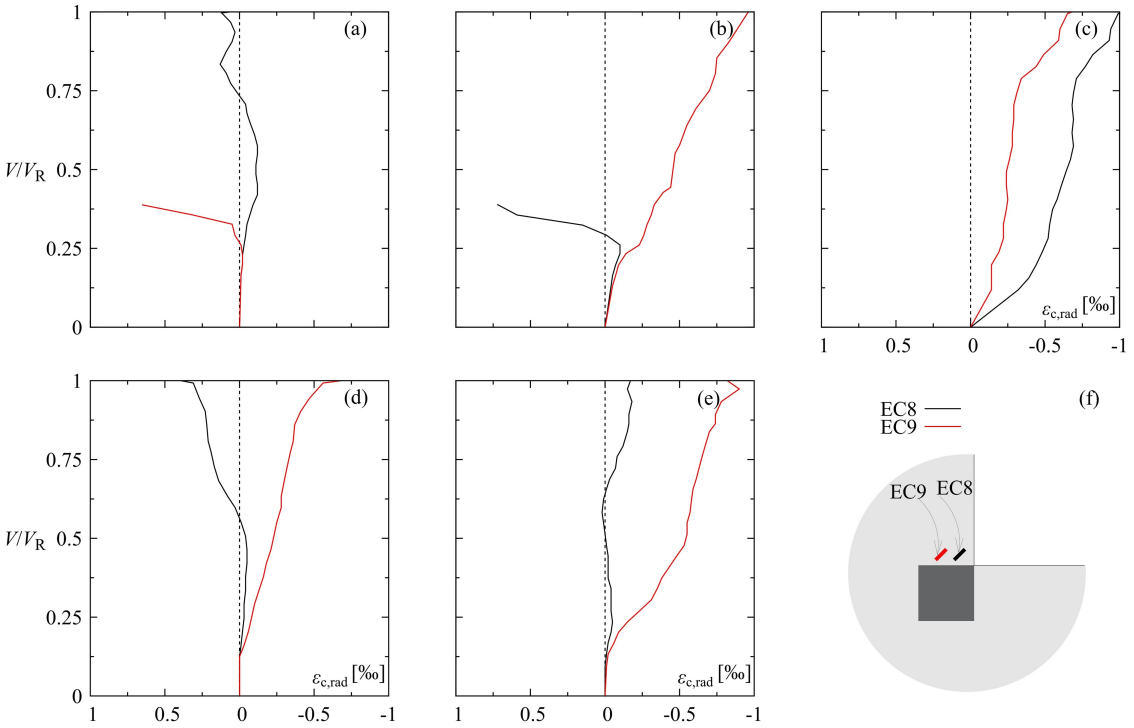

Fig. 5.16 - Radial strains at top surface of test: (a) S3, (b) S4, (c) S5, (d) S6 and (e) S7.

5.5. Comparison to Code Predictions

The accuracy of several codes of practice to predict the punching strength of re-entrant corner is presented in this section (details on the formulation used are given in Chapter 2). The selected codes are EN1992-1-1:2004 (Eurocode 2) [37], FEN 1992-1-1:2023 (draft for future revision of Eurocode 2) [40], ACI 318:19 [39], NBR 6118:2023 [36] and MC2010 (Level of Approximation II, corresponding to a typical design situation) [38].

Their design equations were applied accounting for the pertinent considerations in terms of geometry of the supported area and eccentricity of the shear force. For the comparisons performed, all safety factors were set to 1.0 and the characteristic or specified values of the resistances were replaced by the average ones.

Details of the comparison are presented in Table 5.3 and also in Fig. 5.17. In that Figure, the punching resistance is plotted against the eccentricity of the shear force. As it can be noted, the maximum punching resistance is obtained for a given eccentricity which corresponds to the distance between the centre of gravity of the control section and the axis of the column. For ACI 318:19 with straight corners and a perimeter at 0.5*d*, this eccentricity is 28 mm; for MC2010 and FEN with rounded corners and same distance of perimeter, the eccentricity is 21 mm; while for NBR and EC2, considering a perimeter at 2*d* from the column faces, this eccentricity results 86 mm.

For comparison purposes, the results are plotted in terms of the normalized failure loads $V/b_1 \cdot d \cdot f_c^{0.5}$ (as presented in Fig. 5.10) for each flexural reinforcement ratio (ρ). As expected (for sufficiently high eccentricities), the normalized punching resistance decreases with increasing eccentricity. The curves show in general a similar trend for all cases with a reasonable match to the decay observed in the experimental programme. However, the actual resistance of the specimens is higher than those predicted by codes (best matching being that of NBR 6118).

ACI 318:19 is the most conservative approach. Its degree of conservatism decreases however when the reinforcement ratios are intermediate or low, as well as when the load eccentricity is reduced (S7).

It is interesting to note that both NBR 6118 and EN1992-1-1:2004 provide a good representation of the experimental results, although they are fundamentally empirical. Their

average ratios of experimental to calculated punching resistance (V_R/V_{calc}) are 1.11 and 1.13, respectively (both standards are derived from the MC 1990 [38]).

The results of MC2010 and FEN are also very similar. Both codes are based on the Critical Shear Crack Theory, and result in safer estimates than EN1992-1-1:2004 and NBR 6118 but more accurate than ACI 318:19.

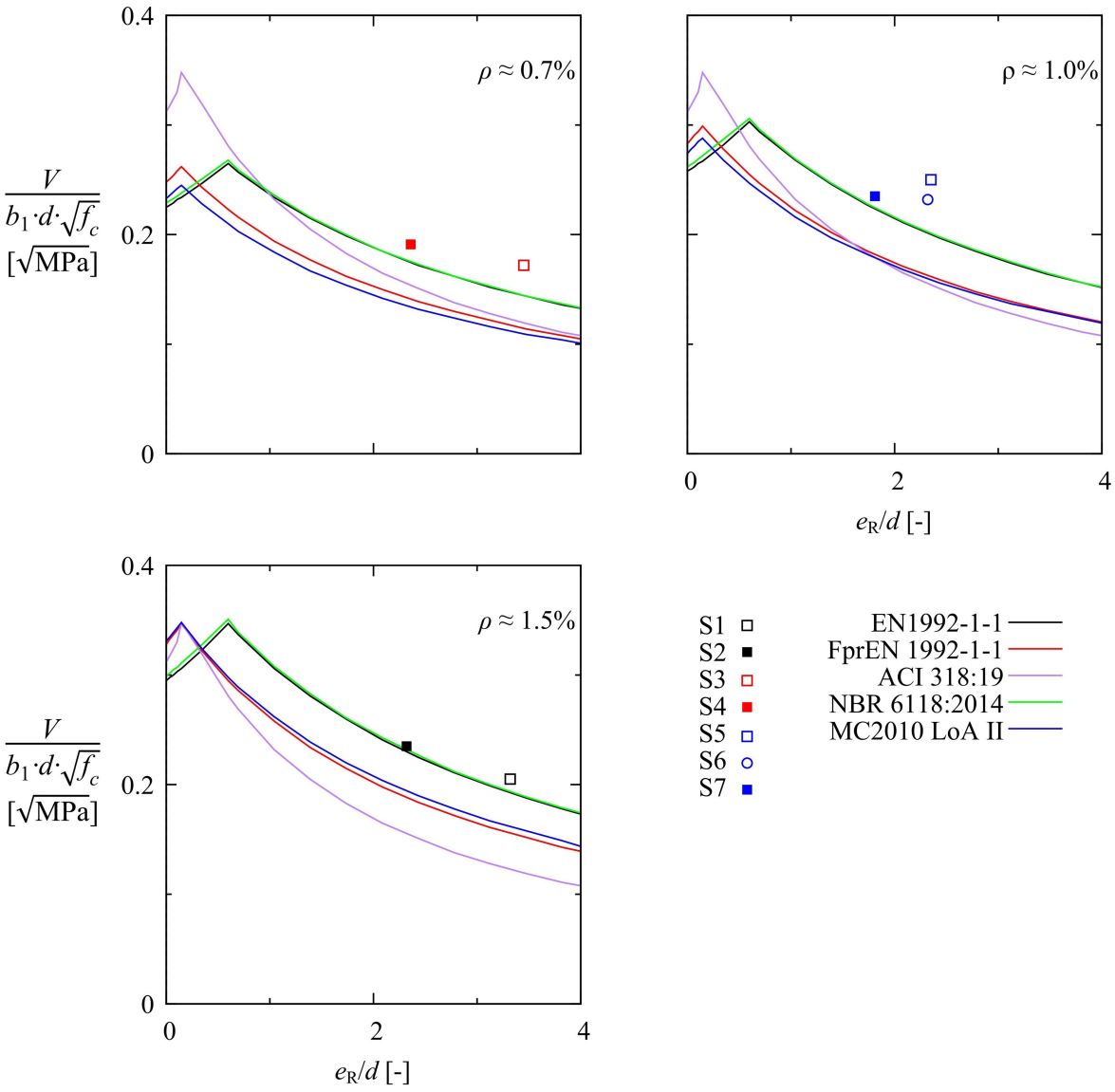

Fig. 5.17. Comparison of predictions and experimental results.

Table 5.3. Summary of experimental and theoretical resistances

Slab	V_R [kN]	NBR 6118		EN-1992		EN-1992		ACI 318		MC2010 - LoAII	
		V_{NBR} [kN]	V_R/V_{NBR} [-]	V_{EC2} [kN]	V_R/V_{EC2} [-]	V_{prEC2} [kN]	V_R/V_{prEC2} [-]	V_{ACI} [kN]	V_R/V_{ACI} [-]	V_{MC10} [kN]	V_R/V_{MC10} [-]
S1	325	303	1.07	301	1.08	243	1.34	193	1.68	248	1.31
S2	372	361	1.03	357	1.04	293	1.27	238	1.57	297	1.25
S3	250	212	1.18	209	1.19	168	1.49	174	1.44	163	1.53
S4	282	259	1.09	256	1.10	208	1.36	224	1.26	201	1.40
S5	358	289	1.19	286	1.25	231	1.55	220	1.62	233	1.54
S6	345	299	1.16	293	1.18	237	1.46	228	1.51	240	1.44
S7	345	328	1.05	324	1.06	264	1.31	261	1.32	272	1.27
		Avge	1.11		1.13		1.39		1.49		1.39
		CoV	0.05		0.06		0.07		0.10		0.08

From this comparison, it can be concluded that typical design equations for the case of re-entrant corners show a variable level of conservatism. In order to make a step forward in the design of these regions, the next section introduces a consistent mechanical model allowing to account for the peculiarities of this connection detail.

5.6. Detailed Analysis and Punching Design of Re-entrant Corner Connections Based on the Critical Shear Crack Theory

5.6.1. Shear Field Analysis

The analysis of the shear field in a flat slab allows investigating the concentrations of shear forces in the critical regions of slab-column connections. This analysis is particularly relevant in situations where significant loads act near supported areas [44], rectangular columns [45] or when openings are present [46]. On the basis of shear fields, the shear-resisting control perimeter can be determined by using Equation (5.3), proposed by Vaz Rodrigues *et al.* [47] and later adopted by MC2010 [39].

$$b_0 = \frac{V}{v_{perp,\max}} \tag{5.3}$$

where b_0 is the length of the shear-resisting control perimeter, V is the total acting shear force and $v_{perp,\max}$ is the maximum unitary shear force perpendicular to a basic control perimeter located at $0.5d$ from the supported area. This equation is typically based on a linear-elastic distribution of the shear field, which ensures robust and simple analyses (although it can be generalised for nonlinear shear fields). Concerning the elastic analysis, it is normally performed considering a reduced value of the Poisson's coefficient ($\nu = 0$) and of the shear modulus ($G = G_{el}/8 = E/16$) to account for the response of cracked concrete [48].

Fig. 5.18 illustrates the influence of eccentricity on the elastic distribution of unitary shear forces, and consequently the resulting reduction in the effective shear resisting perimeter (b_0) as the eccentricity increases for specimens S1, S2 and S7. The analysis of the shear field reveals that the shear forces tend to concentrate around the inner corner of the column for higher eccentricities but are more uniform when the eccentricity is lower and close to the centre of gravity of the basic control perimeter, consistently to previous studies on the shear field response [44]-[45].

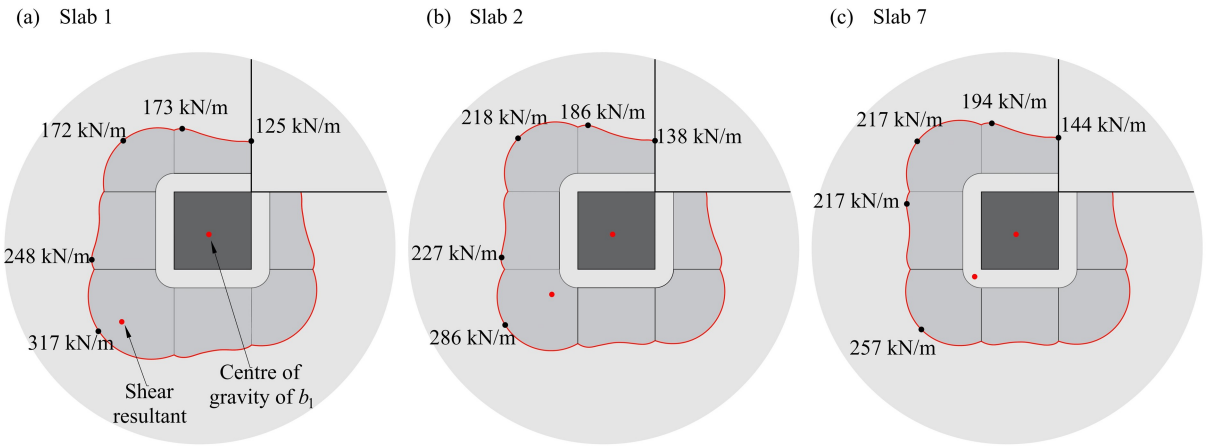

Fig. 5.18. Linear elastic distribution of shear forces (kN/m) along control perimeters at $d/2$ of the applied loads: (a) Slab S1; (b) Slab S2; and (c) Slab S7. (Maximum nominal shear force shown for a total applied load $V = 300$kN).

5.6.2. Punching Resistance

On the basis of the previous results, the punching shear capacity can be assessed in a refined manner by using the principles of the Critical Shear Crack Theory (CSCT). In accordance with this theory, the punching shear strength decreases for increasing crack openings increase. According to this assumption, Muttoni [16] proposed the failure criterion given (5.4), which assumes that the width of the critical crack is proportional to the slab rotation multiplied by the effective depth of the member ($w \propto \psi \cdot d$), a comprehensive review of this theory and more refined approaches can be consulted elsewhere [8]).

$$V_R = \frac{0.75 \cdot b_0 \cdot d \cdot \sqrt{f_c}}{1+15\frac{\psi \cdot d}{d_{g0}+d_g}} \tag{5.4}$$

where b_0 refers to the length of the shear-resisting control perimeter, d to the shear-resisting effective depth (considering the penetration of the supported area), d_g to the maximum aggregate size and d_{g0} to a reference size (set to 16 mm for normal strength concrete). The relationship between the acting shear force and the rotation of the slab may be estimated using different Levels-of-Approximation. Hereafter, the following expression will be used [16] relating the rotations to the level of shear force and the flexural resistance of the slab:

$$\psi = 1.5 \cdot \frac{r_s}{d} \cdot \frac{f_y}{E_s} \left(\frac{V}{V_{flex}}\right)^{3/2} \tag{5.5}$$

where r_s refers to the distance between the centre of the supported area and the point of contraflexure of bending moments, d to the effective flexural depth in the appropriate direction, f_y to yield strength, E_s to the modulus of elasticity of the steel and V_{flex} to the flexural resistance of the slab (calculated according to Annex B). It can be noted that the value of parameter r_s is significantly different at each side of the column. It is relatively high at the inner side ($r_s \approx 1080$ mm) and very low at the side close to the edge ($r_s \approx 200$ mm). This leads to the fact that the rotations at the inner side are also significantly higher than in the side close to the edge (according to Eq. (5.5). Such result is consistent with the experimental results, as can be seen in Fig. 5.9.

As demonstrated in previous works [44],[45], Eq. (4) may be used to assess the resistance of the complete control perimeter or of different sectors composing it. The latter approach allows considering that some regions of the control perimeter may govern the strength (or even be in a softening response) while others have still the capacity to increase their contribution [44]. Such consideration leads in general to more accurate estimates of the punching resistance. In order to apply this methodology to the present case, the distribution of perimeters shown in Fig. 5.19b-c is adopted (consistently with [43,44]). On that basis, the effective length of each sector can be calculated by using Eq. (3). In addition, the value of parameter r_s for each sector is estimated using the results of a linear elastic finite element analysis (Fig. 5.19a).

According to the approach based on sectors [49], the total shear resistance (V_R) can be calculated by adding the shear force contribution at different sectors. In the present case, two governing cases may occur: failure at the inner faces of the column (sector A) or close to the re-entrant edge (sector B). The punching shear resistance is finally determined by summing the calculated contribution for the governing sector and the corresponding shear carried by the other sector.

The latter is estimated proportional to the elastic distribution of shear forces by means of a ratio named λ_i (ratio between the shear force carried by sector "*i*" with respect to the total shear force $\lambda_i = V_{sector,i}/V$). These ratios are given in Fig. 5.19b-c for the different cases investigated. As it can be noted, most of the shear force is actually carried by the inner sides of the column (with a ratio depending upon the eccentricity of the shear force).

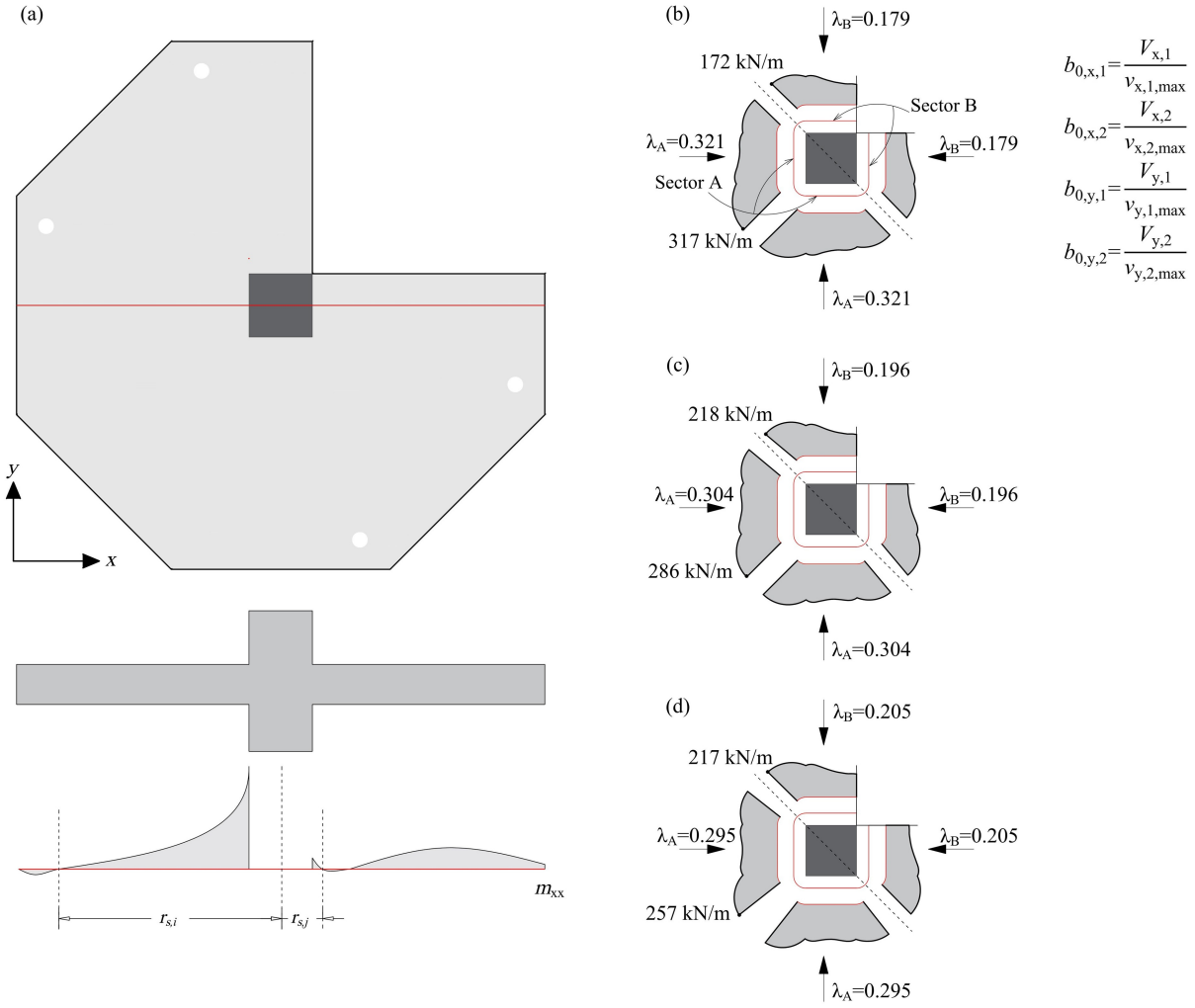

Fig. 5.19 - Definition of support strip widths and reduced control perimeters for the punching shear: (a) definition of r_{sij} distances; shear force distribution for sector A and B (b) Slab 1; (c) Slab 2 and (d) Slab 7.

For instance, in the sector A is governing, $V_{R,A}$ refers to the punching resistance of sector A and the total shear resistance results from adding this term to the corresponding contribution of sector B ($V_{R,B} = \lambda_B V = (\lambda_B/\lambda_A V_{R,A})$. A similar case may result in case sector B were governing, resulting into:

$$V_R = \min \begin{cases} V_{R,A}(1 + \lambda_B/\lambda_A) \\ V_{R,B}(1 + \lambda_A/\lambda_B) \end{cases} \tag{5.6}$$

Table 5.4 presents the calculated values of the punching resistance following this approach (as well as of parameters b_0, r_{sij} and V_{flex}). For all slabs, failure was governed by the concrete strength in sector A, which shows the highest cracking and rotation (Fig. 5.9). The results show consistent agreement between the experimental and theoretical results, with an average ratio of measured-to-calculated resistance equal to 1.02 and a low Coefficient of Variation (7%). It can also be noted that, as sector A was governing, the arrangement of shear reinforcement (specimen S6) had little influence in the test results (and is neglected in the presented analyses).

Table 5.4. The punching shear strength predicted using CSCT.

Slab	b_0 [mm]	$r_{sx,1}$ [mm]	$r_{sx,2}$ [mm]	V_{flex} [kN]	V_R / V_{flex} [-]	V_{CSTC} [kN]	V_R / V_{CSTC} [-]
S1	946	217	1085	656	0.50	335	0.97
S2	1049	175	1065	805	0.46	408	0.91
S3	946	217	1085	308	0.81	233	1.07
S4	1049	175	1065	387	0.73	279	1.01
S5	1049	175	1065	521	0.69	316	1.13
S6	1049	175	1065	539	0.64	326	1.06
S7	1166	162	1060	584	0.59	341	1.01
						Avge	1.02
						CoV	0.07

The CSCT approach is thus observed to be consistent for the punching design of re-entrant slab-column connections. It may be noted that some refinements are possible (as distinguishing between straight and curved segments or considering for the softening response in some regions) but the obtained level of accuracy is already very good.

5.7. Conclusions

This paper investigates on the punching response of re-entrant slab-column connections. To that aim, an experimental programme is presented comprising seven reinforced concrete slabs. This programme was performed with detailed instrumentation allowing to get insights on the mechanical response of the specimens. On that basis, a comparison to current design codes is presented and the mechanical model of the Critical Shear Crack Theory (CSCT) is adapted for a tailored design. The main conclusions of this investigation are listed below:

1. The parameters governing the level of deformation influence the resistance. In particular, lower reinforcement ratios and higher eccentricities, associated to higher levels of deformation for a given acting shear force, are associated to lower punching resistances.
2. The presence of a potential edge reinforcement near to the supported area helps in controlling the cracks observed at edges. Nevertheless, the global behaviour and resistance is little modified if that region is not governing at failure.
3. Reinforcement bars perpendicular to the edges of the re-entrant corners (and thus without continuity) have low levels of strain. On the contrary, those reinforcement presenting continuity are highly efficient to control the deformations and thus to increase the shear resistance.
4. The governing rotation might be parallel to the slab edges or in a diagonal direction. This depends on the level of eccentricity of the shear force.
5. A detailed analysis of the surface strains of the concrete indicate a similar response as that of inner slab-column connections, compatible with the development of a critical shear crack.
6. Design codes reproduce reasonably well the trend that the flexural reinforcement and load eccentricity have on the response when compared to the performed tests. However, they fail in predicting the level of resistance, which appears to be highly conservative in several cases.
7. A mechanical model based on the CSCT shows very good agreement to test results in terms of failure mode and estimated strength. The CSCT allows accounting in a realistic manner for the eccentricity of the shear force and for the different response of the shear-critical regions. This improves the mechanical understanding of the phenomenon and allows for refined evaluations of the response of the connection.

5.8. References

[1] Regúlez B, Faria DMV, Todisco L, Fernández Ruiz M, Corres H. Sustainability in construction: The urgent need for a new ethics. Struct Concr 2023; 24-2:1893-913. https://doi.org/10.1002/suco.202200406

[2] Fürst A, Marti P. Robert Maillart's design approach for flat slabs. Journal of Structural Engineering 1997;123-8:1102-10. https://doi.org/10.1061/(ASCE)0733-9445(1997)123:8(1102)

[3] Megally S, Ghali A. Cautionary note on shear capitals. Concrete International 2002; 24-3:75-83.

[4] Hashemi SS, Sadeghi K, Vaghefi M, Siadat SA. Evaluation of ductility of RC structures constructed with bubble deck system. Int J Civil Eng 2018; 16-5:513-26. https://doi.org/10.1007/s40999-017-0158-y

[5] Nicácio WG, Barros JAO, Melo GSSA. Punching behavior of bubbledeck type reinforced concrete slabs. Struct Concr 2019;21-1;262-77. https://doi.org/10.1002/suco.201900176

[6] Valivonis J, Skuturna T, Daugevičius, M, Šneideris. Punching shear strength of reinforced concrete slabs with plastic void formers. Constr Build Mater 2017, 145: 518-27. https://doi.org/10.1016/j.conbuildmat.2017.04.057

[7] Pei Shuangxi. An investigation into the punching Shear Failure in RC Waffle Slabs Subjected to Concentrated Load. 1994. Tesis Doctoral. University of Abertay Dundee.

[8] Simões JT, Fernández Ruiz M, Muttoni A. Validation of the Critical Shear Crack Theory for punching of slabs without transverse reinforcement by means of a refined mechanical model. Struct Concr 2018;19-1:191-216. https://doi.org/10.1002/suco.201700280

[9] Taylor HP. Investigation of the Dowel Shear Forces Carried by the Tensile Steel in Reinforced Concrete Beams. Tech Rept TRA 431, Cement and Concrete Association 1969, pp24.

[10] Walraven JC. Fundamental Analysis of Aggregate Interlock. ASCE J Struct Eng 1981; 107-11:2245-70. https://doi.org/10.1061/JSDEAG.0005820

[11] Vecchio FJ, Collins MP. The Modified Compression-Field Theory for Reinforced Concrete Elements Subjected to Shear. ACI J 1986; 83-2: 219-31.

[12] Hordijk DA. Tensile and tensile fatigue behaviour of concrete, experiments, modelling and analyses. Heron 1992;37-1:3-79.

[13] Kinnunen S. Punching of concrete slabs with two-way reinforcement, Transactions of the Royal Institute of Technology, No. 198, 112 p. Sweden: Stockholm; 1963.

[14] Nielsen MP, Braestrup MW, Jensen BC, Bach F. Concrete plasticitiy-beam shear-punching shear-shear in joints. Danish Society for Structural Science and Engineering. Copenhagen, Denmark; 1978.

[15] Andrä HP. Zum Tragverhalten von Flachdecken mit Dübelleisten-Bewehrung im Auflagerbereich. Beton-und Stahlbetonbau 1981; 76-3:53-57. (in German)

[16] Muttoni A. Punching shear strength of reinforced concrete slabs without transverse reinforcement. ACI Struct J 2008; 105-4:440-50. https://doi.org/10.14359/19858

[17] Fernández Ruiz M, Muttoni A. Applications of the critical shear crack theory to punching of R/C slabs with transverse reinforcement. ACI Struct J 2009; 106-4:485-94. https://doi.org/10.14359/56614

[18] Broms CE. Tangential strain theory for punching failure of flat slabs. ACI Struct J 2016; 113-1:95-104. https://doi.org/10.14359/51687942

[19] Fraile DH, Setiawan A, Santos JB, Muttoni A. Punching tests on edge slab-column connections with refined measurements. Eng Struct 2023; 288:1-24. https://doi.org/10.1016/j.engstruct.2023.116166

[20] Hanson NW, Hanson JM. Shear and moment transfer between concrete slabs and columns. Portland Cement Association, Research and Development Laboratories 1968; 11-68:2-16.

[21] Stamenkovic A, Chapman JC. Local strength of flat slabs at column heads. CIRIA-Report 39, London; 1972. 81pp.

[22] Narayani N. Shear reinforcement in reinforced concrete column heads. Ph.D. Thesis, Faculty of Engineering, Imperial College of Science and Technology, London, UK, 1971.

[23] Regan PE. Tests of Connections between Flat Slabs and Edge Columns. London, UK: School of Architecture and Engineering, University of Westminster; 1993.

[24] Zaghlool R, Rawdon de Paiva H, Glockner P. Tests of reinforced concrete flat plate floors. J Struct Div Proc Am Soc Civ Eng 1970;96-3:487-507.

[25] Sudarsana IK. Punching shear in edge and corner column slab connections of flat plate structures. University of Ottawa; 2001. PhD thesis.

[26] Ritchie M, Ghali A, Dilger W, Gayed RB. Unbalanced moment resistance by shear in slab-column connections: experimental assessment. ACI Struct J 2006;103-1:74-82. https://doi.org/10.14359/15088

[27] Zaghloul, A. Punching shear strength of interior and edge column-slab connections in CFRP reinforced flat plate structures transferring shear and moment. University of Ottawa; 2007. PhD thesis.

[28] Albuquerque NGB, Melo GS, Vollum RL. Punching shear strength of flat slab-edge column connections with outward eccentricity of loading. ACI Struct J 2016; 113-5:1117-29. https://doi.org/10.14359/51689156

[29] Hammill N, Ghali A. Punching shear resistance of corner slab-column connections. ACI Struct J 1994;91-6:697-705. https://doi.org/10.14359/1502

[30] Stamenkovic A, Chapman J. Local strength at column heads in flat slabs subjected to a combined vertical and horizontal loading. Instit Civil Eng 1974;57-2:205-32.

[31] Walker P, Regan P. Corner column-slab connections in concrete flat plates. J Struct Eng 1987;113-4:704-20.

[32] Desayi P, Seshadri HK. Punching shear strength of flat slab corner column connections. In Part 1. Reinforced Concrete Connections, Department of Civil Engineering, Indian Institute of Science: Bangalore, India, 1997; 122-1:10-20.

[33] Vocke H, Eligehausen R. Durchstanzen von Flachdecken im Bereich von Rand- und Eckstützen. Beton- und Stahlbetonbau 2003; 98:66-73. (in German) https://doi.org/10.1002/best.200300380

[34] Cheng MY, Giduquio MB. Experimental study of corner slab-column connection. ACI Struct J 2014; 111-5:1123-34. https://doi.org/10.14359/51686817

[35] Giduquio MB, Cheng MY, Dlamini LS. Reexamination of strength and deformation of corner slab-column connection with varied slab reinforcement ratio. ACI Struct J 2019; 116-2: 53-63. https://doi.org/10.14359/51712276

[36] Associação Brasileira de Normas Técnicas, Design of Concrete Structures - Procedures, ABNT NBR 6118, 2023.

[37] Design of Concrete Structures—General Rules and Rules for Buildings, EN 1992-1-1. Brussels, Belgium: CEN European Committee for Standardization; 2004, 225 p.

[38] Comité Euro-International du Béton/Fédération Internationale de la Précontrainte: Model Code for Concrete Structures; 1990.

[39] ACI Committee 318. Building Code Requirements for Structural Concrete (ACI 318- 19) and Commentary, 624. Farmington Hills, USA: American Concrete Institute; 2019.

[40] *fib* Model Code for Concrete Structures 2010, *fib*. First Edition UK 2013. https://doi.org/10.1002/9783433604090

[41] FEN 1992-1-1:23. Eurocode 2-Design of concrete structures- Part 1-1: General rules, rules for buildings, bridges and civil engineering structures, Stable version of the draft of the 2nd generation of EN 1992-1-1:23, CEN, Brussels, Belgium, 2023, pp 405.

[42] Ferreira, M. P. (2010). Punção em Lajes Lisas de Concreto Armado com Armaduras de Cisalhamento e Momentos Desbalanceados. Tese de Doutorado em Estruturas e Construção Civil, Publicação E.TD – 007 A/10 Departamento de Engenharia Civil e Ambiental, Universidade de Brasília, Brasília, DF, 275p.

[43] Ferreira M. P., Oliveira M. H., Melo G. S. S.A. Tests on the punching resistance of flat slabs with unbalanced moments. Eng Struct 2019;196:1-13. https://doi.org/10.1016/j.engstruct.2019.109311

[44] Sagaseta J, Muttoni A, Fernández Ruiz M, Tassinari L. Non-axis-symmetrical punching shear around of RC slabs without transverse reinforcement. Mag Concr Res 2011;63-6:441. https://doi.org/10.1680/macr.10.00098

[45] Sagaseta J, Tassinari L, Fernández Ruiz M, Muttoni A. Punching of flat slabs supported on rectangular columns. Eng Struct 2014;77:17-33. https://doi.org/10.1016/j.engstruct.2014.07.007

[46] dos Santos JB, Muttoni A, de Melo GS. Enhancement of the punching shear verification of slabs with openings. Struct Concr 2023;24-2:3021-38. https://doi.org/10.1002/suco.202200714

[47] Vaz Rodrigues R, Fernández Ruiz M, Muttoni M. Shear strength of R/C bridge cantilever slabs. Eng Struct 2008;30:24-33. https://doi.org/10.1016/j.engstruct.2008.04.017

[48] Natário F, Fernández Ruiz M, Muttoni, A. Shear strength of RC slabs under concentrated loads near linear supports. Eng Struct 2014;76:10-23. https://doi.org/10.1016/j.engstruct.2014.06.036

[49] dos Santos JB, Melo GdS, Fernández Ruiz M. Punching performance of flat slabs with openings accounting for the influence of moment transfer and shear reinforcement. Eng Struct 2024;303:1-19. https://doi.org/10.1016/j.engstruct.2024.117461

6. CHAPTER VI: PUNCHING SHEAR IN FLAT SLABS WITH RE-ENTRANT CORNER COLUMNS AND SHEAR REINFORCEMENT

This chapter is the postprint version of the article titled **Punching shear in flat slabs with re-entrant corner columns and shear reinforcement** published in Volume 310 of the journal Engineering Structures in 2024 (DOI: https://doi.org/10.1016/j.engstruct.2024.118098). The authors of this publication are João Paulo de Almeida Siqueira (DSc Candidate), Elaine Jaricuna Pereira de Albuquerque (Professora at UFRR), Miguel Fernández Ruiz (Professor at UPM and DSc advisor during Sandwich Program) and Guilherme Sales de Melo (Full Professor at UnB and thesis director). The complete reference is the following:

- Siqueira J. P. A., Albuquerque E. J. P., Fernández Ruiz M., Melo G. S., *Punching shear in flat slabs with re-entrant corner columns and shear reinforcement*, Engineering Structures, Vol. 310, 24 p., 2024. DOI: 10.1016/j.engstruct.2024.118098.

The main contributions of João Paulo de Almeida Siqueira to the creation of this article were the following:

- Performing all the calculations presented in article;
- Analyse the presented results;
- Production of the figures included in the article;
- Preparation of the manuscript of the article.

6.1. Abstract

Despite the great variety of cases concerning slab-column connections found in practice, most research has concentrated so far on the punching resistance of inner columns without moment transfer. Other cases, such as edge or corner columns, have attracted less research attention despite their practical relevance. Within this context, re-entrant corner columns are a commonly used detail in practice (i.e. columns at corners of openings) where almost no experimental evidence is available and design codes typically extrapolate design recommendations from other cases. In order to advance the knowledge in this field, this paper presents an experimental and theoretical investigation on the punching resistance of slab-column connections in re-entrant corners. The research is addressed at specimens with and without shear reinforcement and introduces the results of an experimental programme on specimens reproducing realistic conditions in terms of size and loading arrangement. The experimental results are first analysed according to several design guidelines, highlighting their shortcomings. On that basis, a theoretical approach for punching design is proposed based on the Critical Shear Crack Theory. Such approach is aimed at understanding the mechanics of punching failure and to lead to consistent predictions on the resistance and deformation capacity of the slab-column connections.

Keywords: flat slab, punching shear, re-entrant corner, shear reinforcement, Critical Shear Crack Theory.

6.2. Introduction

Punching shear in reinforced concrete slabs is typically a brittle failure mode developing in the vicinity of concentrated loads. Such failure is particularly relevant in slab-column connections, as it may propagate leading to the progressive collapse of the structure [1]-[2]. Different alternatives can be adopted to enhance the punching shear response. Some of them allow increasing the failure load but may limit its deformation capacity as, for instance, increasing the flexural reinforcement ratio (see Fig. 6.1a). Others allow increasing both the failure load and also the deformation capacity as for instance increasing the resistance of the concrete (see Fig. 6.1b) or the size of the supported area. One of the most efficient manners to enhance the performance of slab-column connections has been acknowledged to arrange shear reinforcement, which increases in a significant manner both the resistance and the deformation capacity by reinforcing the shear-critical region, see Fig. 6.1c.

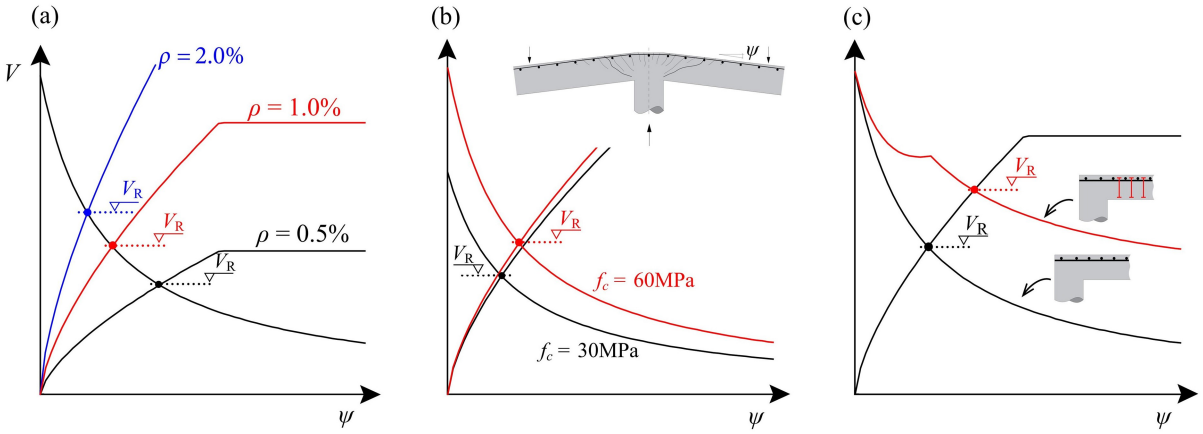

Fig. 6.1 - Enhancement of punching shear resistance (load-rotation response according to the Critical Shear Crack Theory principles [3]-[4]): (a) influence of flexural reinforcement ratio; (b) influence of concrete resistance; and (c) arrangement of punching shear reinforcement.

In the scientific literature, various types of shear reinforcement have been investigated in the past, including bent-up bars [5]-[8], stirrups [5],[9]-[12], headed shear studs[6],[9],[13]-[16] and shearheads [6],[17]. Database investigations relating to various types of reinforcement can be found in the literature [20]-[22]. The large variety of punching shear reinforcement solutions currently available is due to the various possibilities to provide anchorage for the shear reinforcement [18]-[19] as well as due to the search for simple and efficient systems in terms of cost and installation.

Many studies have been conducted so far on the beneficial effect of shear-reinforcement on the punching performance [23]-[30]. They have been based mostly on the response of inner slab-column connections without moment transfer, although some references may be found with moment transfer [31]-[37], edge [19]-[29] or corner [24]-[26], [49]-[52] slab-column connections. According to these studies, three failure modes may govern in general the performance of shear-reinforced slabs. They refer to the maximum punching shear resistance (associated to failures by concrete crushing near to the supported area, Fig. 6.2a), localization of strains in a crack within the shear-reinforced zone (Fig. 6.2b) and punching outside of the shear-reinforced area (Fig. 6.2c).

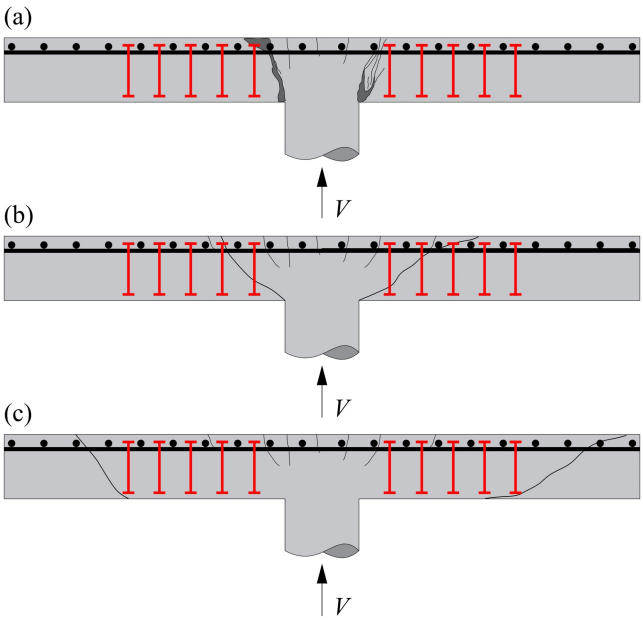

Fig. 6.2. Failure modes in punching for shear-reinforced slabs (adapted from [4]): (a) maximum punching strength; (b) failure within the shear-reinforced zone; and (c) failure outside the shear-reinforced zone.

Despite previous research efforts, many cases are found in practice that have not been investigated specifically and whose design is performed by extrapolation of other situations. One important case for buildings refers to slab-column connections in re-entrant corners. This situation is not only found at corners of L- or C-shaped buildings (Fig. 6.3a), but also at inner patios (Fig. 6.3b). Until recently, tests on slab-column connections at re-entrant column corners were not available in the literature. Recently, Siqueira *et al.* [53] presented the first tests addressed at this case, focusing on slabs without shear reinforcement.

The results showed the relevance of several parameters, such as the moment transfer or flexural reinforcement, as well as the importance of considering a suitable analysis of the shear-field near to the supported area.

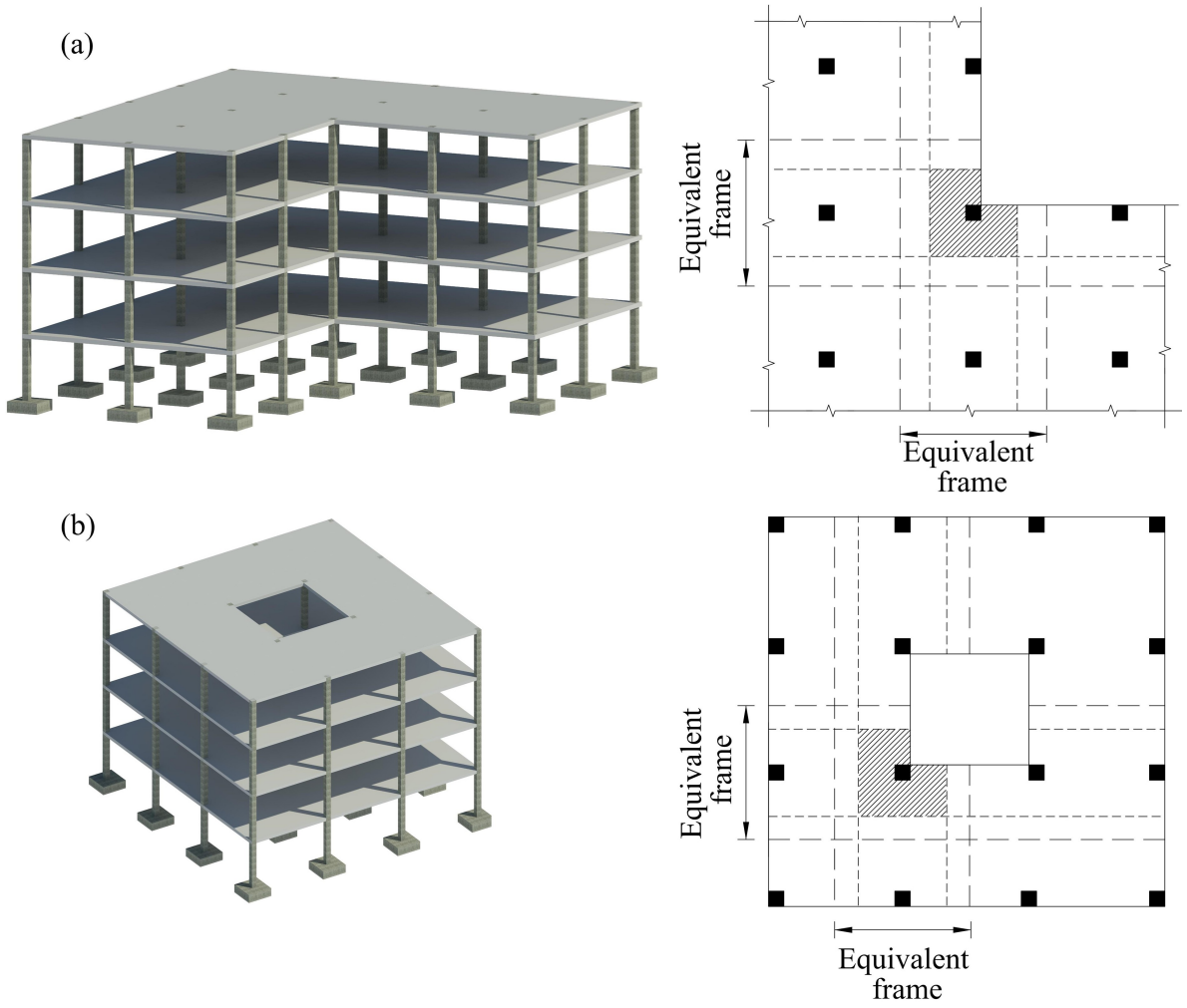

Fig. 6.3. Building with re-entrant corner and equivalent frames: (a) L-shaped building; (b) inner.

In this paper, similar tests in terms of geometry as those of Siqueira *et al.* [53] are introduced, but focusing on the role of shear reinforcement in the response, both in terms of resistance and deformation capacity. The experimental programme includes detailed measurements on the displacements of the slabs, strains in the flexural and shear reinforcement and the concrete strains in the critical shear region. The observed shear resistance is subsequently compared with various codes of practice, showing deficiencies and the need for adjustments in these approaches. Finally, the article discusses a design approach for these connections based on Critical Shear Crack Theory. This analysis extends the previous considerations by Siqueira *et al.* [53] to shear-reinforced slabs, suitably predicting the failure load and mode.

6.3. Experimental Programme

The experimental programme consisted on five specimens equipped with shear reinforcement near to the column region. These specimens were designed consistently with those of a previous experimental programme performed by the authors [53] so that three specimens without shear reinforcement of the previous programme could be used as reference specimens. The tests were aimed at investigating the influence of load eccentricity and shear reinforcement on the punching resistance of slab-column connections. All tests were conducted in the Structural Laboratory of the Universidade de Brasília (Labest-UnB, Brazil).

6.3.1. Specimen Description

The specimens were designed to represent the portion of a slab near a re-entrant corner, both in terms of geometry and acting internal forces (allowing to vary the eccentricity of the shear force at the supported area). The main dimensions of the specimens are depicted in Fig. 6.4 and Fig. 6.5. The specimens had nine sides, with a total in-plane width of 2500 mm and a thickness of 180 mm. They were supported on square reinforced concrete columns (300-mm side), protruding 800 mm on top and 600 mm on bottom, where they were clamped to the testing frame.

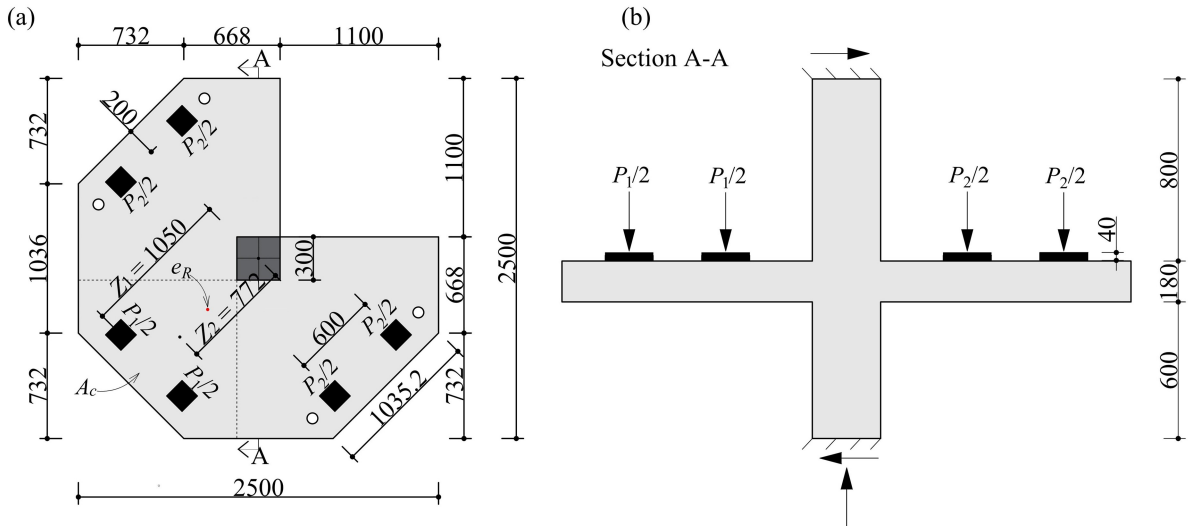

Fig. 6.4 - Slabs dimensions and test setup arrangement: (a) plan view with dimensions; (b) section A-A. (dimensions in [mm])

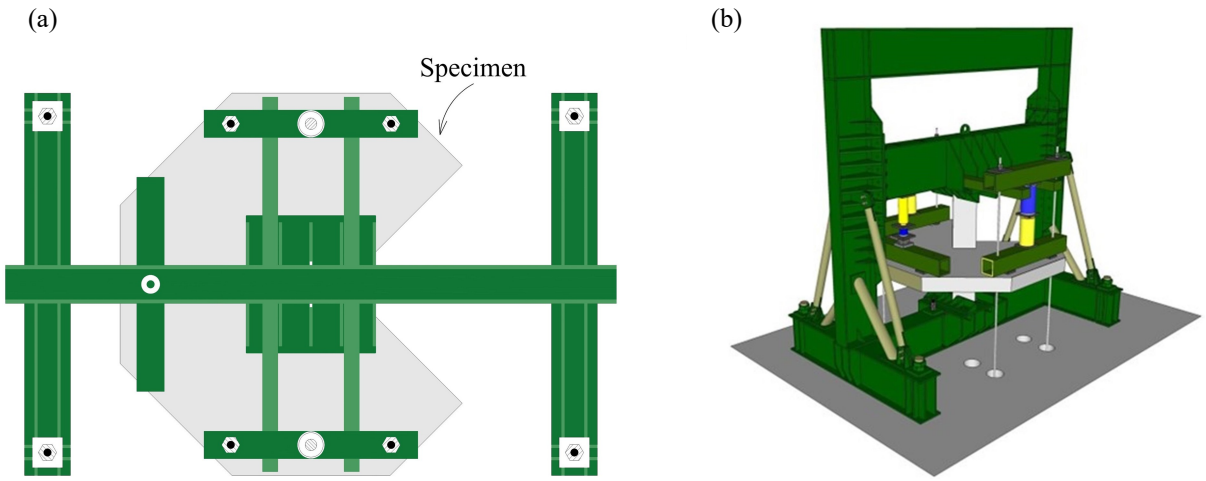

Fig. 6.5 - Test setup arrangement: (a) test rig set-up and (b) 3D visualization section.

The main investigated variables were the eccentricity of the shear force (e_R) and the shear reinforcement ratio. Details for each specimen are given in Table 6.1 and Table 6.2. The mean values of effective depths were obtained from direct measurements in saw cuts of the specimens after testing, varying between 145 and 148 mm (the nominal concrete cover was 20 mm).

Table 6.1 - Main parameters and characteristics of the tested specimens

Test	d [mm]	f_c [MPa]	ρ (1) [%]	ρ_{sw} (2) [%]	P_2/P_1 [-]	e_R [mm]	e_R/d [-]	V_R [kN]	$\frac{V_R}{b_1 \cdot d \cdot \sqrt{f_c}}$ (3)	Failure (4) [-]
S1	148.0	48	1.49	-	0.5	491	3.32	325	0.83	p
S1-1	147.5	48	1.50	0.56	0.5	485	3.29	500	1.62	w
S2	148.0	48	1.49	-	1.0	344	2.32	372	0.96	p
S2-1	144.5	48	1.49	0.32	1.0	348	2.41	513	1.31	w
S2-2	147.0	43	1.55	0.51	1.0	345	2.35	575	1.49	w
S2-3	147.5	43	1.50	0.73	1.0	346	2.35	550	1.49	o
S7	145.0	43	0.95	-	1.5	262	1.81	345	1.11	p
S7-1	146.5	43	1.51	0.56	1.5	264	1.80	640	1.74	o

(1) calculated as $(\rho_x \cdot \rho_y)^{0.5}$ and with $\rho_i = A_i/(s_i \cdot d_i)$

(2) calculated as $\rho_{sw} = \frac{n_t \cdot \frac{\pi}{4} \cdot \emptyset_{sw}}{b_0 \cdot S_r}$

(3) b_1 is the perimeter located at $0.5d$ of the edge of the supported area.

(4) p: punching failure without shear reinforcement; w: punching within shear-reinforced zone and o: punching outside shear-reinforced zone.

Table 6.2 - Details of shear reinforcement of slabs

Test	n_s [-]	n_r [-]	A_{sw} [cm²]	s_0 [mm]	s_r [mm]
S1-1	5	10	78.5	70	90
S2-1	3	10	50.2	70	100
S2-2	4	10	78.5	70	100
S2-3	5	13	102.1	60	90
S7-1	5	10	78.5	70	90

n_s = number of vertical branches of shear reinforcement per radius and n_r = number of vertical branches of shear reinforcement in the perimeter.

The values of the eccentricity of the shear force at failure (e_R) varied between 3.32d (test S1) and 1.80d (test S7-1), aimed at representing realistic cases in practice. Fig. 6.6 shows the evolution of the eccentricity during the tests.

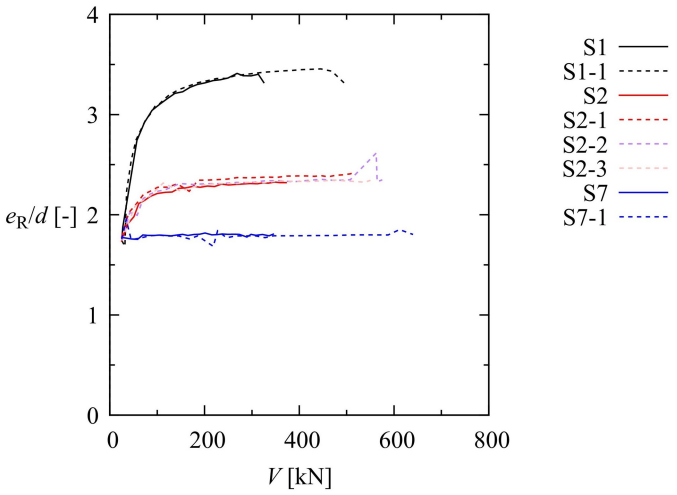

Fig. 6.6 - Load eccentricity of the specimens during the tests.

The flexural reinforcement was uniformly distributed with some adaptions near to the column region. The top layer consisted of 16 mm diameter bars for all specimens, corresponding to a reinforcement ratio equal to 1.5% (25 bars over the width of the member), except for slab S7, where bar spacing was higher resulting into a reinforcement ratio of 0.95% (corresponding to 16 bars over the width of the element). Fig. 6.7a-b shows the arrangement of the flexural reinforcement for both cases. The bottom flexural reinforcement consisted of 12.5 mm bars in all slabs (13 bars in total), as shown in Fig. 6.7c.

Concerning the detailing of the reinforcement at the edges, hooks were provided for the top reinforcement, while the bottom reinforcement was straight (see Fig. 6.7). This does not correspond to typical detailing of edges in flat slabs (where anchorage is usually provided by means of L-shaped reinforcement for top and bottom layer or hooks are provided for the bottom layer) but aims at ensuring full anchorage conditions for the top reinforcement during testing. The column portions were cast monolithically with the slab. Its reinforcement consisted of 8 bars Ø25.0 mm (allowing for transfer of bending moments). These rebars were enclosed by Ø10.0 stirrups, spaced at 100 mm.

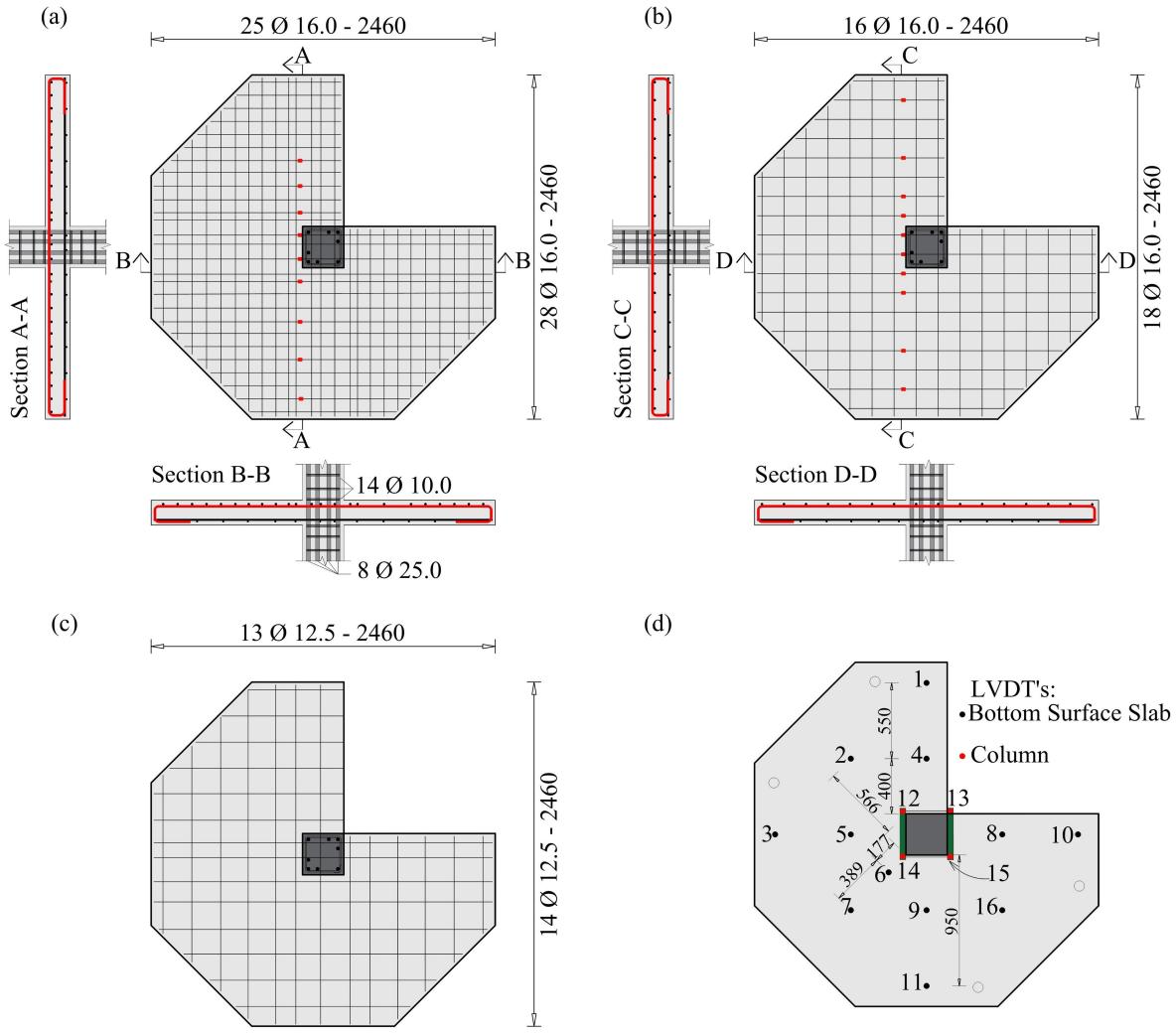

Fig. 6.7 - Flexural reinforcement of slabs and location of strain gages: (a) Slabs S1, S2, S2-1 to S7-1; (b) Slab S7; (c) bottom flexural reinforcement; (d) Positioning of LVDTs on slabs.

With respect to the shear reinforcement, double-headed studs (ribbed bars) with a diameter of 8 mm and 10 mm were used for specimens S2-1 to S7-1. The heads had a diameter equal to three times the bar shaft and were welded to it. Tests of the studs, in which the loading was applied via the heads, showed that ductile failure originated in the shaft region. For installation purposes, the studs were spot-welded to non-structural carrier rails, which were 10 mm wide and 3.2 mm thick. The shear reinforcement was supported at the upper layer of reinforcement by means of the carrier rails, and was arranged following a radial pattern as shown in

Fig. 6.8. The corresponding shear reinforcement ratio (ρ_{sw}) is given in Table 6.1 as defined in [41], varying between 0.32% and 0.73%.

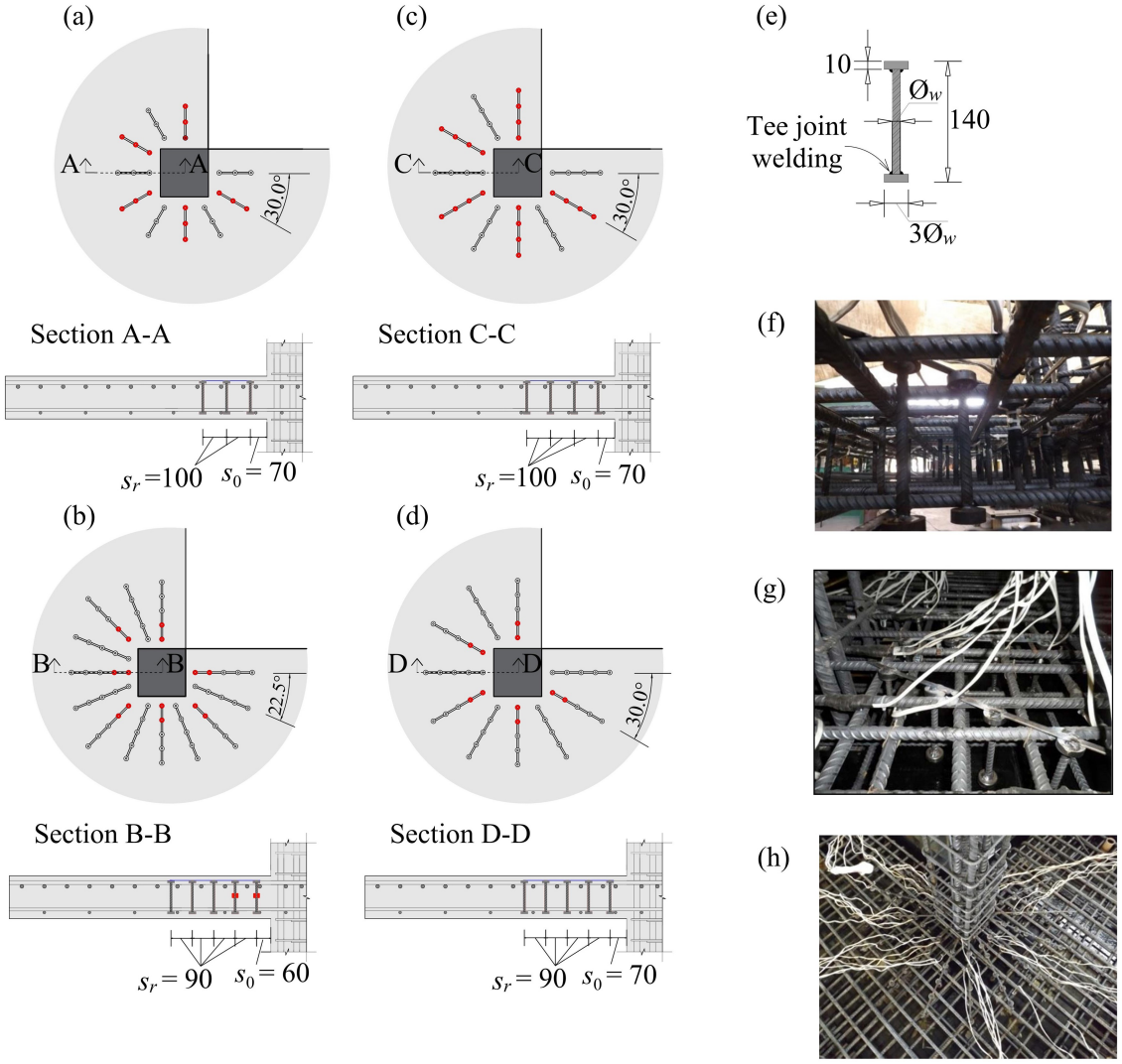

Fig. 6.8 - Shear reinforcement arrangement of the slabs and location of strain gages: (a) slab S2-1; (b) slab S2-3; (c) slab S2-2; (d) slab S1-1 and S7-1; (e) dimensions of the double-headed studs; (f) shear reinforcement in the slab S1-1; (g) shear reinforcement in the slab S2-2; (h) shear reinforcement in the slab S2-3.

6.3.2. Material Properties

The characteristic compressive strength for the concrete was 40 MPa, provided by a local supplier. In the concrete dosage, 50% CEM I and 50% CEM III were used. The water/cement ratio was approximately 0.47. Crushed limestone sand and gravel were used as aggregate, with 9.5 mm of maximum sieve size for the coarse aggregate. The average slump of the concrete mix was 120 mm, and the slabs were moist cured for 7 days.

The compressive strength of concrete, tensile strength and modulus of elasticity were determined by testing standard cylinders (100 mm diameter by 200 mm high). Casting was performed on two test series with all specimens of a given series cast on the same day. The first series included slabs S1, S2, S2-1 and S2-2, while the second comprised slabs S7, S2-3 to S7-1 (refer to Table 6.3). All specimens of one series were tested in two consecutive days, with average testing age of 28 days for one series (S7, S2-3 to S7-1) and 111 days for the other (S1, S2, S2-1 and S2-2). Details on the compressive strength (f_c), tensile strength (f_{ct}) and modulus of elasticity (E_c) at the time of testing are given in Table 6.3.

Concerning the flexural reinforcement, hot-rolled bars were used, exhibiting a well-defined yield plateau. Table 6.3 provides the measured values of yield strength (f_y), tensile strength (f_u) and modulus of elasticity (E_s) based on the average of three control specimens.

Table 6.3 - Properties of concrete and steel

Test	Concrete			Flexural reinforcement			Shear reinforcement			
	f_c [MPa]	f_{ct} [MPa]	E_c [GPa]	Ø [mm]	f_y [MPa]	E_s [GPa]	$Ø_{sw}$ [mm]	f_{yw} [MPa]	f_{uw} [MPa]	E_{sw} [GPa]
S1	48	3.4	29.4	16(1)	558	192	-	-	-	-
S2										
S2-1							8	587	716	187
S2-2							10	560	685	197
S7	43	3.5	32.9	16(2)	572	208	10	528	607	207
S2-3										
S1-1										
S7-1										

(1) f_u = 700 MPa
(2) f_u = 710 MPa

6.3.3. Instrumentation

Vertical displacements of the slab were measured using Linear Variable Displacement Transducers (LVDTs). The LVDTs were positioned at 12 points on the soffit of the slab (targets 1-11 and 16 in Fig. 6.7d) and four LVDTs measured column displacement (targets 12-15). On the basis of the deflections measured with LVDTs, the rotations could be calculated at multiple locations and directions.

Concerning measurement of strains, selected flexural bars were instrumented as shown in Fig. 6.7. Each bar was equipped with two opposed strain gauges (KFG-5-120-C1-11, dimensions 9.4 × 2.8 mm), positioned at the same section. The strain in the reinforcement was then calculated as the average of the two readings (to avoid any potential effect due to bending of the rebars). The shear reinforcement was also instrumented with the same strain gauges. As shown in

Fig. 6.8, in slabs S2-1 and S2-2 all studs along alternate radii were measured (

Fig. 6.8a-b), while in slabs S2-3, S1-1 and S7-1, only the first two studs were instrumented in alternate radii (Fig. 6.8c-d). In addition, surface deformations were also measured on the concrete with strain gages (KC-70-120-A1-11, with dimensions of 80 × 7.5 mm), whose location and details will be provided in the next section.

6.3.4. Test Setup

Testing of the specimens was performed in the custom test rig shown in Fig. 6.5. The specimens were loaded by means of three hydraulic jacks (1 MN of capacity each) connected to two hydraulic pumps. Such load arrangement, as shown in Fig. 6.4a, allowed applying the same load (P_2) at two sides of the specimen, while a different one (P_1) was applied at the third. The loads were measured by means of load cells and were introduced in the specimen by means of spherical hinges on spreader beams supported on square steel plates (side equal to 150 mm and 40 mm thick). Concerning the ends of the columns, they were horizontally fixed to the rig to prevent rotations and to allow for a moment transfer between the slab and the column. The load was applied monotonically until failure, by performing a series of loading steps (with an approximate duration of five minutes each). At the end of each loading step, crack development on the surface was manually tracked and drawn, both on the top and lateral sides.

6.4. Analysis of Test Results

6.4.1. Cracking, rotations and failure mode

Fig. 6.9 and Fig. 6.10 show the load-rotation curves for all slabs depicting the rotations in the reinforcement directions (ψ_x and ψ_y) as well as in the diagonal direction (ψ_{xy}). For each plot, the response for a shear-reinforced slab is presented alongside with the corresponding reference specimen without shear reinforcement. In the same figures, the cracking pattern on the top surface, cracks at of the re-entrant corner faces and saw cut in two selected directions are also given.

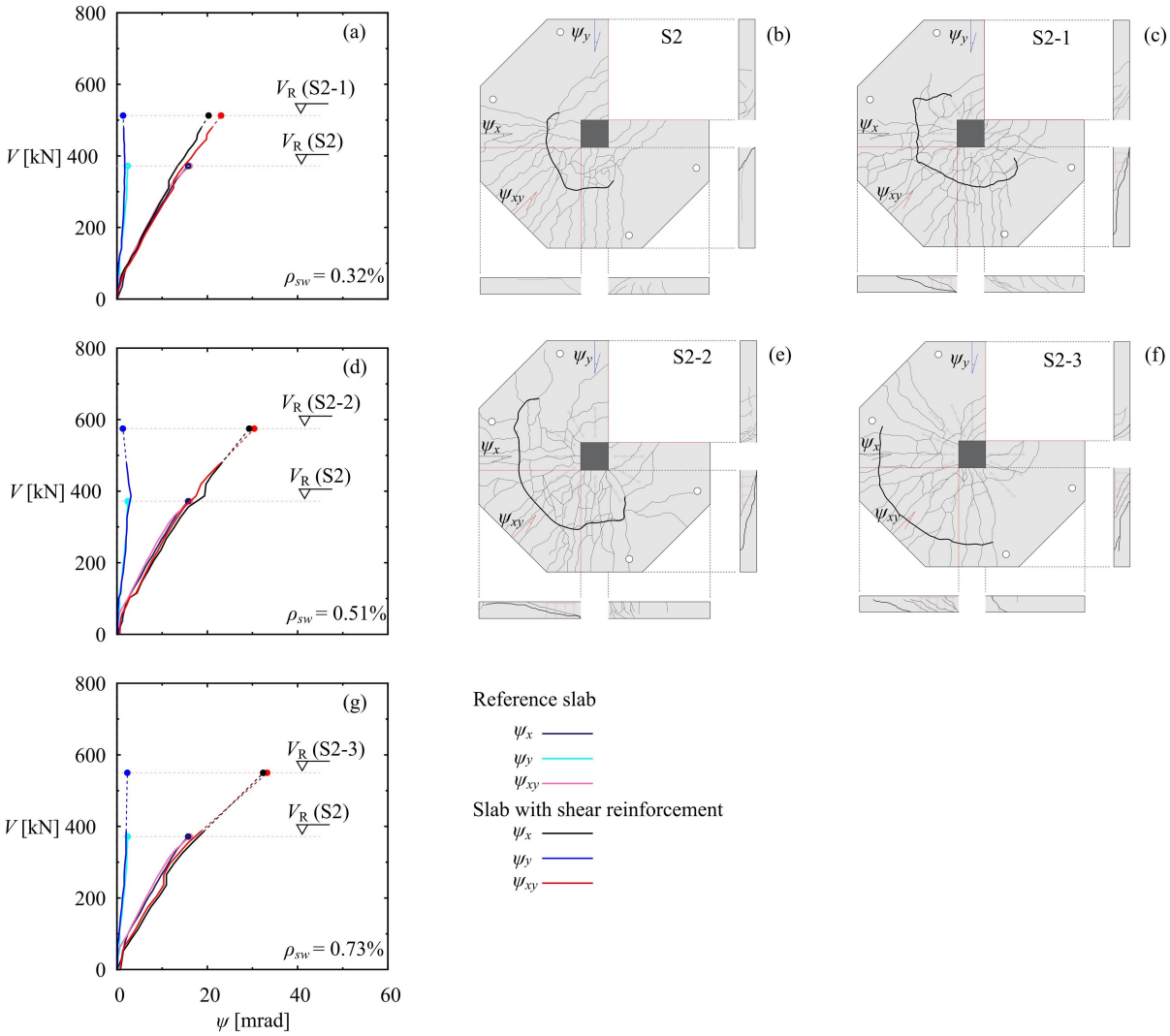

Fig. 6.9 - Load-rotations and cracking pattern top: (a) rotation slab S2 and S2-1; (b) cracking slab S2; (c) cracking slab S2-1; (d) rotation slab S2 and S2-2; (e) cracking slab S2-2; (f) cracking slab S2-3; (g) cracking slab S2-1; and (d) rotation slab S2 and S2-3.

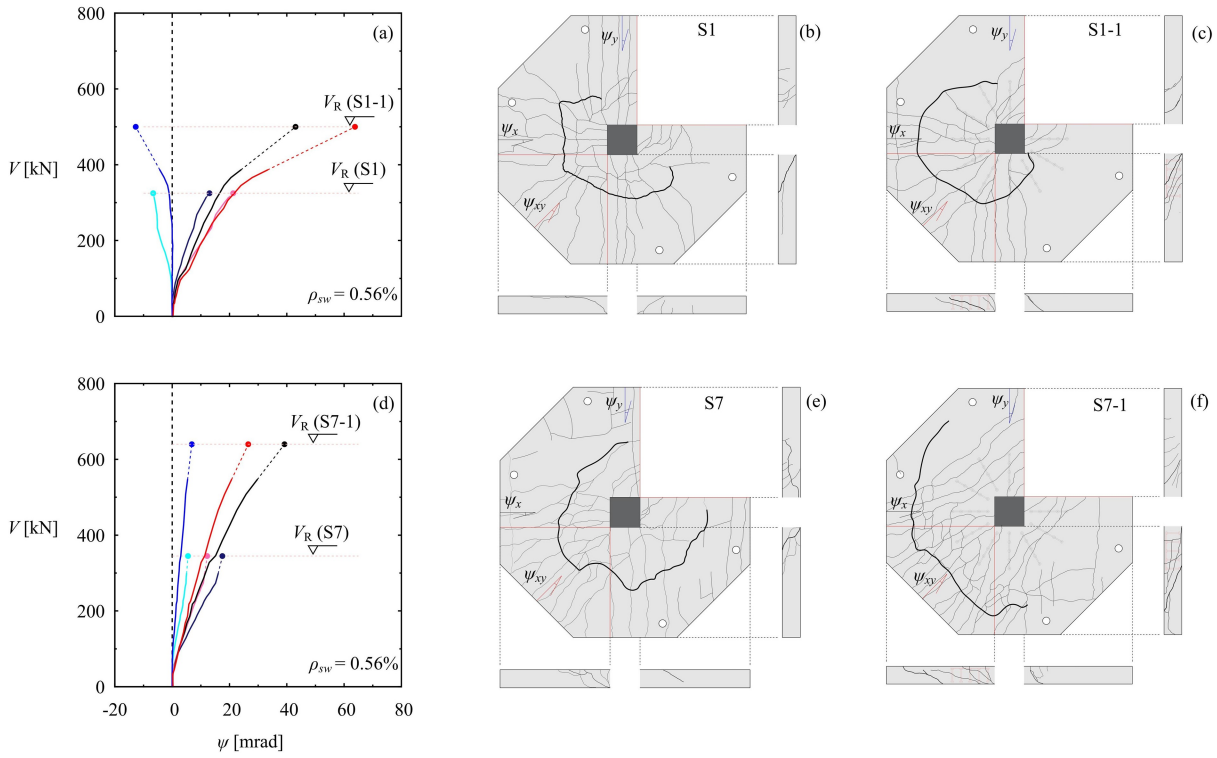

Fig. 6.10 - Load-rotations and cracking pattern top: (a) rotation slab S1 and S1-1; (b) cracking slab S1; (c) cracking slab S1-1; (d) rotation slab S7 and S7-1; (e) cracking slab S7; and (f) cracking slab S1-1.

All slab specimens failed in punching, as confirmed by the development of a punching cone in the saw-cuts. Such failure surface extended from the bottom side of the slab to the top surface. A punching cone was identified in all tests, with the punching cone restricted to the inner region of the slab, except for slab S7, where shear cracking was also observed at the edges (Fig. 6.10e).

Cracking on the top surface developed first at the edges of the column in the inner faces of the slab (opposed to the re-entrant edges) at approximately 16% (S2-1) to 23% (S7) of the failure load. Subsequently, four types of cracks developed on the top surface: (1) cracks radiating from the inner corner of the column and developing outward to the edges, (2) cracks substantially perpendicular to the inner column sides, also developing to the edges, (3) circumferential cracks, perpendicular to the previous ones, at distances from the column that increased with increasing load, (4) torsion cracks in the strips of the slab adjacent to the edges of the re-entrant corner.

Torsion cracks were observed at the edges of the specimens, but the extent of the region where such cracks were observed was influenced by the eccentricity and presence of shear reinforcement. The shear reinforcement increased the overall resistance of the connection and thus torsion cracks developed at larger distances from the column (refer for instance to specimens S7 and S7-1 in Fig. 6.10e-f).

Concerning the eccentricity, lower values (as for specimen S7-1, Fig. 6.10f) were typically associated to larger extents of the cracked zone (as for instance specimen S2-1, Fig. 6.9c). This can also be justified by the higher level of load attained by slabs with lower eccentricities. Concerning the response of the slabs, the shear reinforcement increased both the punching resistance and deformation capacity for the different eccentricities tested (refer to Fig. 6.9 and Fig. 6.10). In all cases, the rotation close to the free edge (ψ_y) was very limited, while the others (ψ_x and ψ_{xy}) had comparable values, particularly for higher levels of eccentricity.

The experimental results show that increasing the shear reinforcement ratio led to an increase on the resistance and deformation capacity (as for instance for slabs S2-1 and S2-2, with an increase of the shear reinforcement ratio ρ_{sw} from 0.32% to 0.51%, refer to Fig. 6.9a,d). Such increase was however limited by the punching resistance outside of the shear-reinforced area (refer to specimen S2-3 of the same series with ρ_{sw} = 0.73% in Fig. 6.9g).

Such results are also shown in Fig. 6.11, where the unitary resistance of the specimens is compared. To that aim, the failure load is normalised by the square root of the concrete strength, the cubic root of the flexural reinforcement ratio, the effective depth and the length of the basic control perimeter. As it can be observed, the normalized failure loads increase with increasing shear reinforcement ratio, but may reach a maximum.

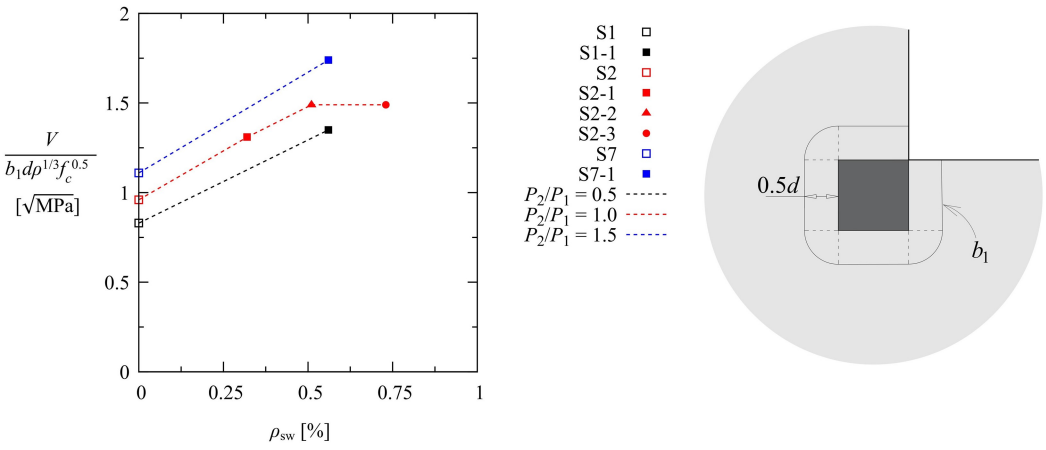

Fig. 6.11 - Normalized strength as a function of the shear reinforcement ratio of all tests.

6.4.2. Detailed measurements

6.4.2.1 Strains in the top flexural reinforcement

Fig. 6.12 shows the profile of strains measured in the flexural reinforcement at the failure load. The recorded strains were higher in the bars located near to the column. On the side of the re-entrant edge, the strains decrease rapidly with increasing distance to the column. On the other side (where the slab was continuous), the decrease in deformation was smoother. As Fig. 6.12 shows, the presence of shear reinforcement had a clear influence on the level of deformation observed in the flexural reinforcement, with higher levels of deformation when shear reinforcement was available. This can be attributed to the higher level of load attained in such tests and to the corresponding increase in the bending moments.

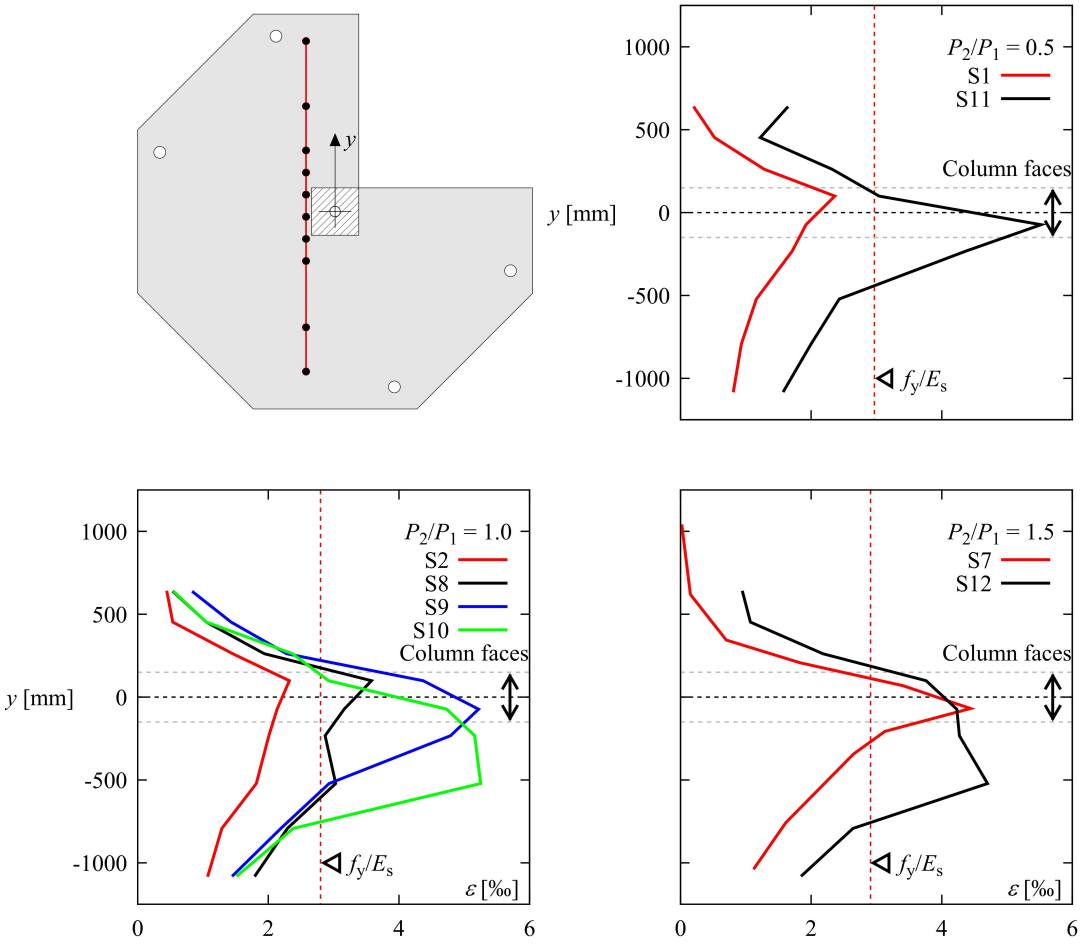

Fig. 6.12 - Profile of strains in the flexural reinforcement of all tests.

6.4.2.2 Strains in the shear reinforcement

Fig. 6.13 and Fig. 6.14 compare the measured axial strains of the shear reinforcement at mid-height for the tested specimens (refer to Fig. 6.13h-i and Fig. 6.14c,f for location of the instrumented bars and to Fig. 6.13j for gauge location). To that aim, the presented results correspond to the average strain of two gauges glued at opposite sides of the shaft (see Fig. 6.13j). Concerning the influence of the amount of shear reinforcement, it can be noted that the strains reduced for higher shear reinforcement ratios. This can be observed by comparing slab S2-3 (ρ_{sw} = 0.73%, Fig. 6.14a,b) to slabs S2-2 and S2-1 (ρ_{sw} = 0.51% and 0.32% respectively, Fig. 6.13a-g). Such result confirms that for higher shear reinforcement ratios, the resistance of the studs was not governing, as already stated in the previous section (Fig. 6.11). This observation is also consistent with the saw cuts where the punching failure surface indicates a development outside of the shear-reinforced area (Fig. 6.9f).

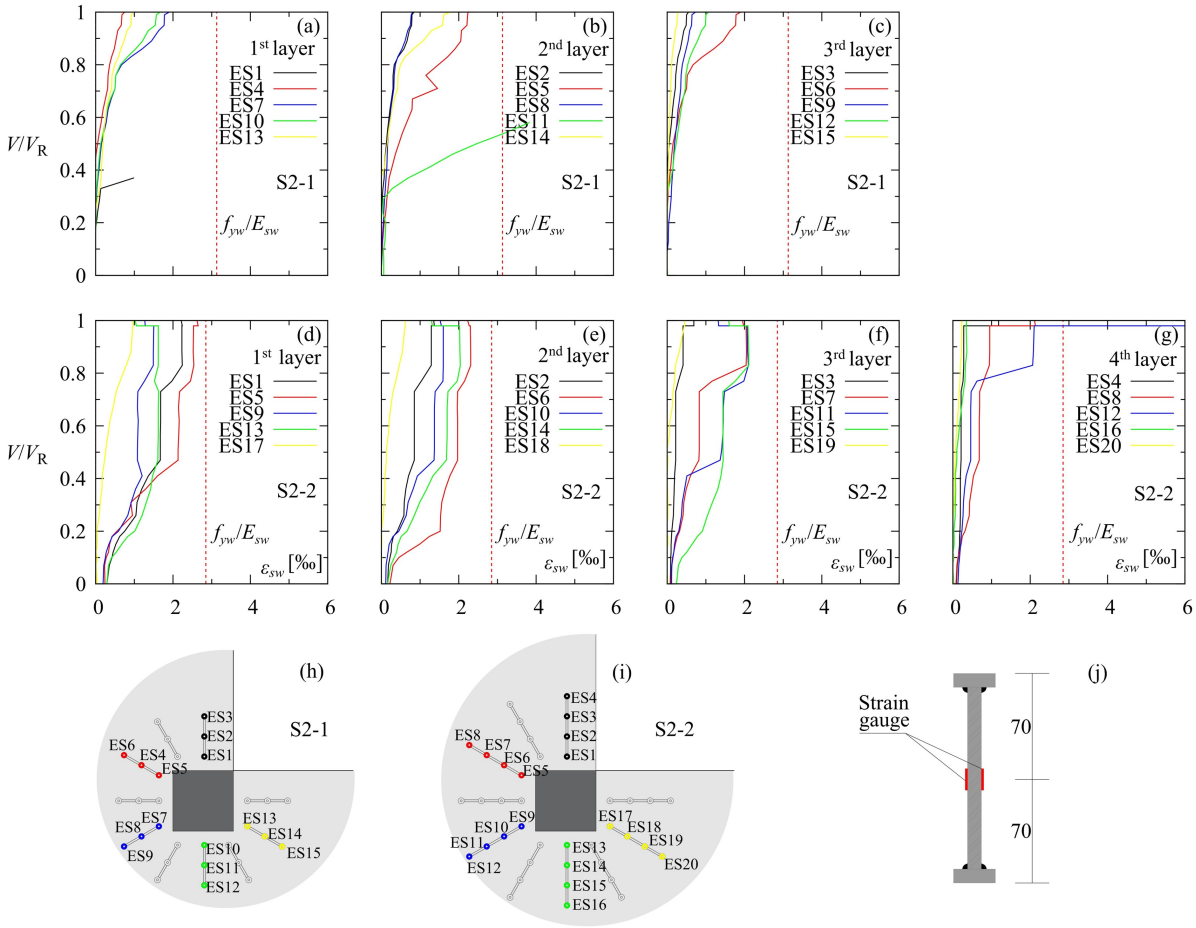

Fig. 6.13 - Measured strains in the shear reinforcement: (a-c) slab S2-1; (d-g) slab S2-2; (h) location of gauges of S2-1; (i) location of gauges of S2-2; and (j) location of gauges in the shaft.

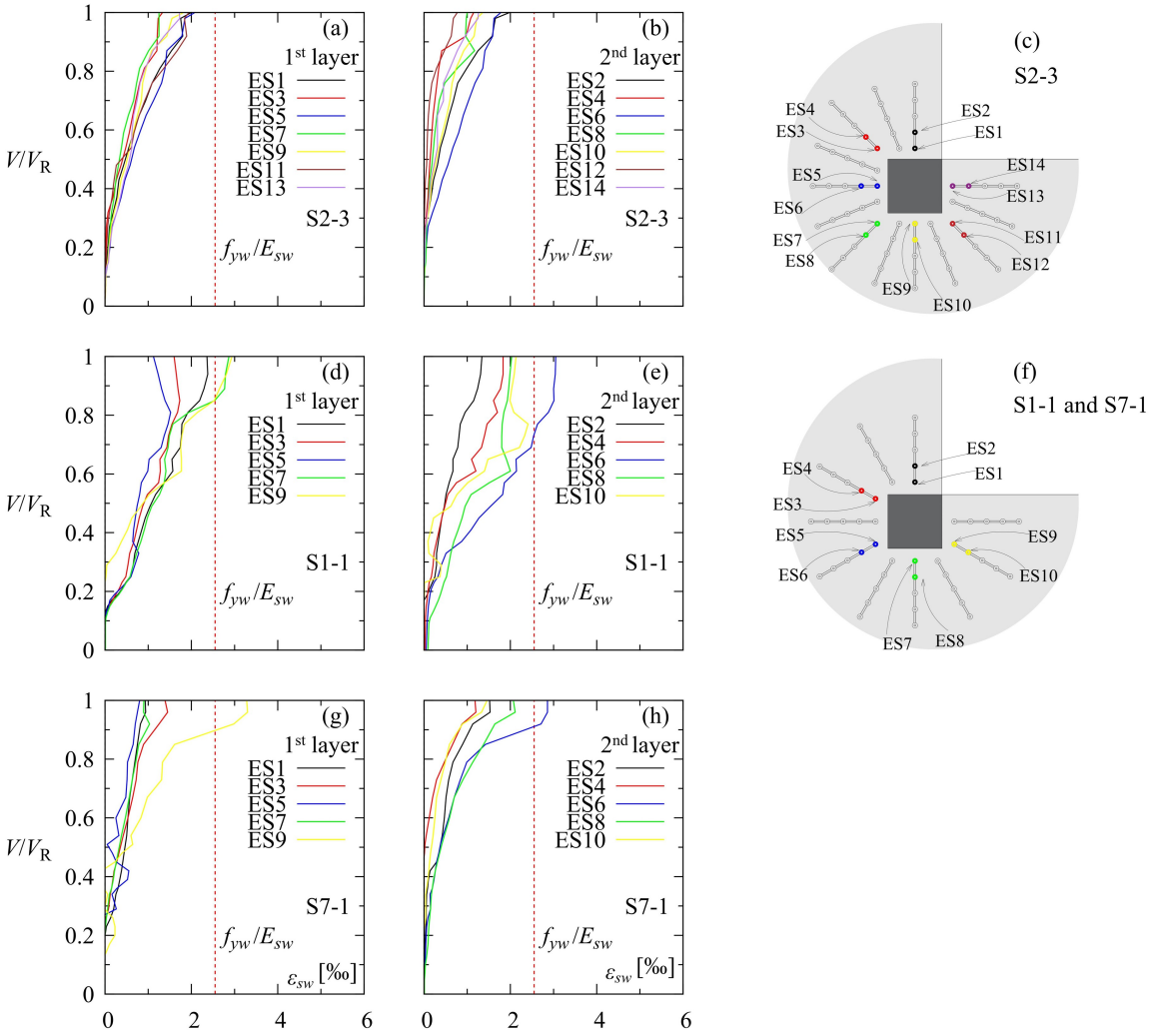

Fig. 6.14 - Measured strains in the shear reinforcement: (a-b) slab S2-3; (c) location of gauges of Slab S2-3; (d-e) slab 11; (f) location of gauges of Slab S1-1 and S7-1; and (g-h) Slab 7-1.

The load eccentricity also shows an influence on the strains of the shear reinforcement. According to the experimental results, it appears that for increasing eccentricity the shear reinforcement experiences higher strains. This can be observed for instance by comparing specimens S1-1 (high eccentricity, Fig. 6.14d,e) and S7-1 (low eccentricity, Fig. 6.14g,h). This result is also consistent with the level of experienced rotation, which is higher for larger eccentricities (as observed in Fig. 6.10).

4.4.2.3 Strains at the concrete surface

The tangential and radial strains of concrete are illustrated in Fig. 6.15 and Fig. 6.16.

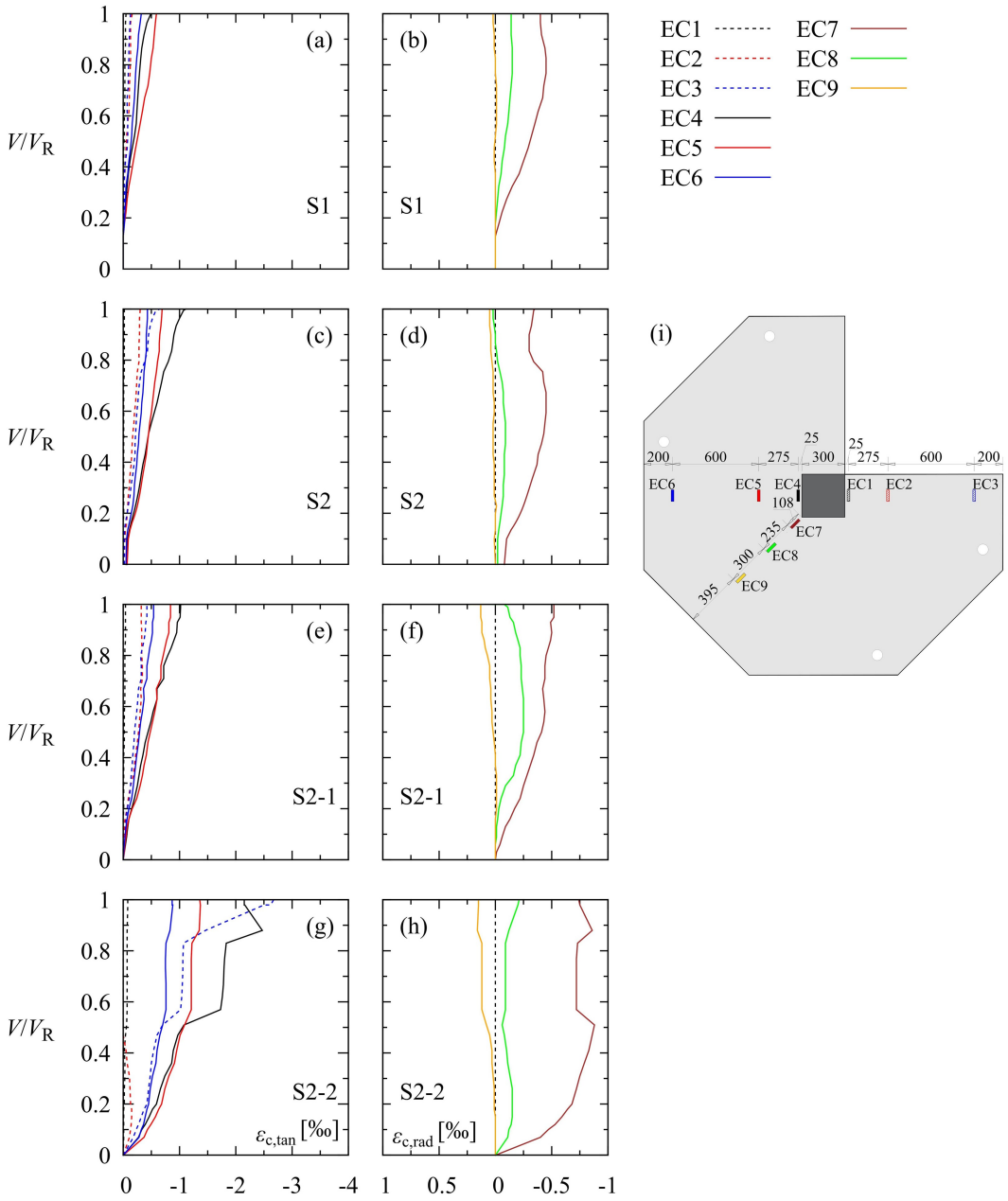

Fig. 6.15 - Surface strains at bottom surface (tangential and radial strains): (a-b) S1; (c-d) S2; (e-f) S2-1; (g-h) S2-2 and (i) location of gauges.

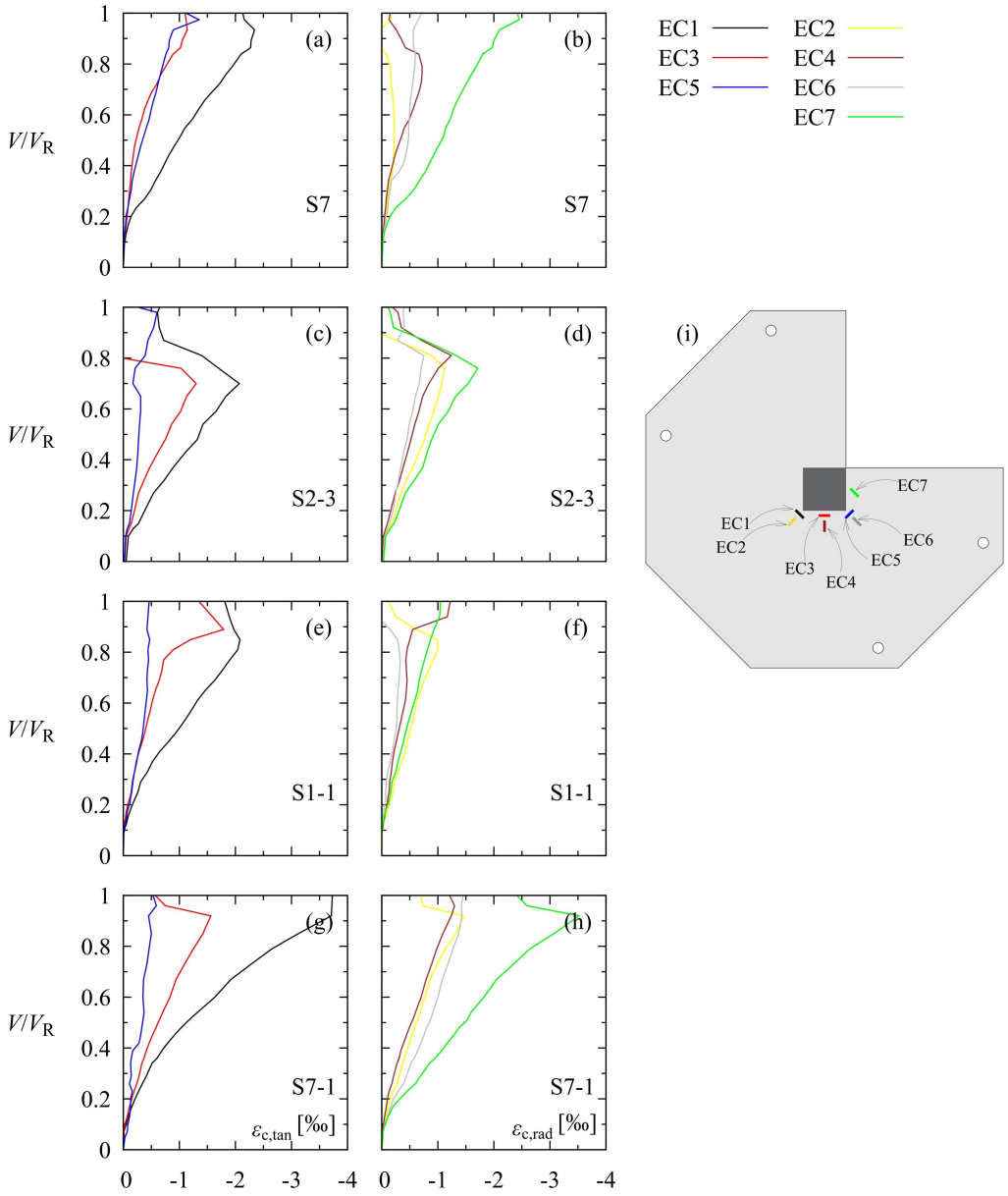

Fig. 6.16 - Surface strains at bottom surface (tangential and radial strains): (a-b) S7; (c-d) S2-3; (e-f) S1-1; (g-h) S7-1 and (i) location of gauges.

The radial strains were typically under compression. Near failure, these strains reduced and, in some cases, turn in tension, consistently with the development of a critical shear crack [3]. Concerning the tangential strains, they showed in general monotonically-increasing compressive strains (as expected for such regions [3]), but sometimes reductions were also observed (as for slab S2-3 and S1-1, refer to Fig. 6.16).

In addition to the conventional radial and circumferential arrangement of gauges, some gauges were also arranged at 45° in an effort to align them with the potential compression struts originating due to torsion moments in this region (Fig. 6.17). Compressive strains were recorded in several gauges indicating potentially relevant torsional moments (Fig. 6.17) but the measurements were not conclusive as the gauges intercepted in several cases flexural cracks (recording thus tensile strains).

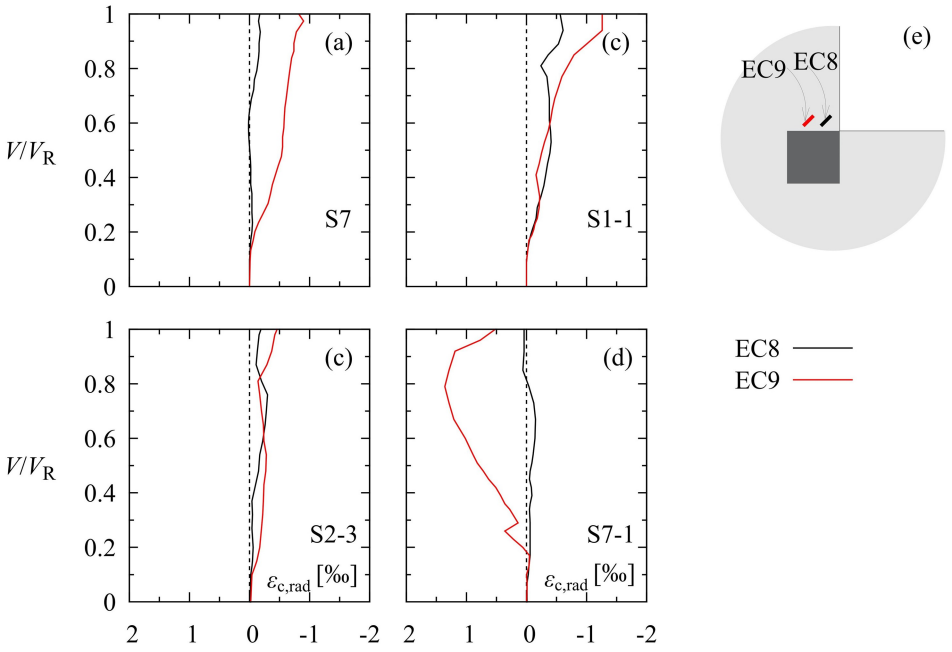

Fig. 6.17 - Radial strains at top surface of test: (a) S7, (b) S2-3, (c) S1-1, (d) S7-1 and (e) location of gauges.

6.5. Comparison to Code Predictions

The accuracy of several codes of practice to predict the punching strength of re-entrant slab-column connections is presented in this section by comparing them to the results of the experimental programme (details on the formulation used for the codes are given in Chapter 2). The selected codes are EN1992-1-1:2004 (Eurocode 2) [55], FEN 1992-1-1:2023 (draft for future revision of Eurocode 2) [41], ACI 318:19 [39], NBR 6118 [36], and MC2010 (Level of Approximation II, corresponding to a typical design situation based on simple analyses) [38]. Their design equations were applied accounting for the geometry of the supported area and the eccentricity of the shear force. For the comparisons performed, all safety factors were set to 1.0 and the characteristic or specified values of the resistances were replaced by the average ones.

Details of the comparison are presented in Table 6.4 and also in Fig. 6.18. In that Figure, the normalized punching resistance ($V/(b_1 d \rho^{1/3} f_c^{0.5})$ as presented in Fig. 6.11) is plotted against the shear reinforcement ratio (ρ_{sw}). As can be observed, the normalized punching resistance increases with increasing shear reinforcement ratio, until the punching shear strength outside the shear-reinforced zone or the maximum punching shear strength governs the resistance. The horizontal plateau for low shear reinforcement ratios is obtained for some codes that consider a constant reduction on the concrete contribution (as NBR, EN1992-1-1 or ACI). On the contrary, for codes where this reduction is gradual (as MC2010 or FEN1992-1-1), such plateau for low shear reinforcement ratios is not observed.

Table 6.4 - Summary of experimental and theoretical resistances also failure modes

Slab	V_R [kN]	Failure Mode	ACI 318 $V_R/V_{R,ACI}$		EN-1992 $V_R/V_{R,EC2}$		EN-1992 $V_R/V_{R,FprEC2}$		MC 2010 - LoAII $V_R/V_{R,MC10}$		NBR 6118 $V_R/V_{R,NBR}$	
				Failure		Failure		Failure		Failure		Failure
S1	325	V_c	1.68	V_c	1.08	V_c	1.34	V_c	1.31	V_c	1.07	V_c
S2	372	V_c	1.57	V_c	1.04	V_c	1.27	V_c	1.25	V_c	1.03	V_c
S7	345	V_c	1.37	V_c	1.06	V_c	1.31	V_c	1.27	V_c	1.05	V_c
S1-1	500	V_{in}	1.52	V_{in}	1.30	V_{max}	1.30	V_{in}	1.32	V_{in}	1.15	V_{max}
S2-1	513	V_{in}	1.61	V_{in}	1.07	V_{in}	1.28	V_{in}	1.31	V_{in}	0.97	V_{in}
S2-2	575	V_{in}	1.52	V_{out}	1.13	V_{max}	1.27	V_{in}	1.26	V_{in}	1.01	V_{max}
S2-3	550	V_{out}	1.27	V_{out}	1.16	V_{max}	1.10	V_{max}	1.09	V_{max}	1.03	V_{max}
S7-1	640	V_{out}	1.35	V_{in}	1.17	V_{max}	1.17	V_{in}	1.22	V_{in}	1.04	V_{max}
		Avge	1.48		1.13		1.25		1.26		1.04	
		CoV	0.09		0.07		0.06		0.05		0.05	

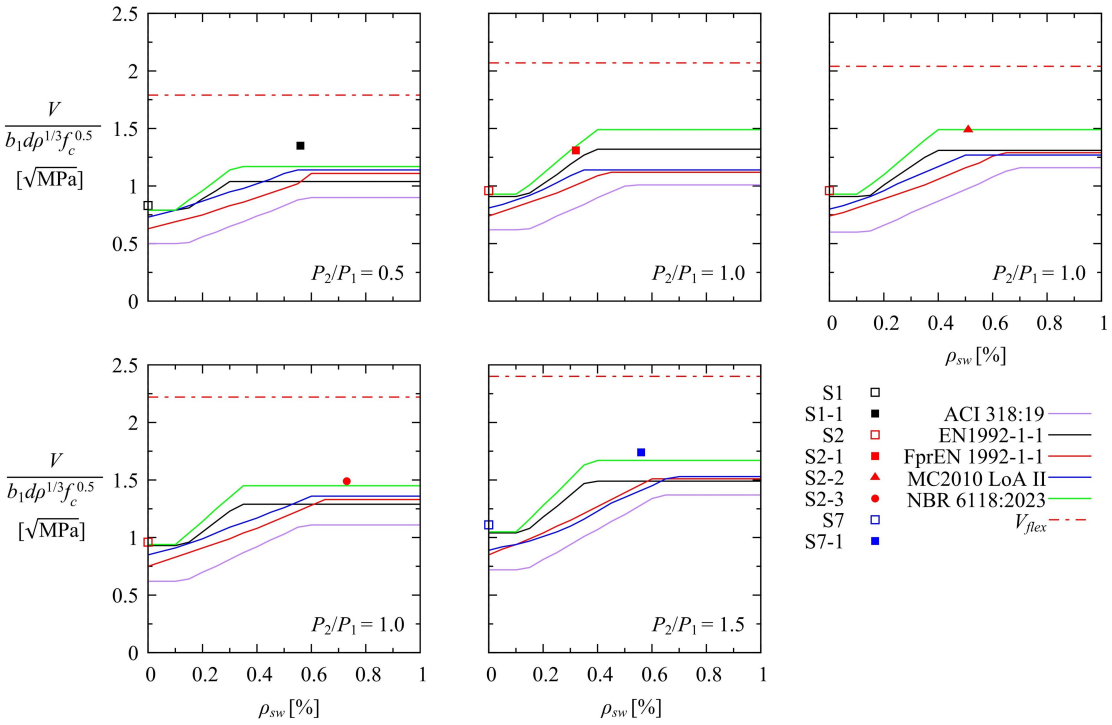

Fig. 6.18 - Code predictions for varying amounts of shear reinforcement and experimental results.

According to the results, ACI 318 underestimates the resistance of all slabs. Both NBR 6118 and EN1992-1-1:2004 (derived from the MC 1990 [56]) provide reasonable estimates of the experimental results, with average ratios of experimental to calculated punching resistance (V_R/V_{calc}) equal to 1.04 and 1.13 with fairly low scatter (CoV ≈ 6.0%). The results of MC2010 and FEN are very similar ($V_R/V_{calc} \approx 1.25$, with a CoV ≈ 5.5%). Both codes are based on the Critical Shear Crack Theory, and result in safer estimates than EN1992-1-1:2004 and NBR 6118 but more accurate than ACI 318.

Despite the fact that failure loads are reasonably predicted for several codes, the prediction of the failure modes is in general not consistent (see Table 6.4). This is observed as an important shortcoming, as the governing criteria for the design are not suitably identified.

6.6. Detailed analysis and punching design of re-entrant corner connections based on the Critical Shear Crack Theory

In this section, the mechanics of the punching failures of re-entrant slab-column connections is investigated in detail on the basis of the physical model of the Critical Shear Crack Theory (CSCT). Such analysis is used to understand the role of several governing parameters and to calculate both the resistance and deformation capacity at failure.

6.6.1. Shear field analysis

A shear field is a useful visualization of the transfer of shear forces within a concrete slab, particularly in cases of eccentric punching (internal columns with unbalanced moments, presence of large openings, edge, corner columns). This analysis can be used to calculate the reduced shear-resisting control perimeter and to identify potential shear-critical regions [60]. To that aim, the shear-resisting control perimeter can be determined by using Equation 6.1, proposed by Vaz Rodrigues *et al.* [61].

$$b_0 = \frac{V}{v_{perp,max}} \tag{6.1}$$

where b_0 is the length of the shear-resisting control perimeter, V is the total acting shear force and $v_{perp,max}$ is the maximum unitary shear force perpendicular to a basic control perimeter located at $0.5d$ from the supported area. This equation is normally based on a linear-elastic distribution of the shear field, which ensures robust and simple analyses (although it can be generalised for nonlinear shear fields). Concerning the elastic analysis, it may be performed considering a reduced value of the Poisson's coefficient ($\nu = 0$) and of the shear modulus ($G = G_{el}/8 = E/16$) to account for the response of cracked concrete [62].

The elastic distribution of unitary shear forces calculated on this basis (elastic shear fields) is illustrated in Fig. 6.19 and Fig. 6.20 at $d/2$ and $d_{v,out}/2$ from the outer perimeter of shear reinforcement, respectively.

These plots show the larger concentrations (and thus reductions in the length of the shear-resisting control perimeter b_0 and $b_{0.5,out}$ respectively) for higher eccentricities, particularly when the basic shear perimeter is closer to the column region. In contrast, when the eccentricity is lower and approaches the centre of gravity of the basic control perimeter, a more uniform distribution of these forces is observed.

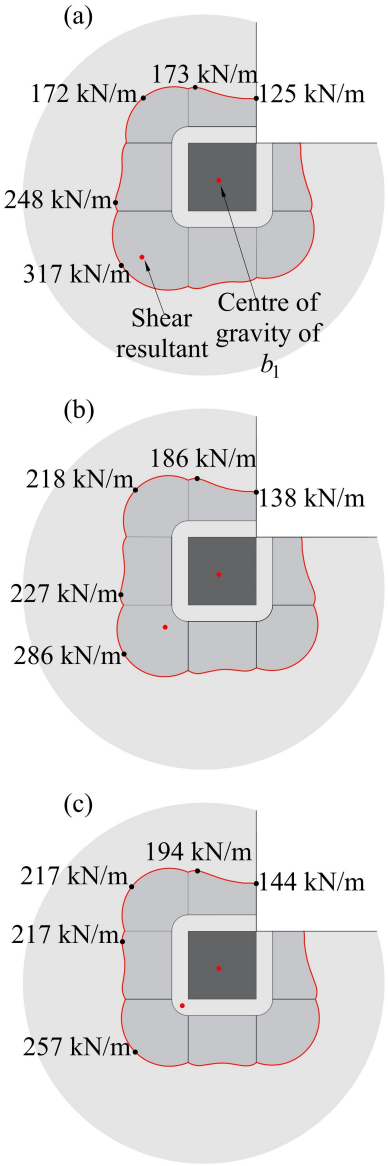

Fig. 6.19 - Linear elastic distribution of shear forces [kN/m] along control perimeters at $d/2$ of the applied loads: (a) Slab S1; (b) Slab S2; and (c) Slab S7. (Maximum nominal shear force shown for a total applied load $V = 300$kN)

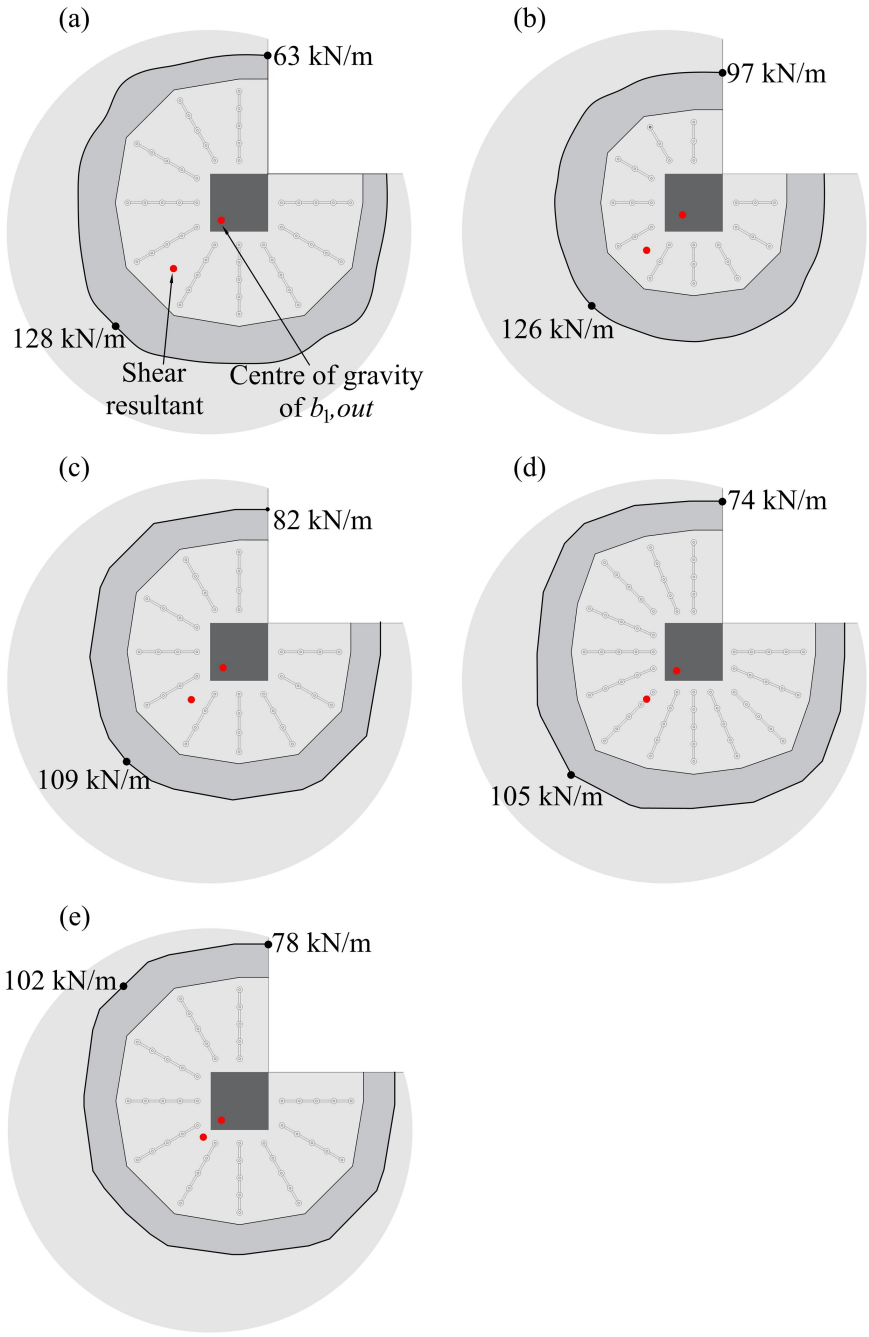

Fig. 6.20 - Linear elastic distribution of shear forces [kN/m] along control perimeters at $d_{v,\text{out}}/2$ of the control perimeter at the outermost perimeter of shear reinforcement: (a) Slab S1-1; (b) Slab S2-1; (c) Slab S2-2; (d) Slab S2-3and (e) Slab S7-1. (Maximum nominal shear force shown for a total applied load V = 300kN)

6.6.2. Theoretical Approach of the Critical Shear Crack Theory

6.6.2.1 Slabs without shear reinforcement

In the following, the Critical Shear Crack Theory (CSCT) will be used to obtain refined estimates of the punching shear resistance. In accordance to this theory, the punching shear strength decreases with increasing slab rotations due to the increase of the width of the critical shear crack. According to this assumption, Muttoni [3] proposed the failure criterion given in Eq. (6.2), which assumes that the width of the critical crack is proportional to the slab rotation multiplied by the effective depth of the member ($w \propto \psi \cdot d$).

$$V_{R,c} = \frac{0.75 b_0 d \sqrt{f_c}}{1+15\frac{\psi d}{d_{g0}+d_g}} \tag{6.2}$$

Where b_0 refers to the length of the shear-resisting control perimeter, d to the shear-resisting effective depth (considering the penetration of the supported area), d_g to the maximum aggregate size and d_{g0} to a reference size (set to 16 mm for normal strength concrete).

Concerning the relationship between the acting shear force and the rotation of the slab, it may be estimated using different Levels-of-Approximation (LoA) [38]. In the following, a LoA III (according to Eq. (6.2) was used to conduct a detailed assessment of the response of the slabs.

$$\psi = 1.2 \frac{r_s}{d} \frac{f_y}{E_s} \left(\frac{m_E}{m_R}\right)^{3/2} \tag{6.3}$$

where r_s refers to the distance between the centre of the supported area and the point of contraflexure of bending moments, d to the effective flexural depth in the appropriate direction, f_y to yield strength, E_s to the modulus of elasticity of the steel, m_E is the average moment per unit width for calculation of the flexural reinforcement in the support strip and m_R is the design average flexural strength per unit width in the support strip for the considered direction. Parameters r_s and m_E were estimated using linear elastic (uncracked) finite element models as recommended in [38]. LoA III was used in the two principal directions (ψ_x and ψ_y). This consideration covers also the xy-direction, as it rotations were comparable to the others (refer to Fig. 6.9 and Fig. 6.10). Such approach proved to be simple and efficient, although more refined alternatives could alternative be used (details on an analysis of the load-rotation curves concerning the response of different sectors can be found elsewhere [53]).

6.6.2.2 Slabs with shear reinforcement

As previously discussed, when shear reinforcement is provided, three failure modes shall be verified: failure within the shear-reinforced area, crushing of concrete struts (maximum punching strength) and failure outside the shear reinforced area. The punching shear strength within the shear-reinforced zone can be calculated as the sum of concrete and shear reinforcement contributions [4] on the basis of Eq. (6.4):

$$V_{R,cs}=V_{R,c}+V_{R,s} \tag{6.4}$$

In this Equation, the concrete contribution ($V_{R,c}$) is given by the failure criterion of the corresponding slabs without shear reinforcement (Eq. (6.2) and the shear reinforcement contribution ($V_{R,s}$) is given by:

$$V_{R,s}=\sigma_{sw}\Sigma A_{sw} \leq f_{yw}\Sigma A_{sw} \tag{6.5}$$

where σ_{sw} is the average stress in the shear reinforcement, ΣA_{sw} is the total area of the activated shear reinforcement in the punching cone (assumed within $0.35d_v$ and d_v) and f_{yw} is the yield strength of the shear reinforcement. Concerning the concentration of shear forces, it was taken into account by multiplying also A_{sw} by the coefficient k_e.()

$$\sigma_{sw}=\frac{E_s\psi}{6}\left(1+\frac{f_b}{f_{yw}}\frac{d}{\emptyset_w}\right) \tag{6.6}$$

where f_b is the average bond stress, $\emptyset_w$ and E_{sw} are respectively the diameter and the modulus of elasticity of the shear reinforcement.

Concerning the maximum punching resistance (crushing of concrete struts), its capacity depends on the opening of the critical shear crack and its roughness, as proposed in [4]. This is accounted for in the CSCT by multiplying the failure criterion of concrete ($V_{R,c}$) by a factor k_{sys}, as given in Eq. (6.2). The value of parameter k_{sys} depends on the type of shear reinforcement and for studs, a value k_{sys} = 2.8 will be used in the following (according to Model Code 2010).

$$V_{R,max} = k_{sys}V_{R,c} \tag{6.7}$$

To calculate the punching resistance outside of the shear-reinforced area, it is considered that the rotations of the critical shear crack concentrate outside of the shear-reinforced area. This approach provides a safe estimate, as a fraction of the total rotation may develop within the shear-reinforced zone [4].

In practice, the only modification compared to the formulation for slabs without shear reinforcement is that the control perimeter selected has to be adapted:

$$V_{\mathrm{R},out} = \frac{0.75 b_{0,out} d_{v,out} \sqrt{f_c}}{1+15\frac{\psi d_v}{d_{g0}+d_g}} \tag{6.8}$$

where $d_{v,out}$ is the shear-resisting effective depth of the outer perimeter of reinforcement. On that basis, $b_{0,out}$ is the outer control perimeter (defined at $0.5d_{v,out}$ from the last perimeter of shear reinforcement). In the present case, the reduction of the control perimeter at the outermost perimeter of shear reinforcement ($b_{0,out,elas}$) due concentration of shear forces were estimated using the shear fields.

6.6.3. Comparison of the CSCT to test results

Table 6.5 summarizes the values of $b_{0,elas}$ and $b_{0,out,elas}$ obtained using Eq. 6.1 for the various tests presented in this paper for control perimeters at $d_v/2$ and $d_{v,out}/2$.

Table 6.5. Control perimeters based on linear-elastic shear fields.

Slab	b_1 [mm]	$b_{1,out}$ [mm]	$b_{0,elas}$ [mm]	$b_{0,out,elas}$ [mm]
S1	1549	-	946	-
S2	1546	-	1049	-
S7	1542	-	1166	-
S1-1	1547	3414	946	2344
S2-1	1540	2678	1049	2381
S2-2	1548	3133	1049	2752
S2-3	1547	3497	1049	2857
S7-1	1545	3414	1166	2727

The punching resistance according to Eq. 6.1 using the punching shear strength formulations of CSCT are summarized in Table 6.6. The shear field combined with the CSCT are able to predict the correct failure mode of tests used for this analysis. All models show fine agreement for the estimate of the failure mode and failure load. The results show consistent agreement between the experimental and theoretical results, with an average ratio of measured-to-calculated resistance equal to 1.03 and a low Coefficient of Variation (4%). It is of particular interest the correct prediction of the failure mode, indicating that the physics of the failure phenomena is suitably captured.

Table 6.6. Comparison of test results with critical shear-crack theory.

Slab	V_u [kN]	Failure (test)	$V_{R,c}$ [kN]	$V_{R,max}$ [kN]	$V_{R,cs}$ [kN]	$V_{R,out}$ [kN]	$V_{R,CSCT}$ [kN]	$V_R/V_{R,CSCT}$ [-]	Failure
S1	325	V_c	329	-	329	-	329	0.99	V_c
S2	372	V_c	370	-	370	-	370	1.00	V_c
S7	345	V_c	323	-	323	-	323	1.07	V_c
S1-1	500	V_{within}	-	545	477	478	477	1.05	V_{within}
S2-1	513	V_{within}	-	633	492	531	492	1.04	V_{within}
S2-2	575	V_{within}	-	617	549	556	549	1.05	V_{within}
S2-3	550	$V_{outside}$	-	630	601	578	578	0.95	$V_{outside}$
S7-1	640	$V_{outside}$	-	686	618	606	606	1.06	$V_{outside}$
							Avge	1.03	
							CoV	0.04	

Representative examples are illustrated in Fig. 6.21, which depicts different failure modes: a slab without shear reinforcement (Fig. 6.21a), failure within the shear-reinforced area (Fig. 6.21b), and failure outside the shear-reinforced area (Fig. 6.21c).

It is interesting to note that the CSCT provides also information on the expected level of strain in the studs (Fig. 6.13 and Fig. 6.14). In general, a satisfactory agreement is found with this respect. For instance, for the investigated specimens S1-1 and S1-7 (Fig. 6.21b,c respectively) the studs are predicted to yield at failure, which agrees with the recorded measurements (Fig. 6.14d-e and Fig. 6.14g-h respectively). As it may be noted, yielding was not recorded for all the studs of these specimens, but the level of strains measured in the studs by strain gages is lower or equal than the maximum expectable strain in the shaft (unless the critical shear crack intercepts the studs at the location of the gauge [4]) accounting for bond conditions.

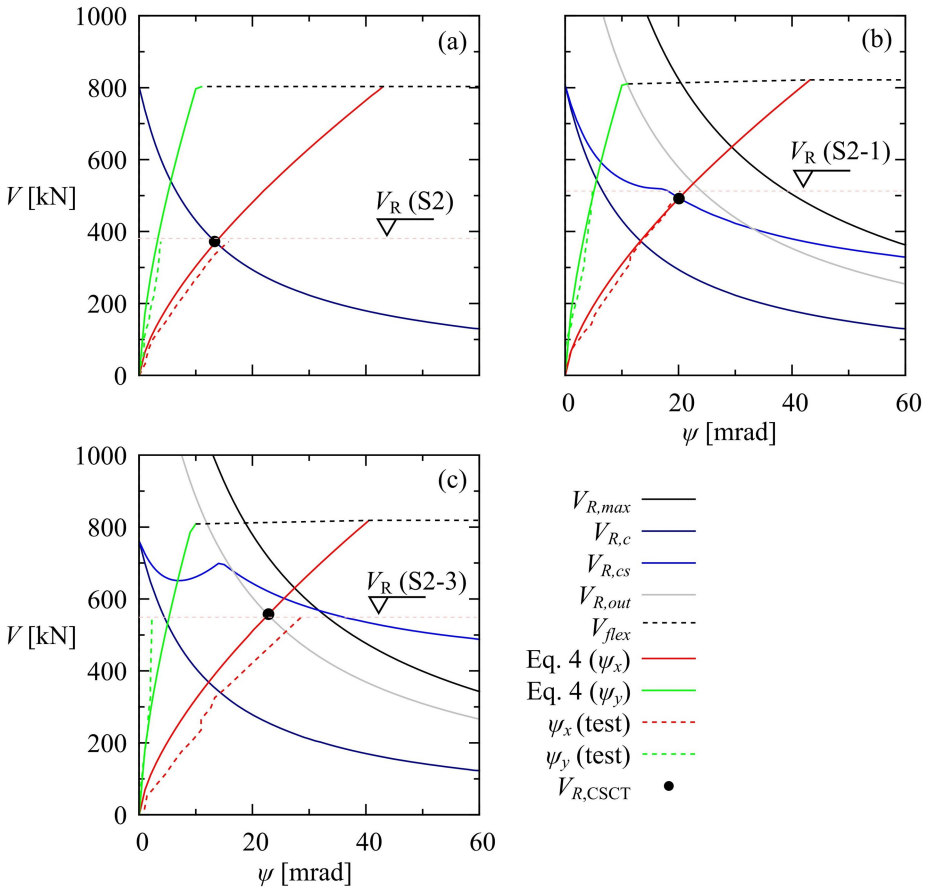

Fig. 6.21 - Failure criteria of the Critical Shear Crack Theory (CSCT) [3]-[4]: (a) slab S2 without shear reinforcement; (b) slab S1-1 with shear reinforcement failing within the shear-reinforced region; and (c) slab S7-1 with shear reinforcement failing outside the shear-reinforced zone.

6.7. Conclusions

In this paper, the punching shear design of re-entrant slab-column connections is investigated. Tests on eight slab-column connections were conducted having the load eccentricity and shear reinforcement as main parameters. The experimental results were later compared to a series of design codes as well as to the theoretical frame of the Critical Shear Crack Theory (CSCT). The main conclusions are presented below:

1. The punching resistance and deformation capacity of flat slabs with re-entrant corner can be significantly increased by incorporating shear reinforcement. Such enhancement in the performance depends largely on the shear reinforcement ratio arranged, but is limited by the resistance outside of the shear-reinforced area or the maximum punching resistance.
2. The slabs with shear reinforcement reach higher levels of deformation. Flexural strains consequently increase, particularly in the region of slab continuity over the column region, while it is less pronounced at the edge region.
3. The activation of the studs is more significant in the slabs with higher levels of eccentricity and shear force. In general terms, it was observed that the most strained studs were located in the area of high concentration of shear stress (diagonal direction at the inner sides of the column for the tested specimens). Concerning the activation of shear reinforcement at the edges, it was consistently lower.
4. A detailed analysis of the surface strains of the concrete indicates that, in the soffit of the slab near to the column, the tangential compressions are higher than the radial compressions, following the same qualitative pattern observed in inner columns. Along the re-entrant edge, however, the radial deformations were more significant, resulting from the combination of bending moments and torsion in this region.
5. Design codes provided conservative estimates of the strength in general, although some codes predicted well the punching resistance (notably EN-1992-1-1:2004 and NBR 6118-2023). However, the prediction of failure modes was not consistent with the experimental observations. This latter fact implied a potential deficiency in the identification of the parameters governing the punching failure.
6. A more consistent approach for design and analysis of this detail can be formulated based on the CSCT. It combines a shear field analysis (to calculate the inner and outer control perimeter) with an estimate of the load-rotation curve (based on a Level-of-Approximation III). This approach provides consistent estimates of the resistance, deformation capacity and also failure mode.

6.8. References

[1] Melo GSSA, Regan PE. Post-punching resistance of connections between flat slabs and interior columns. Mag Concr Res 1998;50(4):319-27. https://doi.org/10.1680/macr.1998.50.4.319

[2] Fernández Ruiz M, Mirzaei Y, Muttoni A. Post-punching behavior of flat slabs. ACI Struct J 2013; 110(5):801-12. https://doi.org/10.14359/51685833

[3] Muttoni A. Punching shear strength of reinforced concrete slabs without transverse reinforcement. ACI Struct J 2008; 105(4):440-50. https://doi.org/10.14359/19858

[4] Fernández Ruiz M, Muttoni A. Applications of the critical shear crack theory to punching of R/C slabs with transverse reinforcement. ACI Struct J 2009; 106-4:485-94. https://doi.org/10.14359/56614

[5] Elstner RC., Hognestad E. Shearing strength of reinforced concrete slabs. Journal Proceedings 1956; 53(7):29-58.

[6] Hawkins NW., Corley WG. Moment transfer to columns in slabs with shearhead reinforcement. ACI Symposium Publication 1974; 42:847-80.

[7] Hallgren M. Punching Shear Capacity of Reinforced High Strength Concrete Slabs. PhD Thesis. Department of Structural Engineering, Royal Institute of Technology, Stockholm, Sweden; 1996.

[8] Tassinari, L. Poinçonnement non symétrique des dalles en béton armé (in French). PhD Thesis. Nr 5030, IS-BETON, Ecole Polytechnique Fédérale de Lausanne, Lausanne, Switzerland; 2011.

[9] Dilger WH., Ghali A. Shear reinforcement for concrete slabs. J Struct Div 1981; 107(12):2403-20. https://ascelibrary.org/doi/10.1061/JSDEAG.0005846

[10] Regan P., Samadian F. Shear reinforcement against punching in reinforced concrete flat slabs. The structural engineer 2001; 79(10):24-31.

[11] Lips S, Fernández Ruiz M, Muttoni A. Experimental Investigation on Punching Strength and Deformation Capacity of Shear-Reinforced Slabs. ACI Struct J 2012; 109(6):889-900. https://doi.org/10.14359/51684132

[12] Schmidt P, Kueres D, Hegger J. Punching shear behavior of reinforced concrete flat slabs with a varying amount of shear reinforcement. Struct Concrete 2020; 21(1):235-46. https://doi.org/10.1002/suco.201900017

[13] Andrä H-P. Zum Tragverhalten von Flachdecken mit Dübelleisten-Bewehrung im Auflagerbereich. BuSt 1981;76(3):53-7. https://doi.org/10.1002/best.198100120

[14] Gomes RB. Punching resistance of reinforced concrete flat slabs with shear reinforcement. PhD Thesis. Polytechnic of Central London, London, UK; 1991.

[15] Birkle G, Dilger WH. Influence of slab thickness on punching shear strength. ACI Struct J 2008;105(2):180-8. https://doi.org/10.14359/19733

[16] Ferreira MP, Melo GS, Regan PE, Vollum RL. Punching of reinforced concrete flat slabs with double-headed shear reinforcement. ACI Struct J 2014;111(2):363-73. https://doi.org/10.14359/51686535

[17] Islam S., Park R. Tests on slab-column connections with shear and unbalanced flexure. J Struct Div 1976; 102(3):549-68. https://doi.org/10.1061/jsdeag.0004296

[18] Beutel R, Hegger J. The effect of anchorage on the effectiveness of the shear reinforcement in the punching zone. Cem Concr Compos 2002;24(6):539-49. https://doi.org/10.1016/S0958-9465(01)00070-1

[19] Monney F, Yu Q, Fernández Ruiz M, Muttoni A. Anchorage of shear reinforcement in beams and slabs. Eng Struct 2022;265(114340):32. https://doi.org/10.1016/j.engstruct.2022.114340

[20] Lips S. Punching of flat slabs with large amounts of shear reinforcement. PhD Thesis. Nr 5409, IS-BETON, Ecole Polytechnique Fédérale de Lausanne, Lausanne, Switzerland; 2011.

[21] Hegger J, Sherif AG, Kueres D, Siburg C. Efficiency of various punching shear reinforcement systems for flat slabs. ACI Struct J 2017;114(3):631-42. https://doi.org/10.14359/51689434

[22] Schmidt P, Kalus M, Hegger J. Critical view on the level of maximum punching strength of flat slabs and column bases using database evaluations. Struct Concr 2021;22(6):3646-60. https://doi.org/10.1002/suco.202100374

[23] Siburg C, Hegger J, Furche J, Bauermeister U. Durchstanzbewehrung für Elementdecken nach Eurocode 2. Beton- Stahlbetonbau 2014;109(3):170-81. https://doi.org/10.1002/best.201300075

[24] Eligehausen R, Vocke H, Clauss A, Furche J, Bauermeister U. Neue Durchstanzbewehrung für Elementdecken. Beton- Stahlbetonbau 2003;98(5):334-44. https://doi.org/10.1002/best.200301700.

[25] Siqueira JPA, Melo GSd. Punching shear in flat slabs with open stirrups as shear reinforcement. Struct Concr 2023; 24(2): 2827-43. https://doi.org/10.1002/suco.202200050

[26] Fernández Ruiz M, Muttoni A, Kunz J. Strengthening of flat slabs against punching shear using post-installed shear reinforcement. ACI Struct J 2010;107(4):434-42. https://doi.org/10.14359/51663816

[27] Einpaul J, Brantschen F, Fernández Ruiz M, Muttoni A. Performance of punching shear reinforcement under gravity loading: Influence of type and detailing. ACI Struct J 2016;113(4):827-38. https://doi.org/10.14359/51688630

[28] Cantone R, Fernández Ruiz M, Bujnak J, Muttoni A. Enhancing punching strength and deformation capacity of flat slabs. ACI Struct J 2019;116(5):261-74. https://doi.org/10.14359/51716842

[29] Walkner R, Spiegl M, Feix J. Concrete screws as a post-installed punching shear reinforcement. Struct Concr. 2021;22:709-725. https://doi.org/10.1002/suco.202000427

[30] Ferreira MP, Pereira Filho MJM., Freitas MVP, Lima Neto AF, Melo GSSA. Experimental resistance of slab-column connections with prefabricated truss bars as punching shear reinforcement. Eng Struct 2021; 233(15):1-14. https://doi.org/10.1016/j.engstruct.2021.111903

[31] Krüger, G. Résistance au poinçonnement excentré des planchers-dalles; EPFL: Écublens, Switzerland; 1999.

[32] Anis NA., Shear strength of reinforced concrete flat slabs without shear reinforcement. PhD Thesis. Imperial College, London; 1970.

[33] Stamenkovic A, Chapman J. Local strength at column heads in flat slabs subjected to a combined vertical and horizontal loading. Instit Civil Eng 1974;57(2):205-32.
[34] Hawkins NM, Bao A, Yamazaki J. Moment transfer from concrete slabs to columns. ACI Struct J 1989;6(86):705-16.
[35] Kamaraldinm K.Punching shear and moment transfer in reinforced concrete flat slabs. PhD thesis. Polytechnic of Central London ;1990.
[36] Ferreira MdP, Oliveira MH, Melo GSSA. Tests on the punching resistance of flat slabs with unbalanced moments. Eng Struct 2019;196:1-13. https://doi.org/10.1016/j.engstruct.2019.109311
[37] Ungermann J, Schmidt P, Christou G, Hegger J. Eccentric punching tests on column bases - Influence of column geometry. Struct Concr. 2022;23(3): 1316-32. https://doi.org/10.1002/suco.202100744
[38] Fraile DH, Setiawan A, Santos JB, Muttoni A. Punching tests on edge slab-column connections with refined measurements. Eng Struct 2023; 288:1-24. https://doi.org/10.1016/j.engstruct.2023.116166
[39] Hanson NW, Hanson JM. Shear and moment transfer between concrete slabs and columns. Res Dev Bull PCA 1968:2-16.
[40] Stamenkovic A, Chapman JC. Local strength of flat slabs at column heads. CIRIA-Report 39, London; 1972. 81pp
[41] Narayani N. Shear reinforcement in reinforced concrete column heads. PhD Thesis. Faculty of Engineering, Imperial College of Science and Technology, London, UK, 1971.
[42] Regan PE. Tests of connections between flat slabs and edge columns. London, UK: School of Architecture and Engineering, University of Westminster; 1993.
[43] Zaghlool R, Rawdon de Paiva H, Glockner P. Tests of reinforced concrete flat plate floors. J Struct Div Proc Am Soc Civ Eng 1970;96-3:487-507.
[44] Sudarsana IK. Punching shear in edge and corner column slab connections of flat plate structures. PhD thesis. University of Ottawa; 2001.
[45] Ritchie M, Ghali A, Dilger W, Gayed RB. Unbalanced moment resistance by shear in slab-column connections: experimental assessment. ACI Struct J 2006;103-1:74-82. https://doi.org/10.14359/15088
[46] Zaghloul, A. Punching shear strength of interior and edge column-slab connections in CFRP reinforced flat plate structures transferring shear and moment. PhD thesis University of Ottawa; 2007.
[47] Albuquerque NGB, Melo GS, Vollum RL. Punching shear strength of flat slab-edge column connections with outward eccentricity of loading. ACI Struct J 2016; 113(5):1117-29. https://doi.org/10.14359/51689156
[48] Hammill N, Ghali A. Punching shear resistance of corner slab-column connections. ACI Struct J 1994;91(6):697-705. https://doi.org/10.14359/1502
[49] Stamenkovic A, Chapman J. Local strength at column heads in flat slabs subjected to a combined vertical and horizontal loading. Instit Civil Eng 1974;57(2):205-32.
[50] Walker P, Regan P. Corner column-slab connections in concrete flat plates. J Struct Eng 1987;113(4):704-20.

[51] Desayi, P.; Seshadri, H.K. Punching shear strength of flat slab corner column connections. In Part 1. Reinforced Concrete Connections, Department of Civil Engineering, Indian Institute of Science: Bangalore, India, 1997; 122(1):10-20.

[52] Vocke H, Eligehausen R. Durchstanzen von Flachdecken im Bereich von Rand- und Eckstützen (in German). Beton- und Stahlbetonbau 2003; 98(2):66-73. https://doi.org/10.1002/best.200300380

[53] Siqueira JPdA, Albuquerque EJP, Fernández Ruiz M, Melo GSSA. Punching shear tests in flat slabs supported on re-entrant corner columns. Eng Struct 2023. (Under Review).

[54] ABNT NBR 6118:2023 - Projeto de Estruturas de Concreto. Associação Brasileira de Normas Técnicas, Rio de Janeiro, Brazil, 2023, 260 pp.

[55] Design of Concrete Structures - General Rules and Rules for Buildings, EN 1992-1-1. Brussels, Belgium: CEN European Committee for Standardization; 2004, 225 p.

[56] Comité Euro-International du Béton/Fédération Internationale de la Précontrainte: Model Code for Concrete Structures; 1990.

[57] ACI Committee 318. Building Code Requirements for Structural Concrete (ACI 318- 19) and Commentary, 624. Farmington Hills, USA: American Concrete Institute; 2019.

[58] *fib* Model Code for Concrete Structures 2010, *fib*. First Edition UK 2013. https://doi.org/10.1002/9783433604090

[59] FEN 1992-1-1:23. Eurocode 2-Design of concrete structures- Part 1-1: General rules, rules for buildings, bridges and civil engineering structures, Stable version of the draft of the 2nd generation of EN 1992-1-1:23, CEN, Brussels, Belgium, 2023, pp 405.

[60] Fernández Ruiz M, Muttoni A. Application of shear stress fields for the analysis and design of reinforced concrete slabs (in Spanish). Hormigón Acero 2009;60(252):73-88.

[61] Vaz Rodrigues R, Fernández Ruiz M, Muttoni M. Shear strength of R/C bridge cantilever slabs. Eng Struct 2008;30(11):3024-33. https://doi.org/10.1016/j.engstruct.2008.04.017

[62] Natário, F., Fernández Ruiz, M., Muttoni, A., Shear strength of RC slabs under concentrated loads near linear supports. Eng Struct 2014;76:10-23. https://doi.org/10.1016/j.engstruct.2014.06.036

7. CONCLUSIONS AND FUTURE RESEARCH

This thesis investigated the punching shear behaviour of flat slabs supported by re-entrant corner (or internal corner) columns. This configuration is not specified in the codes of practice or technical literature. The punching response of flat slabs with re-entrant corner regions is a complex phenomenon, where the resistance and deformation capacity are coupled. Also, the distribution of shear forces near to the supported area plays a major role on the mechanical response, with potential concentrations depending upon the eccentricity of the load.

In addition to Chapters 1 (Introduction) and 7 (Conclusions and Future Research), this document is composed of five chapters. The second chapter presents the code provisions, and the formulations (punching shear and flexural capacities) used for the calculation within this research, as well as the necessary adaptations to consider re-entrant corner connections.

Chapters three to six correspond to three scientific articles that address different aspects related to the theme of this thesis. The fourth chapter presents an additional study that was not included in any of the published articles, but which will be further refined and submitted for publication in a scientific journal in the future.

With the objective of advancing the understanding of punching shear behaviour in flat slabs supported on re-entrant corner columns, an extensive experimental program was conducted as part of this thesis. The campaign comprised fifteen full-scale reinforced concrete specimens, designed to investigate the influence of key parameters on slab-column connection performance. The variables studied included the flexural reinforcement ratio, the presence of edge reinforcement near the re-entrant corner, the load eccentricity, and the use and amount of shear reinforcement.

A comparative analysis of the key design standards (ACI 318:2019, Eurocode 2:2004, ABNT NBR 6118:2023, fib Model Code 2010 and EN 1992-1-1:2023) was also presented. While all these standards offer consolidated procedures for verifying punching shear in internal, edge and corner (or external corner) columns, none of them explicitly address slab-column connections in re-entrant corners.

To enable these standards to be applied to the case under investigation, specific adaptations were made, particularly with regard to the definition of critical perimeters, in order to extend the existing criteria for columns positioned in re-entrant regions.

The experimental results demonstrate that shear deformations have a significant impact on the overall deformation state within the shear-critical region at the point of failure. Additionally, the geometric positioning of the re-entrant corner column intensifies stress concentrations and impacts the behaviour of the connection.

These observations highlight the need to explicitly incorporate shear deformations and the effects of re-entrant geometry into a mechanical theory that seeks to consistently describe the mechanism of shear failure by punching in slab-column connections, both in terms of load resistance and associated deformations. In addition, the results demonstrate the importance of future updates to design codes to consider this type of configuration, currently absent from the standards, to provide more appropriate criteria for the design and evaluation of slabs supported by re-entrant corner columns.

Punching shear in flat slabs with re-entrant corner columns

The third chapter conducts a comparison of two specimens: a re-entrant corner slab and an inner slab-column connection (both with similar geometry and material properties). The main conclusions are listed below:

1. The results of the comparison showed that the position of the column had a significant influence on the punching resistance and deformation capacity. The unitary resistance showed that the capacity of the re-entrant corner slab was approximately 50% lower than that of the inner slab-column connection.
2. The yielding of the flexural reinforcement was confined to an area close to the column, with the maximum strains occurring within the column width. On the side of the column where the slab edge was discontinuous, the strains decreased rapidly with increasing distance from the column, approaching zero. This strain distribution closely resembles the behaviour observed in interior connections (e.g., specimens RS and results reported in the literature) and in edge-column specimens (e.g., PHS1, Fraile *et al.*), respectively.

Punching shear tests in flat slabs supported on re-entrant corner columns

The results of an experimental campaign of full-scale reinforced concrete flat slabs (180 mm thickness) supported on re-entrant corner columns without shear reinforcement were presented in Chapter 5 of this thesis. The main conclusions are listed below:

1. The influence of the flexural reinforcement ratio on punching shear capacity and rotation is well recognised in tests on interior slab-column connections and was also confirmed for the re-entrant corner specimens investigated in this study. Higher reinforcement ratios led to increased punching resistance. For example, slab S2 (ρ = 1.5%) could withstand a punching load that was 4% higher than slab S5 (ρ = 1.0%) and 32% higher than slab S4 (ρ = 0.7%).
2. Regarding the eccentricity of the shear force, the test results revealed a pronounced influence of load eccentricity. The punching shear capacity decreased by approximately ~10-13%, when compared with the reference. In contrast, the slab rotation at failure increased significantly.
3. The use of the reinforcement at the edges in the specimen S6 suggests that it is effective. This is because reductions in displacements along the re-entrant edges were observed. There was also improved control of crack development in this area. However, the test results also indicate that its contribution to increasing the ultimate punching shear capacity is limited.
4. Design codes reproduce reasonably well the trend that the flexural reinforcement and load eccentricity have on the response when compared to the performed tests. However, they fail in predicting the level of resistance, which appears to be highly conservative in several cases.
5. In general, the design approaches reflect the anticipated trend of a decrease in punching shear capacity as the load eccentricity increases, which is consistent with the experimental observations. However, when the absolute resistance levels were compared, it was found that none of the standards accurately predicted the measured capacities. This was anticipated since existing codes do not explicitly address slab-column connections at re-entrant corner columns. Therefore, specific adaptations were required in this work to enable the application of the codes to this configuration.
6. Despite these limitations, all design provisions produced estimates that were conservative with regard to punching shear resistance. Of these, NBR 6118 produced

predictions closest to the experimental results, whereas ACI 318 proved to be the most conservative.

7. The Critical Shear Crack Theory provides a suitable frame for analysis of the punching resistance of this case, with accurate estimates of the strength (V_R / V_{CSTC} = 1,02) and a low Coefficient of Variation. To that aim, different sectors may be considered in the control perimeter.
8. The Critical Shear Crack Theory (CSCT) is a suitable and physically consistent framework for analysing the punching shear behaviour of flat slabs supported on re-entrant corner columns. This theory relies on a mechanical description of the failure mechanism and makes it possible to account for the influence of rotation, shear deformation, and the non-uniform shear stress distribution inherent to this connection. When adapted to the present case, the theory provided accurate strength predictions with a low coefficient of variation, thus demonstrating its applicability in situations not explicitly covered by current design codes.
9. In addition, the shear-field approach proved to be an effective tool for understanding the internal stress flow near the column-slab connection. This methodology enabled the rational definition of the control perimeter for re-entrant corner layouts and the identification of critical regions with elevated shear demand. Overall, combining the CSCT with shear-field analysis provides a consistent approach to evaluating the punching shear resistance in flat slabs with re-entrant corner columns.

Punching shear in flat slabs with re-entrant corner columns and shear reinforcement

Chapter 6 presents the results of tests conducted on five specimens of re-entrant slab-column connections with shear reinforcement. These results are then compared with those for the reference slabs described in Chapter 3. The main conclusions are:

1. The punching resistance and deformation capacity of flat slabs with re-entrant corners can be significantly increased by incorporating shear reinforcement, consistent with the results observed in slabs with internal columns. In compared with slabs without shear reinforcement, the punching strength and rotation capacity increased significantly. As the amount of shear reinforcement increases, so do the failure loads, but this is limited by the resistance outside the shear-reinforced area or the maximum punching resistance.

2. The activation of the shear reinforcement dependents of the level of load eccentricity and the specific regions of the slab (the inner faces of the column or near the edges). Accordingly, slabs subjected to higher load eccentricities exhibited greater mobilization of the shear reinforcement. The most strained studs were consistently located in the regions of maximum shear demand, particularly in the diagonal zones adjacent to the inner faces of the column.
3. The design approaches provided by current standards generally underestimate the shear capacity due to punching. Even when modifications were introduced to the control perimeter outside the shear-reinforced region, the design provisions still failed to correctly identify the governing failure mode. Although all provisions provided safe estimates of the expected load, the incorrect identification of the failure mechanism compromises the reliability of the design.
4. The ACI 318-11 provisions produced more conservative predictions than the experimental results obtained in this study. By contrast, NBR 6118 once again produced the most accurate estimates of punching shear capacity of all the design codes evaluated.
5. In this chapter, the results were refined using the Critical Shear Crack Theory (CSCT) in combination with a Level-of-Approximation III (LoA III) formulation and a shear-field approach in order to define the control perimeter outside of the shear-reinforced region. This integrated methodology provides a more consistent, mechanically sound approach to analysing slab-column connections at re-entrant corners. Consequently, it provides consistent estimates of the resistance, deformation capacity and the governing failure mode.

Future research

Some questions remain open with respect to the punching shear behaviour of ***slab-column connections supported on re-entrant corners***. Further experimental, numerical and theoretical investigation is still required to approach a consensus in this topic. Some possible ideas for future research are listed below.

With respect to experimental works:

Additional experimental research on re-entrant corner slab–column connections involving relatively thick slabs, varying column dimensions, exploring different load eccentricity, column geometries (such as rectangular and circular columns), and assessing different types of shear reinforcement would be valuable to further validate the findings of this study.

Another relevant topic for future research would be the investigation of columns in which one dimension is significantly larger than the other, such as columns with rectangular cross-sections (e.g., 0.30 m × 0.60 m), a configuration often found in building structures. In such cases, the slab torsional stiffness along the longer side of the column is expected to be higher, potentially leading to eccentricities different from those considered in the present study. Accounting for this effect may provide a more comprehensive understanding of punching shear behavior in practical design situations.

With respect to code design improvements:

An interesting strategy to improve current design codes would be the development of nonlinear numerical models for the experimentally tested specimens using the finite element method. Once validated, these computational models would enable extensive parametric studies, including variations in several geometric and mechanical parameters as well as different levels of load eccentricity. By comparing the numerical outcomes with the predictions of existing design provisions, valuable insights could be obtained to support the refinement and improved calibration of current code formulations.

APÊNDICE: RECOMENDAÇÕES PARA A ABNT NBR 6118:2023

Conforme discutido no Capítulo 2, referente às prescrições normativas, a ABNT NBR 6118:2023 [1] não contempla de forma explícita o caso específico de pilares de canto reentrante. Em razão dessa lacuna normativa, torna-se necessária a adoção de adaptações e interpretações das recomendações existentes para a estimativa das cargas de ruptura por punção em lajes lisas apoiadas nesses elementos.

De acordo com a norma, para pilares internos, quando há transferência de momentos fletores nas direções ortogonais, devem ser consideradas conjuntamente as parcelas correspondentes no cálculo da resistência à punção. Para pilares de borda, quando não atua momento no plano paralelo à borda livre, considera-se apenas a parcela de momento perpendicular à borda. Por outro lado, quando atua momento no plano paralelo à borda livre, devem ser consideradas simultaneamente as parcelas de momento paralela e perpendicular à borda.

No caso dos pilares de canto, a norma estabelece que se aplique o procedimento previsto para pilares de borda quando não atua momento no plano paralelo à borda livre. Entretanto, como o pilar de canto apresenta duas bordas livres, a verificação deve ser realizada separadamente para cada uma delas, considerando-se, em cada análise, o momento fletor cujo plano seja perpendicular à borda livre adotada.

Conforme Wight e MacGregor (2009) [2], na equação para verificação da transferência combinada de cisalhamento e momento em ligações laje-coluna do ACI 318:2019 [3] foi originalmente derivada assumindo a atuação do momento fletor em apenas uma direção principal por vez. Em aplicações usuais em edifícios, a prática corrente consiste em empregar essa equação para verificar a tensão máxima de cisalhamento no perímetro crítico, considerando a ação combinada do esforço cortante e do momento em uma única direção. Dessa forma, a verificação deve ser realizada separadamente para ambas as direções ortogonais principais, adotando-se a situação mais crítica para o dimensionamento. Contudo, em situações particulares, associadas a vãos elevados ou a disposições estruturais incomuns, pode ser adotada a verificação da tensão de cisalhamento máxima considerando a atuação simultânea de momentos fletores nos dois eixos principais.

Dessa forma, para o tratamento específico dos pilares de canto reentrante, identificam-se, nas normas em geral, três abordagens possíveis para considerar a presença de momentos fletores: (i) a consideração independente dos momentos atuantes nas direções ortogonais (direções x e y); (ii) a consideração conjunta dessas parcelas, por meio da soma de suas contribuições; ou (iii) a utilização de um momento fletor resultante.

A última abordagem, baseada na consideração de um momento fletor (ou excentricidade) resultante equivalente, esteve presente nas recomendações formuladas pelo Prof. Paul Regan durante a fase de concepção dos ensaios em pilares de canto reentrante. Contudo, como a norma brasileira fundamenta a verificação da punção na consideração dos momentos atuantes nas direções ortogonais, e não em um momento resultante único, a adoção da consideração conjunta das parcelas de momento em cada direção mostra-se mais coerente.

Abordagem (i) - Verificação independente dos momentos em cada direção

As Equações (1) e (2) são aplicadas quando a verificação da resistência à punção é realizada de forma independente para cada direção ortogonal (*x* e *y*), considerando a atuação do momento em uma direção por vez:

$$\tau_S = \frac{F_S}{u_i^* d} + \frac{K \ |M_{S,x} - M_{S,x}^*|}{W_{p,x} d} \quad (1)$$

$$\tau_S = \frac{F_S}{u_i^* d} + \frac{K \ |M_{S,y} - M_{S,y}^*|}{W_{p,y} d} \quad (2)$$

Abordagem (ii) - Verificação considerando a sobreposição dos momentos

A Equação (3) é aplicada quando se considera a sobreposição das parcelas de momento atuantes nas direções ortogonais:

$$\tau_S = \frac{F_S}{u_i^* d} + \frac{K_x |M_{S,x} - M_{S,x}^*|}{W_{p,x} d} + \frac{K_y |M_{S,y} - M_{S,y}^*|}{W_{p,y} d} \quad (3)$$

Abordagem (iii) - Verificação com momento fletor resultante equivalente

A Equação (4) é empregada quando a verificação é realizada a partir de um momento fletor resultante:

$$\tau_S = \frac{F_S}{u_i^* d} + \frac{K \ |M_{S,xy} - M_{S,xy}^*|}{W_{p,xy} d} \quad (4)$$

$M_{S,x}$ e $M_{S,y}$ representam os momentos fletores atuantes em relação ao centro do pilar. Já $M^*_{S,x}$ e $M^*_{S,y}$ correspondem aos momentos resultantes da excentricidade do perímetro crítico reduzido em relação ao centro do pilar.

De forma análoga, $M_{S,xy}$ e $M^*_{S,xy}$ correspondem, respectivamente, ao momento fletor resultante combinado nas direções ortogonais e ao momento equivalente associado à excentricidade resultante do perímetro crítico reduzido em relação ao centro do pilar.

A Fig. 1 ilustra os perímetros críticos adaptados, definidos a uma distância de 2d em relação à face do pilar. Os termos W_{py} e W_{px} correspondem ao módulo de resistência plástica do perímetro relativo ao centro geométrico do perímetro cheio (u_1). E o termo $W_{p,xy}$ calculado conforme apresentado na Eq. (2.16), conforme apresentado no Capítulo 2.

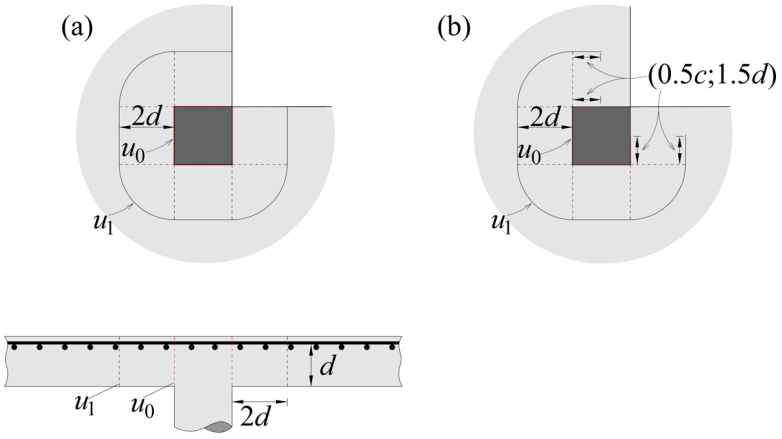

Figura 1. Perímetro crítico para pilares de canto reentrante: (a) Perímetro crítico completo e (b) Perímetro crítico reduzido.

Os coeficientes K_x e K_y correspondem à parcela do momento fletor transmitida ao pilar por meio do cisalhamento nas direções x e y, respectivamente. Para sua determinação, adotam-se os valores do coeficiente K conforme apresentados na Tabela 19.2 da norma, com a devida modificação da razão geométrica: substitui-se C_1/C_2 por $C_2/2C_1$. C_1 representa a dimensão da seção transversal do pilar paralela à excentricidade da força e C_2 representa a dimensão perpendicular à excentricidade.

Tabela 1 - Valores de K (Tabela 19.2 NBR 6118:2023)

C_1/C_2	0,5	1,0	2,0	3,0
K	0,45	0,60	0,70	0,80

Tabela 2 - Valores de K_x e K_y (adaptado – NBR 6118:2023)

C_1/C_2	0,5	1,0	2,0	3,0
K_x	0,375	0,45	0,60	0,65
K_y	0,60	0,45	0,375	0,375

A tensão solicitante, pode ser reescrita na Eq. (5), onde surge o parâmetro β (semelhante ao adotado no Eurocode 2), que pode ser obtido por meio da Eq. (3).

$$\tau_S = \beta \frac{F_S}{u_i^* d} \tag{5}$$

$$\beta = \frac{u_1}{u_1^*} + \frac{k_x |M_{S,x} - M_{S,x}^*|}{W_{p,x} F_S} + \frac{k_y |M_{S,y} - M_{S,y}^*|}{W_{p,y} F_S} \tag{6}$$

Os momentos $M^*_{S,x,}$ e $M^*_{S,y}$ surgem da excentricidade entre o centro do pilar e o centro geométrico do perímetro crítico, correspondendo às distâncias x^*_{cp} e y^*_{cp} respectivamente. O centro geométrico do perímetro (u1) e do perímetro crítico reduzido (u_1^*) podem ser calculados pelas expressões abaixo:

$$x_{cp} = \frac{\pi d \left(\frac{4d}{\pi} + \frac{c_x}{2}\right)}{u_1} \tag{7}$$

$$x_{cp}^* = \frac{\pi d \left(\frac{4d}{\pi} + \frac{c_x}{2}\right) + \frac{c_x^2}{4}}{u_1^*} \tag{8}$$

O valor de $W_{p,x}$ para pilares de canto reentrante podem ser calculados pela expressão abaixo:

$$W_{p,x} = \frac{c_x^2}{2} + c_y c_x + 4 d c_y + 12 d^2 + \frac{\pi d c_x}{2} + 2 x_{cp}^2 + \pi d x_{cp} \tag{9}$$

Os valores de $W_{p,y}$, y_{cp} e y^*_{cp} são obtidos substituindo-se os índices x por y nas equações.

A tensão resistente na ausência de armaduras de punção é dada por:

$$\tau_{R,1} = 0.182 k_e (100 \rho f_c)^{1/3} \tag{10}$$

onde k_e é um fator que leva em conta o *size effect*, que foi incorporado na última atualização da norma e ρ é a taxa de armadura de flexão da laje igual à largura do pilar mais 3d de cada lado (limitado a 2%).

$$k_e = 1 + \sqrt{200/d} \leq 2 \tag{11}$$

Para a carga característica pode ser obtida pela Eq. 9:

$$V_{c,\,NBR} = 0.182 \left(1 + \sqrt{\frac{200}{d}}\right) (100 \rho f_c)^{1/3} u_1 \, d \tag{12}$$

A Tabela 3 apresenta a comparação entre as cargas resistentes à punção obtidas experimentalmente (V_R) e as estimativas fornecidas pela ABNT NBR 6118:2023 (V_{NBR}), considerando as três abordagens propostas para o tratamento dos momentos fletores em pilares de canto reentrante. Observa-se que a abordagem (i), baseada na verificação independente dos momentos em cada direção, resulta, em média, em valores mais conservadores. Por outro lado, as abordagens (ii) e (iii) conduzem a estimativas mais próximas dos valores experimentais, com médias de V_R/V_{NBR} superiores à unidade e coeficientes de variação reduzidos, indicando maior consistência e melhor representatividade do comportamento observado experimentalmente.

Tabela 3 - Estimativas das cargas pelas três abordagens.

Laje	f_c [MPa]	ρ [%]	d [mm]	$e_{R,x}=e_{R,y}$ [mm]	e_R [mm]	V_R [kN]	Abordagem (i)		Abordagem (ii)		Abordagem (iii)	
							V_{NBR} [kN]	V_R/V_{NBR} [-]	V_{NBR} [kN]	V_R/V_{NBR} [-]	V_{NBR} [kN]	V_R/V_{NBR} [-]
S1	48	1.49	148	348	491	325	359	0.91	305	1.06	304	1.07
S2	48	1.49	147	243	344	372	414	0.90	369	1.01	361	1.03
S3	44	0.67	143	348	496	250	252	0.99	214	1.17	213	1.18
S4	44	0.65	145	241	344	282	298	0.95	265	1.06	260	1.09
S5	44	1.00	141	235	336	358	333	1.08	296	1.21	291	1.23
S6	44	0.94	146	239	341	345	341	1.01	304	1.14	298	1.16
S7	43	0.95	145	185	262	345	367	0.94	337	1.02	328	1.05
S8	53	0.96	144	361	511	309	302	1.02	256	1.21	254	1.22
							Média	0.97		1.11		1.13
							CoV	0.06		0.07		0.06

Referências

[1] ABNT NBR 6118:2023 - Projeto de Estruturas de Concreto. Associação Brasileira de Normas Técnicas, Rio de Janeiro, Brazil, 2023, 260 pp.

[2] MacGregor, J. G., and Wight, J. K., Reinforced Concrete - Mechanics and Design, 5th edition, New Jersey, 2009.

[3] ACI Committee 318. Building Code Requirements for Structural Concrete (ACI 318- 19) and Commentary, 624. Farmington Hills, USA: American Concrete Institute; 2019.